



# Practical Antenna Design for Wireless Products

Henry Lau

# **Practical Antenna Design for Wireless Products**

For a complete listing of titles in the  
*Artech House Antennas and Electromagnetics Analysis Library*  
turn to the back of this book.

# **Practical Antenna Design for Wireless Products**

Henry Lau



**ARTECH  
HOUSE**

BOSTON | LONDON  
[artechhouse.com](http://artechhouse.com)

**Library of Congress Cataloging-in-Publication Data**

A catalog record for this book is available from the U.S. Library of Congress.

**British Library Cataloguing in Publication Data**

A catalogue record for this book is available from the British Library.

**Cover design by John Gomes**

ISBN 13: 978-1-63081-325-3

**© 2019 ARTECH HOUSE**

**685 Canton Street**

**Norwood, MA 02062**

All rights reserved. Printed and bound in the United States of America. No part of this book may be reproduced or utilized in any form or by any means, electronic or mechanical, including photocopying, recording, or by any information storage and retrieval system, without permission in writing from the publisher.

All terms mentioned in this book that are known to be trademarks or service marks have been appropriately capitalized. Artech House cannot attest to the accuracy of this information. Use of a term in this book should not be regarded as affecting the validity of any trademark or service mark.

10 9 8 7 6 5 4 3 2 1

# Contents

<b>Preface</b>	<b>9</b>
<b>Acknowledgments</b>	<b>13</b>
<b>1 Fundamental Concepts</b>	<b>15</b>
1.1 Introduction	15
1.2 Antenna Fundamentals	16
1.2.1 Basic Types of Antenna	16
1.2.2 Multiband and MIMO	20
1.3 Radiation Mechanism	23
1.3.1 Source of Radiation	23
1.3.2 Characteristics of Radiation	26
References	33
<b>2 Specifications and Performances</b>	<b>35</b>
2.1 Introduction	35
2.2 Specifications and Performances	35
2.2.1 Radiation Pattern	35
2.2.2 Beam Solid Angle	38
2.2.3 Radiation Power Intensity	39
2.2.4 Directivity and Effective Aperture	40
2.2.5 Aperture Concept, Effective Aperture, and Directivity	41
2.2.6 Gain	43
2.2.7 Polarization	45
2.2.8 Efficiency	48
2.2.9 Impedance Matching	49
2.2.10 Friis Transmission and Receiving Formulas	51
References	53

<b>3</b>	<b>Basic Antenna Elements</b>	<b>55</b>
3.1	Introduction	55
3.2	Antenna Elements	55
3.2.1	<i>Quarter-Wavelength Monopole or Half-Wavelength Dipole Antenna</i>	55
3.2.2	<i>Loop Antenna</i>	62
3.2.3	<i>Patch Antenna</i>	66
	References	72
<b>4</b>	<b>Advanced Antenna Elements</b>	<b>75</b>
4.1	Introduction	75
4.2	Miniature Antennas for Portable Electronics	76
4.2.1	<i>Inverted-L and Inverted-F Antennas</i>	76
4.2.2	<i>Meandered Line</i>	81
4.2.3	<i>Multiband Antenna</i>	83
4.2.4	<i>Dielectric Loaded</i>	85
	References	89
<b>5</b>	<b>Electromagnetic Simulation and Software</b>	<b>93</b>
5.1	Introduction	93
5.2	Electromagnetic Simulation Methods	94
5.2.1	<i>MoM</i>	94
5.2.2	<i>Differential Equation Techniques</i>	95
5.3	Antenna Simulation Tools	97
5.3.1	<i>Numerical Electromagnetics Code</i>	98
5.3.2	<i>Momentum</i>	100
5.3.3	<i>FEKO</i>	100
5.3.4	<i>High-Frequency Structure Simulator</i>	101
5.3.5	<i>CST</i>	101
5.3.6	<i>EM.Cube</i>	102
5.3.7	<i>Sonnet</i>	102
5.3.8	<i>WIPL-D Pro</i>	102
5.3.9	<i>AWR Microwave Office</i>	103
5.3.10	<i>Antenna Magus</i>	104
5.3.11	<i>AntSyn</i>	106
	References	107
<b>6</b>	<b>Measurements</b>	<b>111</b>
6.1	Introduction	111
6.2	Measuring Equipment	112
6.3	Antenna Ranges	113
6.4	Far-Field Pattern Measurement	116
6.5	Gain Measurement	116
6.6	Directivity	119
6.7	Efficiency Measurements	120

6.8	Phase Measurement	120
6.9	Polarization Measurement	121
6.10	TRP and TIS Measurements	122
6.11	SAR Measurement	124
	References	125
<b>7</b>	<b>Impedance Matching</b>	<b>127</b>
7.1	Introduction	127
7.2	Impedance Matching	128
7.3	Smith Chart	129
7.4	Matching Topology and Elements	132
7.4.1	<i>Series Element</i>	132
7.4.2	<i>Shunt Element</i>	135
7.4.3	<i>Matching Topologies</i>	138
7.5	Matching Elements	139
7.5.1	<i>Inductor</i>	139
7.5.2	<i>Capacitor</i>	141
7.5.3	<i>Transmission Line</i>	145
7.6	Practical Considerations	145
7.6.1	<i>Impedance Measurement with VNA</i>	145
7.6.2	<i>Balanced or Unbalanced</i>	146
7.6.3	<i>Ground Effect</i>	148
	References	154
<b>8</b>	<b>Practical Implementation Strategies and Design Examples</b>	<b>157</b>
8.1	Introduction	157
8.2	Understanding the Requirements	158
8.2.1	<i>Internal or External</i>	158
8.2.2	<i>Polarization and Directivity</i>	159
8.2.3	<i>Operating Frequency, Size, and Geometry</i>	165
8.3	Implementation Considerations and Strategies	168
8.3.1	<i>RF PCB Layout Techniques and Practices</i>	169
8.3.2	<i>Antenna Location and Placement</i>	169
8.3.3	<i>Ground Plane</i>	171
8.3.4	<i>Enclosure</i>	173
8.3.5	<i>Mechanical Design, PCB Design, and Teamwork</i>	175
	References	183
<b>9</b>	<b>Future Trends</b>	<b>187</b>
9.1	Introduction	187
9.2	IoT Technology	188
9.2.1	<i>IoT Devtices</i>	188
9.2.2	<i>Enabling Technologies</i>	188
9.3	Antenna Designs for IoT Applications	190

9.3.1	<i>Smarthome Applications</i>	190
9.3.2	<i>Wearable Devices</i>	191
9.3.3	<i>Commercial Application</i>	203
9.4	Antenna Technologies for the Future	208
9.4.1	<i>Fractal Antennas</i>	208
9.4.2	<i>Polymer</i>	209
9.4.3	<i>Metamaterials</i>	210
9.4.4	<i>3-D Printed Antennas</i>	211
	References	212
	<b>About the Author</b>	<b>217</b>
	<b>Index</b>	<b>219</b>

## Preface

I have been working on radio frequency (RF) solutions for more than 27 years, covering circuit, printed circuit board (PCB), and antenna designs; my entire career has been almost all about wireless technology. I have seen or developed many successful and some less-successful wireless products during my engineering and management careers. Most of the less successful products typically have difficulties with obtaining certification on electromagnetic interference/electromagnetic compatibility (EMI/EMC) compliance or have short communication range compared to the competitors' products. Those issues are all related to RF design, particularly on the antenna design. Besides providing consultancy or design services to help companies correct the problems, I decided to share my design experience on antennas to the industry by teaching and presenting in RF-related courses and seminars organized by the Institute of Electrical and Electronics Engineers (IEEE), EDICON, *Microwave Journal*, and a few others about 10 years ago. Teaching has been fun and enjoyable to me. However, the number of students, engineers and managers who attended my courses and seminars were still limited. A few years ago, Patrick Hindle from *Microwave Journal* referred me to Artech House with the possibility of writing a book on antenna design. This posed a great opportunity for me to share my antenna design experience with a larger group of people. That was when the writing of the book started.

This book is written as a comprehensive design guide or handbook covering antenna fundamentals, basic antenna designs, simulation, and measurement to practical implementation strategies so readers can use them to design antennas with optimum performance in actual products and systems. With an emphasis on practicality, this book does not address too deeply the underlying theories of antennas. Interested readers can find references at

the end of each chapter for greater detail. This book can also help antenna designers, circuit designers, and design managers bridge the gap between electromagnetic theory and its application in the design of practical antennas in actual products.

The book is organized into 9 chapters covering different aspects of antenna designs. Chapter 1 presents introductory remarks on commonly used antennas on the market so that readers can get an idea of what will be discussed in more detail later in the book. Their basic properties and features will be highlighted as well. The radiation mechanism of antennas will be described and illustrated to show how and why antenna radiates. It provides a fundamental concept to explain how electromagnetic fields are generated and used as a medium for wireless communications.

Chapter 2 provides insights on the specifications and performances of different antennas. The antenna parameters of radiation pattern, beam solid angle, directivity, effective aperture, gain, polarization, and efficiency will be discussed. A basic understanding of them is important to antenna or system designers to identify their impact on overall system performance.

Followed by the brief introduction in Chapter 1 to the commonly used antennas on the market, Chapter 3 discusses those antennas in more detail and with practical examples. Their key antenna parameters are derived mathematically for performance comparison and their advantages and disadvantages will be highlighted in different applications and products.

If designed properly, the commonly used antennas discussed in Chapter 3 such as the dipole or monopole offer good performance. However, the required size of the antenna is large for optimum performance. To address the size issue, Chapter 4 provides some advanced design techniques to miniaturize and optimize the antenna despite the limited size of the product. That is particularly important for handheld wireless devices that call for small size, light weight, and low power consumption.

Chapter 5 focuses on the discussion of electromagnetic simulation and software for antenna design. They are useful to predict and optimize the antenna performance for complex structures as it would be very difficult or impossible to find the analytical solutions for analysis. With the electromagnetic simulators, the design effort and development time can be minimized and shortened, respectively. Some of the commonly used electromagnetic simulators, both commercial and free, are discussed.

Antenna performance can be affected by the environment (i.e., having finite ground plane, proximity to adjacent components or metal objects). Modeling all the environmental conditions for simulation is quite involved, and the simulation time is lengthy. Instead of simulation, measurement is

more direct and effective to validate the designs. Antenna measurement is the main discussion in Chapter 6. In addition to the fundamental parameters of antennas, measurements on other RF parameters mandated by regulatory authorities are also addressed.

Besides the fundamental antenna parameters presented in Chapter 6, another parameter, impedance, is also very important as it plays a crucial role in determining the overall efficiency of an antenna. Chapter 7 presents the basic theory of S-parameters, impedance measurement equipment, and techniques. Impedance matching topologies and matching elements with practical considerations are also discussed in detail.

Chapter 8 discusses the design issues and considerations of antennas from product and system perspectives. The importance of understanding the specifications and requirements of the antenna is identified, and the system analyses and considerations are then provided. Since PCB layout design, component placement, and mechanical design are also the key design elements determining the ultimate performance of the antenna, their relevance and special design rules are also presented. To offer more design details and insights, several design examples on commercial products are used for illustration.

Chapter 9 identifies the future trends on antennas for Internet of Things (IoT) devices due to their recent popularity and huge market potential as predicted. In addition, technology-specific design trends based on new materials and design approaches are also presented. More different materials, structures, fabrication processes, and combinations of them are expected to come out in the future, which may improve antenna performance dramatically.



## **Acknowledgments**

I sincerely thank Patrick Hindle of *Microwave Journal* for introducing me to Artech House about writing this book. He arranged several webinars for me on antenna and radio frequency printed circuit board (RF PCB) designs, which also inspired me to write this book.

Sherry Hess, David Vye, and Derek Linden from National Instruments deserve special thanks for providing the antenna design and simulation tools to facilitate the development of the book.

I particularly acknowledge Artech House's editorial and production staff. David Michelson, Stephen Solomon, and many other editorial staff members assisted me with continuous guidance and patience to produce and arrange my manuscript. I also express my sincere gratitude to the reviewers for their kind review of the manuscript, which greatly improved and refined it.

Last, but not least, I express my deepest appreciation to my family members, Ludy, Harmon, and Fiona, for their understanding and patience during the writing of this book and their help with reviewing the book.



## CHAPTER

# 1

### Contents

1.1 Introduction

1.2 Antenna Fundamentals

1.3 Radiation Mechanism

## Fundamental Concepts

### 1.1 Introduction

The purpose of this chapter is to provide an overview on commonly used antennas on the market, particularly for wireless products. Those antennas are dipoles, monopoles, loops, and helical and printed circuit boards (PCBs). Most advanced antennas such as multiple-input and multiple-output (MIMO) and multiband are also introduced. Readers can get a glance of what will be discussed in more detail later in this book. Their basic properties and features will be highlighted here. The radiation mechanism of antennas will be described and illustrated so that readers can understand how and why antenna radiates. It also serves as a fundamental concept to explain how electromagnetic fields are generated and used as a medium for wireless communications. The information is particularly useful to students, engineers, or design managers who have no prior knowledge on antennas.

## 1.2 Antenna Fundamentals

### 1.2.1 Basic Types of Antenna

Dipole is one of the fundamental antenna elements used in practice and for mathematical analysis. It basically consists of two linear conductors with the signal fed at the center as shown in Figure 1.1. Depending on the length of the dipole, it could be short or long.

A linear conductor is often called a short dipole when the length  $L$  is very short compared to the wavelength ( $L \ll \lambda$ ). The radiation power is typically proportional to the length  $L$  and thus a longer antenna would have a better radiation performance. In spite of the advantage, a long antenna would require more space whereas space would be scarce in most wireless handheld devices. Since a dipole is differential in nature, it would require a differential signal source or a balun to transform a single-ended source to a differential one.

As shown in Figure 1.2, a monopole is one-half of a dipole and is mounted vertically above a reflecting plane or is simply called a ground plane [1]. According to the image theory, the electromagnetic fields above the ground plane can be found by using the equivalent source in free space, which is simply a dipole antenna of twice the length as shown in Figure 1.1. The radiation pattern of a monopole above the ground plane is identical to that of a dipole but the impedance of a monopole is just one-half. A monopole is particularly attractive when small size is needed since a monopole has just half the size of a dipole. Many wireless handheld devices (i.e., walkie-talkies, tablet PCs) are using monopole antennas as the main PCB acts as a ground plane for the monopole as shown in Figure 1.3.

Relatively broadband, helical antennas (helix) [2, 3] is another simple but practical electromagnetic radiator. The most popular helix is a traveling wave antenna in the form of a corkscrew that produces radiation along the axis of the helix antenna. The helix in most cases is used with a ground

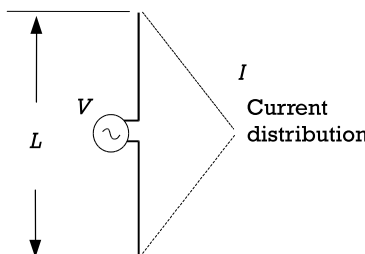


**Figure 1.1** Dipole antenna.

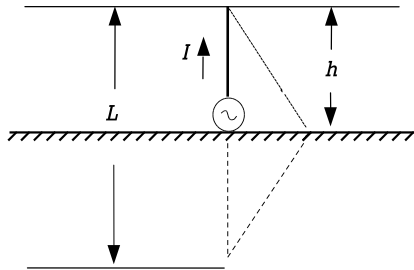


**Figure 1.2** Monopole antenna.



**Figure 1.3** Monopole antenna on a handheld device.

plane as shown in Figure 1.4. The advantages of using helix are its wide bandwidth, easy construction, and real input impedance and circular polarization. The radiation characteristics are dependent on its relative size and geometry to the wavelength. There are two modes, normal and axial, under which the helix can operate. In the normal mode of operation, the dimensions of the helix are small compared to the wavelength with the maximum radiation normal to the helix's axis. The radiation pattern is omnidirectional and similar to an electrically short dipole or monopole. The helix operating in the normal mode is commonly used in handheld devices, portable radios, and Family Radio Service (FRS). When the dimensions of the helix are comparable to a wavelength, the helix operates in the axial mode



**Figure 1.4** Helix antenna with ground plane.

and functions as a directional antenna. Under this mode of operation, the maximum radiation intensity is along the axis of the helix with only one major lobe as shown in Figure 1.5. The waves being radiated are circularly polarized. The helix operating in the axial mode is commonly used for the satellite or point-to-point communication.

A loop antenna is an inexpensive and versatile antenna that can be in different forms such as circle, square, or triangle [2]. It consists of a loop of wire or other metallic conductor with its end connected to a balanced source as shown in Figure 1.6. There are two distinct types of loop antenna: electrically small and electrically large. For a small loop antenna, its size is much smaller than a wavelength. The large loop antenna is also called the resonant loop antenna as its circumference is close to the wavelength of operation. Small loop antennas have very poor radiation efficiency. They are typically used in small devices such as pagers, portable radios, and keyless entry devices. The typical frequency range of operation is from 3 MHz to

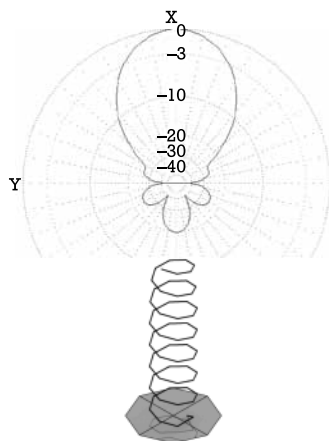


**Figure 1.5** Helix antenna with a major lobe along its axis.

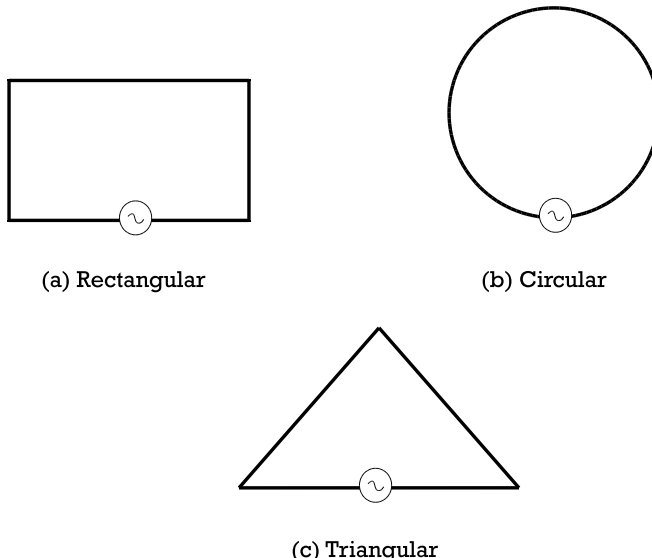


**Figure 1.6** Various loop antennas.

900 MHz. Figure 1.7 shows a rectangular loop antenna used in a 400-MHz pager. With careful design techniques, the loop antenna can fit and perform reasonably well in small handheld devices.

Similar to an infinitesimal dipole, the radiation pattern of a small loop antenna has a null perpendicular to and a maximum along the plane of the loop. When the loop's length approaches one wavelength, the maximum shifts from the plane of the loop to the perpendicular axis. The large loops are commonly used in arrays to offer directional property. Typical examples

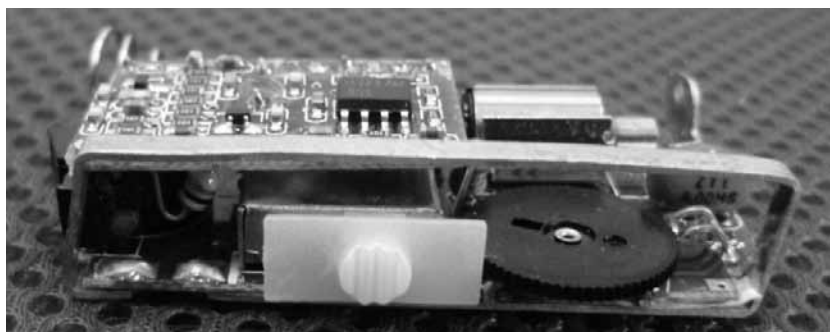


**Figure 1.7** Rectangular loop antenna in a 400-MHz pager.

are helical or quad array antennas. With proper phase difference between loops and the loop circumference, the maximum radiation is directed toward the axis of the loop, forming an end-fire antenna.

The PCB antenna is gaining much popularity in recent years due to the proliferation of wireless connectivity with smartphones. Since the operating frequency of either Bluetooth or WiFi devices is at either 2.4 GHz or 5.6 GHz, this makes the PCB antenna very attractive due to its simplicity in design, small size, and low cost. The PCB antenna comes in many different forms (i.e., inverted-L, inverted-F, meandered line). Literally, any trace printed on a PCB can be a PCB antenna. Figure 1.8 shows an inverted-F antenna printed on a Bluetooth module. PCB antennas are used mainly as an internal antenna for handheld devices since they occupy very little space with reasonable performance. Furthermore, most PCB antenna types are monopole in nature and a monopole has to work with a ground plane. PCB antennas are thus particularly suitable since they could make use of the ground area of the main PCB. In any good RF layout, the main board is usually flooded with ground patches, which form a good ground plane for the PCB antennas.

### 1.2.2 Multiband and MIMO

The demand on multiband antennas has been increasing due to the surge on the sales of smartphones in recent years. To be compatible to the existing

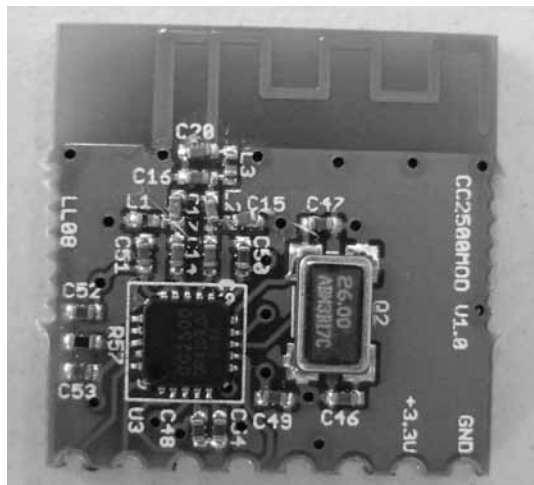


**Figure 1.8** Inverted-F antenna printed on a Bluetooth module.

cellular networks, most cellphones have to cover multiband frequencies to cover all the available frequency bands of different cellular generations of network (i.e., GSM/GPRS, 3G, or 4G) [4]. In addition, there are regional variations on the operating frequency for different countries. For example, many GSM phones can support four bands (850/900/1,800/1,900 MHz) and are usually referred to as quad-band phones or world phones to account for the regional frequency band variations. With such a phone, one can travel internationally using the same handset. For a 3G phone, it has to cover both GSM and 3G bands and results in a hexa-band cellular antenna of 850/900/1,700/1,800/1,900/2,100 MHz.

It would be ideal if the smartphones have an individual antenna for each frequency band. Unfortunately, space is a scarce commodity in cell-phones as more components are put inside the phone to add more features. This leads to the requirement of multiband single antenna to cover all the required frequencies. There are several implementation approaches on multiband design, noticeably using PCB, ceramic block, or flexible tape. They all use a meandered line approach, as shown in Figure 1.9. The design details will be discussed in Chapter 4.

In wireless communications, MIMO is a technology using multiple transmit and receive antennas to exploit multipath propagation to increase the capacity of a radio link [5]. MIMO is now being used in many wireless communication standards including IEEE 802.11ac/n, 3G, WiMax, and Long Term Evolution of 4G. MIMO had been referred to the use of multiple transmit and receive antennas for beamforming and diversity to enhance the performance of a single data signal. Nowadays, MIMO refers to a technique of sending and receiving multiple data signals over the same radio channel simultaneously with multipath propagation. MIMO can be



**Figure 1.9** The 800/900/1,800/1,900-MHz quad-band antenna.

categorized into three main techniques as diversity coding, precoding, and spatial multiplexing. Precoding is a multistream beamforming technique by which spatial processing occurs at the transmitter only. With appropriate gain and phase weightings, signal power is maximized at the receiver input when the same signal is emitted from each of the transmit antennas. Beamforming can increase the received signal level by adding signals that emit from different antennas constructively while reducing the multipath fading effect. With the spatial multiplexing technique [7, 8], a high-rate signal is split into multiple lower-rate streams, which are transmitted from different transmit antennas in the same frequency channel. Reliable parallel-channel stream  $s$  can be established if signals that arrive at the receiver antennas have sufficient different spatial signatures and the receiver has accurate channel state information (CSI). Spatial multiplexing is thus a very powerful method to increase channel capacity at higher signal-to-noise ratios but requires a MIMO antenna configuration. When there is no channel knowledge at the transmitter, diversity coding methods can be used by which signal is emitted from each of the transmit antennas with full or near orthogonal coding. Spatial multiplexing can be combined with diversity coding if the channel information is available at the transmitter.

In cellular MIMO systems, multiple antenna elements are used at the base station as well as the user mobile unit. In the base station where space is abundant, having multiple antennas is not a problem. The antennas are usually placed with a separation of a quarter or half wavelength to achieve low coupling and low correlation among themselves which are required to achieve high data rates offered by MIMO technology. As an illustration, Figure 1.10 shows two WiFi antennas forming spatial diversity with physical separation. However, such spacing is not possible in the mobile device (i.e., a smartphone having a small form factor). The limited space in a smartphone will make the field correlations and mutual coupling increase which



**Figure 1.10** MIMO antenna used in a wireless router.

results in lower diversity performance of the MIMO antenna system. Because of the space requirement, many small MIMO antennas have been being developed with creative ideas for smartphones, noticeably the dielectric loaded antenna or the PCB antenna [9].

## 1.3 Radiation Mechanism

### 1.3.1 Source of Radiation

A good understanding of the antenna radiation mechanism is helpful to develop the right antennas for the right applications. The first step is to understand what an antenna is. An antenna can be defined as a structure comprising a region of transition between a guided wave and a free-space wave as shown in Figure 1.11. The transmission line is used to guide the RF or microwave energy from one place to another. Ideally, the energy would be transmitted with minimum losses. The losses include the attenuation, heat dissipation, radiation and mismatch loss on the transmission line. The transmission line can be a 2-wire transmission line, coaxial cable or waveguide, which will try to confine within itself the energy being transmitted.

The generator shown in Figure 1.11 sends a uniform traveling wave along the transmission line. When the wave reaches the open ends, it radiates as a free-space wave. The wave guided in the transmission line is a

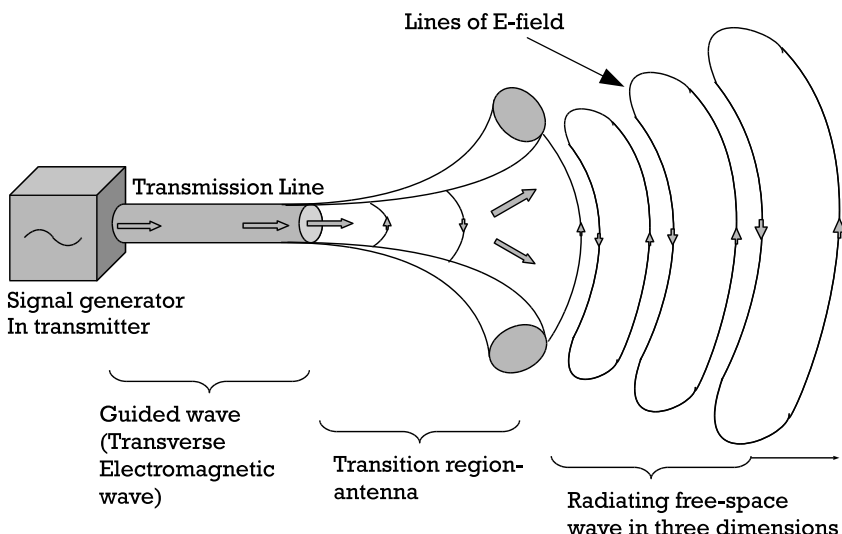


**Figure 1.11** Antenna is the transition region between a transmission line and free-space.

plane wave and becomes a spherically expanding wave at the open ends. Although the currents flowing from the generator through the transmission line stop at both ends, the fields generated by them keep on going. The region of the transition from the guided wave to the free-space wave is defined as an antenna.

The antenna can thus be considered as a transformation device converting currents from a circuit into electromagnetic photons radiating into free space. Although the antenna is illustrated as a transmitting device in Figure 1.11, it can also act as a receiving device converting photons back into currents towards the load.

To understand in more detail about how radiation is generated by the antenna, it has been suggested to examine how electrons move inside the conductor [10].

Assuming that there is a pulse of charge moving in the  $x$ -direction in a straight conductor, a momentary electric current  $I$  is generated by the moving charge as given by

$$I = q_L \frac{dx}{dt} \quad (1.1)$$

where  $q_L$  is charge per unit length, C/m, and C is in Coulomb.

The total current can be found by multiplying the length  $l$  of the pulse as

$$Il = q_L l \frac{dx}{dt} = qv \quad (\text{A m}) \quad (1.2)$$

where  $q$  is the total charge of pulse (C) and  $v$  is velocity (m/s).

The time derivative of the above equation gives

$$\frac{dI}{dt} l = q \frac{d^2x}{dt^2} = q\dot{v} \quad (\text{A m/s}) \quad (1.3)$$

where  $\dot{v}$  is the acceleration of charge (m/s<sup>2</sup>) or

$$Il = q\dot{v} \quad (1.4)$$

where  $q$  = electric charge (C),  $l$  = length of current element (m),  $I$  = time-varying current (A/s), and  $\dot{v}$  = acceleration (m/s<sup>2</sup>).

Also, the power  $P$  radiated by an accelerated charge can be found as:

$$P = \frac{\mu^2 q^2 \dot{v}^2}{6\pi Z} \quad (\text{W}) \quad (1.5)$$

where  $\mu$  = permeability of medium (H/m).

It is thus evident that, to have radiation from an antenna, there would be a time-varying current traveling along the conductor with acceleration.

As shown in Figure 1.12(a, b), either a stationary charge or a moving charge with constant speed on the conductor does not radiate since there

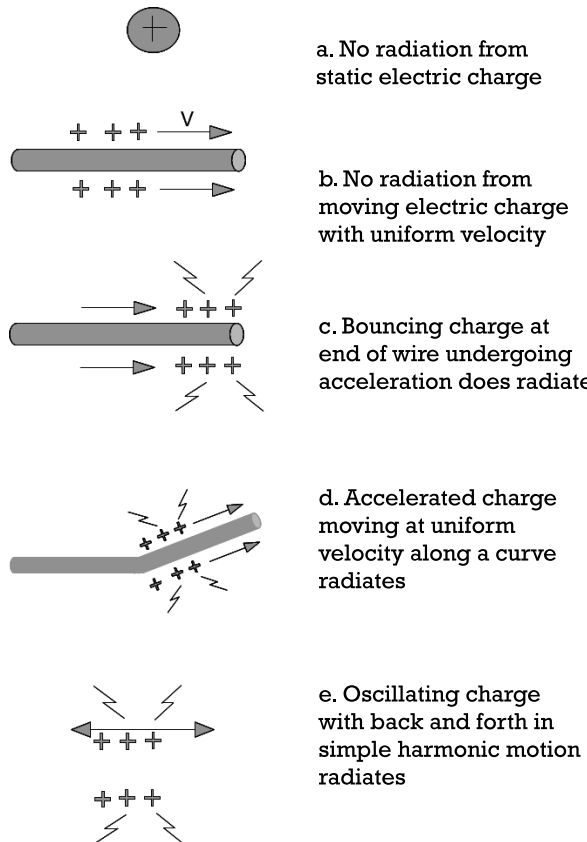


**Figure 1.12** Radiation due to different motions of electric charge.

is no acceleration occurred. When charges reach the end of the conductor, they bounce back (Figure 1.12(c)). The change of direction on the charges creates acceleration and results in radiation. A charge moves at a constant velocity along a curved conductor and it will accelerate at the curved region and radiates.

### 1.3.2 Characteristics of Radiation

The origin of radiation from an antenna has just been discussed. It will be explained mathematically that the radiation is created by the electromagnetic field generated by the signal source. The radiated power on both hypothetical point source and oscillating electric dipole will be derived based on the electromagnetic field that they induced. The theoretical and mathematical work to be introduced will be very helpful on understanding the characteristics of any other antennas since both signal sources are the fundamental building block.

Assuming that there is a current with current density  $J$  flowing in a conductor as shown in Figure 1.13, a scalar potential is induced and can be expressed as:

$$V(\mathbf{r}) = \frac{1}{4\pi\epsilon} \int \frac{\rho(\mathbf{r}')}{R} dV' \quad (1.6)$$

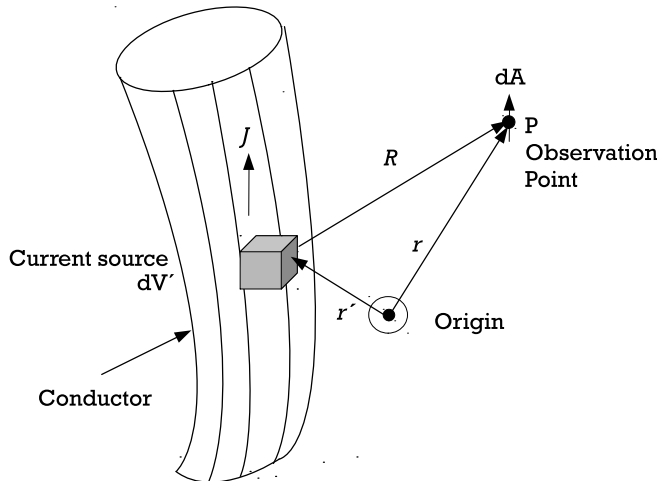


**Figure 1.13** Potential functions due to a current source.

where  $\epsilon$  is the permittivity of the medium and  $\rho$  is electric charge in Coulomb.

The electric field associated with this potential is

$$\mathbf{E} = -\nabla V \quad (1.7)$$

The current source also generates a vector potential of

$$\mathbf{A}(r) = \frac{\mu}{4\pi} \int \frac{J(r')}{R} dV' \quad (1.8)$$

The magnetic field due to this magnetic potential is

$$\mu H = \nabla \times \mathbf{A} \quad (1.9)$$

As explained in the previous section, stationary charges will not radiate and thus (1.6) and (1.7) alone are not useful for antenna analysis. Now, assuming that the signal source changes with time, (1.6) and (1.7) can be generalized to account for the time-varying property as

$$V(r, t) = \frac{1}{4\pi\epsilon} \int \frac{\rho(r', t)}{R} dV' \quad (1.10)$$

and

$$\mathbf{A}(r, t) = \frac{\mu}{4\pi} \int \frac{J(r', t)}{R} dV' \quad (1.11)$$

with  $R = |\mathbf{r} - \mathbf{r}'|$ .

Since the observation point and the signal source are located in different positions, there is a finite time delay between the variation of the signal source and the corresponding potential changes at the observation point. To account for the time delay, (1.10) and (1.11) are again rewritten as

$$V(r, t) = \frac{1}{4\pi\epsilon} \int \frac{\rho(r', t - R/v)}{R} dV' \quad (1.12)$$

$$A(r,t) = \frac{\mu}{4\pi} \int \frac{J(r',t-R/v)}{R} dV' \quad (1.13)$$

These new potentials are often called retarded potentials for the reason that they have been delayed or retarded by a time delay of  $R/v$ . The time delay  $R/v$  represents the interval required from the disturbance to travel a distance of  $r$  with the speed of light  $v$  ( $3 \times 10^8$  m/s). It can also be explained as that the disturbance of the potential experienced at the observation point at time  $t$  is due to the time variation of the signal source occurred at an earlier time  $t - R/v$ .

Given the two retarded potentials, the electric and magnetic fields can be derived from these two Maxwell's equations

$$\mu H = \nabla \times A \quad (1.14)$$

$$E = -\nabla V \quad (1.15)$$

It is generally not necessary to evaluate (1.12) as one can apply another Maxwell's equation to find  $E$  from  $H$  by taking its curl and integrating with respect to time as

$$\nabla \times H = \epsilon \dot{E} \quad E = \frac{1}{\epsilon} \int \nabla \times H dt \quad (1.16)$$

Using an alternating current element is an excellent example of calculating the electromagnetic field induced in free space using the retarded vector potentials. As shown in Figure 1.14, a filamentary current  $I$  flowing along an elemental length  $dl$  on a conductor will produce an approximated current element  $Idl$ . This approximation can be justified as the conductor length  $dl$  is short such that the current is constant along the length. Any physical antennas can be considered to have a large number of such building-block current elements joining from end to end, although the isolated current element appears to be unrealistic and impractical. Having a specified current distribution, the electromagnetic field of any actual antenna can be calculated if the electromagnetic field of the building blocks is known.

The goal of the following analysis is to find the radiated power for a sinusoidal current element at an arbitrary point  $P$ . For a sinusoidal signal, the current element becomes  $Idl \cos \omega t$  and locates at the origin of a spherical

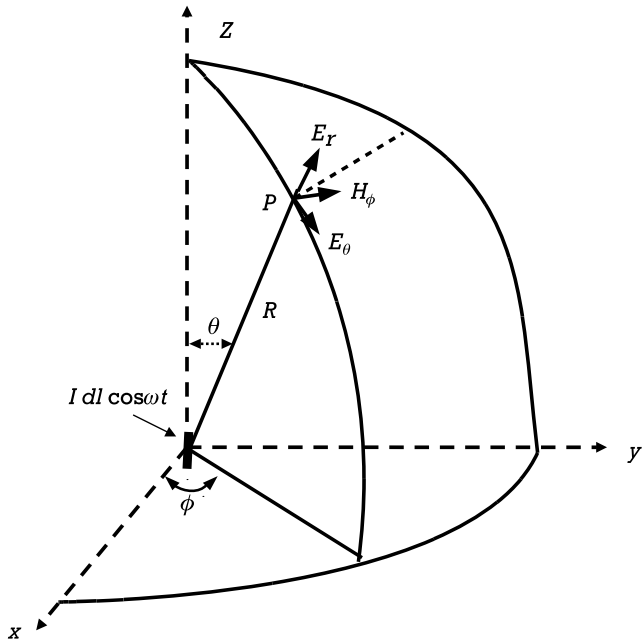


**Figure 1.14** An alternating current element at the origin of a spherical coordinate system.

coordinate system. The vector potential  $\mathbf{A}$  can be found by integrating the retarded vector potential (1.13) over the volume of the current element. The volume integration is the integration of the cross-sectional area of the conductor and along the conductor's length. The integration of the current density  $J$  over the cross-sectional area becomes  $I$  as the current density is assumed constant along the length. The subsequent integration over the length gives  $Idl$ .

The resultant vector potential of this sinusoidal current element is thus expressed as

$$A_z = \frac{\mu}{4\pi} \frac{Idl \cos \omega \left( t - \frac{r}{v} \right)}{r} \quad (1.17)$$

Only the  $z$ -axis component exists as the vector potential has the same direction as the current element.

The curl of a vector can be expressed in three spherical components as [10]

$$(\nabla \times A)_\theta = \left[ \frac{1}{r \sin \theta} \frac{\partial (A_r)}{\partial \phi} - \frac{1}{r} \frac{\partial (r A_\phi)}{\partial r} \right] \quad (1.18)$$

$$(\nabla \times A)_r = \frac{1}{r \sin \theta} \left[ \frac{\partial}{\partial \theta} (\sin \theta A_\varphi) - \frac{\partial (A_\theta)}{\partial \varphi} \right] \quad (1.19)$$

$$(\nabla \times A)_\varphi = \frac{1}{r} \left[ \frac{\partial}{\partial r} (r A_\theta) - \frac{\partial A_r}{\partial \theta} \right] \quad (1.20)$$

Due to the symmetry of the current element along the  $\Phi$ -direction,

$$\partial/\partial \theta = 0 \quad (1.21)$$

and with the current element in Figure 1.14, it can be shown that

$$\begin{aligned} A_\theta &= -A_z \sin \theta \\ A_r &= A_z \cos \theta \\ A_\varphi &= 0 \end{aligned} \quad (1.22)$$

The curl of the magnetic potential  $A$  finally gives three terms in spherical coordinates as

$$\mu H_\theta = (\nabla \times A)_\theta = 0 \quad (1.23)$$

$$\mu H_r = (\nabla \times A)_r = 0 \quad (1.24)$$

$$H_\varphi = \frac{1}{\mu r} \left[ \frac{\partial}{\partial r} (r A_\theta) - \frac{\partial A_z}{\partial \theta} \right] \quad (1.25)$$

Putting (1.17) and (1.22) into (1.25) gives

$$H_\phi = \frac{Idl \sin \theta}{4\pi} \left[ \frac{\cos \omega \left( t - \frac{r}{v} \right)}{r^2} - \frac{\omega \sin \omega \left( t - \frac{r}{v} \right)}{rv} \right] \quad (1.26)$$

The components of the electric field strength  $\mathbf{E}$  can be found by taking the curl and time integral of (1.16)

$$\begin{aligned} E_r &= \frac{2Idl \cos \theta}{4\pi \epsilon} \left( \frac{\sin \omega t'}{\omega r^3} + \frac{\cos \omega t'}{r^2 v} \right) \\ E_\theta &= \frac{Idl \sin \theta}{4\pi \epsilon} \left( \frac{\sin \omega t'}{\omega r^3} + \frac{\cos \omega t'}{r^2 v} - \frac{\omega \sin \omega t'}{rv^2} \right) \\ E_\phi &= 0 \end{aligned} \quad (1.27)$$

The instantaneous power flow density is governed by the Poynting vector as

$$\vec{\mathbf{P}} = \vec{\mathbf{E}} \times \vec{\mathbf{H}} \quad (1.28)$$

which has both  $\theta$  and  $r$  components of

$$\begin{aligned} P_\theta &= -E^r H_\theta \\ &= \frac{I^2 dl^2 \sin 2\theta}{16\pi^2 \epsilon} \left( \frac{\omega \sin \omega t'}{2r^3 v^2} - \frac{\cos 2\omega t'}{r^4 v} - \frac{\sin 2\omega t'}{2\omega r^5} \right) \end{aligned} \quad (1.29)$$

and

$$\begin{aligned} P_r &= -E_\theta H_\phi \\ &= \frac{I^2 dl^2 \sin^2 \theta}{16\pi^2 \epsilon} \left( \frac{\omega^2 (1 - \cos 2\omega t')}{2r^2 v^3} - \frac{\omega \sin 2\omega t'}{r^3 v^2} - \frac{\sin 2\omega t'}{2\omega r^5} \right) \end{aligned} \quad (1.30)$$

The average of  $P_\theta$  is zero as the average value of all the terms in (1.29) is zero. On the other hand, the average value of the radial component of the Poynting vector is due to the first term only in (1.30) as

$$P_{r(ave)} = \frac{\eta}{2} \left( \frac{\omega I dl \sin \theta}{4\pi r v} \right)^2 \quad (1.31)$$

By integrating  $P_{r(ave)}$  over a spherical surface centered at the current element gives the total radiated power as

$$\begin{aligned} P_{total} &= \oint_S P_{r(ave)} da \\ &= \int_0^\pi \frac{\eta}{2} \left( \frac{\omega I dl \sin \theta}{4\pi r v} \right)^2 2\pi r^2 \sin \theta d\theta \\ &= \frac{\eta \omega^2 I^2 dl^2}{12\pi v^2} \\ &= \frac{\eta \omega^2 I_{eff}^2 f^2 dl^2}{6\pi v^2} \end{aligned} \quad (1.32)$$

where  $2\pi r^2 \sin \theta d\theta = da$  is the incremental surface area and  $I_{rms}$  is the effective current of the maximum current  $I$ .

Or the total power can also be expressed as

$$P_{total} = R_{rad} I_{eff}^2 \quad (1.33)$$

where

$$R_{rad} = 80\pi^2 \left( \frac{dl}{\lambda} \right)^2 \quad (1.34)$$

which is called the radiation resistance of the current element  $I$ . Both (1.33) and (1.34) give some insights to antenna designers on how to design and optimize antennas. It can be realized that both the current and radiation resistance should be maximized to have the maximum radiated power by the current element. The radiation resistance is a function of the length of the current element in this simple example. It can be implied that the radiation is higher for a longer antenna and so is the radiated power. It will be shown later in the book that a quarter-wavelength dipole antenna has a higher resistance than a short dipole antenna. The analytical expression on the radiation resistance of other antennas with different sizes and shapes will become very complicated when the structures become more complex.

The amount of current flowing through the antenna is a function of the impedance of the signal source and the impedance of the antenna as a load. A matching network may be added between the signal source and the load for maximum power transfer. The impedance of the antenna is a function of its loss and radiation resistances. Both resistances are also a function of the size and geometry of the antenna. Finding their analytic expressions if there are any is quite involved for complex antenna structures. Simulation tools (to be discussed in Chapter 5) will be needed to find the characteristics and performance of antennas more easily.

## References

- [1] "Monopole Antenna – Antenna Theory," last modified October 25, 2016, <http://www.antenna-theory.com/antennas/monopole.php>.
- [2] Kraus, J. D., *Antennas*, New York: McGraw-Hill, 1988.
- [3] Balanis, C. A., *Antenna Theory: Analysis and Design*, New York: John Wiley & Sons, 1997.
- [4] Miao, G., et al., *Fundamentals of Mobile Data Networks*, New York: Cambridge University Press, 2016.
- [5] "MIMO," Wikipedia, last modified March 17, 2019, <https://en.wikipedia.org/wiki/MIMO>.
- [6] Lipfert, H., "MIMO OFDM Space Time Coding – Spatial Multiplexing, Increasing Performance and Spectral Efficiency in Wireless Systems, Part I Technical Basis," *Technical Report*, Institut für Rundfunktechnik, August 2007. [7] Golbon-Haghghi, M. -H., "Beamforming in Wireless Networks," *InTech Open*, 2016, pp. 163–199.
- [8] Kshetrimayum, R. S., *Fundamentals of MIMO Wireless Communications*, New York: Cambridge University Press, 2017.
- [9] Sharawi, M. S., *Printed MIMO Antenna Engineering*, Norwood, MA: Artech House 2014.
- [10] Jordan, E. C., and K. G. Balmain, *Electromagnetic Waves & Radiating Systems*, 2nd Edition, Upper Saddle River, NJ: Prentice Hall, 1968.



## **CHAPTER**

# **2**

### **Contents**

- 2.1 Introduction
- 2.2 Specifications and Performances

## **Specifications and Performances**

### **2.1 Introduction**

Followed by the introduction of commonly used antennas on the market and the mathematical analysis on radiation mechanism, this chapter continues to provide more insights on the specifications and performances of different antennas. This is particularly important to the antenna or system designers to understand what they are and their significance on overall system performance. The basic parameters of radiation pattern, beam solid angle, directivity, effective aperture, gain, polarization, and efficiency will be discussed. The chapter will then be concluded by the introduction of Friis transmission and receiving formulas, which are also important to wireless system considerations.

### **2.2 Specifications and Performances**

#### **2.2.1 Radiation Pattern**

An antenna radiation pattern or radiation pattern is the variation of the radiation properties by an antenna as a function of space coordinates

of the observation point. Typically, it is defined in the far-field region and presented by a mathematical function or a graphical representation of the radiated power or field. A convenient set of coordinates is shown in Figure 2.1 in which the field pattern is represented as a function of its distance  $r$  from the origin of the antenna in the direction of  $\theta$  and  $\Phi$ . Unless the antenna is a point source in which its radiation pattern is isotropic, most antennas exhibit certain directional property. As illustrated in Figure 2.2, the field pattern has the main lobe peaked at  $\theta = 0$  ( $z$  direction). There are also some minor lobes in the side and back directions. The nulls between the lobes have minimum radiation.

As mentioned above, the radiation pattern can be defined by the radiated field or power. The radiated field can be specified by four components as:

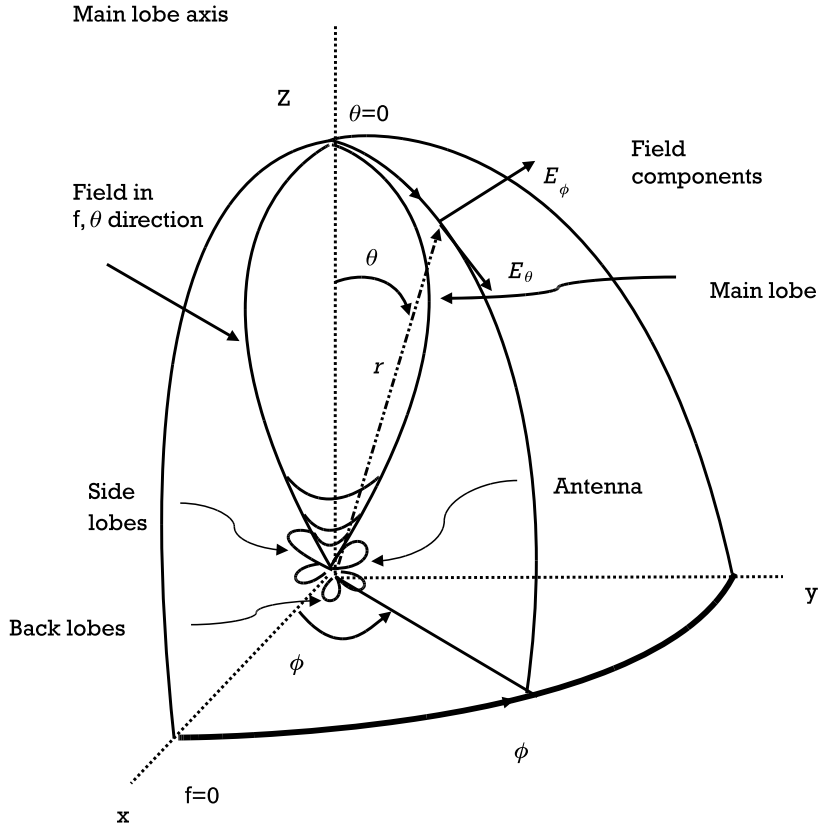


**Figure 2.1** Field pattern represented in a function of its distance  $r$ .

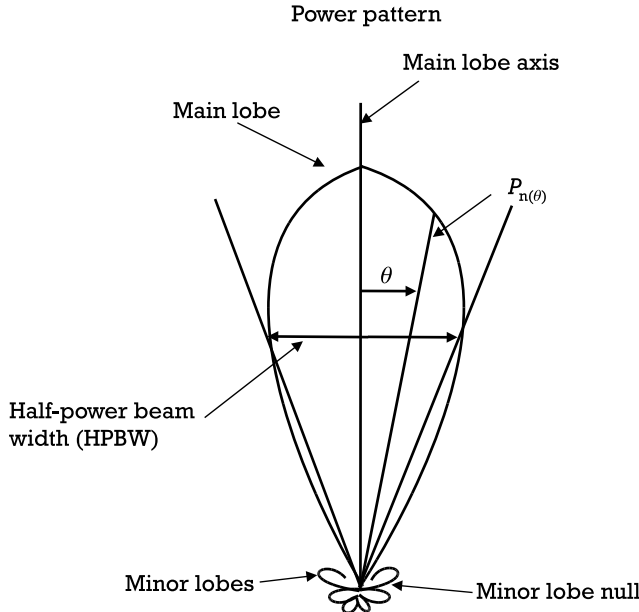


**Figure 2.2** Principal plane pattern in polar coordinates.

$$\begin{aligned}
 &E_\phi(\theta, \phi) \\
 &E_\theta(\theta, \phi) \\
 &\delta_\theta(\theta, \phi) \\
 &\delta_\phi(\theta, \phi)
 \end{aligned} \tag{2.1}$$

where  $E_\theta(\theta, \Phi)$  and  $E_\phi(\theta, \Phi)$  are the  $\theta$ - and  $\Phi$ -components of the electric field, respectively, as a function of  $\theta$  and  $\Phi$  angles and  $\delta_\theta(\theta, \Phi)$  and  $\delta_\phi(\theta, \Phi)$  are the phases of the corresponding field.

The field can be normalized by dividing it by its maximum value to provide a normalized field pattern as:

$$E_\theta(\theta, \phi)_n = \frac{E_\theta(\theta, \phi)}{E_\theta(\theta, \phi)_{\max}} \tag{2.2}$$

It is dimensionless and has a maximum value of unity. It gives a very convenient way to identify the antenna's directional property by evaluating its field strength relative to the peak.

In addition to field strength, the radiation pattern can also be expressed in terms of power density or Poynting vector  $S(\theta, \Phi)$  as introduced in (1.28). Although the Poynting vector is a vector as implied by its name, its magnitude is used here with the direction pointing radially outward in the far field.

It can also be normalized with respect to its maximum value by dividing its maximum value as:

$$P_n(\theta, \phi) = \frac{S(\theta, \phi)}{S(\theta, \phi)_{\max}} \quad (2.3)$$

where  $S(\theta, \Phi)$  is the magnitude of the Poynting vector of  $[E^2_\theta(\theta\Phi) + E^2_\phi(\theta\Phi)]/Z_o$ ,  $\text{Wm}^{-2}$ ,  $S(\theta, \Phi)_{\max}$  is the maximum magnitude the Poynting vector  $Z_o$  is the intrinsic impedance of space of  $376.7 \Omega$ .

It is also dimensionless and has a maximum value of unity.

In order to examine the direction property of the antenna more easily, the field pattern can better be presented along the principal plane. Such a pattern is called the principal plane pattern in which the plane cuts through the main lobe axis. Using the example in Figure 2.1, there are two principal planes being at right angle with each other as defined by the  $x$ - $z$  and  $y$ - $z$  planes. Typically, two principal planes may be sufficient to represent a single field component. If the pattern is symmetrical around the  $z$ -axis, one cut will be sufficient for. Figure 2.2 shows the principal plane pattern in polar coordinates of the antenna having the three-dimensional (3-D) radiation pattern as shown in Figure 2.1. It can also be presented in rectangular coordinates with decibel scale to show the details of the nulls and minor lobes in Figure 2.3.

Despite that the radiation patterns provide a complete presentation of the antenna radiation characteristics, other important antenna parameters can be expressed in single scalar quantities for antenna performance comparison. They will be discussed in more detail in the following sections.

### 2.2.2 Beam Solid Angle

The beam solid angle of an antenna is given by the integral of the normalized power pattern over a sphere as [1]:

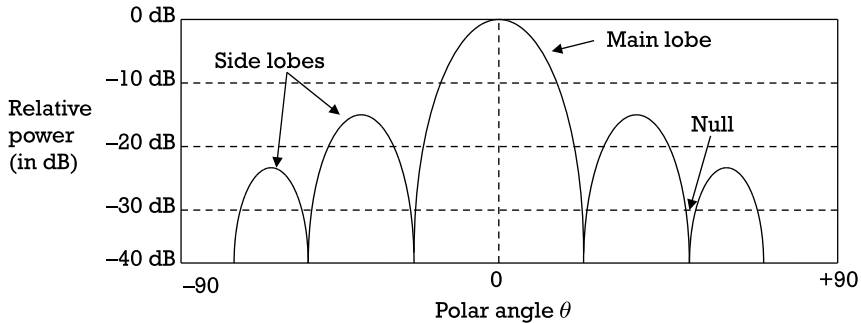


**Figure 2.3** Field pattern in rectangular coordinates with decibel scale.

$$\Omega_{Area} = \int_0^{2\pi} \int_0^{\pi} P_n(\theta, \phi) d\Omega \quad (2.4)$$

where

$$d\Omega = \sin \theta d\theta d\Phi$$

With minor lobes being neglected, it is often approximated by the angles subtended by the half-power points on the main lobe in the two principal planes as:

$$\Omega_A \sim \theta_{HP} \phi_{HP} \quad (2.5)$$

where  $\theta_{HP}$  and  $\phi_{HP}$  are the corresponding half-power beamwidths.

The approximation is illustrated in Figure 2.4 where the beam solid angle of an actual pattern is equivalent to the same solid angle subtended by the spherical cap of the cone-shaped pattern with half-power beamwidth. This parameter is often used as a figure of merit for easy performance comparison if the primary concern is to know how focused the signal is beaming to or from.

### 2.2.3 Radiation Power Intensity

As a far-field parameter, radiation intensity is defined as the power radiated from an antenna per unit solid angle in a given direction.

The total radiated power can be related as:

$$P_{rad} = \oint_{\Omega} (\theta, \phi) d\Omega \quad (2.6)$$

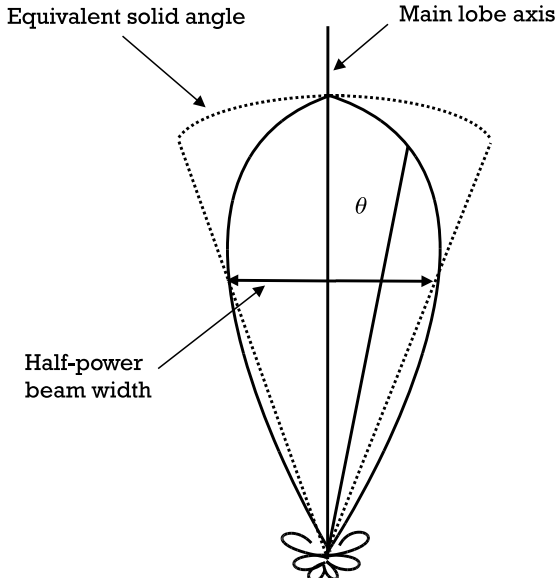


**Figure 2.4** Equivalent solid angle.

where  $U$  is the radiation intensity (watts per square degree or steradian).

For an isotropic source in which the radiation intensity is constant in all angles  $\theta$  and  $\Phi$ , the radiated power is:

$$P_{rad} = 4\pi U_{ave} \quad (2.7)$$

or

$$U_{ave} = \frac{P_{rad}}{4\pi} \quad (2.8)$$

#### 2.2.4 Directivity and Effective Aperture

Directivity is one of the mostly quoted parameters of antennas. It is a measure of how directionally an antenna radiates. It is defined as the ratio of the maximum radiation intensity to the average radiation intensity over the entire sphere as:

$$D = \frac{U(\theta, \phi)_{\max}}{U_{ave}} \quad (2.9)$$

It can also be expressed as the ratio of the maximum magnitude of the Poynting vector to the average one at a certain distance as:

$$D = \frac{S(\theta, \phi)_{\max}}{S_{ave}} \quad (2.10)$$

By integrating the magnitude of the Poynting vector over a sphere and dividing by  $4\pi$  gives the average value as:

$$S(\theta, \phi)_{ave} = \frac{1}{4\pi} \int_0^{2\pi} \int_{\pi}^{\pi} S(\theta, \phi) d\Omega \quad (\text{W m}^{-2}) \quad (2.11)$$

Putting (2.11) into (2.10), the directivity can be expressed as:

$$D = \frac{1}{\frac{1}{4\pi} \int_0^{2\pi} \int_{\pi}^{\pi} P_n(\theta, \phi) d\Omega} = \frac{4\pi}{\Omega_A} \quad (2.12)$$

The last expression relates directivity to beam solid angle. It can be shown that the greater directivity is, the smaller the beam solid angle is and the more energy the antenna will radiate to a certain direction.

### 2.2.5 Aperture Concept, Effective Aperture, and Directivity

To illustrate the aperture concept, it is assumed that there is a field of a uniform plane field propagating to a receiving electromagnetic horn antenna as shown in Figure 2.5. The antenna will absorb the plane wave's energy and convert into receiving power. Assuming the antenna extracts all the power from the wave over its entire surface  $A_p$ , the total power received by the horn can be defined as:

$$P = SA_p \quad (\text{W}) \quad (2.13)$$

where  $S$  is the Poynting vector or power density ( $\text{W/m}^2$ ).

As illustrated, the electromagnetic horn can be considered as an aperture, which can extract power from incoming waves. The power extracted

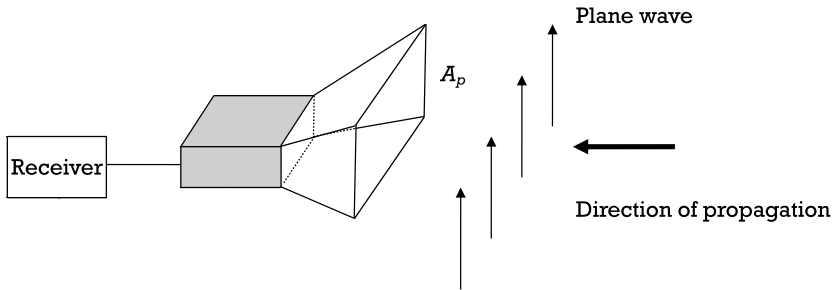


**Figure 2.5** Uniform plane wave incident upon a horn antenna with physical aperture  $A_p$ .

is proportional to the physical aperture or area of its mouth. In this example, the physical area of the horn is the same as the effective aperture. In reality, the effective aperture may not always be the same as the physical area. A large antenna could still be a poor receiving or transmitter antenna, but good design techniques can bring them close together.

To illustrate further, it is assumed that there is a radiating aperture as shown in Figure 2.6 with an electric field strength of  $E_a$ . The power radiated by this aperture is:

$$P = A_p \frac{|E_a|^2}{Z} \quad (2.14)$$

where  $A_p$  is the antenna physical aperture ( $\text{m}^2$ ) and  $Z$  is the intrinsic impedance of the medium ( $\Omega$ ).

At a distance of  $r$  and a direction broadside to the radiating aperture, the power experienced at the observation point  $b$  is:

$$P = \Omega_A r^2 \frac{|E_r|^2}{Z} \quad (2.15)$$

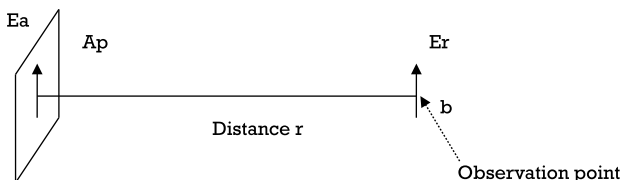


**Figure 2.6** Field experienced at observation point  $b$  due to a radiating aperture.

where  $\Omega_A$  is the beam solid angle of the antenna (sr).

The electric field strength  $E_a$  and  $E_r$  can be related as [1]:

$$|E_r| = A_p \frac{|E_a|}{r\lambda} \quad (2.16)$$

Putting (2.16) into (2.15) gives:

$$A_p = \frac{\Omega_A}{\lambda^2} \quad (2.17)$$

Assuming the field is uniform across the antenna physical aperture  $A_p$  and also equals to its maximum effective aperture  $A_{em}$ , (2.17) becomes:

$$A_{em} = \frac{\Omega_A}{\lambda^2} \quad (2.18)$$

This shows that the maximum effective aperture is its beam area divided by the wavelength squared.

Putting (2.12) into (2.18) gives:

$$A_{em} = \frac{\lambda^2}{4\pi} D \quad (2.19)$$

This equation shows a very important relation that the maximum effective aperture of any antenna is the product of its directivity and the square of the wavelength divided by  $4\pi$ .

## 2.2.6 Gain

Antenna power gain or simply gain is another key parameter describing the performance of an antenna. It relates to both the electrical efficiency and the directional property of the antenna. Its gain being a transmitting antenna determines how effective the antenna can turn its input power into radio signal pointed into a particular direction. Similarly, as a receiving antenna, its gain describes how effective it converts incoming radio signal into electrical signal.

The gain is defined as the ratio of its radiation intensity  $U(\theta, \Phi)$  in a given direction to the mean radiation intensity of a lossless isotropic source as:

$$G(\theta, \phi) = \frac{U(\theta, \phi)}{U_{lossless_{ave}}} \quad (2.20)$$

From (2.8), the average radiation intensity of a lossless isotropic source is

$$U_{lossless_{ave}} = P_{in}/4\pi$$

The gain can be defined as:

$$G(\theta, \phi) = 4\pi \frac{U(\theta, \phi)}{P_{in}} \quad (2.21)$$

When the direction is not specified, the power gain is usually defined in the direction of maximum radiation as:

$$G = 4\pi \frac{U_{max}}{P_{in}} \quad (2.22)$$

For a nonideal antenna, less than 100% of the input power  $P_{in}$  will be turned into radiated power. The radiated power can be related to the input power as:

$$P_{rad} = e_{total} P_{in} \quad (2.23)$$

where  $e_{total}$  is the total antenna efficiency.

Equation (2.15) can be rewritten as:

$$G = e_{total} 4\pi \frac{U_{max}}{P_{rad}} \quad (2.24)$$

or

$$G = e_{total} D \quad (2.25)$$

which shows that the antenna gain is a function of the total antenna efficiency and directivity. The total efficiency will be discussed in more detail in the following section. It is also worthwhile to point out that the antenna being discussed is a passive type. Unlike an active antenna, which has the power source and amplifier to provide active gain, the gain of a passive antenna comes from concentrating the radiated power into a certain beam angle and direction. This is desirable for applications in which the direction between the communicators is known and fixed. In applications where the direction is unknown or omnidirectional property is desired, an active antenna will be needed to provide additional gain.

### 2.2.7 Polarization

Polarization is one of key fundamental characteristics of an antenna. Before addressing the polarization of the antenna, the polarization of a plane electromagnetic wave will be discussed first [2]. A plane wave is an electromagnetic wave with the electric and magnetic fields traveling in a single axis. There is no field in the two orthogonal axes such that the electric and magnetic fields are perpendicular to each other and to the direction that the plane wave is traveling. The plane wave is illustrated in Figure 2.7 where the wave is traveling in the  $z$ -direction with the E-field and H-field oriented in the  $x$ - and  $y$ -direction, respectively. If the electric field lies in the  $x$ -direction only, this wave is said to be linearly polarized in the  $x$ -direction.

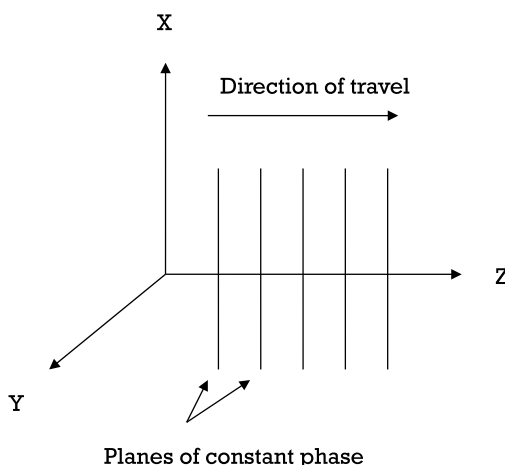


**Figure 2.7** A plane wave with E-field traveling in the  $z$ -direction.

As a function of time and position, the electric field can be given by (see Figure 2.8(a)):

$$E = \cos\left[2\pi f\left(t - \frac{z}{c}\right)\right]\hat{x} \quad (2.26)$$

where  $c$  is speed of light and  $\hat{x}$  is a unit vector pointing to the  $x$ -direction.

The electric field of the wave traveling in the  $z$ -direction may have both  $x$ - and  $y$ -components as shown in Figure 2.8(b). In this general case, the wave is elliptically polarized and can be expressed in terms of two linearly polarized components with one in the  $x$ -direction and one in the  $y$ -direction expressed as:

$$E_x = E_1 \cos\left[2\pi f\left(t - \frac{z}{c}\right)\right] \quad (2.27)$$

$$E_y = E_2 \cos\left[2\pi f\left(t - \frac{z}{c}\right) + \delta\right] \quad (2.28)$$

where  $E_1$  is the amplitude of the  $x$ -direction component,  $E_2$  is the amplitude of the  $y$ -direction component, and  $\delta$  is the phase angle by which  $E_y$  leads  $E_x$ .

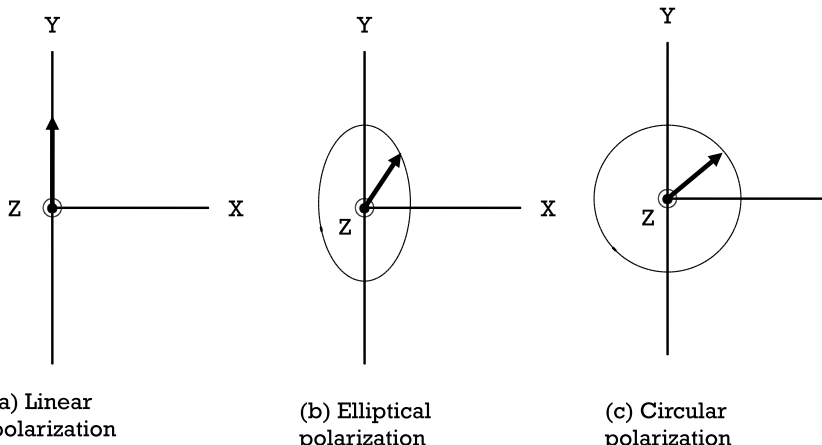


**Figure 2.8** Different polarizations for a wave traveling out of the page: (a) linear polarization, (b) elliptical polarization, and (c) circular polarization.

The composite vector field  $\mathbf{E}$  can be found by combining the  $x$ - and  $y$ -components as defined in (2.27) and (2.28), respectively, as:

$$\mathbf{E} = E_1 \cos\left[2\pi f\left(t - \frac{z}{c}\right)\right] \hat{x} + E_2 \cos\left[2\pi f\left(t - \frac{z}{c}\right) + \delta\right] \hat{y} \quad (2.29)$$

where  $\hat{y}$  is a unit vector pointing to the  $y$ -direction.

At a position  $z$ , the electric vector  $\mathbf{E}$  rotates as a function of time. The tip of the vector traces out an ellipse, which is called the polarization ellipse. It can be characterized by the axial ratio, which is the ratio of the major to minor axes of the polarization ellipse as:

$$AR = \frac{E_2}{E_1} \quad (2.30)$$

The wave is linearly polarized in the  $x$ - and  $y$ -direction for  $E_2 = 0$  and  $E_1 = 0$ , respectively. However, the wave is circularly polarized if  $E_1 = E_2$  and  $\delta = \pm 90^\circ$ . For  $\delta = +90^\circ$ , the wave is left-hand circularly polarized (LHCP). It will be right-hand circularly polarized (RHCP) when  $\delta = -90^\circ$ .

Applying the same principle of wave polarization, the polarization of an antenna refers to the polarization of the far field radiated by the antenna. If an antenna radiates a linearly polarized wave, the antenna is described as a linearly polarized antenna. As an example, a monopole or dipole antenna (to be discussed in the next chapter) is one type of linearly polarized antennas. Similarly, an antenna radiating a circularly polarized wave is called the circularly polarized antenna. A helical antenna is one type of circularly polarized antennas.

The polarization property of antennas is important for antenna-to-antenna communications due to their reciprocity property. According to the reciprocity principle, the transmitting and receiving property are the same. That means if a horizontally polarized antenna transmits horizontally polarized fields, it will receive horizontally polarized fields as well. However, a vertically polarized antenna will not be able to receive the horizontally polarized fields generated by a horizontally polarized antenna. There is no communication between two orthogonally polarized antennas. Assuming there are two communicating antennas with polarization vectors separated by an angle  $\Phi$ , the polarization loss factor (PLF) [3] due to the polarization mismatch is defined as:

$$PLF = \cos^2 \phi \quad (2.31)$$

If both antennas are polarized in the same way, there is no power loss due to the polarization mismatch since the angle between their radiated fields is zero.

### 2.2.8 Efficiency

The total antenna efficiency accounts for all the losses on the antenna, which include the input mismatch, polarization, and dielectric and conduction losses as:

$$\epsilon_{total} = \epsilon_i \epsilon_c \epsilon_d \epsilon_p \quad (2.32)$$

where  $\epsilon_i$  = impedance mismatch efficiency,  $\epsilon_c$  = conduction efficiency,  $\epsilon_d$  = dielectric efficiency, and  $\epsilon_p$  = polarization efficiency [3].

The impedance mismatch efficiency is also expressed as the reflection coefficient of  $1 - |\Gamma|^2$ .

where

$$\Gamma = \frac{Z_{in} - Z_t}{Z_{in} + Z_t} \quad (2.33)$$

and  $Z_{in}$  is the antenna impedance and  $Z_t$  is the terminal impedance.

The terminal impedance is the impedance of the system port to which the antenna connects. It will be the output port of a transmitter or receiver if the antenna is used as a transmitting or receiving element, respectively. The impedance mismatch efficiency indicates how well the antenna is matched to the terminal.

The conduction efficiency accounts for the loss on the metal conductor as heat dissipation of the antenna structure. The dielectric efficiency accounts for the dielectric loss incurred at the dielectric material if any used by the antenna. The dielectric loss is the inherent dissipation of electromagnetic energy such as heat in the dielectric material. Since it is very difficult to separate the conduction and dielectric losses in measurements [3–5], it is more convenient to combine them as the radiation efficiency as:

$$\epsilon_r = \epsilon_c \epsilon_d \quad (2.34)$$

Equation (2.32) can then be rewritten as:

$$e_{total} = e_r e_p \left(1 - |\Gamma|^2\right) \quad (2.35)$$

and the gain expressed in (2.25) becomes:

$$G = e_r e_p \left(1 - |\Gamma^2|\right) D \quad (2.36)$$

Antenna designers will try to design an antenna with the highest gain as much as possible. Most of the determining parameters are function of the antenna's geometry, operating frequency as well as the comprising materials. In many situations, those determining parameters or variables are conflicting with each other on the overall efficiency. Analytic solutions may not be possible to find to account for all the variables for optimization. Computer design and simulation tools will be needed to help optimizing the performance of the antenna. This will be addressed in detail in Chapter 5.

### 2.2.9 Impedance Matching

Antennas are typically designed to a reference impedance of  $50\Omega$ . However,  $75\Omega$  is also commonly used from very high frequency (VHF) to ultrahigh frequency (UHF) range. The antenna is usually connected to the transmitter output or receiver input depending on whether it is used as a transmitting or receiving antenna, respectively. Ideally, the antenna impedance should be conjugately matched to the terminal impedance in order to maximize the gain of the antenna as highlighted in (2.25). However, the terminal impedance may not always be matched to the antenna due to other constraints or requirements. In this situation, an impedance matching network can be added between the terminal and the antenna to transform the antenna impedance to the conjugate of the impedance of the terminal or vice versa.

For the VHF to UHF range, lumped-element matching networks are commonly used. Although there are many different matching networks that can be designed, L-sections are very practical and simple to design as shown in Figure 2.9 [6]. Capacitors and surface-mounted inductors with high circuit-Q values are commonly used on matching networks without incurring too much signal loss. For lower dissipation loss, air coils as an inductor can be used at the expense of larger size. If designed properly, the matching network can provide filtering function to suppress harmonic contents or image noise on a transmitter or receiver, respectively.

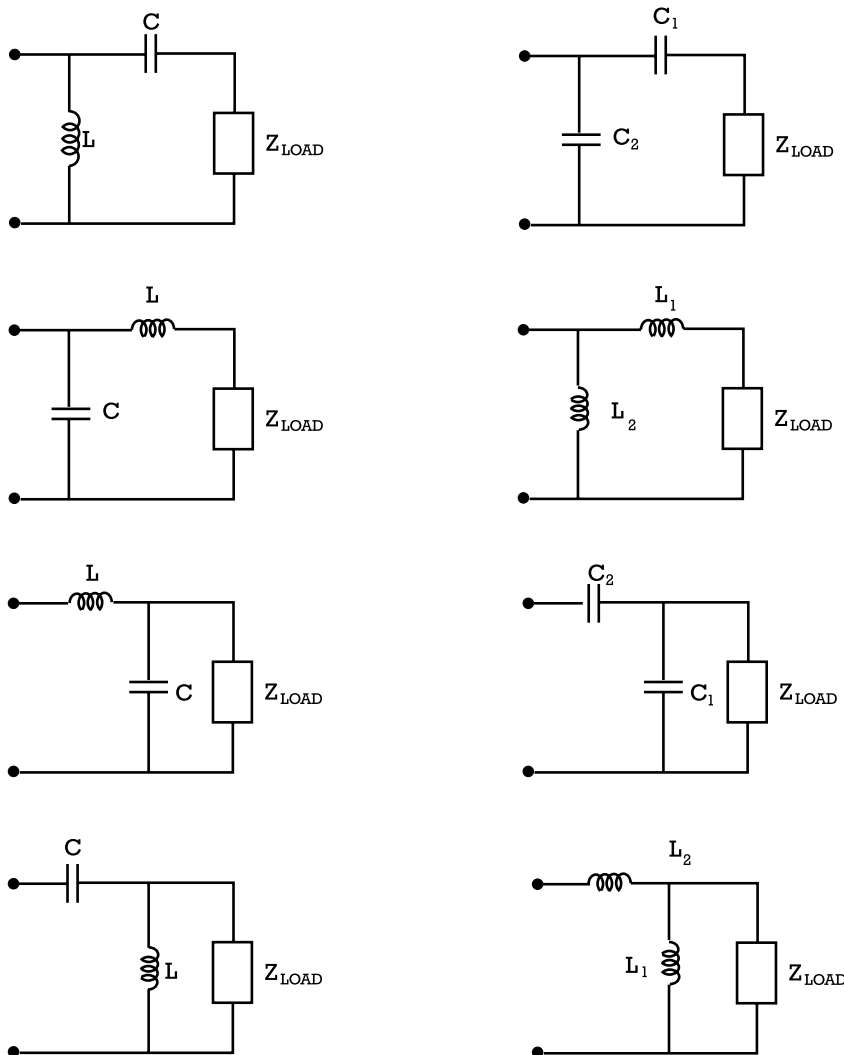


**Figure 2.9** L-type matching networks.

For microwave frequencies higher than 2 GHz, the surface-mounted or air coil inductor is either having too much high-frequency loss or being too low in self-resonant frequency [7, 8] to be used. Instead, distributed circuit elements such as microstrip line, stripline, or coplanar waveguide [9] can be used up to 20 GHz.

### 2.2.10 Friis Transmission and Receiving Formulas

For many radio frequency and microwave communication systems, both the Friis transmission and receiving formulas are very useful to design and optimize for the best communication range. The Friis transmission equation determines the power received due to the power transmitted between two antennas with a distance of  $r$  as shown in Figure 2.10. Assuming the input power at the terminal of the transmitter is  $P_t$  for an isotropic antenna, the power density  $S_r$  at distance  $r$  from the transmitter is:

$$S_r = \frac{P_t}{4\pi r^2} \quad (2.37)$$

If the antenna is non-isotropic and has a gain of  $G_t$ , the power density becomes:

$$S_r = \frac{P_t G_t}{4\pi r^2} \quad (\text{W}) \quad (2.38)$$

Assuming the receiving antenna has an effective aperture of  $A_{er}$ , the power collected by the receiving antenna is thus:

$$P_r = \frac{P_t G_t A_{er}}{4\pi r^2} \quad (\text{W}) \quad (2.39)$$

Putting (2.19) into (2.39), the power collected can be expressed as:

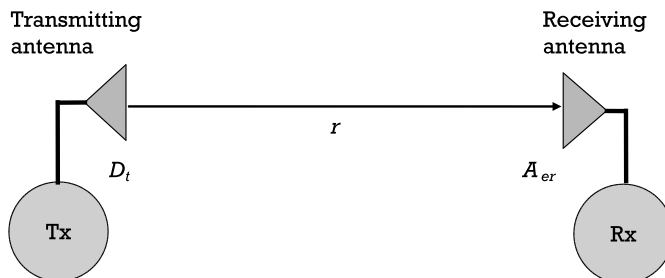


**Figure 2.10** Power received due to the power transmitted between two antennas with a distance of  $r$ .

$$P_r = \frac{\lambda^2 P_t D_t D_r}{(4\pi r)^2} \quad (\text{W}) \quad (2.40)$$

or

$$\frac{P_r}{P_t} = \frac{\lambda^2 D_t D_r}{(4\pi r)^2} \quad (\text{W}) \quad (2.41)$$

It is assumed that the antenna efficiency is 100%. Equation (2.41) is known as the Friis transmission equation relating the receiving power to the transmitting power. The inverse of the term  $(\lambda/4\pi)^2$  in the equation is called the free-space path loss. It accounts for the loss due to the energy spreading as the electromagnetic wave radiates spherically. It should be noted that in order to maximize the power received, the term  $(\lambda/4\pi)^2$  should be maximized assuming both the transmitting and receiving antenna directivities are kept constant at all frequencies. This suggests operating the complete communication system at a lower frequency, which results in a longer wavelength.

Equally important, the Friis receiving equation [10] indicates how well the receiver system is designed on sensitivity performance. The sensitivity of a receiver is determined by the minimum signal level; a system can detect with an acceptable signal-to-noise ratio as:

$$P_{in(\min)} = -174 \text{ dBm/Hz} + NF + 10 \log(B) + SNR_{\min} \quad (2.42)$$

in dBm

where  $B$  is the system noise bandwidth and  $NF$  is the noise figure of the system defined as:

$$NF = \frac{SNR_{in}}{SNR_{out}} \quad (2.43)$$

in dB

where  $SNR_{in}$  and  $SNR_{out}$  is the signal-to-noise ratio at the input and output, respectively.

Since in a typical receiver, there will have multiple stages of amplifier and mixer as shown in Figure 2.11. The total noise figure is governed by the Friis receiving equation as:



**Figure 2.11** Receiver chain with cascading stages with different gain and noise figure.

$$NF_{tot} = 1 + (NF_1 - 1) + \frac{(NF_2 - 1)}{AP_1} + \dots + \frac{(NF_m - 1)}{AP_1 \dots AP_m} \quad (2.44)$$

where  $NF_{tot}$  is the equivalent total noise figure,  $NF_m$  is the noise figure of the  $m$  stage,  $AP$  is the available gain of the  $m$  stage, all are expressed as ratios, not in decibels.

It can be shown that the total noise figure is dominated by both the noise figure and the gain of the first stage on the receiver chain. Many system design books or references would suggest optimizing the performance of the low noise amplifier (LNA) since it is typically the first stage on the receiver chain. For a complete receiver, the antenna instead would be the first stage on the receiver chain. For a passive network such as antenna, the noise figure is the attenuation of the antenna. The attenuation can be considered as the efficiency of the antenna as formulated in (2.32). A slight degradation on the efficiency of the antenna will have direct and dominating effect on degrading the receiver sensitivity. The system or product designers should also pay special attention to the performance of the antenna in addition to that of the receiver.

## References

- [1] Kraus, J. D., *Antennas*, New York: McGraw-Hill, 1988.
- [2] Kraus, J. D., *Electromagnetics*, 3rd ed., McGraw-Hill, New York, 1984.
- [3] Balanis, C. A., *Antenna Theory: Analysis and Design*, New York: John Wiley & Sons, 1997.
- [4] Ramo, S., J. R. Whinnery, and T. Van Duzer, *Fields and Waves in Communication Electronics*, Third Edition, New York: John Wiley & Sons, 1994.
- [5] Chen, L. F., et al., *Microwave Electronics: Measurement and Materials Characterization*, New York: Wiley, 2007.
- [6] Gonzalez, G., *Microwave Transistor Amplifiers: Analysis and Design*, Second Edition, Upper Saddle River, NJ: Prentice Hall, 1997.

- [7] Bahl, I. J., *Lumped Elements for RF and Microwave Circuits*, Norwood, MA: Artech House, 2003.
- [8] Sobot, R., *Wireless Communication Electronics: Introduction to RF Circuits and Design Techniques*, New York: Springer, 2012.
- [9] Edwards, T., *Foundations for Microstrip Circuit Design*, New York: John Wiley & Sons, 1983.
- [10] Vizmuller, P., *RF Design Guide: Systems, Circuits, and Equations*, Norwood, MA: Artech House, 1995.

## **CHAPTER**

# **3**

### **Contents**

- 3.1 Introduction
- 3.2 Antenna Elements

## **Basic Antenna Elements**

### **3.1 Introduction**

Chapter 2 gives a brief introduction to the fundamentals of various commonly used antennas on the market. This chapter will continue to discuss those antennas in more detail and with more practical examples. Their advantages and disadvantages will be highlighted in different applications and products. Derivatives of them will also be presented so that readers can use the knowledge to come up with optimal antennas for their particular applications.

### **3.2 Antenna Elements**

#### **3.2.1 Quarter-Wavelength Monopole or Half-Wavelength Dipole Antenna**

##### **3.2.1.1 Radiation Characteristic**

In Section 1.3.2, the radiated power and resistance are derived for a small current element. Although the small current element is hypothetical and cannot be implemented, it is useful for theoretical analysis. A more practical structure is an elementary dipole with a very short

length relative to its wavelength. The signal is fed to the center of the short dipole as shown in Figure 3.1. Unlike the small current element, the current on this short dipole is no longer constant along the conductors. For the length  $l$  of the conductor being smaller than a wavelength, the current distribution can be approximated as having a maximum at the center to zero at both ends as shown in Figure 3.1. The average current on the short dipole is only one-half of that of the small current element having constant  $I$  throughout its entire length. Its radiated power is thus only one-quarter of the small current elements. Its radiation resistance is also only one-quarter of that of the small current element as:

$$R_{rad(\text{short-dipole})} = 20\pi^2 \left( \frac{l}{\lambda} \right)^2 \quad (3.1)$$

The assumption of having an average current of  $I/2$  on the short dipole may not be true for longer antennas. It is necessary to know the current distribution along the conductor of the antenna in order to find the radiated power.

The current distribution can be found by solving the Maxwell's equations along the antenna with the appropriate boundary conditions. Although it is possible to find the solution analytically, the task is very involved and difficult. Without knowing the exact solution, we could still assume a certain current distribution. It has been found that a sinusoidal current distribution is a very close estimate [1]. In Figure 3.2, Figure 3.1 has been redrawn with a sinusoidal current. The current on the conductors can be expressed as:

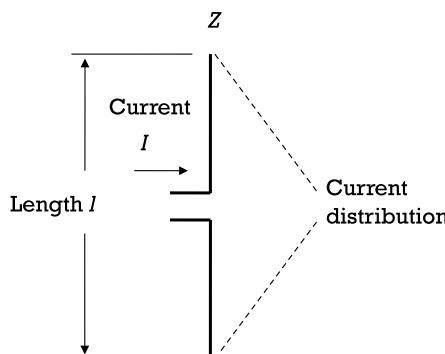


**Figure 3.1** Current distribution on a short dipole.

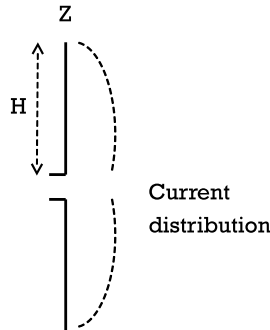


**Figure 3.2** Dipole antenna with sinusoidal current distribution.

$$I = I_{\max} \sin \beta(H - z) \quad (3.2)$$

for  $z > 0$ , where  $H$  is the half-length of the dipole,  $\beta$  is the phase-shift constant, radian per unit length,  $z$  is the position along the vertical dipole, and

$$I = I_{\max} \sin \beta(H + z) \quad (3.3)$$

for  $z < 0$ .

The same procedures as used in Section 1.3.2 can be applied here to find the electric and magnetic field strengths with  $H = \pi/4$  for a quarter-wave monopole as:

$$H_\phi = j \left( \frac{\cos\left(\frac{\pi}{2}\cos\theta\right)}{\sin\theta} \right) \left( \frac{I_{\max} e^{-j\beta r}}{2\pi r} \right) \quad (3.4)$$

$$E_\theta = j \left( \frac{\cos\left(\frac{\pi}{2}\cos\theta\right)}{\sin\theta} \right) \left( \frac{60I_{\max} e^{-j\beta r}}{r} \right) \quad (3.5)$$

For a quarter-wave monopole or a half-wave dipole, the magnitude of the electric and magnetic field can be expressed as:

$$H_\phi = \left( \frac{\cos\left(\frac{\pi}{2}\cos\theta\right)}{\sin\theta} \right) \left( \frac{I_{\max}}{2\pi r} \right) \quad (3.6)$$

$$E_\theta = \left( \frac{\cos\left(\frac{\pi}{2}\cos\theta\right)}{\sin\theta} \right) \left( \frac{60I_{\max}}{r} \right) \quad (3.7)$$

Since  $H_\phi$  and  $E_\theta$  are in phase, the corresponding Poynting vector is just the product of the two. The effective Poynting vector, which accounts for the radiation, is half of the peak value as:

$$P_{ave} = \left( \frac{\cos^2\left(\frac{\pi}{2}\cos\theta\right)}{\sin^2\theta} \right) \left( \frac{\eta I_{\max}^2}{8\pi^2 r^2} \right) \quad (3.8)$$

For a monopole antenna, the total radiated power can be found by integrating the above Poynting vector over a hemisphere as:

$$\begin{aligned} \oint P_{ave} da &= \oint P_{ave} 2\pi r^2 \sin\theta d\theta \\ &= \int_0^{\frac{\pi}{2}} \frac{\cos^2\left(\frac{\pi}{2}\cos\theta\right)}{\sin\theta} d\theta \left( \frac{\eta I_{\max}^2}{4\pi} \right) \end{aligned} \quad (3.9)$$

where  $da = 2\pi r^2 \sin\theta d\theta$ .

Using the substitution method [1], (3.8) can be reexpressed as:

$$\begin{aligned} P_{rad} &= \frac{0.609\eta I_{\max}^2}{4\pi} \\ P_{rad} &= \frac{0.609\eta I_{eff}^2}{2\pi} = 36.5I_{eff}^2 \end{aligned} \quad (3.10)$$

where  $I_{eff}^2 = I_{\max}^2/2$  is the effective current.

The radiation resistance is thus  $36.5\Omega$  for a quarter-wavelength monopole. It is assumed that the monopole is mounted on an infinite ground

plane. The power radiated by a half-wavelength dipole is twice as much since the radiation occurs through the complete sphere rather than just the hemisphere. The corresponding radiation resistance is  $73\Omega$  given the same current.

### 3.2.1.2 Directional Property of Dipole Antenna

Antennas typically have two main functions. One is to convert the electrical signal from a signal source to an electromagnetic wave or power into free space. The conversion ideally can be done most effectively and efficiently through the antenna and the matching network as discussed in Chapter 2. The second function is to radiate energy to certain directions. Alternatively, the radiating energy can be suppressed in some undesired directions. Since the dipole antenna is the fundamental element for study, analysis, and practical use, it is worthwhile to study its directional characteristic.

Recalling from Chapter 1, the radiating field represented by (1.27) for an elementary current element or oscillating electric dipole is:

$$E_\theta = \frac{Idl \sin \theta}{4\pi\varepsilon} \left( -\frac{\omega \sin \omega t'}{rv^2} \right) \quad (3.11)$$

The magnitude of the term for the field strength accounted for radiation is thus:

$$\begin{aligned} E_\theta &= \frac{\omega Idl \sin \theta}{rv^2 4\pi\varepsilon} \\ &= \frac{60\pi Idl \sin \theta}{r\lambda} \end{aligned} \quad (3.12)$$

where  $\theta$  is the angle between the axis of the elementary dipole and the radius vector from the dipole to the observation point.

If the dipole is placed vertically, the radiation is uniform along the  $x$ - $y$  plane for  $\theta$  being  $90^\circ$ . The horizontal radiation pattern is thus a circle as shown in Figure 3.3(a). For any vertical planes passing through the  $z$ -axis, the radiation pattern has a figure-8 shape as shown in Figure 3.3(b) since the field strength varies as  $\sin \theta$ . A 3-D plot on the field pattern is shown in Figure 3.3(c) to show the famous donut-shape pattern.

For a dipole antenna, its corresponding radiation field strength has already expressed by (3.6, 3.7). For a dipole with any length  $L$ , its radiation field strength can be expressed as [1]:

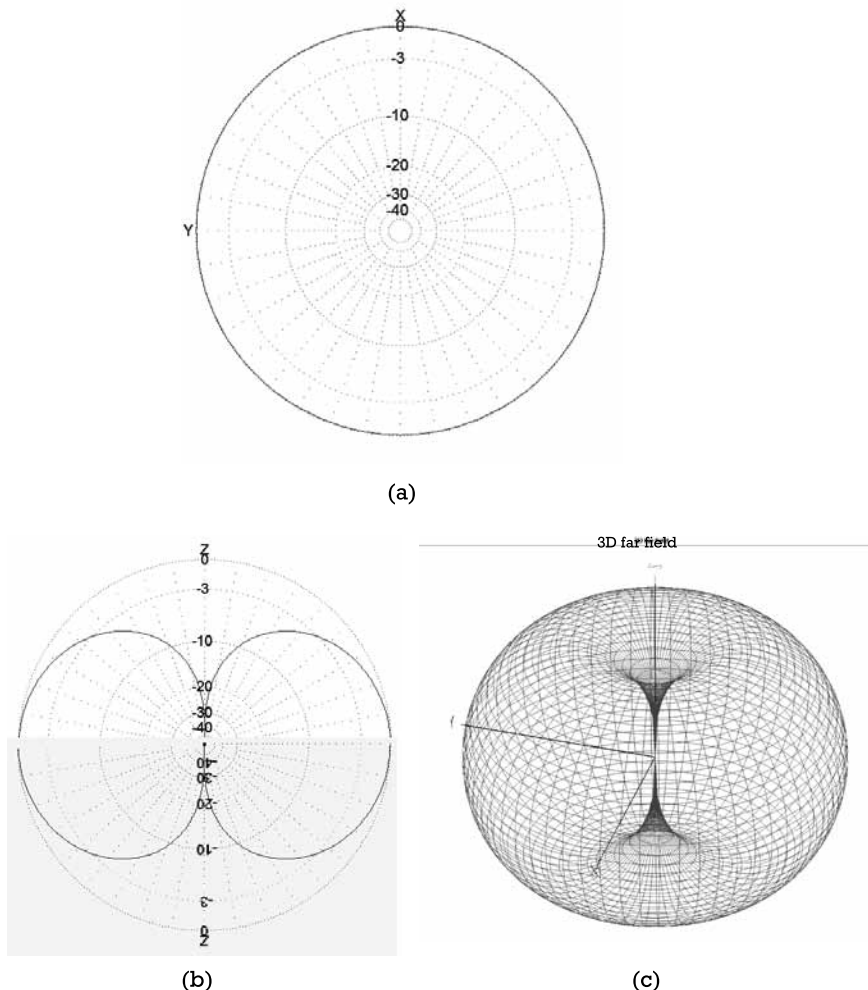


**Figure 3.3** (a) Horizontal field pattern, (b) vertical field pattern, and (c) 3-D field pattern of a small dipole.

$$E_\theta = \frac{60I}{r} \left[ \frac{\cos \beta L - \cos(\beta L \cos \theta)}{\sin \theta} \right] \quad (3.13)$$

Figure 3.4 shows the vertical field pattern for a dipole with various lengths to illustrate how its directivity varies with its length. As shown in Figure 3.4(a), a half-wavelength dipole is only slightly more directional

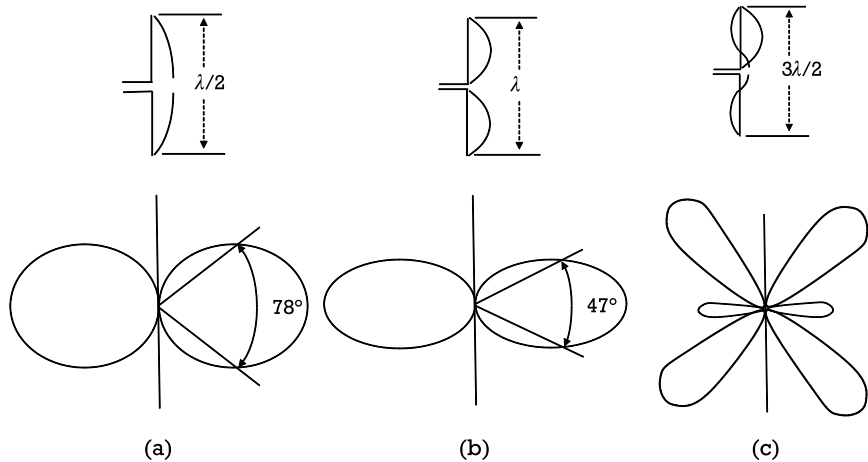


**Figure 3.4** Radiation patterns for: (a) a half-wavelength dipole, (b) a wavelength dipole, and (c) a one-and-a-half-wavelength dipole.

than the short dipole as its half-power beamwidth is  $78^\circ$  as compared to  $90^\circ$  of a short dipole. For one wavelength, the half-power beamwidth becomes  $47^\circ$ . As the length increases beyond one wavelength, the number of side-lobes increases. As shown by the beamwidth, the directivity of a dipole antenna increases with its length. On the contrary, the efficiency of the dipole antenna decreases with its length as the ohmic loss on the conductor will go up. One may have to optimize the antenna among the required gain and directivity.

### 3.2.1.3 Quarter-Wavelength Monopole or Half-Wavelength Dipole Antenna for Wireless Communication Devices

Monopole and dipole antennas have been used intensively in many wireless communication systems and devices such as mobile phones, cordless telephones, WiFi routers, and walkie-talkies due to their simple construction. Although simple in design, their directivity, efficiency, and gain are greatly influenced by their electrical length. The radiation power is typically proportional to the length  $L$  and thus a longer antenna would have a better radiation performance. The electrical length, in turn, is related inversely to the frequency of operation. A long antenna would require more space where space would be scarce in most wireless handheld devices.

Many short-range, low-power wireless devices (SRD) such as garage door openers, video monitoring devices, and smart-home remote

controllers typically operate at 315 MHz/433 MHz, 868 MHz/915 MHz, and 2.4 GHz/5.6 GHz [2, 3]. The length of a quarter-wavelength monopole is 24 cm for 315 MHz and 8.2 cm for 915 MHz. Except used on a base unit, the required length of 24 cm for 315 MHz is prohibitively long to be used on a handheld device. The 915-MHz operation still requires an antenna length of 8.2 cm, which may be allowed by some devices. The 2.4-GHz/5.6-GHz operating frequency would be preferred for a monopole antenna due to its shorter physical length. However, the associated free-space path loss as introduced in Section 2.2.10 is higher than that at 315/433 MHz. Unless an additional power amplifier is used, 2.4-GHz/5.6-GHz devices such as Bluetooth, a wireless mouse, or a baby monitor typical have a very short communication distance.

Monopoles are traditionally external to the device as shown in Figure 1.3 for best performance. They are either fixed or retractable and made of straight wire or helix [4] with plastic cover. As the recent trend is to make wireless devices such as a cellphone small, the external monopole antenna would be very intrusive visually and physically to the users. Many wireless devices are thus required to use an internal antenna, which makes the design more challenging. Other forms of antenna types such as inverted-L or inverted-F or meandered would be more suitable.

### **3.2.2 Loop Antenna**

A loop antenna is an inexpensive and versatile antenna, which can be in different forms such as circle, square, or triangle [5]. It consists of a loop of wire or other metallic conductors with its end connected to a balanced source as shown in Figure 1.6. There are two distinct types of loop antenna: electrically small and electrically large. For a small loop antenna, its size is much smaller than one wavelength. The large loop antenna is also called the resonant loop antenna as its circumference is close to the wavelength of operation. Although small loop antennas have a very low radiation efficiency, they are typically used in receivers such as pagers or transmitter such as keyless entry devices. Figure 1.7 shows a rectangular loop antenna used in a 400-MHz pager. With careful and creative design techniques, the loop antenna can fit and perform reasonably well in small handheld devices.

Due to its low cost and versatility, a loop antenna has been widely used for many applications covering the frequency range from 300 KHz to 900 MHz. A loop can be in different forms such as a circle and a polygon of a square, triangle, or rectangle.

A circular loop is shown in Figure 3.5 with a radius of  $a$  in the  $x$ - $y$  plane. Assuming that the radius is much smaller than a wavelength ( $a \ll \lambda$ ), the current within the loop can be approximated as constant  $I_0$  along the loop. The fields from the small circular loop are expressed as [4]:

$$E_{\phi_{loop}} = \eta \frac{(\pi a)^2 I_0 e^{-jkr}}{\lambda^2 r} \sin \theta \quad (3.14a)$$

$$H_{\theta_{loop}} = \frac{-E_\phi}{\eta} \quad (3.14b)$$

The far-field radiated electric field pattern in the  $x$ - $z$  or  $y$ - $z$  plane has a variation of  $\sin \theta$  with a direction that resembles the same field pattern of a short dipole as expressed in (3.11) except that the electric and magnetic fields are interchanged. The electric field is horizontally polarized in the  $x$ - $y$  plane. Due to this similarity, a small loop is often referred as the dual of a dipole antenna. Similarly, the far-field radiated fields at the principal plane for a square loop shown in Figure 3.6 can be expressed as:

$$E_{\phi_{square}} = \eta \frac{\pi L^2 I_0 e^{-jkr}}{\lambda^2 r} \sin \theta \quad (3.15a)$$

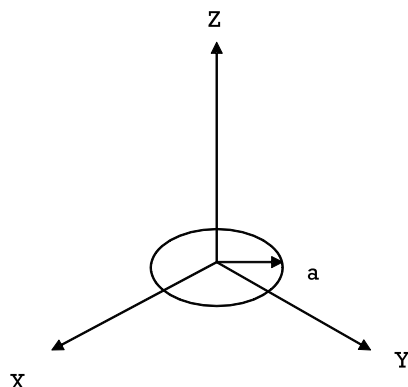


**Figure 3.5** A circular loop antenna.

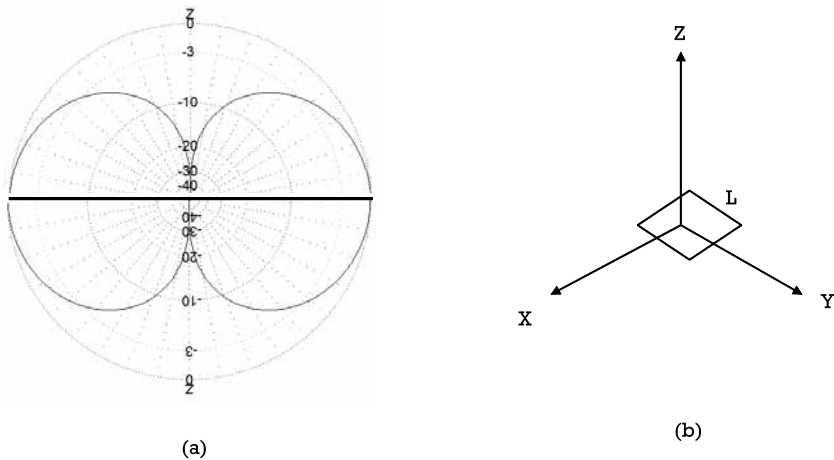


**Figure 3.6** Far-field radiated field: (a) at the principal plane and (b) for a square loop.

$$H_{\theta_{square}} = \frac{-E_\phi}{\eta} \quad (3.15b)$$

where  $L$  is the length of the square.

As suggested by (3.14) and (3.15), the far-field radiation pattern of a small square loop at the principal plane is identical to that of the small circular loop.

The radiation resistance of the small loop can be derived as [4]:

$$R_r = 20\pi^2 \left( \frac{C}{\lambda} \right)^4 \quad (3.16)$$

where  $C$  is the circumference of the loop,  $2\pi a$ .

As a comparison and assuming that the circumference is  $\lambda/2$  for the small circular loop, the radiation resistance calculated by (3.16) is only  $0.77\Omega$ , which is very low as compared to  $73\Omega$  of a half-wavelength dipole. Small loop antennas thus have very poor radiation efficiency and they are seldom used for transmission in radio frequency (RF) communication except under the special circumstances of low power and short range. Despite its low radiation resistance, it is still useful in receiver applications where the receiving signal to noise is large enough. Due to its small size, it is of

ten used as an electromagnetic interference/electromagnetic compatibility (EMI/EMC) signal sniffer probe as shown in Figure 3.7.

Modern communication systems and devices require long communication distance; other ways to improve the antenna efficiency are needed to improve the product's competitiveness. One way is to increase the number of turns so that the magnetic field passes through all the loops. The corresponding radiation resistance can be found by multiplying the radiation resistance of the single loop by  $N^2$  as [6]:

$$R_{rN} = N^2 20\pi^2 \left( \frac{C}{\lambda} \right)^4 \quad (3.17)$$

Unlike the dipole or monopole, the smaller-than-resonant loop antenna is inductive and needs capacitive compensation to yield the pure resistive impedance. Receivers usually have to compensate for the small loop's low efficiency. This compensation may mean putting more gain into the receiver's front end, which may be costly, requires lower noise, or degrades the overall receiving intermodulation performance.

The loop efficiency can be increased with a few simple steps. Both theoretical analysis and field tests show that a loop antenna using flat-strip conductors, such as PCB traces, has an efficiency 1.5 to 2 dB greater than that of a loop antenna using round-wire conductors of the same cross-sectional area [7]. This improvement on efficiency results from the fact that the antennas with flat-strip conductors have lower skin-effect loss in the rectangular conductor than in the round-wire conductors. This method is the cheapest and easiest-to-achieve in antenna design. Similar analysis shows



**Figure 3.7** EMI/EMC signal sniffer probe (From: [10]. Reprinted with permission of Kenneth Wyatt of Wyatt Technical Services LLC.)

that using two coplanar loops instead of a single one provides a 3-dB increase in efficiency as long as the loops are not packed closer than about 1/10 wavelength. However, in most pagers and similar designs, the loops are close together due to space constraint, the gain advantage decreases to about 1.5 to 2 dB. This is still impressive considering the low cost of implementation. However, each loop turn increases the inductance of the antenna, which makes impedance matching more difficult and sensitive to component tolerances.

Another way to increase the radiation sufficiency is to insert a ferrite core or rod inside the loop. The ferrite material has the capability to increase the magnetic flux inside the loop to increase the radiation resistance [8, 9]. The corresponding radiation resistance can be found as:

$$R_{rf} = N^2 20\pi^2 \left(\frac{C}{\lambda}\right)^4 \left(\frac{\mu_e}{\mu_o}\right)^2 \quad (3.18)$$

and

$$\mu_{eff} = \frac{\mu_f}{1 + (\mu_f - 1)D} \quad (3.19)$$

where  $\mu_o$  is the permeability of free space,  $\mu_{eff}$  is the effective permeability of the ferrite core,  $\mu_f$  is the permeability of the ferrite material, and  $D$  is the demagnetization factor.

The effective permeability of most ferrite can be as high as 50 and it can increase the radiation resistance dramatically. Because of the increased radiation resistance and low cost, many amplitude modulation (AM) radios are using a multturn coil antenna with ferrite rod or bar inserted. The impedance of the loop is inductive and can be tuned out by a parallel capacitor to feed to the input of the front-end amplifier for the receiver. Unfortunately, most ferrite material exhibits very high loss at high frequencies. Ferrite-loaded antennas are confined to applications with operating frequencies below 100 MHz.

### 3.2.3 Patch Antenna

A patch or microstrip antenna has been used in many consumer, industrial, and space applications due to its thin planar structure, low cost, simple fabrication, and installation. In spite of all the advantages, the microstrip

antenna has some performance limitations such as low efficiency, narrow frequency bandwidth, and high Q. Nevertheless, its versatility and more advanced designs on performance improvement still make it attractive in many applications. There are many analysis methods for patch antennas including the transmission line, cavity, and moment method [11].

The typical shapes of the patch antenna are rectangular, square, elliptical, or circular, while the rectangular patch is the most common configuration. Figure 3.8 shows a typical patch antenna fed by a microstrip transmission line. The patch is of length  $L$  and width  $W$  with usually two metal layers having the top layer for the feeding transmission line and the patch antenna and the bottom layer for the ground plane. Both layers are made of high-conductivity metal such as copper. For higher performance, the copper conductor could be gold-plated. Between the two metal layers is the substrate consisting of a dielectric material having a relative permittivity of  $\epsilon_r$ . For low-cost, high-yield but less performance sensitivity applications operating at frequencies lower than 3 GHz, the antenna can be fabricated with a standard PCB fabrication process with FR-4 substrate since FR-4 is a standard PCB substrate material. For high-performance and high-operating frequencies, other substrate materials such as Duroid, Teflon, or PTFE can be used. Their dielectric constant varies from 2 to 10.

Based on the transmission line model and assuming  $L$  of a half-wavelength  $\lambda/2$ , the patch antenna can be considered as a resonating open-end transmission line with a perfect reflection at the open end. Since the end of the patch is open circuit, the current is zero at the end. It is maximum and minimum at the center and beginning of the patch, respectively. The voltage is at a maximum of  $+V$  at the end, while it is at a minimum of  $-V$  at the

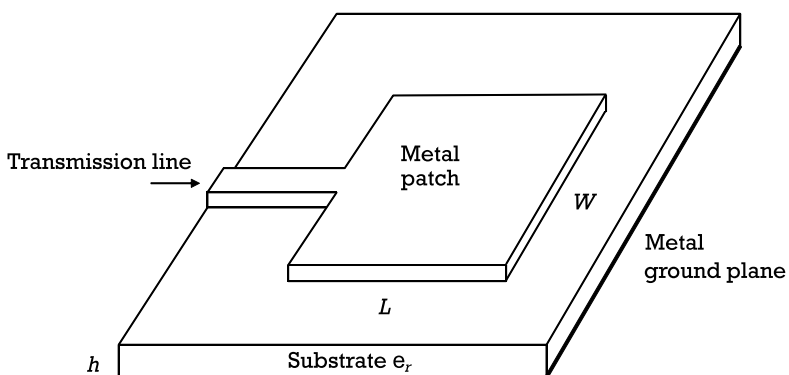


**Figure 3.8** Patch antenna fed by a microstrip transmission line.

beginning. As illustrated in Figure 3.9, there are fringing E-fields near the surface at both ends. Since they are in phase along the y-direction, they add up in phase and produce radiation.

The center frequency of operation can be approximated by:

$$f_r = \frac{1}{2L_{\text{eff}} \sqrt{\mu_o \epsilon_o \epsilon_{\text{ref}}}} \quad (3.20)$$

where  $\epsilon_o$  is the permittivity of free space,  $\epsilon_{\text{ref}}$  is the effective permittivity of the substrate, and  $L_{\text{eff}}$  is the effective length as defined by:

$$L_{\text{eff}} = L + 2\Delta L \quad (3.21)$$

where  $L$  is length of the patch and

$$\Delta L = (h)(0.412) \frac{(\epsilon_{\text{ref}} + 0.3)\left(\frac{W}{h} + 0.264\right)}{(\epsilon_{\text{ref}} - 0.258)\left(\frac{W}{h} + 0.8\right)} \quad (3.22)$$

where  $h$  is the thickness of the substrate and  $W$  is the width of the patch.

The width  $W$  of the microstrip antenna determines the input impedance, bandwidth, and radiation pattern. The larger the width is, the lower the input impedance becomes. For a square patch, the input impedance

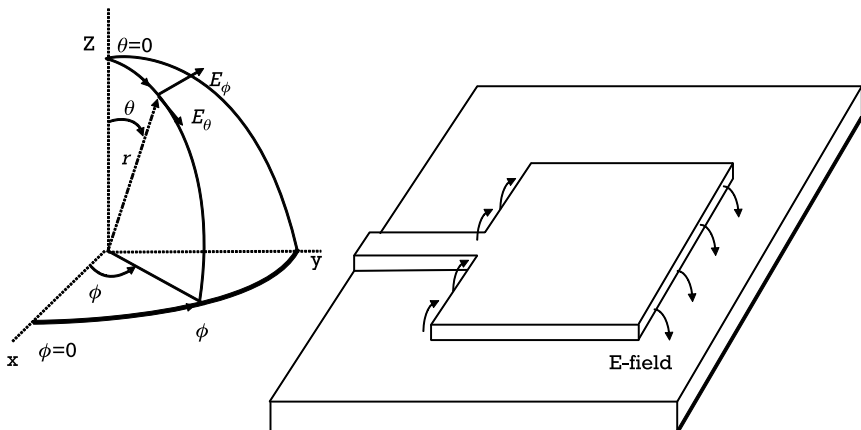


**Figure 3.9** Patch antenna with fringing E-fields near the surface at both ends.

varies from  $200\Omega$  to  $300\Omega$ . The radiation pattern of a rectangular patch can be approximated as:

$$E_\theta = \cos\left(\frac{kL}{2}\sin\theta\cos\phi\right)(\cos\phi)\begin{Bmatrix} \sin\left(\frac{kW\sin\theta\sin\phi}{2}\right) \\ \left(\frac{kW\sin\theta\sin\phi}{2}\right) \end{Bmatrix} \quad (3.23)$$

$$E_\phi = \cos\left(\frac{kL}{2}\sin\theta\cos\phi\right)(\cos\theta\sin\phi)\begin{Bmatrix} \sin\left(\frac{kW\sin\theta\sin\phi}{2}\right) \\ \left(\frac{kW\sin\theta\sin\phi}{2}\right) \end{Bmatrix} \quad (3.24)$$

where  $k$  is  $2\pi/\lambda$ .

The total radiated field is given by:

$$E_{total} = \sqrt{E_\theta^2 + E_\phi^2} \quad (3.25)$$

The bandwidth and efficiency can be increased by using a thinner substrate and with a lower dielectric constant.

As discussed previously, the input impedance of a square patch is very high if the patched is fed at the end. It can be reduced to  $50\Omega$  by increasing the width, which will occupy much space. Methods to lower the input impedance without increasing the size are desirable. As recalled, the voltage is maximum at both ends and decreases in magnitude towards the center. The current is minimum at both ends but increases in magnitude towards the center. The input impedance governed by  $V/L$  decreases when the fed is placed towards the center as shown in Figure 3.10 [4, 11]:

$$Z_{in}(I) = Z_{in}(0)\cos^2\left(\frac{\pi I}{L}\right) \quad (3.26)$$

where  $I$  is the distance of the insert feed from the end and  $Z_{in}(0)$  is the input impedance for  $I=0$ .

Another commonly used method is to use a quarter-wavelength transmission line to transform the high input impedance of the patch to a lower system impedance of  $50\Omega$  or  $75\Omega$  as shown in Figure 3.11.

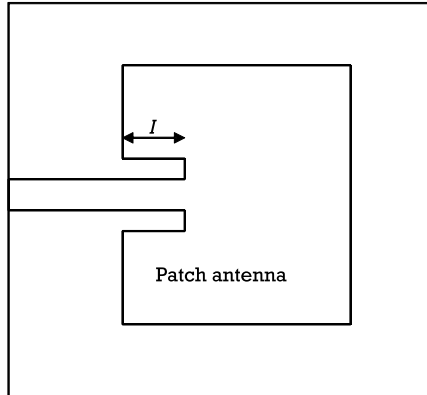


**Figure 3.10** Patch antenna with an insert feed.

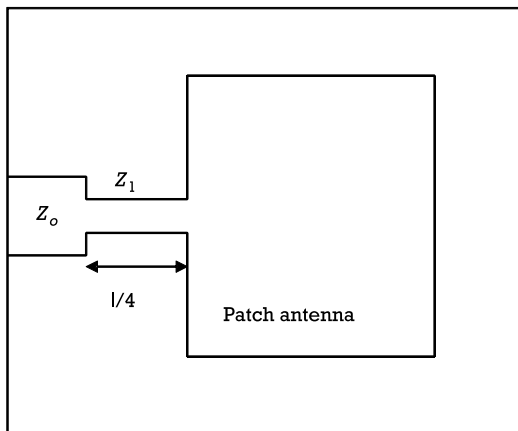


**Figure 3.11** Patch antenna with a quarter-wavelength impedance transformer.

Due to its simplicity and versatility in design, patch antennas have been used extensively in many communication devices. Two major applications are the radio frequency identification device (RFID) [12] and Global Positioning System (GPS) antennas. Figure 3.12 shows RFID antenna panels installed in a vending machine. The antennas will scan all the products inside to which RFID tags are attached so that the central system can track and manage their quantities. The operating frequency of the RFID antenna is

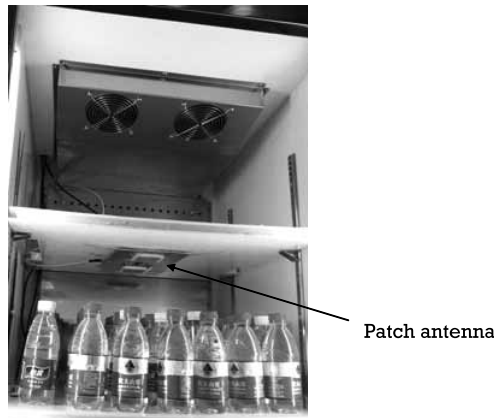


**Figure 3.12** RFID antenna panel installed in a vending machine.

902 to 928 MHz, which has a moderate length of wavelength. As indicated in (3.20), the dielectric constant of the substrate determines the required geometry. There are a wide variety of dielectric material to be used for the patch antenna. Figure 3.13 shows some commercial RFID patch antennas using ceramic, FR-4, and air as the substrate. The size shrinks with the dielectric constant of the substrate being used. The dielectric constant of ceramic varies from 10 to 90 so that the patch can become very small.

Similarly, the GPS antenna shares a few similarities with the RFID antenna. First, the surface of both antennas is perpendicular to the direction of the incoming signal. They expect to receive signals from the front but not the back side. Therefore, the patch antenna is particularly suitable for both applications since the back side of it is the ground. The energy is focused and radiated from the front side with higher gain than the dipole antennas. The RFID antenna points to the object to be scanned while the GPS antenna points to the sky where the satellite signals come in. Second, both antennas require circular polarization [4, 13]. The circular polarization is actually desirable for many antennas. For an RFID reader antenna, it can ensure that an RFID tag can be detected regardless, whether it is placed vertically or horizontally. A right-hand circularly polarized (RHCP) wave becomes left-hand circularly polarized (LHCP) when reflected from a surface. The GPS signal will have some immunity to signal fading effects of reflected waves interfering with the desired wave since GPS signals from satellites are RHCP.

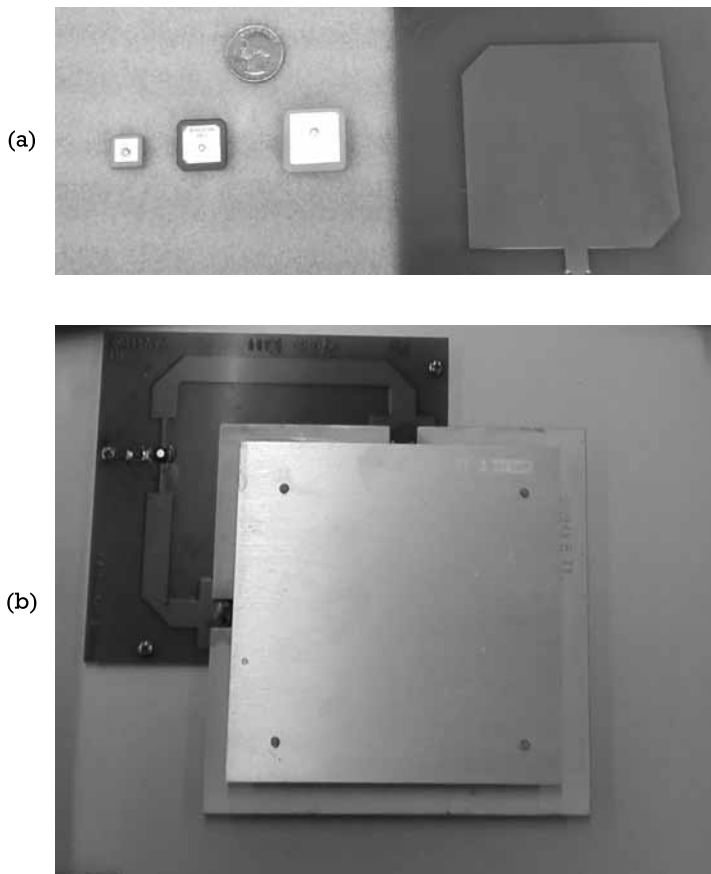


**Figure 3.13** RFID patch antenna using ceramic and FR-4 as dielectric materials.

## References

- [1] Jordan, E. C., and K. G. Balmain, *Electromagnetic Waves & Radiating Systems*, 2nd ed., Upper Saddle River, NJ: Prentice Hall, 1968.
- [2] Loy, M., R. Karingattil, and L. Williams, *ISM-Band and Short Range Device Regulatory Compliance Overview*, Texas Instruments Application Report SWRA048, May 2005.
- [3] Micrel Incorporated, "How to Go Through FCC Compliance Testing Using the MICRF112," *Application Note 55*, 2007.
- [4] Balanis, C. A., *Antenna Theory: Analysis and Design*, New York: John Wiley & Sons, 1997.

- [5] Kraus, J. D., *Antennas*, New York: McGraw-Hill, 1988.
- [6] Smith, G. N., "Radiation Efficiency of Electrically Small Multiturn Loop Antennas," *IEEE Trans. on Antennas and Propagation*, Vol. AP-20, No. 5, September 1972, pp. 656–657.
- [7] Lau, H., "Performance Concerns Guide the Design of Pager Antennas," *Microwaves & RF*, December 1995, pp. 95–106.
- [8] Islam, M. A., "A Theoretical Treatment of Low-Frequency Loop Antennas with Permeable Cores," *IEEE Trans. on Antennas and Propagation*, Vol. AP-11, No. 2, March 1963, pp. 162–169.
- [9] Rumsey, V. H., and W. L. Weeks, "Electrically Small Ferrite Loaded Loop Antennas," *IRE Convention Rec.*, Vol. 4, Part 1, 1956, pp. 165–170.
- [10] Wyatt, K. "An EMC Troubleshooting Kit—Part 1 a (Emissions)," EDN.com, June 2, 2012, <http://www.edn.com/electronics-blogs/the-emc-blog/4378152/An-EMC-Troubleshooting-Kit--Part-1a-Emissions->.
- [11] Pozar, D. M., and D. H. Schaubert, *Microstrip Antennas, the Analysis and Design of Microstrip Antennas and Arrays*, New York: John Wiley & Sons, 1995.
- [12] Lehpamer, H., *RFID Design Principles*, Second Edition, Norwood, MA: Artech House, 2012.
- [13] "Polarization of Antennas—Antenna Theory," <http://www.antenna-theory.com/basics/polarization.php#polarization>.



## **CHAPTER**

# **4**

### **Contents**

- 4.1 Introduction
- 4.2 Miniature Antennas  
for Portable Electronics

## **Advanced Antenna Elements**

### **4.1 Introduction**

Chapter 3 provides a detailed analysis of some commonly used antennas. Practical application examples are illustrated. If designed properly, those antennas such as dipole or monopole offer good antenna performance. However, the required size of the antenna is typically very large in order to achieve the optimum performance. With the proliferation of Internet-of-Things (IoT) technology, handheld wireless devices and terminals are in huge demand. Those hand-held devices call for small size, light weight, and low power consumption. Since more components are being put into the devices in order to implement the increasing number of product features, the space left for putting the required antenna is decreasing. Unfortunately, the size of the antenna limits the antenna's efficiency, bandwidth, and gain [1, 2]. There is always a trade-off between the volume and performance of the antenna. The best

antenna design approach is to excite the whole volume of the antenna for full radiation. This chapter will provide some advanced design techniques to miniaturize and optimize the antenna, despite the limited size of the product.

## 4.2 Miniature Antennas for Portable Electronics

### 4.2.1 Inverted-L and Inverted-F Antennas

One of the most popular techniques on antenna miniaturization is bending and folding. Although the antenna efficiency of a dipole or monopole is very high, its length is very long. It is typically used as an external antenna. An inverted-L antenna can reduce the size of a monopole while offering an acceptable performance by bending the top portion of the monopole, as shown in Figure 4.1. It occupies much less space than a monopole as long as there is enough space along the horizontal axis.

Recalling that the radiation impedance of a quarter-wavelength monopole is  $36.5\Omega$ , a matching network is usually required to transform the impedance to a system impedance of  $50\Omega$  for most applications. Impedance transformation is typically needed for an inverted-L antenna as its radiation resistance will be lower than  $36.5\Omega$  due to the ground plane effect [1, 2]. The capacitance is also very large as the coupling from the bent segment is higher than a monopole due to its closer proximity to the ground plane.

The added matching network will unavoidably attenuate the RF signal due to the losses associated with the matching elements. Figure 4.2 shows the high-frequency equivalent circuit of the matching elements such as capacitor and inductor. The loss is usually due to the ohmic and high-frequency losses. The high-frequency loss is a result of either the dielectric or ferrite loss depending on how the matching components are constructed.

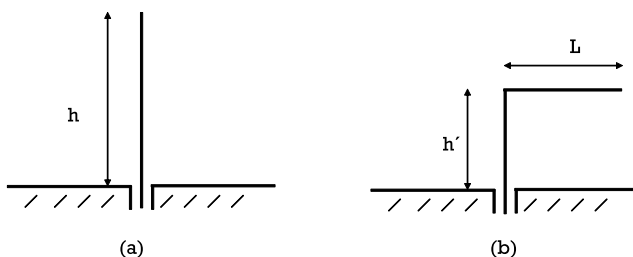


**Figure 4.1** (a) A monopole mounted on a ground plane with a height of  $h$ . (b) An inverted-L antenna showing height reduction ( $h' < h$ ).

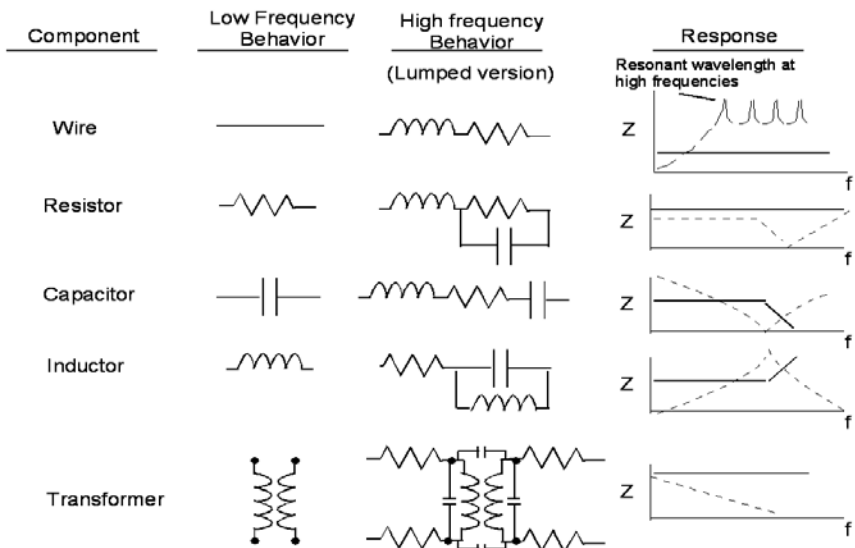


**Figure 4.2** High-frequency behavior of matching elements.

For frequencies lower than 3 GHz, surface-mounted capacitors and inductors are commonly used in the matching networks. The dielectric loss accounts for the high-frequency loss for the surface-mounted capacitors while either the dielectric or ferrite loss accounts for the inductors depending on the material being used [3]. The losses are represented by the resistors in the equivalent circuits in Figure 4.2. More details about matching will be discussed in Chapter 7.

For frequencies higher than 3 GHz, distributed elements will be more applicable for matching as they incur lower loss. However, they occupy much more space than the surface-mounted components. The best approach is to avoid using any external matching elements by designing the antenna such that its sectional elements are both matching and radiating elements simultaneously. The inverted-F antenna shown in Figure 4.3 is a good example. It is similar to an inverted-L antenna but with three segments: upper arm, feeding conductor, and shorting arm. The upper arm is bent along the  $x$ -axis as the main radiating segment while the signal is injected through the feeding conductor.

There are several approaches to analyze the characteristics of an inverted-F antenna. The first method is using the transmission line equivalent model [3–8]. As shown in Figure 4.4, the inverted-F antenna can be considered as an open-ended transmission line. The impedance at the open end is

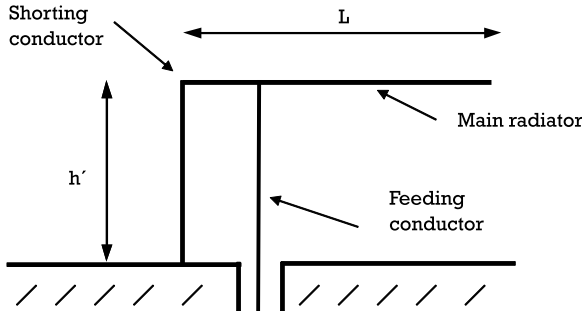


**Figure 4.3** An inverted-F antenna mounted on a ground plane.

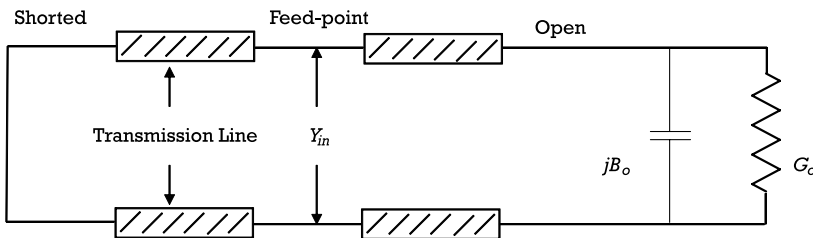


**Figure 4.4** An equivalent transmission-line model.

typically very high and can be modeled as an equivalent admittance of  $jB_o + G_o$  with maximum voltage but zero current. However, the impedance at the short end is zero with maximum current but zero voltage. As the feeding point moves from the short end towards the open end, the impedance changes from very low to very high impedance. The impedance's variation with location along the antenna is similar to the impedance variation at different feeding location of the patch antenna discussed in Chapter 3. At a certain location along the transmission line (antenna), the impedance will be very close to the system impedance of  $50\Omega$ . The transmission line of the conductor of the antenna acts as both matching and radiating elements.

The second method is using the equivalent lumped-element model. As shown in Figure 4.5, the main conductor behaves as a monopole and its impedance becomes very close to  $36.5\Omega$  (with an infinite ground plane) or lower depending on its distance to the ground when its length is one-quarter wavelength. If its length is slightly shorter than one-quarter wavelength, its impedance becomes capacitive. The main conductor will become a capacitive divider with feeding input at the dividing node between  $C_1$  and  $C_2$ . The capacitive dividing ratio between  $C_1$  and  $C_2$  is a function of the location

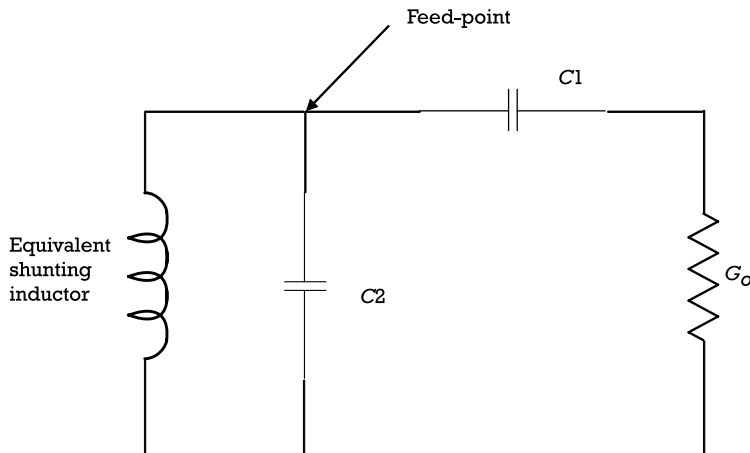


Figure 4.5 A lumped-equivalent model.

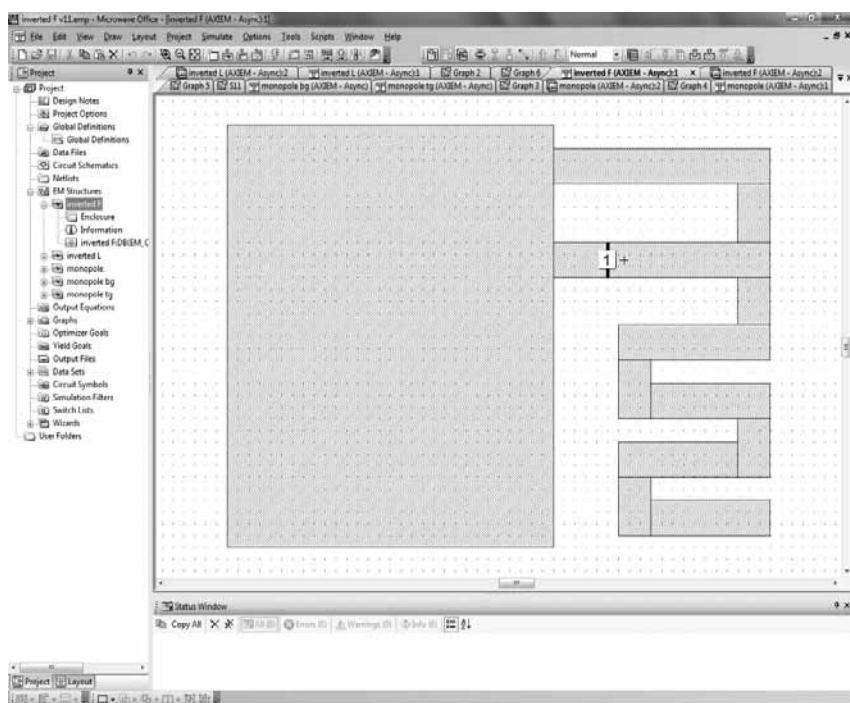
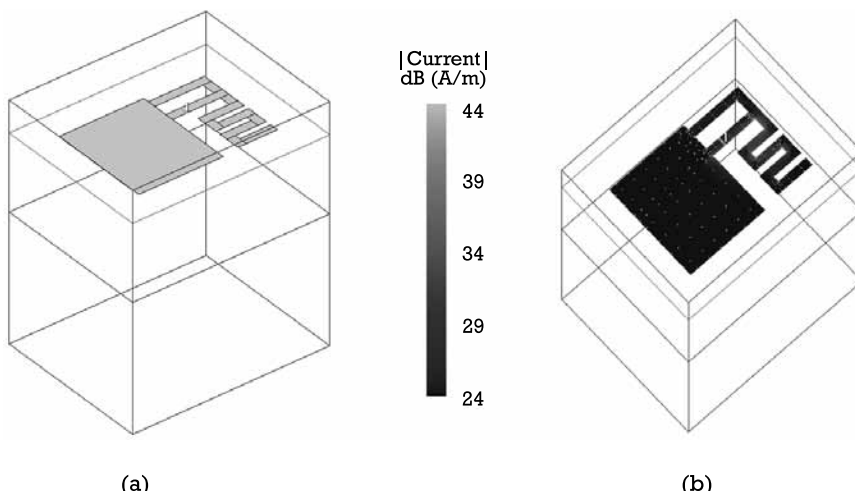


Figure 4.6 Layout of inverted-F antenna created in Microwave Office of AWR Design Environment platform. (Courtesy of National Instruments.)

of the feed point. The shunting shorted-conductor can be represented as an equivalent inductor to resonate with the capacitive divider.

It is getting more difficult or impossible to find the analytical solution when the antenna structure is complex. Another method is to run simulations using an antenna design tool. As a design example, Figure 4.6 shows the layout of a modified, printed inverted-F PCB antenna created for simulation using a commercial electromagnetic (EM) simulator [9]. The design is an inverted-F antenna with a meandered main pole. Meandering is another popular technique on antenna miniaturization that will be discussed in the following section. Details on electromagnetic simulations and optimizations for antenna designs will be discussed in the next chapter. For most electromagnetic simulations, creating the layout of the antenna is the first step. Once the layout is created, the substrate material and dimensions need to be specified. The simulator can then extract the layout for electromagnetic simulation after the enclosure is specified. The enclosure is needed to set the finite boundaries to limit the space for electromagnetic field analysis. Figure 4.7(a) shows the antenna in 3-D layout view with enclosure for simulation. The simulator will try to find the current distributions on the conductors of the antenna by an interactive electromagnetic solver. Once the solution is found, the antenna properties such as gain, efficiency and radiation pattern can then be calculated. Figure 4.7(b) shows the current distribution on the



**Figure 4.7** (a) Antenna in 3-D layout view with enclosure for simulation, and (b) simulated current density on the antenna conductor using the electromagnetic simulator module Axiem. (Courtesy of National Instruments.)

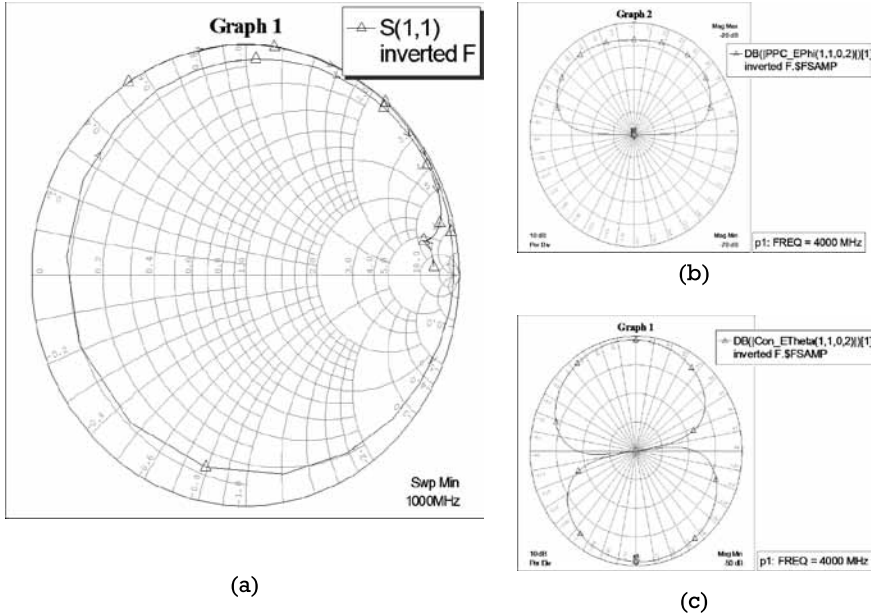


**Figure 4.8** (a) Simulated input impedance of the antenna, (b) antenna radiation pattern,  $E_\phi$ , and (c) antenna radiation pattern,  $E_\theta$ . (Courtesy of National Instruments.)

conductors of the antenna by which the antenna properties are calculated. The simulation results are shown in Figure 4.8. The simulated input impedance shown in Figure 4.8(a) may not always be  $50\Omega$ . The optimizer offered by the antenna design tool can adjust the geometries and substrate parameters of the antenna to achieve the specified requirements automatically. It can then bring the impedance to the required system impedance of  $50\Omega$ .

#### 4.2.2 Meandered Line

Meandered line antennas are developed primarily for miniaturization and are used extensively for small handheld devices due to their small sizes [10–13]. As shown in Figure 4.9, a typical meander line dipole consists of periodic segments of vertical and horizontal branches. The physical length of the meander line dipole can be formulated as:

$$L_d = 2N(W + L) \quad (4.1)$$

where  $L$  is the length of each meander segment,  $W$  is the width of each meander line segment, and  $N$  is the number of meander line segment.

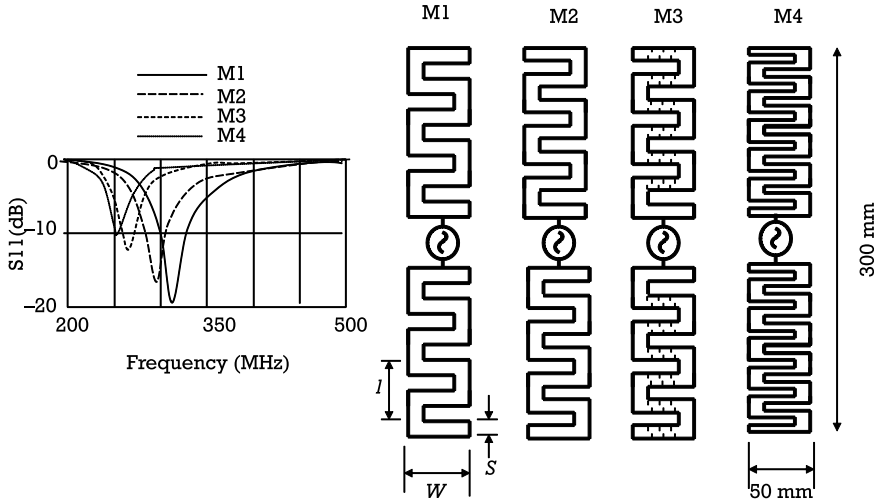


**Figure 4.9** Resonant frequencies for different meandered dipoles. (Based on results from [14].)

Given the same height, the meander line dipole would have a longer physical length than a straight dipole resulting in a lower resonant frequency. Figure 4.9 illustrates the shift in resonant frequency using meandered structures based on the research results of reference [14]. Assuming the resonant frequency of a conventional dipole is 500 MHz, the resonant frequency of M1 dipole shifts to 320 MHz due to extended length as result of meandering. The resonant frequency of M2 and M4 dipole shifts further down to 300 MHz and 260 MHz, respectively, due to the existence of more meander segments. Submeandering can also be implemented to increase the length of the M3 dipole as shown in Figure 4.9, which results in a further decrease in resonant frequency.

Since the downward shift in resonant frequency is due to the increase in the physical length of the dipole, the size of the antenna can be shrunk by meandering while keeping the same operating frequency. This is the reason why meander line antennas are used extensively for small handheld devices.

There is a relationship between antenna efficiency, resonant frequency, and geometry of a meander dipole as proposed by [14]. The radiation efficiency  $\eta$  can be expressed as:

$$\eta = \frac{1}{\frac{Nw}{l} \frac{\lambda}{s} \frac{R_s}{R_d} \frac{1}{4\pi} + 1} \quad (4.2)$$

where  $R_d$  is the radiation resistance,  $R_s$  is the conductor skin resistance, and  $s$ ,  $N$ ,  $l$ , and  $w$  is the meander dipole's dimensional parameter of width, number of turns, pitch, and length, respectively.

It can be shown that radiation efficiency drops with an increase in the number of turns despite a decrease in the resonant frequency. One has to optimize the geometry of the meander line antenna for optimum performance in terms of size, efficiency, bandwidth, and input impedance.

#### 4.2.3 Multiband Antenna

The sales of smartphones in recent years have been surging leading to a great demand for internal and miniature antennas. In order to be compatible to the existing cellular networks, most cellphones have to operate in multiple frequencies to cover all the available frequency bands of different cellular generations of network (i.e. GSM/GPRS, 3G, or 4G). In addition to the cellphone frequency bands, WiFi, GPS, and Bluetooth frequency bands are also desirable to be incorporated in smartphones as those features become standard nowadays. In order to integrate all the features into a smartphone, a multiband antenna has to be designed to use the precious board space effectively.

As conducted by many researchers, a number of design techniques have been reported focusing on multiband small antennas [15–24]. Although a few of them address only two to three bands, some researchers [23, 24] report that their hex-band or even penta-band antenna can cover all the above bands. Among their designs, inverted-F antenna or planar inverted-F antenna (PIFA) offers the best compromise between performance and board space. Since inverted-F occupies less space than PIFA and can be implemented as a planar element in PCB, design techniques for multiband using inverted-F antenna will only be discussed. The design concept from [24] will be used to illustrate how to design an antenna to cover all the frequency bands for GSM (880–960 MHz), DCS (1,710–1,880 MHz), PCS (1,850–1,990 MHz), UMTS2100 (1,920–2,170 MHz), WLAN + Bluetooth (2,400–2,480 MHz), and WiMAX (2,500–2,690 MHz).

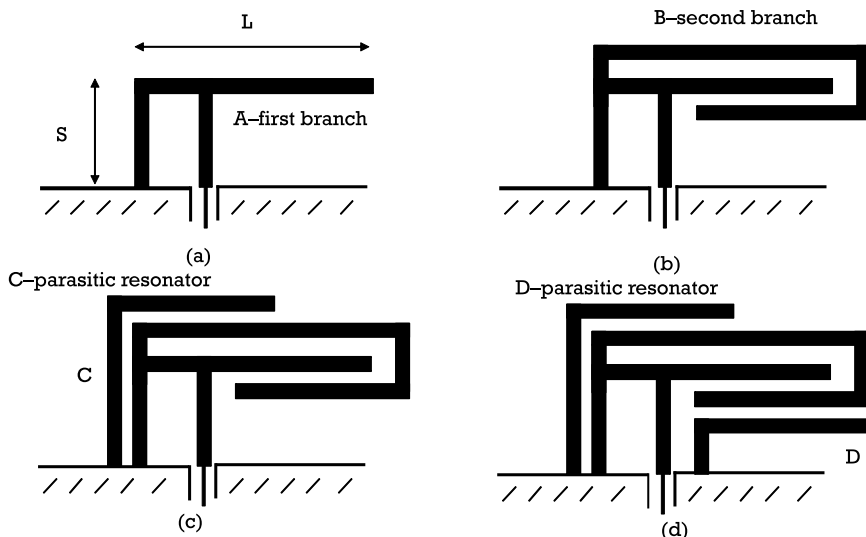
Recall from Section 4.2.1 that an inverted-F antenna resembles a monopole antenna with an additional shunting wire to the ground. As shown in

Figure 4.10(a), the resonant frequency of the inverted-F antenna can be expressed as:

$$f_{res} = \frac{v}{(L + S)4} \quad (4.3)$$

where  $v$  is velocity of light,  $L$  is the length of the main pole, and  $S$  is the length of the shunting conductor.

If sized properly, the antenna will resonate at 1,800 MHz (DCS) with impedance close to  $50\Omega$ . Another branch  $B$  having a longer length can be added as shown in Figure 4.10(b) to resonate at 900 MHz (GSM) to form a dual-band antenna. A third or fourth branch may be added to introduce more resonant frequencies. However, the interaction between impedance of different resonating branches makes it difficult to match all frequency bands simultaneously since all the branches are connected in parallel. Instead of direct connection, the parasitic resonator  $C$  is placed close to the second resonator  $B$ . Due to electromagnetic coupling, the parasitic element  $C$  is excited by the driven resonator  $B$ . The combination of resonators  $B$  and



**Figure 4.10** Multiband inverted-F antenna: (a) single band, (b) dual band with two branches, (c) tri-band with parasitic resonator, and (d) quad-band with parasitic impedance compensator.

$C$  forms a dipole antenna with a resonant frequency of 2,150 MHz to cover the UMTS2100 band.

For the WLAN (2,400–2,480 MHz) and WiMAX (2,500–2,690 MHz) bands, additional parasitic resonators may be added to cover them. However, this will occupy more space and their close proximity will start to influence each other on the resonant frequencies and impedance. Such interaction will make it very difficult to match the antenna at all the required frequencies. Instead of using several parasitic elements for the individual frequencies, [24] came up with a wideband approach to cover the last three bands spanning from 1,900 MHz to 2,700 MHz since the frequencies are very close to each other. Another parasitic element  $D$  is placed very close to branch  $B$  of the inverted-F antenna. Since antenna branch  $B$  resonates at 900 MHz, it will also resonate at a half-wavelength at 1,800 MHz. At frequencies higher than 1,800 MHz, its impedance will become inductive. If the size of the parasitic element  $D$  is properly chosen, its impedance becomes capacitive and will neutralize the inductance on the antenna branch  $B$  due to their electromagnetic coupling. Such arrangement can cover the required frequency band from 1,900 MHz to 2,700 MHz without affecting the original resonant modes at 900 MHz and 1,800 MHz.

As illustrated in Section 4.2.1, it would be much easier to predict and optimize complicated designs such as the mentioned multiband antenna with an electromagnetic simulator. The quad-band antenna shown in Figure 1.9 is used as a design example. It has multiple meandered dipoles coupled with each other and is implemented in an FR-4 PCB substrate. Its 3-D layout is created for electromagnetic simulation as shown in Figure 4.11(a). The simulated and optimized input impedance is shown in Figure 4.11(b) with a good match at the required frequencies of 800, 900, 1,800, and 1,900 MHz.

#### 4.2.4 Dielectric Loaded

Material loading is a very common and effective way to shrink down antenna size. It is also one of the slow-wave approaches to put high-contrast materials at a strategic location on the antenna structure. The electromagnetic wave will travel along the material-loaded path with a wave velocity  $v_s$  smaller than the speed of light  $c$  [25–27] as:

$$v_s = \frac{c}{\sqrt{\mu_r \epsilon_r}} \quad (4.4)$$

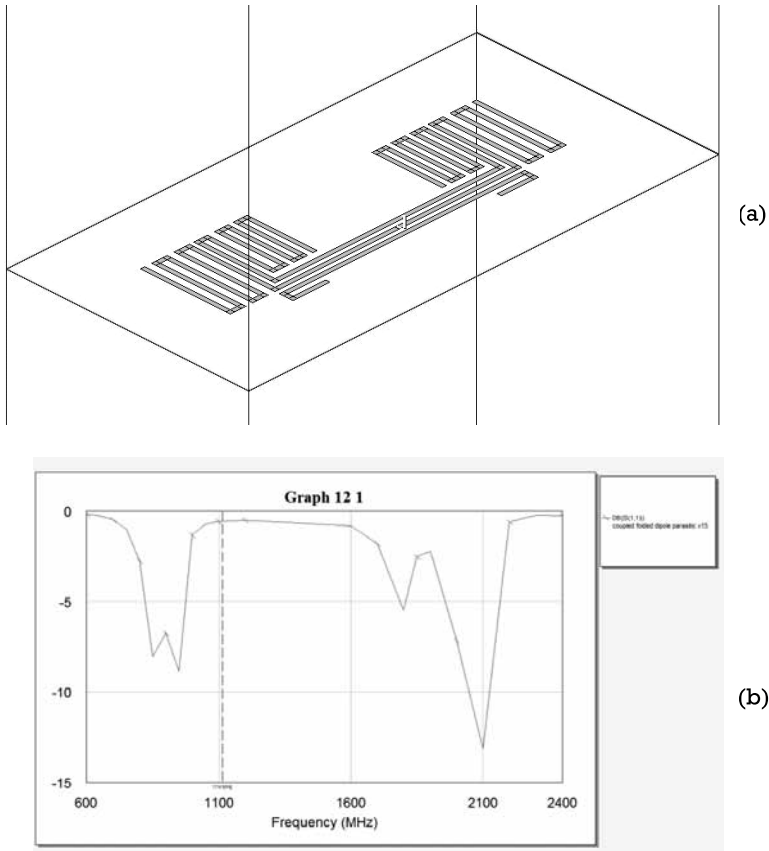


**Figure 4.11** (a) A quad-band meandered dipole antenna in a 3-D layout view, and (b) simulated input impedance of the antenna using the electromagnetic simulator module Axiem.

where  $\mu_r$  is the relative permeability of the loaded material and  $\epsilon_r$  is the relative permittivity of the loaded material.

Although the loss of commercially available magnetic materials is relatively high for operating frequencies above 300 MHz [2], much research is still being conducted to decrease the high-frequency loss since magnetic materials can improve antenna bandwidth. Since the high-frequency loss on magnetic materials is very high, dielectric materials ( $\epsilon_r$  only) are still the mainstream and the most popular element for antenna miniaturization.

As a result of its low cost and low loss, ceramic is the most commonly used dielectric material for high-frequency and microwave antenna designs. There are two major types of ceramic that have been commonly used:

high-temperature and low-temperature ceramics. Typically, ceramic comes in powder form and requires heating process for sintering with a temperature of  $>1,600^{\circ}\text{C}$  and  $<1,000^{\circ}\text{C}$  for high and low-temperature ceramic, respectively. Depending on the ratio of the mixing compounds, the dielectric constant of ceramic can be 6, 9, 16, 37, or even up to 140 [28, 29].

In addition to being an antenna material, low-temperature ceramic is also used as the substrate in a low-temperature cofired ceramic (LTCC) [29] packaging technique for RF and microwave module and component miniaturization. LTCC has advantages compared to other packing technologies since the ceramic supports structures with any resistive, conductive, and dielectric materials, and passive devices are fired below  $1,000^{\circ}\text{C}$  due to a special composition of the material. Typical passive devices are capacitors, resistors, inductors, filters, and transformers. LTCC also has the ability to embed those passive elements in a multilayer structure for module miniaturization. Due to its multilayer structure, many chip antennas for Bluetooth, WiFi, or ZigBee applications are developed using LTCC technology for antenna miniaturization [30]. Despite the advantages, the dielectric constant offered by LTCC is typically less than 10. Such a low dielectric constant prohibits the antenna from further miniaturization.

On the contrary, the high-temperature ceramic offers a wide range of dielectric constant from 6 up to 140. Because of its high dielectric constant, the high-temperature ceramic is used extensively in GPS and RFID patch antennas for size reduction as discussed in Chapter 3. Similarly, it is also used as the substrate in component packaging using the cofiring technology. This high-temperature cofired ceramic (HTCC) technology has the advantages of mechanical rigidity and hermeticity, which are needed in high-reliability and high-performance devices to guard against moisture, heat, thermal expansion, and corrosive elements. Distributed circuit elements such as transmission lines, transformers, filters, directional couplers, and combiners can be integrated on the same substrate with microwave monolithic integrated circuit (MMIC) to form a complete high-performance microwave module.

The performance of many standard antennas can be enhanced by loading with a dielectric material. For example, a wire monopole antenna as shown in Figure 4.12 can be coated with a dielectric material to extend its electrical length while maintaining the frequency characteristics and physical length as reported in [31–33]. The coating not only reduces the required length of the antenna for resonance but also provides insulation between the metallic wire and the surrounding medium. In addition to size reduction, dielectric loading can also increase the frequency bandwidth of

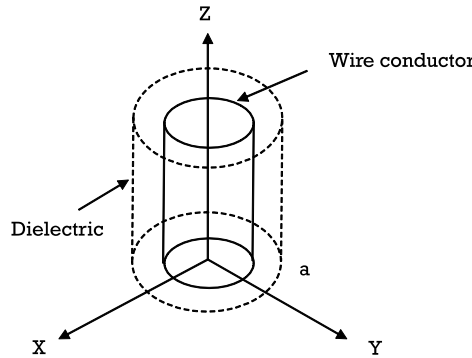


**Figure 4.12** Wire antenna coated with dielectric material.

a monopole antenna when the dielectric is located and sized properly [34]. Figure 4.13 illustrates such a monopole with epoxy dielectric in a thin disc placed on top of the ground plane. Another typical antenna that often uses dielectric loading is the helical antenna. As reported in [35], a novel structure of loading with ceramic stub can reduce the size of an axial mode helix antenna by a factor of 4 while maintaining comparable radiation properties to a conventional helix with the same number of turns. Similarly, a quadrifilar helix antenna loaded with a hollow ceramic rod with dielectric constant of 40 can reduce its size significantly with only 2.7% of an air-loaded quadrifilar helix antenna in volume [36].

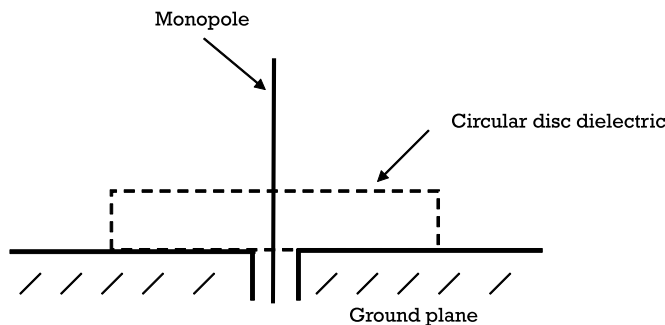


**Figure 4.13** Dielectric-loaded monopole for bandwidth enhancement.

## References

- [1] Balanis, C. A., *Antenna Theory: Analysis and Design*, New York: John Wiley & Sons, 1997.
- [2] Volakis, J., C. -C. Chen, and K. Fujimoto, *Small Antennas: Miniaturization Techniques & Applications*, New York: McGraw-Hill, 2009.
- [3] Hui, L., et al., "A Small Printed Antenna for Bluetooth Wireless Communication," *Progress in Electromagnetics Research Symposium Proceedings*, July 2015, pp. 2190–2194.
- [4] Zhu, Q., K. Fu, and Y. Li, "The Analysis of Planar Inverted-F Antennas with Equivalent Models," *Journal of University of Science and Technology of China*, Vol. 35, No. 2, April 2005, pp. 144–147.
- [5] Gallo, M., et al., "Design of an Inverted F Antenna by Using a Transmission Line Model," *Proceedings of the 5th European Conference on Antennas and Propagation*, April 2011, pp. 635–637.
- [6] Jung, J., H. Lee, and Y. Lim, "Modified Meander Line Monopole Antenna for Broadband Operation," *Electronics Letters*, Vol. 43, No. 22, 2007, pp. 508–510.
- [7] Misman, D., et al., "The Effect of Conductor Line to Meander Line Antenna Design," *Antennas and Propagation Conference Proc.*, March 2008, pp. 17–18.
- [8] Khaleghi, A., "Dual Band Meander Line Antenna for Wireless LAN Communication," *IEEE Trans. on Antennas and Propagation*, Vol. 55, No. 3, 2007, pp. 1004–1009.
- [9] National Instruments, "NI AWR Design Environment," product home page and trial version download, 2019, <http://www.awr.com/software/products/ni-awr-design-environment>.
- [10] Fenwick, R. C., "A New Class of Electrically Small Antennas," *IEEE Trans. on Antennas and Propagation*, Vol. 13, May 1965, pp. 379–383.
- [11] Rashed, J., and C. T. Tai, "A New Class of Wire Antennas," *IEEE Antennas and Propagation Society International Symposium*, Vol. 20, 1982, pp. 564–567.
- [12] Rashed, J., and C. T. Tai, "A New Class of Resonant Antennas," *IEEE Trans. on Antennas and Propagation*, Vol. 39, September 1991, pp. 1428–1430.
- [13] Nakano, H., et al., "Shortening Ratios of Modified Dipoles," *IEEE Trans. on Antennas and Propagation*, Vol. 32, April 1984, pp. 385–386.
- [14] Tsutomu, E., et al., "Resonant Frequency and Radiation Efficiency of Meander Line Antennas," *Electronics and Communications in Japan*, Vol. 83, 2000, pp. 52–58.
- [15] Liao, W. -J., S. -H. Chang, and L. -K. Li, "A Compact Planar Multiband Antenna for Integrated Mobile Devices," *Progress in Electromagnetics Research*, Vol. 109, 2010, pp. 1–16.

- [16] Sze, J. -Y., and T. -H. Hu, "Compact Dual-Band Annular-Ring Slot Antenna with Measured Grounded Strip," *Progress in Electromagnetics Research*, Vol. 95, 2009, pp. 299–308.
- [17] Ku, C. H., et al., "Folded Dual-Loop Antenna for GSM/DCS/PCS/UMTS Mobile Handset Applications," *IEEE Antennas and Wireless Propagation Letters*, Vol. 9, 2010, pp. 998–1011.
- [18] Wang, C. -J., and C. -H. Lin, "A Circularly Polarized Quasi-Loop Antenna," *Progress in Electromagnetics Research*, Vol. 84, 2008, pp. 333–348.
- [19] Bhatti, R. A., Y. -T. Im, and S. -O. Park, "Compact PIFA for Mobile Terminals Supporting Multiple Cellular and Non-Cellular Standards," *IEEE Trans. on Antennas and Propagation*, Vol. 57, No. 9, September 2009, pp. 2534–2540.
- [20] Liu, Z. D., P. S. Hall, and D. Wake, "Dual-Frequency Planar Inverted-F Antenna," *IEEE Trans. on Antennas and Propagation*, Vol. 45, No. 10, October 1997, pp. 1451–1458.
- [21] Li, P., et al., "A Novel Quad-Band (GSM850 TO IEEE 802.11A) PIFA for Mobile Handset," *Progress in Electromagnetics Research*, Vol. 137, 2013, pp. 539–549.
- [22] Sanchez-Montero, R., et al., "Hybrid PIFA-Patch Antenna Optimized by Evolutionary Programming," *Progress in Electromagnetics Research*, Vol. 108, 2010, pp. 221–234.
- [23] Li, G., et al., "Design of a Compact UWB Antenna Integrated with GSM/WCDMA/WLAN Bands," *Progress in Electromagnetics Research*, Vol. 136, 2013, pp. 409–419.
- [24] Chi, Y. -J., and C. -W. Chiu, "Hex-Band Multi-Standard Planar Antenna Design for Wireless Mobile Terminal," *Advanced Transmission Techniques in WiMAX*, InTech, January 18, 2012.
- [25] Fujimoto, K., and H. Morishita, *Modern Small Antennas*, New York: Cambridge University Press, 2013.
- [26] Walter, C. H., *Travelling Wave Antennas*, New York: Dover, 1965.
- [27] Chang, K. (ed.), *Encyclopedia of RF Microwave Engineering*, Vol. 3, New York: John Wiley & Sons, 2005, pp. 4744–4760.
- [28] Skyworks Solutions, Inc., "Technical Ceramics Dielectric and Magnetic Materials," *Technical Brochure*, 2017.
- [29] Imanaka, Y., *Multilayered Low Temperature Cofired Ceramics (LTCC) Technology*, New York: Springer, 2005.
- [30] Ullah, U., et al., "Antenna in LTCC Technologies: A Review and the Current State of the Art," *IEEE Antennas and Propagation Magazine*, Vol. 57, No. 2, April 2015.

- [31] Adekola, A., A. I. Mowete, and A. Ogunsola, "On the Problem of Dielectric Coated Thin Wire Antenna," *Progress in Electromagnetics Research Symposium Proceedings*, August 18–21, 2009, pp. 4744–4760.
- [32] Lamensdorf, D., "An Experimental Investigation of Dielectric Coated Antennas," *IEEE Trans. on Antennas and Propagation*, Vol. 15, No. 6, 1967, pp. 767–771.
- [33] Moore, J. and M. A. West, "Simplified Analysis of Coated Wire Antennas and Scatterers," *Proc. IEE Microwave and Antennas Propag.*, Vol. 142, No. 1, February 1995, pp. 14–18.
- [34] Zivkovic, I., "Dielectric Loading for Bandwidth Enhancement of Ultra-Wide Band Wire Monopole Antenna," *Progress in Electromagnetics Research*, Vol. 30, 2012, pp. 241–252.
- [35] Rahim, T., "Theory of Helix Antenna," *ResearchGate Publication*, February 16, 2015.
- [36] Wang, Y. -S., and S. -J. Chung, "A Miniature Quadrifilar Helix Antenna for Global Positioning Satellite Reception," *IEEE Trans. on Antennas and Propagation*, Vol. 57, No. 12, December 2009.



## **CHAPTER**

# **5**

### **Contents**

- 5.1 Introduction
- 5.2 Electromagnetic Simulation Methods
- 5.3 Antenna Simulation Tools

## **Electromagnetic Simulation and Software**

### **5.1 Introduction**

As illustrated in Chapters 1 and 2, the required mathematics are quite involved in order to find an analytical expression of the basic antenna parameter such as the radiation resistance of a simple antenna structure of a monopole or dipole. It would be even more difficult or impossible to find the analytical solution for more advanced antennas with a complicated structure as presented in Chapter 3. To minimize the design effort and shorten the development time, electromagnetic simulators can be used to predict and optimize the antenna performance. Computer-aided analysis and optimization is so efficient that it is now replacing the traditional trial-and-error design approach.

There are many different software packages, both commercial and free on the market. Despite being free of charge, some of the free design tools can be used to design many standard antennas such as monopole and helical

antennas. This chapter will introduce some of the commonly used electromagnetic simulators on the market.

## 5.2 Electromagnetic Simulation Methods

Most electromagnetic simulators try to find the numerical solution of Maxwell's equations in differential or integral form. Integral-equation methods, such as the Method of Moments (MoM), use the integral-equation form of Maxwell's equations to formulate the electromagnetic problem. The Green's function tensor is the kernel of the integrals. The differential equation methods on the other hand are derived from Maxwell's curl equations. The finite element method (FEM), the finite-difference time-domain method (FDTD), and the finite integration technique (FIT) are the most popular differential-equation-based methods derived directly from Maxwell's curl equations. They try to solve the partial differential equations of the electromagnetic problem. Except the MoM, which is a surface-discretization method, all the other mentioned methods are volume-discretization-based.

### 5.2.1 MoM

The MoM is the boundary element method in solving electromagnetic problems. It is a numerical computational method of solving linear partial differential equations [1] being formulated as integral equations. It makes use of Maxwell's equations in integral equation form to formulate the electromagnetic problem in terms of unknown currents flowing on the object. The interaction between the currents and the fields can be described by the kernel of the integrals and formulated by the Green's function tensor. Since the problem formulated by the Green's function tensor already includes the electromagnetic influence by infinite space, simulation covers the surrounding environment without making any approximations. The corresponding solution thus covers all the background medium space. One of the most important antenna analyses, the far-field radiation, is also included in the solution automatically and analytically.

The MoM [2] has been popular since the 1980s as it calculates only the boundary values instead of the values over the whole space. It basically models the antenna structure with small metallic surface patches and applies the boundary conditions upon those surface patches. It is very computationally efficient for small surface-to-volume ratio [3]. In many other problems, it is significantly less efficient than the volume-discretization methods such as the FEM to be discussed in the next section.

Since MoM typically requires fully populated matrices for computation, the storage requirements and computational time will grow according to the square of the problem size. It is less computationally efficient as compared to the FEMs in which the storage requirements grow linearly with the problem size.

### 5.2.2 Differential Equation Techniques

The most popular differential equation-based methods are the FEM, the FDTD method, and the FIT. They are derived simply from Maxwell's curl or the Helmholtz wave equations. The differential equation techniques are very efficient solving small and full 3-D volumetric geometry with inhomogeneous media where the element is discretized. As the number of unknowns is proportional to the resolution and the volume to be modeled, these techniques will be less effective when solving open-space problems where the number of discretized element is enormous. The open-space issue can be alleviated by applying the approximation techniques such as the absorbing boundary conditions and perfectly matched layers (PML) to truncate the space to be analyzed.

#### 5.2.2.1 FEM

Being a frequency-domain solver, the FEM [3–6] is a method based on solving partial differential equations formulated by a variational expression. It divides space into elements of tetrahedron which are the simplest volume entities. Using tetrahedrons has the advantage of approximating arbitrary geometries. Fields inside the tetrahedrons are expressed as a number of basic polynomial functions. The variation of the functions is set to zero which yields a large linear system of equations. A matrix eigenvalue is solved to find the fields at all the nodes at each frequency.

Two typical methods can be used to solve the linear systems of equations, namely, the direct and iterative solvers. The direct solver finds the system solution directly resulting from the FEM discretization. Although the memory requirement is very high as it increases quadratically with the number of tetrahedrons, multiple-port excitation can be simulated simultaneously. However, the iterative solver uses a special algorithm to transfer the original system of equations into a new one in an attempt to minimize the system error. The iterative process repeats until the system error reaches a predefined minimum. While the iterative solver may take longer than the direct solver to reach the final solution depending on the iteration step

chosen, the memory requirement is much less. Frequency-domain solver is particularly suitable in solving problems with periodicity such as phased arrays, frequency-selective structures, and bandgap antennas.

### 5.2.2.2 FDTD

The FDTD [7–10] technique is a grid-based, differential time-domain numerical modelling method. Maxwell's equations in partial differential form are modified to central-difference equations. The time derivative of the H-field is dependent on the curl of the E-field, while the time derivative of the E-field is dependent on the curl of the H-field. The electric field is solved at a given instant in time and the magnetic field is solved at the next instant. The process is repeated in a cyclic manner with a time-stepping algorithm introduced by Yee [7]. These waves propagate in the 3-D Yee's lattice in which appropriate values of permittivity and permeability to each electric field and magnetic field components can be assigned, respectively, without slowing the speed of computation. Such versatility makes FDTD technique efficient when simulating 3-D antenna structures with inhomogeneous media.

FDTD is a popular and easy-to-understand computational electromagnetic (CEM) technique in which the implementation is very simple as a full-wave solver. It is much easier to implement a basic FDTD solver than the MoM and FEM solvers. If the time step is small enough, solutions with a wide frequency range can be found with a single simulation since it is a time-domain method.

### 5.2.2.3 FIT

The FIT [11–13] discretizes the integral form of Maxwell's equations in meshes with unknowns of electric voltages and magnetic fluxes on the mesh faces. It is a spatial discretization technique to solve the field problems numerically in time and frequency domains with preservation of basic properties of the continuous equations such as conservation of charge and energy. The approach of this technique is to apply the Maxwell equations in integral form to a set of discretized grids. It has not only very high flexibility in geometric modeling and boundary handling but also can use arbitrary material distributions and material properties such as dispersion, nonlinearity, and anisotropy.

The FIT has been enhanced over the years since its introduction in 1977 [11]. This technique is the basis for many commercial simulation tools since

it covers the full range of electromagnetics from DC up to high frequency as well as the optical applications. With its unique dual-orthogonal grid and explicit time integration scheme, FIT is computational and memory-efficient, which is important for transient field analysis in radio frequency and microwave applications [12].

#### 5.2.2.4 Transmission Line Matrix Method

The transmission line matrix (TLM) [14] method is a space and time-discretizing technique to compute 3-D electromagnetic structures. It is a special FDTD technique with a mesh of transmission lines interconnected at nodes as the computational domain. The method is based on Huygens' model of wave propagation and scattering. The propagation and scattering of voltage impulses through the network are analogous to the propagation of electromagnetic fields in arbitrary media. Since it is a time-domain simulator, the reflected voltage impulses due to the incident impulses can be computed by the scattering matrix. They then propagate to the neighboring nodes for the next time step as incident voltage impulses. The electromagnetic fields can then be computed by the incident voltage impulses. The transmission line matrix can be solved directly by a circuit solver such as the commonly known simulation program with integrated circuit emphasis (SPICE) or the derivative of SPICE from U.C. Berkely, HSPICE.

TLM can compute complex 3-D electromagnetic structures with different permeability, permittivity, and electric and magnetic conductivities. It can also run free-space simulation by applying the PML technique. Similar to the FDTD method, TLM is one of the most powerful time-domain simulation methods.

### 5.3 Antenna Simulation Tools

There are not many antenna-only design tools on the market as most of them are part of their electromagnetics or microwave design suites. Both antenna-only and electromagnetic simulation tools will be addressed in this section. Since most commercial antenna or electromagnetic simulators are very expensive, it is worth the effort to understand their capabilities, features, and limitations before the final purchase decision is made.

Despite being free of charge, some of the noncommercial design tools can be used for many standard antennas such as monopole, helical, or patch antennas. Those tools will be adequate if the objective is to design a particular antenna for a particular wireless product.

### 5.3.1 Numerical Electromagnetics Code

Based on the MoM technique, the Numerical Electromagnetics Code (NEC) [15–17] is a very popular antenna simulation tool for wire and surface antennas. It uses an interactive method to find the solutions of the integral equation of the electric and magnetic fields. The currents on the wires are then found based on the MoM solution to calculate the antenna impedance and the radiation pattern.

NEC was first developed by Lawrence Livermore National Laboratory in the 1970s. Since the code was released for public use, many commercial and noncommercial versions such as NEC-2 to NEC-4 [18], MININEC [19], EZnec [20], or MMANA-GAL [21] were developed based upon the original code or the same underlying methods.

NEC breaks the antenna into a number of segments for analysis. With an iterative solver, NEC determines the induced voltages and currents at each of these segments based on the diameter of the conductor and the operating frequency. In some arrangements of the wires that the induced currents will reinforce or cancel the currents in other wires, NEC will sum them up to determine the net current in each of the conductors. Once all the currents in each conductor are known, the resultant radiation characteristic can then be calculated.

As an illustration, a very popular Yagi antenna as shown in Figure 5.1 is simulated with a free version of MMANA-GAL antenna design software.

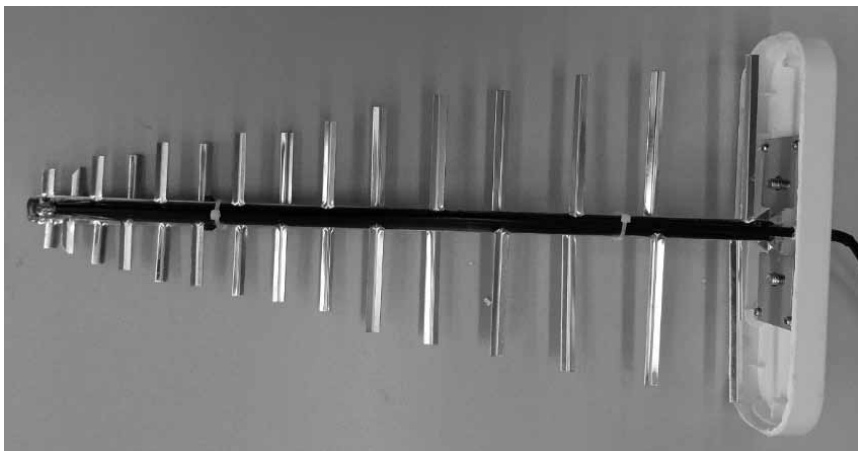


**Figure 5.1** A 15-element Yagi antenna. (Courtesy of Lexiwave Technology (Hong Kong) Limited.)

The antenna is modeled by wire segments and its geometry can be entered by the simple graphical input or tabular form as shown in Figure 5.2. For simplicity, only six elements are modeled in the simulator. Once the antenna is constructed and the operating frequency is specified, the solver can find the solutions almost instantaneously. The 3-D radiation pattern can then be plotted as shown in Figure 5.3 along with the calculated results of gain, front-to-back ratio, and input impedance. Larger or more complicated antennas will require the professional version, which allows more segments to be simulated along with more features.

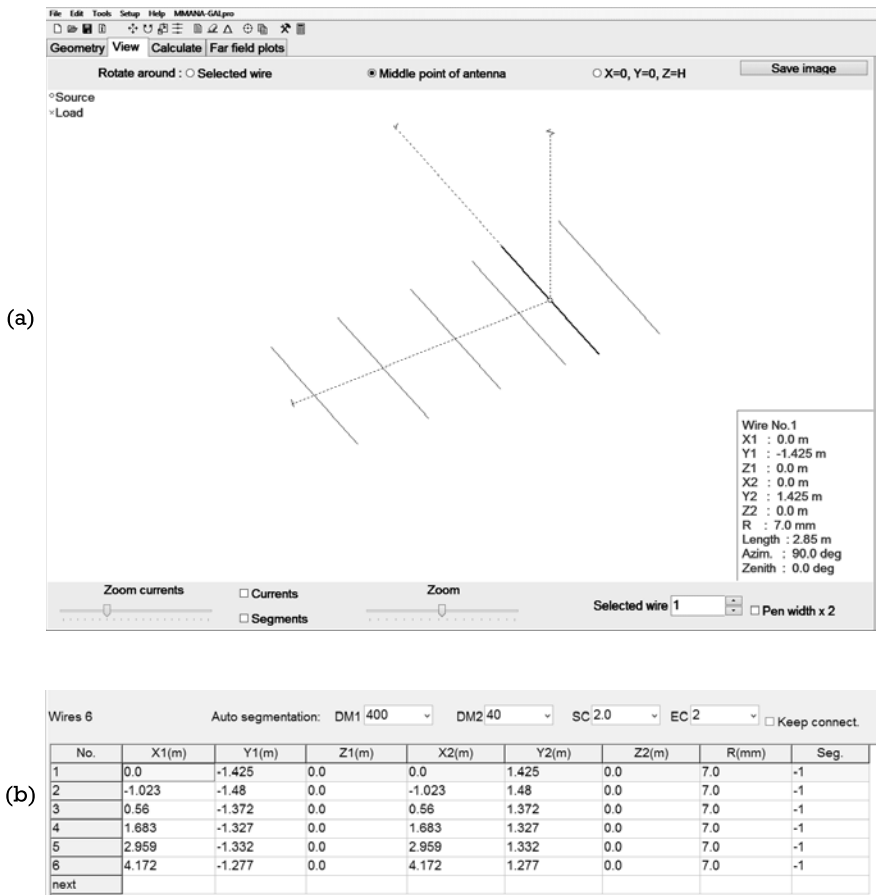


**Figure 5.2** (a) A six-element Yagi antenna modeled by wires in MMANA-GAL, and (b) the geometry of the Yagi antenna can be provided in a table.

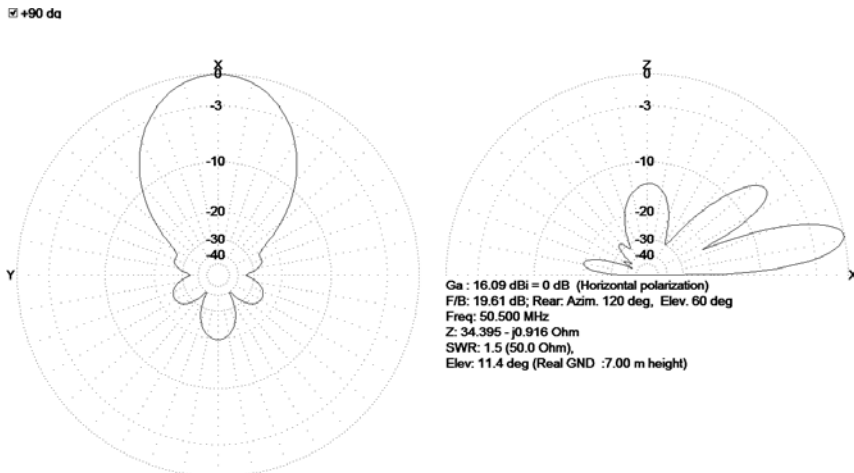


**Figure 5.3** Radiation pattern after simulation.

### 5.3.2 Momentum

As a design module of the ADS Design Suite of Keysight, Momentum [22] is 3-D planar electromagnetic simulation software that solves the integral equations with the MoM. It was developed as a 3-D planar simulator for passive circuit analysis. Combining full-wave and quasi-static electromagnetic solvers, it provides insight into electromagnetic behavior of RFIC, MMIC, RF board, and antenna designs. In addition to ADS, the Momentum simulation engine is also integrated in Genesys and Cadence Virtuoso software packages to support various design flows and applications. This allows cosimulation of integrated circuits (ICs), packages, and boards in high-frequency and high-speed applications. The visualization of surface currents and planar antenna radiation in 3-D space provides valuable insights for engineers to identify the locations of problem areas. Its model composer creating custom parameterized electromagnetic-based component libraries allows engineers to run simulations and optimization much easier and faster.

### 5.3.3 FEKO

Similar to Momentum, FEKO [6, 23, 24] is also based on the MoM. It combines with other methods such as FEM, FDTD, Physical Optics Approach (GO), and Unified Theory of Diffraction (UTD) to analyze a broad spectrum of electromagnetic problems related to antenna design and placement,

radar cross section and electromagnetic compatibility. Truly arbitrary 3-D structures can be modeled by the solver with dielectric volumes solved in the Surface Integral Equation, the Volume Integral Equation, or a hybrid approach with FEM. Its hybridization of different solvers allows efficient and accurate analysis of multiscale, complex, and electrically large problems. Its unique features include powerful meshing algorithms for surface or volume, flat or curvilinear mesh generation with adaptive or manual refinement, and modeling with metamaterials and composites.

#### 5.3.4 High-Frequency Structure Simulator

A high-frequency structure simulator (HFSS) [25] is one of the first electromagnetic tools on the market and subsequently becomes the de facto standard. The main purpose of HFSS is to design antennas and complex RF electronic circuit elements including filters, transmission lines, and packaging with 3-D visualization on electromagnetic fields. Due to its flexibility and generality, it is very popular and used extensively in industrial and product design environments. HFSS uses various electromagnetic solvers including its highly accurate FEM, the large scale MoM technique, the ultra-large scale asymptotic methods of physical optics (PO), and shooting and bouncing rays (SBR) to solve a wide range of microwave, RF, and high-speed digital applications. Its adaptive meshing technique automatically determines and generates the appropriate mesh/grid for the solver. Coupled with multi-threading capability, the meshing process uses a robust volumetric meshing technique to reduce the required memory size and simulation time.

#### 5.3.5 CST

As part of CST Studio Suite [26, 27], CST Microwave Studio (CST MWS) is an electromagnetic tool for 3-D simulation of high-frequency devices of antennas, filters, couplers, and planar and multilayer structures. In addition to its flagship solver module using the FIT, CST MWS also includes modules based on different time-domain and frequency-domain methods including FEM, MoM, Multilevel Fast Multipole method (MLFMM), and SBR with distinct advantages in their own domains. The time-domain solver can find the broadband behavior of the device being modeled in one simulation run given a sufficient fine time step. As a general purpose of electromagnetic simulator with automatic direct meshing and many different types of solver, CST is a close competitor to HFSS.

### 5.3.6 EM.Cube

EM.Cube [28] is a simulation suite for electromagnetic modeling of RF system engineering problems and has a highly integrated modular architecture. The core is a general-purpose parametric CAD modeling input environment CubeCAD. In addition to its core FDTD solver, it has other computational modules offering a mix of full-wave, static, and asymptotic numerical solvers in both time and frequency domains to provide the ultimate solution to many electromagnetic needs. Different meshing techniques can be used corresponding to the solvers chosen for simulation. It is one of the affordable software packages due to its modular structure. Users can start with a basic product configuration and expand it over time with higher modeling needs.

### 5.3.7 Sonnet

Sonnet [29] is another affordable and popular electromagnetic simulator on the market. It uses the shielded domain MoM technique to perform 3-D planar circuit analysis and model extraction. It provides interfaces to work with other major high-frequency CAE design tools such as Cadence Virtuoso, MATLAB, ADS, and MWO. As a stand-alone simulator, Sonnet is very easy to use with intuitive menu controls.

Its patented conformal meshing technology allows fast simulation with less memory on curved geometries and off-grid circuit elements than the regular rectangular or triangular meshing techniques. Sonnet's unique technique of Adaptive Band Synthesis (ABS) can adaptively select the frequency simulation points with uneven frequency steps on the specified frequency band. The overall simulation time is greatly reduced while maintaining high precision on the detailed spectral behavior.

### 5.3.8 WIPL-D Pro

WIPL-D Pro [30, 31] is another affordable 3-D electromagnetic simulation for RF and Microwave applications. The software can create complex 3-D models using wires, plates and predefined 3-D objects as building blocks as illustrated in Figure 5.4. Its solver is based on the MoM with quadrilateral meshing and higher-order basis functions and runs simulation with less memory requirements. With its WIPLD Pro CAD optional module, complex structures with solid modeling can be created more easily or imported from various CAD formats with fully automated meshing process. The software



**Figure 5.4** Modeling a monopole antenna on a cellular phone near a human head using WIPL-D.

package is useful for modeling and simulation on passive components such as resonators, filters, and antennas.

### 5.3.9 AWR Microwave Office

Similar to ADS Design Suite, AWR Microwave Office [32] is part of the NI AWR Design Environment platform, which provides modeling and simulation on RF and microwave components, linear and nonlinear circuits, systems, and electromagnetic cosimulations. The user interface is intuitive and friendly, providing project management and design entry on high-frequency circuits and systems from a comprehensive library of RF components. Its simulation solvers include APLAC, AXIEM, and Analyst. APLAC is a harmonic-balance simulator performing linear and nonlinear circuit analysis with various harmonic-balance modes. AXIEM is a 3-D planar electromagnetic tool to design passive structure, transmission line, large planar antenna, and patch array designs using a proprietary MoM approach for full-wave analysis. It uses a heuristic meshing approach to automatically fracture structures with triangular and rectangular elements. With its fast solver technology, complex antenna arrays can be simulated by AXIEM entirely. A rectangular patch antenna is constructed and modeled using AXIEM as shown in Figure 5.5(a). Figure 5.5(b) illustrates the design of a  $4 \times$

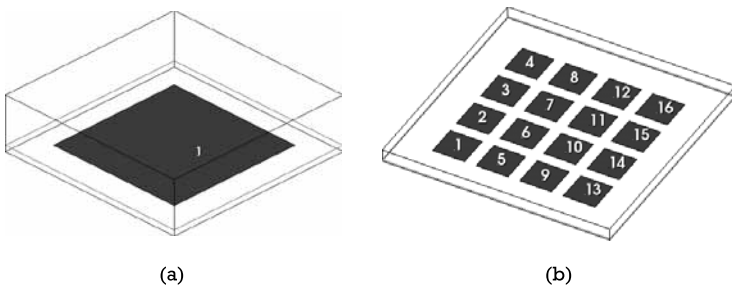


**Figure 5.5** (a) Modeling of a single patch antenna as a basic element using AXIEM, and (b) a  $4 \times 4$  antenna array consisting of 16 basic patch elements.

4 antenna array using 16 single-patch elements. Its antenna postprocessing function not only visualizes surface currents on antennas and provides near-field and far-field radiation patterns but also calculates key antenna parameters such as gain, directivity, efficiency, and return loss. Figure 5.6 shows the radiation pattern as well as the input impedance of the antenna array after simulation. Its adaptive meshing algorithm uses a volumetric tetrahedron meshing technique to provide meshing automatically with a minimal setup effort or manual intervention as shown in Figure 5.7. Similar to Sonnet, the simulation result will contain large error on antenna structures with finite substrate size because of the solver's inherent assumption of infinite substrate size. For a more accurate result, its full 3-D FEM simulation module Analyst can be used to model true 3-D structures with arbitrary substrate size.

### 5.3.10 Antenna Magus

Antenna Magus [33] is different from all the other software packages mentioned before as it provides not only antenna simulation but also synthesis. It helps engineers to choose and optimize antennas according to the specified parameters given a vast library of sample antennas. Each antenna can be designed for a range of target specifications such as operating frequency, impedance and gain. The synthesis algorithm adjusts the physical parameters automatically to match the design objectives. Compared to the general electromagnetic analysis tools, the analysis time for Antenna Magus is much shorter due to the approximations being made in simulation since the software knows the topology and the environment of the antenna. Another useful feature, Antenna Magus, provides is tweaking. It allows users to change the designed parameters within certain boundaries. Once the

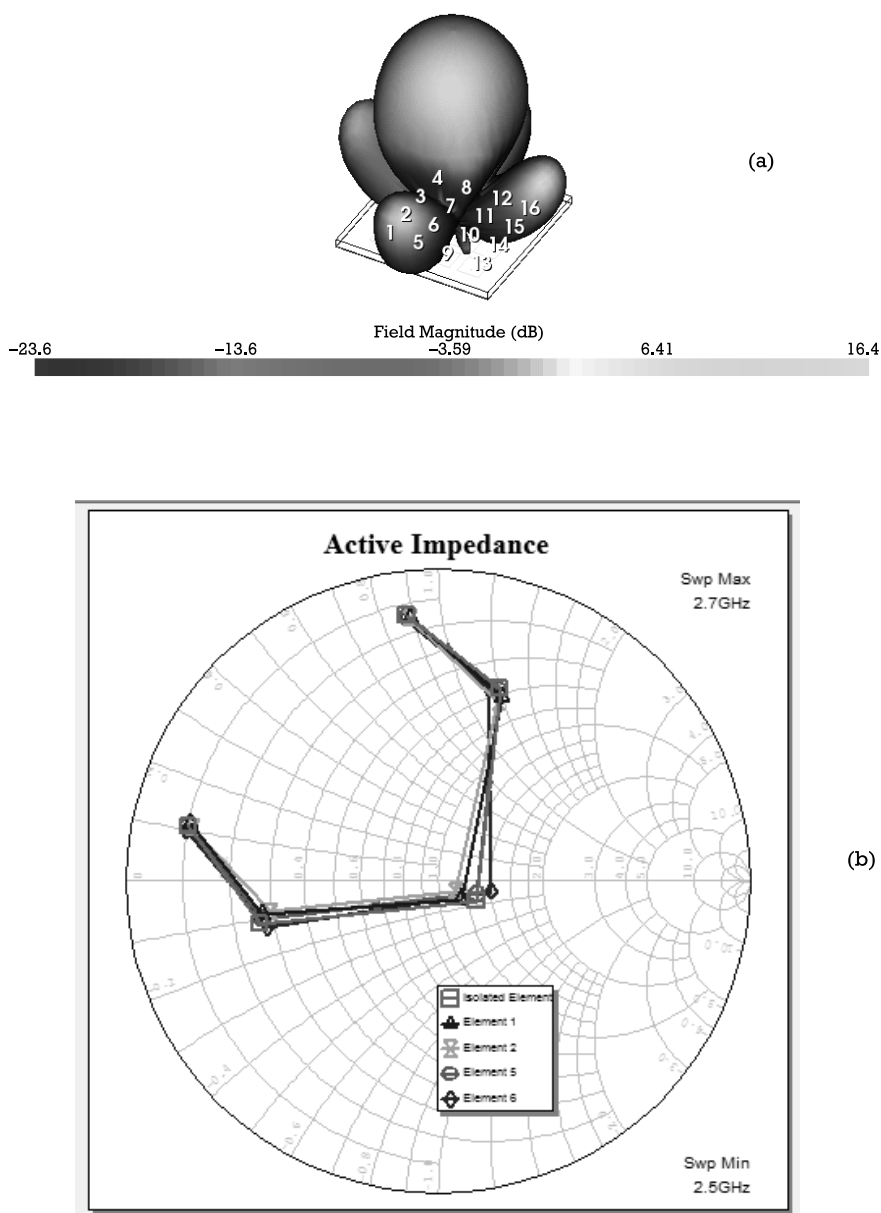


**Figure 5.6** Simulation results: (a) radiation pattern, and (b) input impedance.

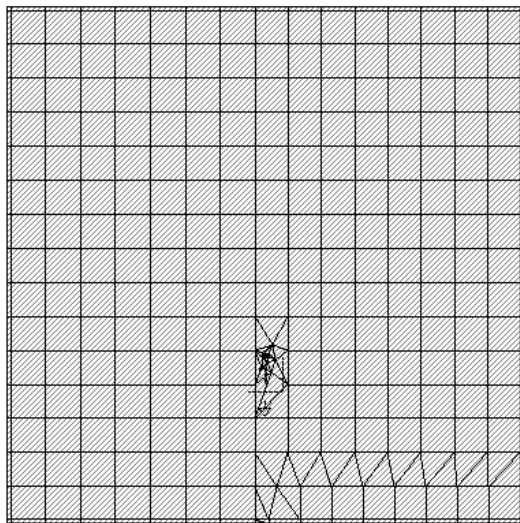


**Figure 5.7** Automatic meshing on a patch antenna with AXIEM.

design is satisfied by the engineer, it can then be exported to the general electromagnetic simulators such as FEKO or CST for further simulation and refinements.

### 5.3.11 AntSyn

AntSyn [34] is another design tool offered by National Instruments as an additional product of its AWR Design Environment platform. It is an automated antenna design, synthesis, and optimization tool, which produces antenna designs as outputs by taking the antenna engineering requirement matrix such as impedance, gain, operating bandwidth, and radiation efficiency. Different to Antenna Magus, AntSyn uses a browser-based interface and cloud-based resources for fast computation and large memory utilization. It employs a proprietary evolutionary algorithm to generate antenna structures with higher performance than would otherwise be developed by traditional methods. A diverse range of antenna types such as electrically small, phased-array, multiband, broadband, planar, or wire are available for synthesis and optimization. The final design structures can be exported to NI AWR Design Environment's software such as Microwave Office, Analyst, or CST for further simulation and optimization.

## References

- [1] "Boundary Element Method," last modified January 17, 2018, [https://en.wikipedia.org/wiki/Boundary\\_element\\_method#CITEREFWalton2008](https://en.wikipedia.org/wiki/Boundary_element_method#CITEREFWalton2008).
- [2] Harrington, R. F., *Field Computation by Moment Methods*, New York: Macmillan, 1968.
- [3] Vandenbosch, G. A. E., and A. Vasylchenko, "A Practical Guide to 3D Electromagnetic Software Tools, Microstrip Antennas," *InTech*, 2011.
- [4] Jin, J. M., *The Finite Element Method in Electromagnetics*, 2nd ed., New York: John Wiley & Sons, 2002.
- [5] Volakis, J. L., A. Chatterjee, and L. C. Kempel, *Finite Element Method for Electromagnetics*, New York: IEEE Press/Oxford University Press, 1997.
- [6] Courant, R. L., "Variational Methods for the Solution of Problems of Equilibrium and Vibration," *Bulletin of the American Mathematical Society*, 1943, pp. 1–23.
- [7] Yee, K. S., "Numerical Solution of Initial Boundary Value Problems Involving Maxwell's Equations in Isotropic Media," *IEEE Trans. on Antennas and Propagation*, Vol. 14, 1966, pp. 302–307.
- [8] Taflove, A., *Computational Electrodynamics: The Finite Difference Time Domain Method*, Norwood, MA: Artech House, 1997.
- [9] Sullivan, D. M., *Electromagnetic Simulation Using the FDTD Method*, New York: Wiley-IEEE Press, 2000.
- [10] Davidson, D. B., *Computational Electromagnetics for RF and Microwave Engineering*, Second Edition, New York: Cambridge University Press, 2014.
- [11] Weiland, T., "A Discretization Method for the Solution of Maxwell's Equations for Six Component Fields," *Electronics and Communications AEU*, Vol. 31, No. 3, 1977, pp. 116–120.
- [12] Bossavit, A., and L. Kettunen, "Yee-Like Schemes on a Tetrahedral Mesh, with Diagonal Lumping," *Int. J. Numer. Model.*, Vol. 42, 1999, pp. 129–142.
- [13] Celuch-Marcysiak, M., and W. K. Gwarek, "Comparative Study of the Time-Domain Methods for the Computer Aided Analysis of Microwave Circuits," *Int. Conf. on Comp. in Electromagnetics*, November 1991, pp. 30–34.
- [14] Weiner, M., *Electromagnetic Analysis Using Transmission Line Variables*, New York: World Scientific Publishing Company, 2001.
- [15] Gerald, B., and A. Poggio, "NEC Part I: Program Description—Theory," *Technical report*, Lawrence Livermore Laboratory, January 1981.

- [16] Gerald, B., and A. Poggio, "NEC Part II: Program Description—Code," *Technical report*, Lawrence Livermore Laboratory, January 1981.
- [17] Gerald, B., and A. Poggio, "NEC Part III: Program Description – User's Guide," *Technical report*, Lawrence Livermore Laboratory, January 1981.
- [18] Voors, A., "NEC Based Antenna Modeler and Optimizer," product homepage, <http://www.qsl.net/4nec2/>.
- [19] Lewallen, R., "MININEC: The Other Edge of the Sword," *QST Magazine*, February 1991, pp. 18–22.
- [20] W7EL, "EZNEC Antenna Software," product homepage, <https://web.archive.org/web/20161219004922/http://eznec.com/>.
- [21] Mori, M., A. Schewelew, and I. Gontcharenko, "MMANA-GAL," product homepage, <http://hamsoft.ca/pages/mmana-gal.php>.
- [22] Keysight Technologies, "Momentum 3D Planar EM Simulator," product homepage, <https://www.keysight.com/en/pc-1887116/momentum-3d-planar-em-simulator?nid=-33748.0.00&cc=US&lc=eng&cmpid=zzfindees-of-momentum>.
- [23] FEKO, HyperWorks, Altair, "High Frequency Electromagnetics and Antenna Design," product homepage, <https://altairhyperworks.com/product/FEKO>.
- [24] Altair Engineering, Inc., "Numerical Methods in FEKO," white paper.
- [25] ANSYS, "ANSYS HFSS," product brochure.
- [26] Y. Schols, W. De Raedts, and G. A. E. Vandenbosch, Computer Simulation Technology CST, "CST Microwave Studio," product homepage, <https://www.cst.com/products/cstmws>.
- [27] Vasiolchenko, A., "A Benchmarking of Six Software Packages for Full-Wave Analysis of Microstrip Antennas, Antennas and Propagation," *The Second European Conference on Antennas and Propagation*, 2007.
- [28] EMAG Technologies Inc., "EM.CURE," product home page, <https://emagtech.com/em-cube/>.
- [29] Sonnect Software, Inc. "Discover Sonnet" *Product Brochure*, <http://www.sonnetsoftware.com/>.
- [30] WIPL-D d.o.o., "WIPL-D Pro," product home page, <https://www.wipl-d.com/index.php>.
- [31] WIPL-D d.o.o., "WIPL-D Pro CAD," product home page, <https://www.wipl-d.com/products.php?cont=wipl-d-pro-cad>.
- [32] National Instruments, "NI AWR Design Environment," product home page, [http://www.awr.com/software/products/ni\\_awr\\_design\\_environment](http://www.awr.com/software/products/ni_awr_design_environment), trial version download, <http://www.awrcorp.com/try>.

- [33] Magus (Pty) Ltd, "Antenna Magus," product home page, <http://www.antennamagus.com/overview.php>.
- [34] National Instruments, "AntSyn: Antenna Synthesis Module," product home page, <http://www.awrcorp.com/products/additional-products/antsyn-antenna-synthesis-module>.



## CHAPTER

# 6

### Contents

- 6.1 Introduction
- 6.2 Measuring Equipment
- 6.3 Antenna Ranges
- 6.4 Far-Field Pattern Measurement
- 6.5 Gain Measurement
- 6.6 Directivity
- 6.7 Efficiency Measurements
- 6.8 Phase Measurement
- 6.9 Polarization Measurement
- 6.10 TRP and TIS Measurements
- 6.11 SAR Measurement

## Measurements

### 6.1 Introduction

Analytical methods for designing various standard antennas were presented in the last few chapters. For advanced antennas with complicated structures, electromagnetic simulators can be used to predict the performance. With the sophistication and advancement of the simulation tools, the characteristics of most antennas can be simulated. However, the antenna performance will be affected by the environment (i.e., finite ground plane, proximity to adjacent components, or metal objects). The task to model all the environmental conditions is quite involved and the simulation time is thus very lengthy. Measurement is more direct and effective to validate the antenna design. This chapter will highlight the measurement techniques and equipment setups on measuring the fundamental parameters of antennas. The desired measurements of an antenna include radiation pattern, gain, efficiency, impedance, and polarization.

Antenna is one of the most critical components in wireless products. Although its characteristics play a major role in determining the RF

performance of the products, other RF parameters such as specific absorption rate (SAR), total radiated power (TRP), and total isotropic sensitivity (TIS) are also important as they are examined and mandated by regulatory authorities. Due to their importance, their measurement techniques and setups will also be addressed.

## 6.2 Measuring Equipment

According to the reciprocity theorem [1], an antenna can be used as either a transmitting or receiving antenna. However, it is more convenient to perform antenna measurements with the test antenna (antenna under test) in the receiving mode as the transmitter is typically bulky and heavy. However, a receiver can be small and less expensive. If the test antenna is reciprocal, its receiving characteristics such as radiation pattern and gain should be identical to its transmitting ones. At RF and microwave frequencies, it is necessary to have frequency and output power stability to achieve precise measurements. It is therefore desirable to place the equipment on a stable and vibration-free platform. Due to such importance, the transmitting equipment is typically held stationary while the receiving equipment can be movable and rotatable.

A typical antenna measurement setup is illustrated in Figure 6.1. The source or transmitting antenna is typically a standard antenna with known antenna characteristics such as gain and radiation pattern within the testing frequency range. The antenna should also have the right polarization. The transmitter should provide a stable output power and an accurate test frequency. Preferably, the frequency can be selectable to accommodate a wide range of antennas operating in different frequencies. A wide range of affordable RF and microwave signal generators can be used as the transmitter.

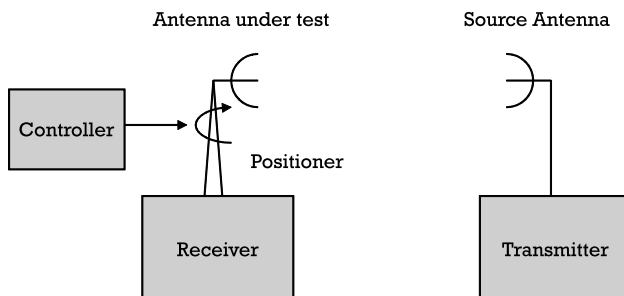


**Figure 6.1** A typical antenna measurement system.

The receiver must detect the field strength or power received from the test antenna. A simple bolometer can be used to detect the energy of incident electromagnetic waves. For a more accurate measurement with higher sensitivity, selectivity, and dynamic range, a spectrum analyzer can be used. If phase measurement is needed, a dual-channel spectrum analyzer can be used [2]. In order to measure the radiation pattern of the test antenna, a positioning system is used to rotate the test antenna in various planes.

### 6.3 Antenna Ranges

Once all the measuring equipment and antennas are available, the next critical step is to find a suitable place and environment to take the measurement. The ideal condition is to illuminate the test antenna by plane waves, which have a wave front with field vectors being constant over an area that extends well beyond the aperture of the test antenna. The condition can be approximated by placing the test antenna far from the transmitting antenna. If the distance is larger than the far-field region  $2D^2/\lambda$ , the maximum phase error of the incident field is  $22.5^\circ$  from an ideal plane wave [3]. Such a phase error is still acceptable to most measurements. Finding a test site large enough to reach the far-field requirement is typically not a big problem, but securing that it is reflection-free and interference-free is a real challenge. To have accurate measurements, it is needed to minimize unwanted reflections from nearby objects from either surrounding walls or the ground. This requires open sites (open ranges) in rural areas with flat terrain to have free-space propagation condition. Since finding a large, open site with a free-space propagation condition is a rare commodity, an alternative is to use anechoic chambers.

Besides the difficulties of finding suitable free space test sites, other challenges in antenna measurements are equipment being expensive, antenna being large to be accommodated, uncontrollable outdoor environment in outdoor sites, and the requirement of whole antenna system (e.g., on-craft mounted antenna) to be measured.

There are two types of antenna measurement sites (antenna ranges), namely, indoor and outdoor ranges. They can further be categorized as free-space ranges, reflection ranges, and compact ranges.

Free-space ranges are either indoor or outdoor measurement sites that are designed to allow reflection-free propagation. The outdoor free-space ranges are built such that all the reflections from nearby objects and the ground are suppressed as much as possible. The most popular free-space

ranges are elevated ranges, slant ranges, compact ranges, and anechoic chambers.

Elevated ranges are outdoor ranges where the source and test antennas are mounted on high towers or buildings to achieve a clear line of sight more easily for free-space propagation as shown in Figure 6.2 [3, 4]. The terrain beneath is smooth and the source antenna has high directivity so that any reflected signals from the ground or the buildings behind are minimized.

Slant ranges occupy less space than the elevated ranges as the source antenna is mounted on the ground while the test antenna is mounted on a tower (see Figure 6.3). The tower must be nonconducting and the source antenna is preferred to have low sidelobes and narrow beamwidth to minimize reflections from surrounding buildings. For low measuring frequencies, the slant ranges still require a large, open space to avoid reflections from surrounding buildings.

All the outdoor ranges discussed above have major drawbacks of uncontrollable test conditions such as being interfered by external electromagnetic sources, having reflections as well as different weather conditions. Using indoor antenna ranges such as anechoic chamber offers an excellent alternative to outdoor sites. An anechoic chamber is a large room built with steel sheets on the walls, floor, and ceiling to form a Faraday cage to shield against external interference and electromagnetic noise. All the inner surfaces of the chamber are covered by RF absorbing elements as shown in Figure 6.4. The typical shape of the absorbing element is a pyramid or wedge. While pyramids absorb incident normal waves the best, wedges work much better than pyramids for waves parallel to their ridges [3, 5]. Despite its convenience and having a controlled environment, its major drawback is size

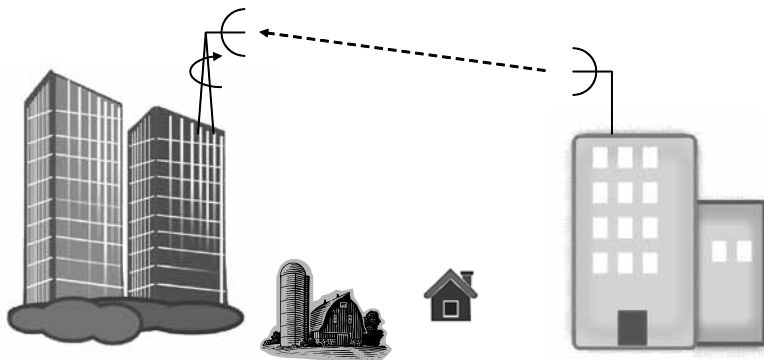


**Figure 6.2** Illustration of an elevated range.

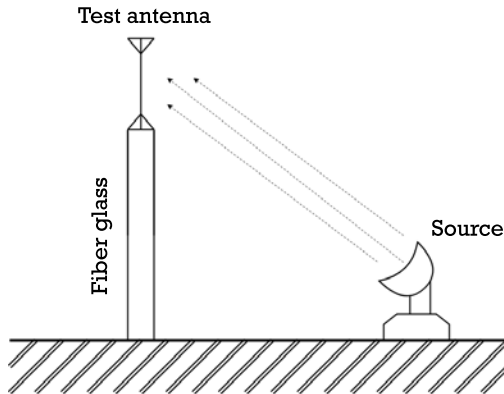


**Figure 6.3** Illustration of a slant range.

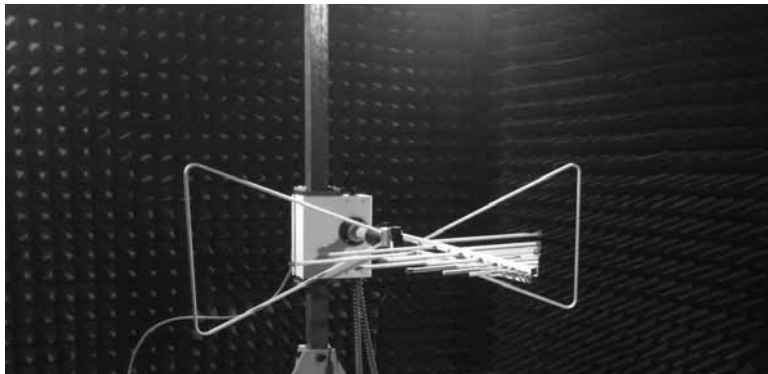


**Figure 6.4** An anechoic chamber with absorbing material. (Courtesy of Lexiwave Technology (Hong Kong) Limited.)

requirement. The antennas have to have a separation of a few wavelengths to simulate far-field conditions for accurate measurements. Although it is desirable to have the anechoic chambers as large as possible, cost and practical constraints often limit their size.

To overcome the above size problem for an anechoic chamber, compact ranges can be used. In this approach, the source antenna radiates towards a reflector with a shape that reflects the spherical wave into a plane wave (see Figure 6.5). The typical shape of the reflector is parabolic, similar to a satellite dish antenna whose size is several times that of the test antenna.

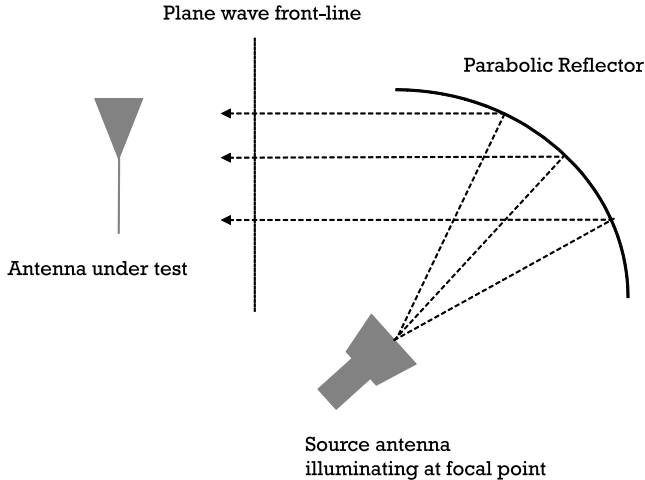


**Figure 6.5** Compact range with an offset source antenna.

In order not to block the reflected rays, the source antenna should be offset from the reflector as shown in Figure 6.5.

#### 6.4 Far-Field Pattern Measurement

Given that the equipment and a suitable antenna range are provided, antenna measurements can then be performed. The first measurement to be discussed is the far-field radiation pattern. It is measured on the surface of a sphere of constant radius. The coordinate system of choice for measurement is the spherical one such that any position on the sphere is identified by the directional angles  $\theta$  and  $\Phi$  (see Figure 6.6). As discussed earlier, the radiation pattern for the test antenna is the same for both transmit and receive modes according to the reciprocity theory. For illustration, the test antenna is measured as a receiving antenna. The test antenna is rotated using the test setup as shown in Figure 6.1 while the receiving power is measured at each position. The magnitude of the radiation pattern is then determined by the receiving power.

#### 6.5 Gain Measurement

In the previous section, the measurement of the radiation pattern of an antenna is presented. However, it is only a relative radiation pattern. The exact value of the peak gain is unknown. The measurement only provides

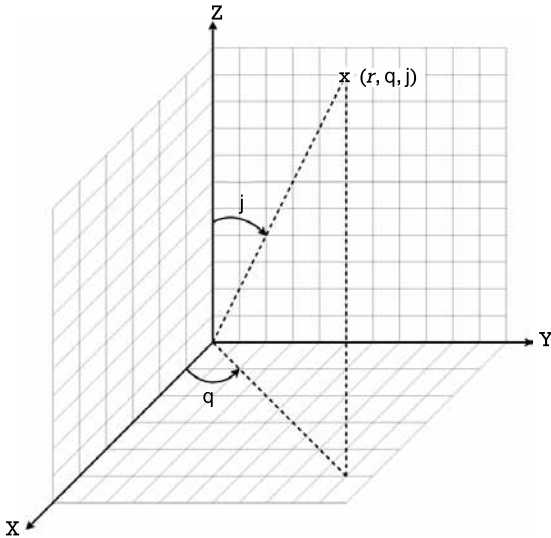


**Figure 6.6** Spherical coordinate system.

the shape of the radiation pattern which in turns indicates how directive the test antenna is. A commonly used method for gain measurement is the gain-comparison method. It requires the same environment as the pattern measurements except that a standard antenna for comparison is used. The standard antenna is a test antenna with known gain and polarization. Typical standard antennas are half-wavelength dipole antenna and pyramid horn antenna of 2.15 dB and 15–20 dB gain, respectively.

On the gain-comparison method, two sets of measurement are performed as shown in Figure 6.7. A reference transmit power  $P_o$  is injected into a transmitting antenna. Its absolute gain is not critical for the measurement. On the first measurement, the receiving power  $P_{ANT}$  is measured when putting the test antenna in receiving mode. While keeping the same setup, the receiving power  $P_{STD}$  is remeasured with the test antenna replaced by a standard antenna. It is assumed that the measuring antenna is properly matched to the receiver and oriented for maximum power. Applying the Friis's transmission formula, the gain of the two antennas relating to the transmitting antenna can be found as:

$$G_{ANT\ dB} + G_{odB} = 20 \log_{10} \left( \frac{4\pi R}{\lambda} \right) + 10 \log_{10} \left( \frac{P_{ANT}}{P_o} \right) \quad (6.1)$$

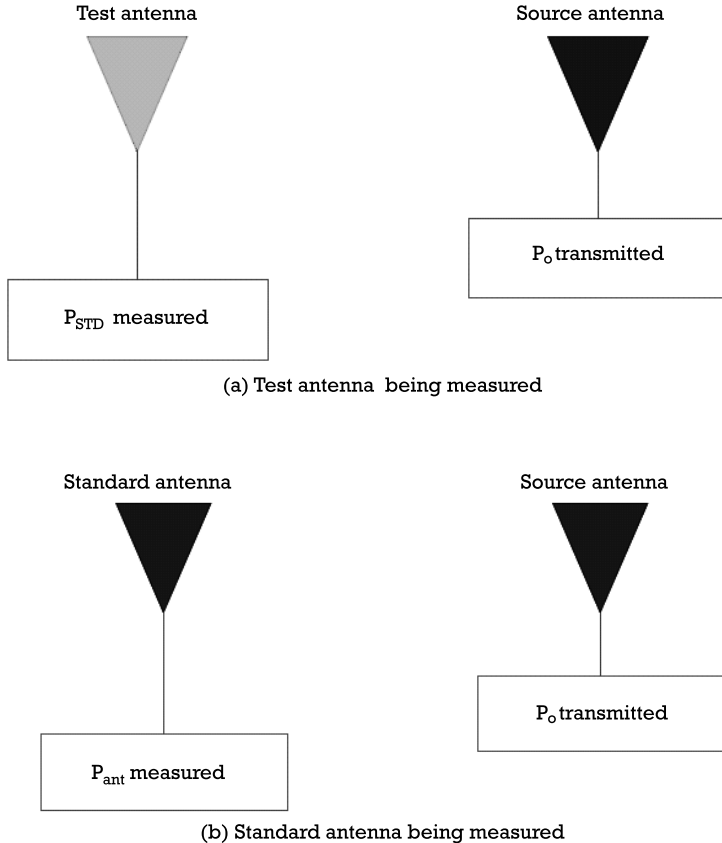


**Figure 6.7** Gain-comparison measurement.

$$G_{STD\ dB} + G_{o\ dB} = 20 \log_{10} \left( \frac{4\pi R}{\lambda} \right) + 10 \log_{10} \left( \frac{P_{STD}}{P_o} \right) \quad (6.2)$$

where  $G_{ANT}$  is the gain of the test antenna in decibels,  $G_{STD}$  is the gain of the standard antenna in decibels, and  $G_o$  is the gain of the transmitting antenna in decibels.

From (6.1), the expression on the gain of the test antenna can be found as:

$$G_{ANT\ dB} = G_{STD\ dB} + 10 \log_{10} \left( \frac{P_{ANT}}{P_{STD}} \right) \quad (6.3)$$

If the test antenna is polarized such as circularly or elliptically, two standard antennas with linear vertical and horizontal polarization have to be used to obtain the corresponding polarized field components. The total gain of the test antenna can be found by two measured field components as:

$$G_{ant\ dB} = 10 \log_{10} (G_{antv} + G_{anth}) \quad (6.4)$$

where  $G_{antv}$  is the gain of the test antenna measured by a vertically linearized standard antenna and  $G_{anth}$  is the gain of the test antenna measured by a horizontally linearized standard antenna.

## 6.6 Directivity

As illustrated in Section 2.2.4, directivity is defined as the ratio of the maximum radiation intensity to the average radiation intensity over the entire sphere as:

$$D = \frac{U(\theta, \phi)_{\max}}{U_{ave}}$$

It can be rewritten as:

$$D = 4\pi \frac{U(\theta_o, \phi_o)_{\max}}{\int_0^{2\pi} \int_0^{\pi} U(\theta, \varphi) \sin \theta d\theta d\varphi} \quad (6.5)$$

where  $U(\theta_o, \Phi_o)_{\max}$  is the max radiation intensity at direction  $\theta_o, \Phi_o$ .

In practice, the radiation intensity is sampled over a sphere of constant radius  $R$ . The optimum spacing will depend on the designed accuracy and the directive property of the antenna.

Similarly, if the test antenna is polarized, standard antennas with linear vertical and horizontal polarization have to be used to obtain the corresponding polarized components. The total directivity of the test antenna can be found by two measured components as:

$$D_{ant\ dB} = 10 \log_{10} (D_{antv} + D_{anth}) \quad (6.6)$$

where  $D_{antv}$  is the directivity of the test antenna measured by a vertically linearized standard antenna and  $D_{anth}$  is the gain of the test antenna measured by a horizontally linearized standard antenna.

Two measurements will be required if the antenna is polarized circularly or elliptically such that the total directivity can be expressed as:

$$D_o = D_\theta + D_\phi \quad (6.7)$$

where  $D_\theta$  is the partial directivity for  $\theta$ -component measurement and  $D_\phi$  is the partial directivity for the  $\phi$ -component measurement.

## 6.7 Efficiency Measurements

Recalling (2.3), the efficiency is expressed as:

$$\epsilon_r \epsilon_p = \frac{G}{(1 - |\Gamma|^2)D}$$

Assuming the antenna is perfectly matched and aligned for maximum gain, the radiation efficiency can be calculated as:

$$\epsilon_r = \frac{\text{Gain}}{\text{Directivity}} \quad (6.8)$$

where gain and directivity can be found by the measurements introduced in the previous two sections.

## 6.8 Phase Measurement

In Section 6.4, the magnitude of the receiving power is used to describe the radiation pattern. However, in order to have a complete description of the radiation pattern, the phase information is also needed in addition to the magnitude of the receiving power. Assuming an antenna transmits at a frequency of  $f$ , its fields travel in the  $y$ -direction can be expressed as:

$$E = \hat{x}A^{jC}e^{j2\pi ft} + \hat{z}Be^{jD}e^{j2\pi ft} \quad (6.9)$$

There are two independent and orthogonal components of  $E$ -field traveling along the  $x$ -axis and  $z$ -axis. Their magnitudes are  $A$  and  $B$  for the

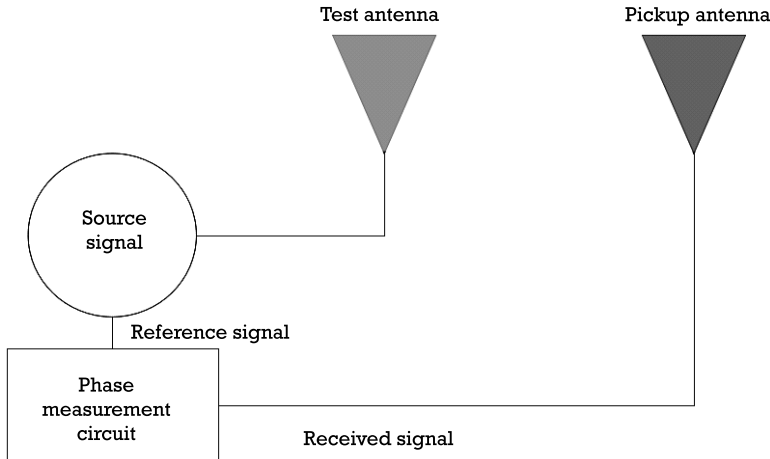


**Figure 6.8** Phase measurement setup.

$x$ -components and  $z$ -components, respectively. Their phases are C and D for the  $x$ -components and  $z$ -components, respectively.

A simple test setup as shown in Figure 6.8 can be used to measure phase. The test antenna is driven by a signal source and the signal source is also fed into a phase measurement equipment. The receiving antenna picks up the radiating field and feeds into the phase measurement equipment for phase comparison. The equipment can determine the relative phase of the field by comparing the locations of the maxima and minima of the receiving signal. The receiving antenna should be linearly polarized to pick up just one component of the receiving field. The other orthogonal component can be picked up by rotating the receiving antenna.

This measurement works well provided that the phase measurement equipment is close to the test antenna. A standard antenna with known phase characteristic can be used to compare with the test antenna to find the phase information if the test antenna is far from the equipment.

## 6.9 Polarization Measurement

Antenna polarization is determined by the axial ratio, the tilt angle, and the sense of rotation, clockwise or counterclockwise. Three typical measurement methods can be classified as (1) partial method, (2) comparison method, and (3) absolute method. The partial method such as the polarization-pattern method can produce the axial ratio and the tilt angle in a given

direction of radiation. The signal under this polarization-pattern method depends on the polarization of the test antenna as well as the angle of the probe's rotation. When testing as illustrated in Figure 6.9, the signal level is recorded and plotted against the angle of rotation. The polarization pattern is then obtained from the considered direction of radiation. Although simple in test setup and procedures, this method cannot provide the sense of rotation. In order to find the information, two circularly polarized probe antennas can be used, one being clockwise and the other being counter-clockwise. The one that gives the stronger signal determines the sense of rotation. The comparison method can provide complete polarization information as a polarization standard is used. The absolute method such as the three-antenna method can provide the complete information without the use of polarization standard.

## 6.10 TRP and TIS Measurements

The measurements discussed so far are purely on the antenna itself. As will be introduced in the subsequent chapters, the radiation characteristic of the antenna will change when it is put on the products or systems than it is alone. The TRP [6] and TIS [7] are two important parameters of wireless communication products, particularly for cellular phones. TRP is a measure of how much power a device radiates. It could be just an antenna, a complete product, or a system with the antenna. A receiving antenna measures the power radiated by the device over all angles in a 3-D measurement. The power is then summed up and the result becomes TRP.

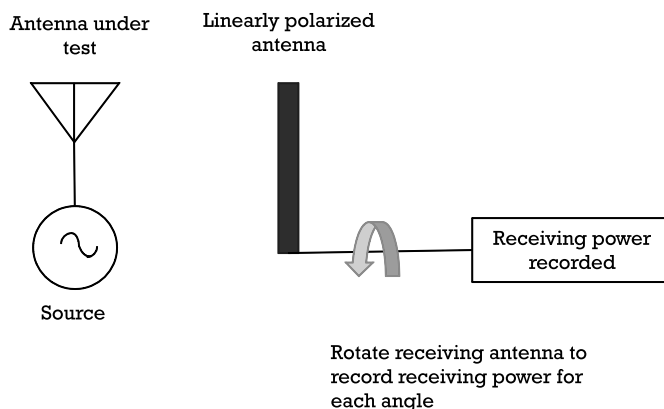


**Figure 6.9** Antenna polarization measurement.

Assuming that an antenna has a radiation pattern of  $U(\theta, \Phi)$  as expressed in (3.2), the total radiated power can be found by integrating over  $\theta$  and  $\Phi$  across a sphere as:

$$P_{TRP} = \int_0^{2\pi} \int_0^{\pi} U(\theta, \phi) \sin \theta d\theta d\phi \quad (6.10)$$

To account for the polarization property of the device, the power due to the vertical and horizontal fields has to be measured. Equation (6.10) can be rewritten as:

$$P_{TRP} = \int_0^{2\pi} \int_0^{\pi} (U_\theta(\theta, \phi) + U_\phi(\theta, \phi)) \sin \theta d\theta d\phi \quad (6.11)$$

TRP is an effective and direct way to know how well the antenna and the radio device as a whole transmits signal power. It is also one of the key technical requirements for a cellphone to be certified by wireless carriers. Without the certification, the cellphone is not allowed to connect to the carrier network.

TIS is also a key parameter to be specified and certified by wireless carriers. Similar to TRP, TIS is a parameter that depends not only on the antenna but also the radio. The sensitivity of a receiver is the smallest amount of signal received by a receiver for a reliable communication. For an analog modulation system such as FM radio, the figure of merit for reliable reception is a 12-dB signal-to-noise ratio at the audio output. For a digital modulation system, the threshold would be represented in bit-error rate (BER) of, for example, 1% at the baseband.

Similar to TRP, TIS can be found by measuring the average sensitivity of a receiving device over the entire 3-D sphere. The device is put inside an anechoic chamber for measurement. The transmit antenna is fed with an RF signal with modulation from a signal generator or a communication test set. For testing with a signal generator, the device will need to have a way to indicate the success of reliable reception such as producing an audible sound or flashing a light-emitting diode (LED). It would be more convenient if using a communication tester as the digital data output from the device can be fed to the same tester for BER detection and determination. The transmit power level is lowered until the sensitivity threshold is reached. The power

found is the effective isotropic sensitivity  $EIS(\theta_o, \Phi_o)$  for a particular angle. TIS is the average EIS value over the entire sphere of angles as:

$$TIS = \frac{4\pi}{\int_0^{2\lambda\pi} \left[ \frac{1}{EIS_\theta(\theta_o, \phi_o)} + \frac{1}{EIS_\phi(\theta_o, \phi_o)} \right] \sin \theta_o d\theta_o d\phi_o} \quad (6.12)$$

## 6.11 SAR Measurement

SAR [8] is a measure of how much RF energy is absorbed by human body and is defined as the power absorbed per unit mass of tissue. It is usually averaged over a small volume or the whole body and can be defined from the electric field within the tissue as:

$$SAR = \frac{1}{Vol} \int_S \frac{\sigma(r) |E(r)|^2}{\rho(r)} dr \quad (6.13)$$

where  $\sigma$  is the sample electrical conductivity,  $\rho$  is the density of the sample,  $E$  is the electric field in root mean square (RMS), and  $Vol$  is the volume of the sample.

SAR is critical to cellphone design particularly on the antennas, as all cell phones must meet the U.S. Federal Communications Commission (FCC) or European Union's (EU) RF exposure standard if they are sold in the United States or Europe, respectively [9]. The FCC or EU has set a limit in a concern that the cellphone users may suffer health issue if their brains are exposed to too much RF radiation. The antenna design is critical to the SAR level as its radiation efficiency and location determine how much power the cellphone will radiate to the head of the user. The SAR level can be lowered by reducing the output power of the power amplifier on the transmitter. However, there is another key parameter, TRP, which is also governed by the carrier companies to ensure a minimum average TX power over all angles for reliable communication. The requirements on SAR and TRP are thus contradictory. One way to solve the dilemma is to place the antenna at the bottom of the cellphone. It will thus not radiate too much to the user's head while maintaining the required TRP level.



**Figure 6.10** SAR test set. (Source: DASY6-The Gold Standard SAR Testing and Beyond, product poster. Reprinted with permission of Schmid & Partner Engineering AG.)

Specialized equipment has to be used to measure SAR on radiation from cellular phones as shown in Figure 6.10. It has a robotic arm moving a measuring probe along a hollow tub. The tub replicates the shape of a human head and is filled with fluid to simulate the human tissue with correct conductivity and density. The fluids will be different for difference frequencies as the property of human issue is frequency-dependent. The cellular phone is placed on the edge of the tub so that the probe can measure its transmit power through the head region [10].

## References

- [1] IEEE Standard Test Procedures for Antennas, IEEE Std. 149-1979, 1979, distributed by Wiley-Interscience.
- [2] Balanis, C. A., *Antenna Theory: Analysis and Design*, New York: John Wiley & Sons, 1997.
- [3] Kraus, J. D., *Antennas*, New York: McGraw-Hill, 1988.
- [4] “Monopole Antenna: Antenna Theory,” <http://www.antenna-theory.com/antennas/monopole.php>.

- [5] DeWitt, B. T., and W. D. Burnside, "Electromagnetic Scattering by Pyramidal and Wedge Absorber," *IEEE Trans. on Antennas and Propagation*, 1988.
- [6] "Total Radiated Power (TRP) – Antenna Theory," <http://www.antenna-theory.com/definitions/trp.php>.
- [7] "Total Isotropic Sensitivity (TIS) – Antenna Theory," last modified October 25, 2016, <http://www.antenna-theory.com/definitions/tis.php>.
- [8] U.S. Federal Communications Commission, "Specific Absorption Rate (SAR) for Cellular Telephones," Proceedings & Actions, <https://www.fcc.gov/general/specific-absorption-rate-sar-cellular-telephones>.
- [9] Means, D. L., and K. W. Chan, "Evaluating Compliance with FCC Guidelines for Human Exposure to Radio Frequency Electromagnetic Fields," Office of Engineering and Technology, Federal Communications Commission, June 2001.
- [10] "Human Exposure to Radio Frequency Fields from Hand-Held and Body-Mounted Wireless Communication Devices - Human Models, Instrumentation, and Procedures—Part 1: Procedure to Determine the Specific Absorption Rate (SAR) for Hand-Held Devices Used in Close Proximity to the Ear (Frequency Range of 300 MHz to 3 GHz)," IEC 62209-1:2005, IEC Standard, <https://webstore.iec.ch/publication/6588>.

## CHAPTER

# 7

### Contents

- 7.1 Introduction
- 7.2 Impedance Matching
- 7.3 Smith Chart
- 7.4 Matching Topology and Elements
- 7.5 Matching Elements
- 7.6 Practical Considerations

## Impedance Matching

### 7.1 Introduction

Chapter 6 highlighted the measurement techniques and equipment setups for measuring the fundamental parameters of antennas including radiation pattern, gain, efficiency, and polarization. Another important parameter, impedance, was not addressed in Chapter 6, but is included in this chapter for detailed discussions as it relates directly to the design effort on impedance matching. It plays a very important role in determining the overall efficiency of an antenna (see Section 2.2.8). The basic theory of S-parameters will be covered, followed by an introduction on impedance measuring equipment such as the network analyzer. Different matching topologies and matching elements will be presented. The high-frequency characteristic of the matching elements will be discussed and their effects on the antenna will be highlighted. Practical considerations on impedance measurement and designing the matching networks will also be presented in detail.

## 7.2 Impedance Matching

According to the maximum power transfer theorem [1–3], the resistance of the load must equal the resistance of the signal source to obtain the maximum external power from the source with finite internal resistance as:

$$R_s = R_L \quad (7.1)$$

The theorem can be extended to AC circuit that maximum power transfer occurs when the load impedance equals the complex conjugate of the source impedance as shown in Figure 7.1

$$Z_L = Z_s^* \quad (7.2)$$

where  $Z_L$  is the complex source impedance of  $R_L + X_L$  and  $Z_s$  is the complex source impedance of  $R_s + X_s$ .

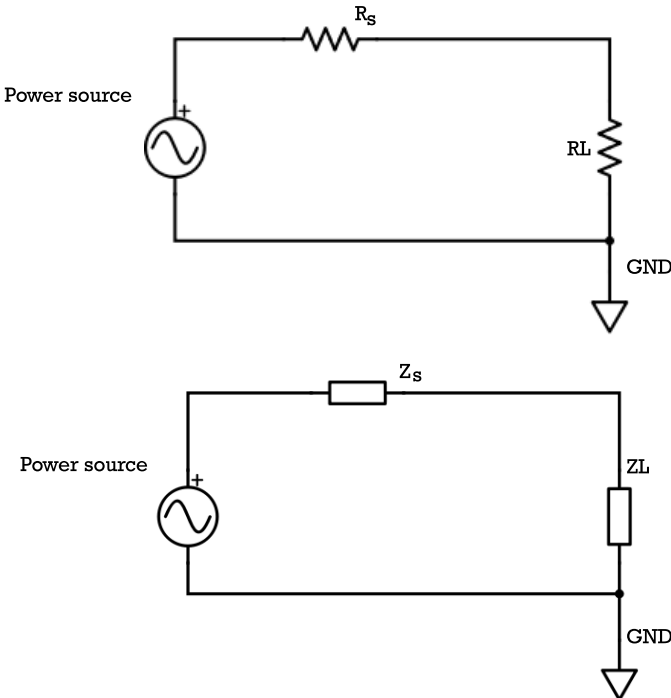


**Figure 7.1** Maximum power transfer.

Impedance matching is the practice to design a network to bring the input impedance of an electrical load to the internal impedance of the signal source to maximize the power transfer or minimize signal reflection from the load. The network is also called the impedance transformation network. The matching network is usually consisted of either lumped or distributed elements depending on the operating frequencies.

### 7.3 Smith Chart

At microwave frequencies, transmission lines are often used as a matching element in antenna matching circuits. The analysis of transmission lines is very cumbersome in the analytic form and very hard to use for circuit design on impedance matching. The Smith chart is a convenient tool to visualize the impedance of a transmission line as a function of frequency. It was invented by Phillip H. Smith (1905–1987) [4, 5] as a graphical aid for electronics and electrical engineers to solve problems with transmission line and matching circuits. It is also very useful to design the matching network by a graphical approach. The Smith Chart is also used to display the antenna impedance physically when measured with a vector network analyzer (VNA) [6]. Multiple parameters such as impedances, admittances, and reflection coefficient can be plotted on the same Smith chart. Therefore, it is a very convenient tool to design single-port or multiport matching circuit for an antenna, amplifier, or oscillator.

The Smith chart is shown in Figure 7.2 which is the representation of all impedances in the reflection coefficient plane, called the  $\Gamma$  plane as expressed:

$$\Gamma = \frac{Z - Z_o}{Z + Z_o} \quad (7.3)$$

where  $Z_o$  is the characteristic impedance of the transmission line or the reference impedance of the system. The normalized impedance can be expressed as:

$$z = \frac{Z}{Z_o} = \frac{R + jX}{Z_o} = r + jx \quad (7.4)$$

Equation (7.3) can be rewritten as:

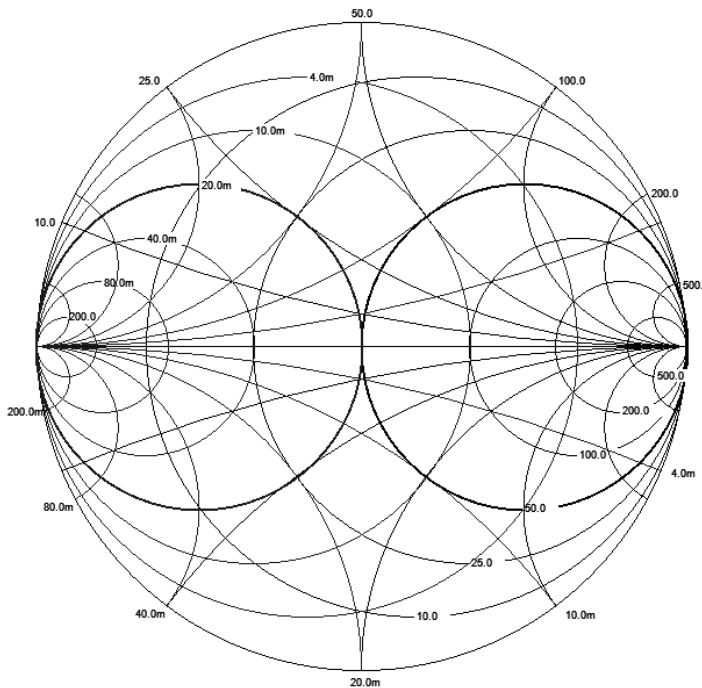


**Figure 7.2** Smith chart.

$$\Gamma = \frac{z - 1}{z + 1} \quad (7.5)$$

This expression relates the transformation of the normalized load impedance to the reflection coefficient. As an illustration for the transformation, assuming the impedance of the input and the system are both  $50\Omega$ , the normalized input impedance is 1 and the reflection coefficient is therefore 0 according to (7.3). The impedance of being 1 in the  $z$  plane maps to the center of the  $\Gamma$  plane (point A) where the reflection coefficient is 0 (see Figure 7.3). Similarly, for  $z = 0$ , the reflection coefficient becomes  $-1$ . It then maps to point B where  $U$  is  $-1$  and  $V$  is zero. As a further illustration, for an impedance of constant resistance  $z = 1 + jx$ , its reflection coefficient becomes

$$\Gamma = \frac{jx}{2 + jx} \quad (7.6)$$

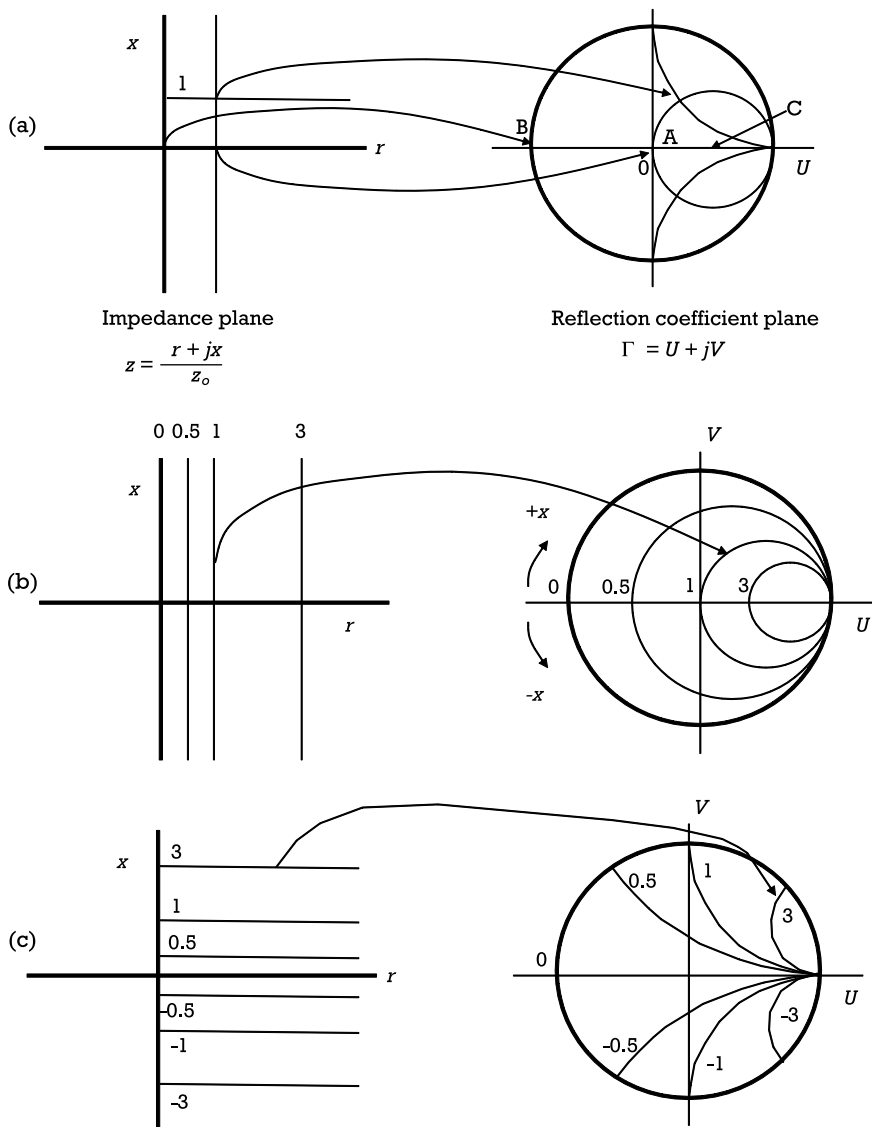


**Figure 7.3** (a) Conformal mapping from impedance to Smith chart, (b) mapping of constant resistance circles, and (c) mapping of constant reactance circles.

As shown in Figure 7.3(b), all the various points along  $z = 1 + jx$  are mapped to a circle of a radius  $1/2$  with the center at point C where  $U$  is  $1/2$  and  $V$  is 0. The circle is called the constant resistance circle for a resistance

of 1. Different constant resistance lines shown in Figure 7.3(b) map to different constant resistance circles in the  $\Gamma$  plane. Similar mapping on impedance of constant reactance lines to constant reactance circle in the  $\Gamma$  plane can be shown in Figure 7.3(c) [7, 8]. As shown, there is a one-to-one correspondence mapping from the  $z$  plane to the  $\Gamma$  plane. The graph of plotting the constant resistance and constant reactance circles together for all  $z$  values is the Smith chart for  $\text{Re}[z]$  being  $\geq 0$ . It could be observed that the upper half and lower half represent positive and negative reactances, respectively.

The Smith chart can also be used as an admittance chart with the following mapping:

$$\Gamma' = \frac{y - 1}{y + 1} \quad (7.7)$$

where  $y$  is the normalized admittance of  $Y/Y_o$  and  $Y_o$  is the reference admittance.

$\Gamma$  and  $\Gamma'$  admittance is related as:

$$\Gamma' = -\Gamma \quad (7.8)$$

When the Smith chart is used as an impedance chart, it is called the Z Smith chart. When it is used as an admittance chart, it is called the Y Smith chart. Graphically, the Y Smith chart is the mirror image of the Z Smith chart along the  $y$ -axis (Figure 7.4). The numeric scaling is the same for both charts. As shown later, the Z and Y Smith chart is more convenient for series and parallel components, respectively, on impedance matching. The superposition of both charts forms the ZY Smith chart as shown in Figure 7.5, which is often used for impedance matching with both series and parallel elements.

## 7.4 Matching Topology and Elements

### 7.4.1 Series Element

This section will discuss various approaches to achieve conjugate impedance match between the source and the load with a few examples. Assuming that the load impedance is at point A in Figure 7.6(a), which has an impedance of  $50 + j50$ , a series capacitor can be added to bring the impedance to the center point along the constant resistance circle on the Smith

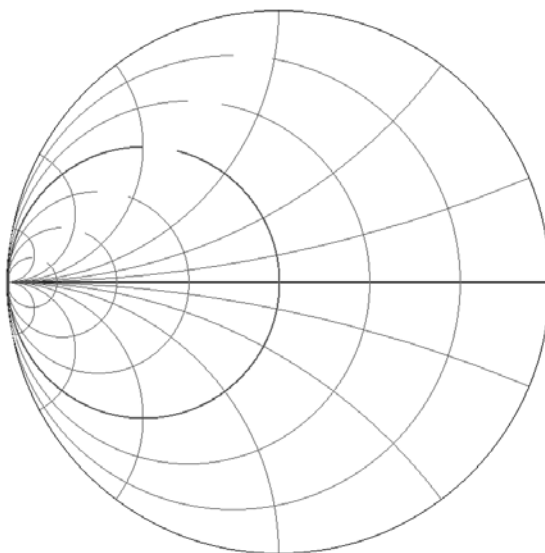


**Figure 7.4** Y Smith chart.

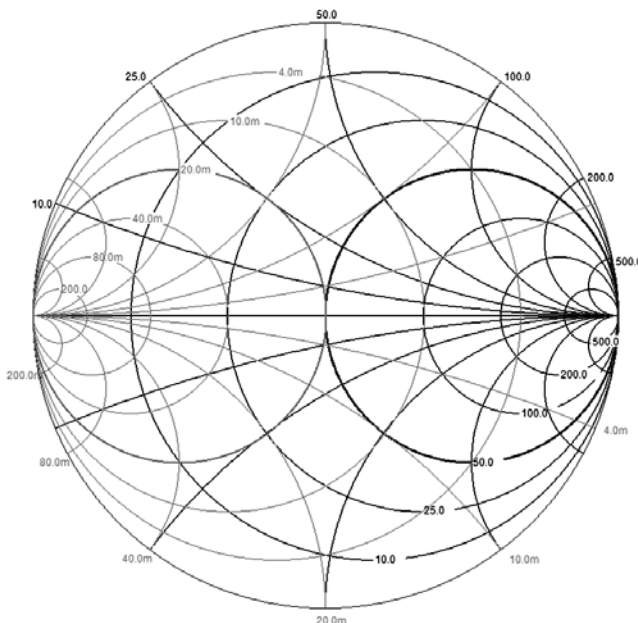


**Figure 7.5** ZY Smith chart.

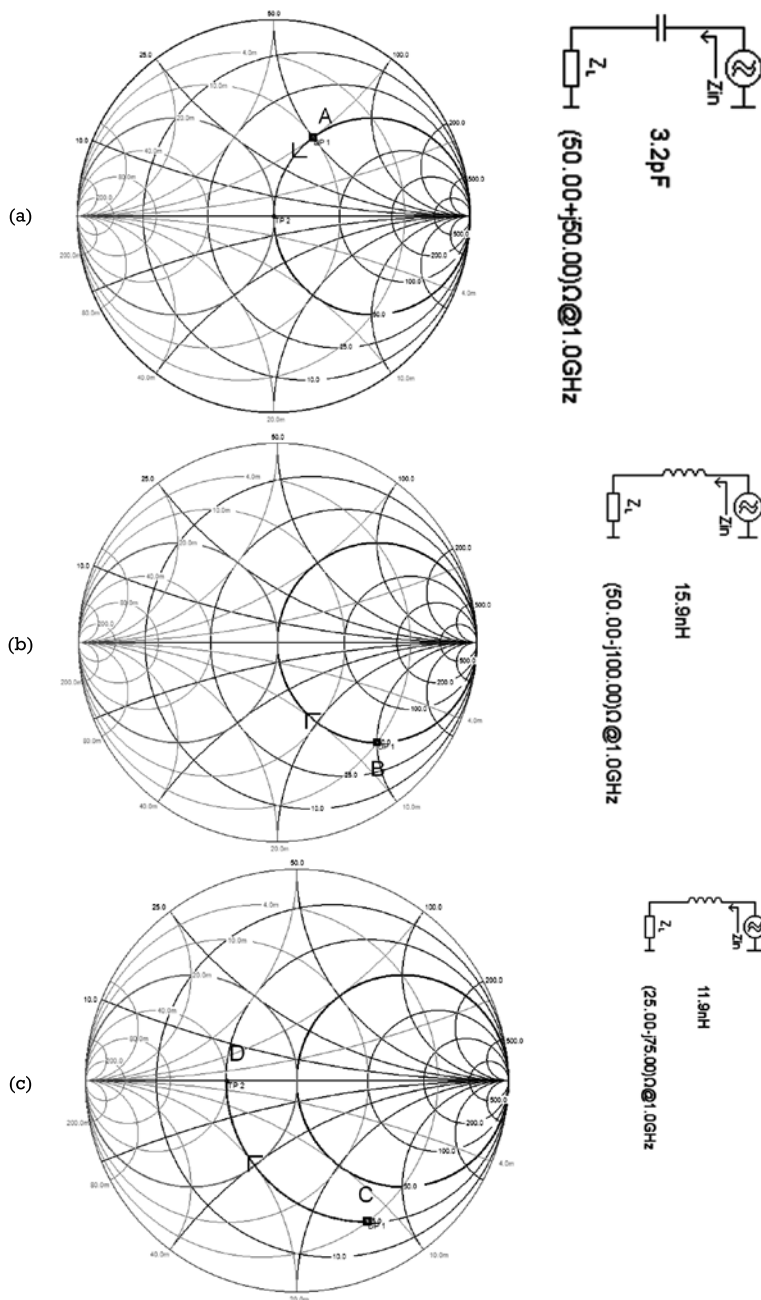


**Figure 7.6** (a) Adding series capacitor for matching, (b) adding series inductor for matching, and (c) adding series inductor but cannot match.

chart as mentioned in the previous section. The impedance of capacitor  $Z_c$  is given by:

$$Z_c = \frac{-j}{2\pi f C} \quad (7.9)$$

The resultant input impedance after the series capacitor is:

$$\begin{aligned} Z_{in} &= Z_L + Z_c \\ &= 50 + j50 + Z_c \end{aligned} \quad (7.10)$$

For a given frequency and with a suitable value of  $Z_c$ , the reactance can be made to be  $-50$ , which cancels out the positive reactance of the load impedance. The resultant input impedance becomes  $50\Omega$ , which matches to the source impedance of  $50\Omega$ . If the operating frequency is 1 GHz, the required value of the series capacitor is found to be 3.2 pF. The reactance of the capacitor just cancels out the reactance of the load impedance, making the load impedance pure resistive of  $50\Omega$ .

As a second example, the load impedance is assumed to be  $50 - j100$  and is represented in point B in the Smith chart in Figure 7.6(b). In this case, a series inductor can be used to move the impedance clockwise to the center of the Smith chart along the constant resistance circle. The required value of the series inductor to give a reactance of  $j100$  at 1 GHz is 1.59 nH. Similar to the case of using a series capacitor, the reactance of the inductor just cancels out the reactance of the load impedance, making the resultant load impedance to the source impedance of  $50\Omega$ .

As a third example, the load impedance is assumed to be  $25 - j75$  at point C in the Smith chart of Figure 7.6(c). This time, adding a series element can move the impedance along the constant  $25\Omega$  circle but can never go to the center point. It will require a shunt element to match to  $50\Omega$ , which will be discussed in the following section.

#### 7.4.2 Shunt Element

A series inductor for the impedance shown in Figure 7.7(a) can be added to bring point C to point E, which lies on the constant admittance circle of 20 mS. A shunt inductor can then be added in parallel to move the impedance along the constant admittance circle to the center again as shown in Figure 7.7(b). The matching network with a series and shunt elements is

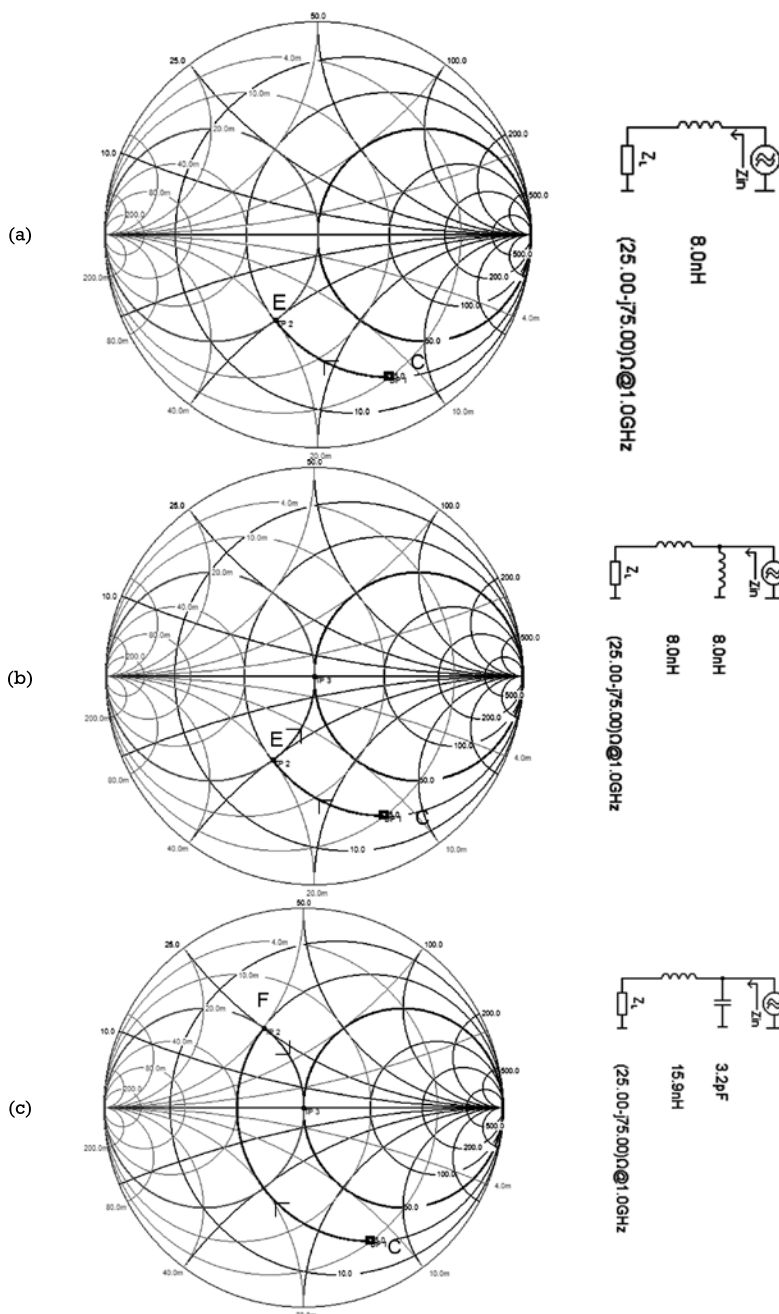


**Figure 7.7** Matching using the shunt element: (a) adding a series inductor, (b) adding a parallel inductor, and (c) adding a series inductor and then a parallel shunt capacitor.

commonly called the L-network. Given the same load impedance and if the series inductor is made larger in value, point C will be moved to point F on the other side of the constant admittance circle (see Figure 7.7(c)). A shunt capacitor can then be used to bring point F to the center again.

Instead of using a series element, a shunt element can also be used for matching. As shown in Figure 7.8(a), a shunt inductor is added in parallel to the load. The impedance will go to point G on the constant resistance circle.

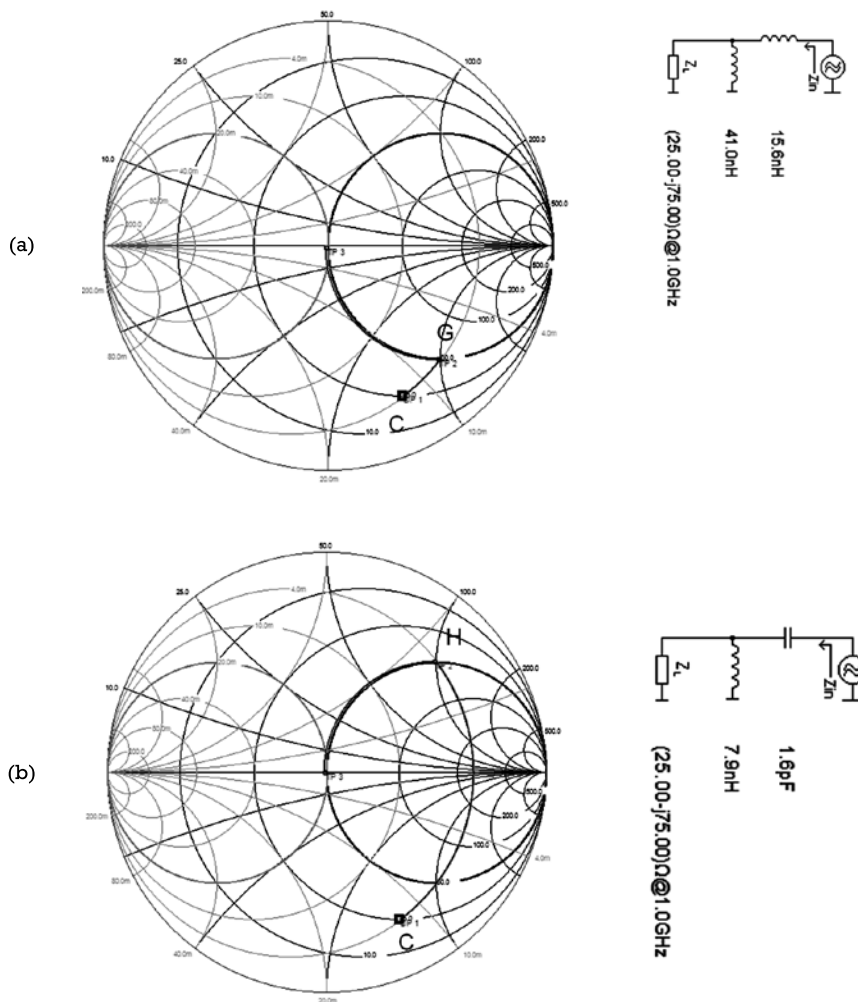


**Figure 7.8** Matching with a shunt element: (a) adding a shunt inductor and then a series inductor, and (b) adding a shunt inductor and then a series capacitor.

circle. A series inductor can then bring the impedance to the center. With a shunt inductor of a lower inductance value, point C moves to point H, which is also on the constant resistance circle but on the positive reactance side. Point G can then be brought to the center with a series capacitors (Figure 7.8(b)). As can be seen, there is more than one way to match any impedance on the Smith chart to  $50\Omega$  with an L-network. Figure 2.9 in Chapter 2 shows eight possible approaches to design the L-network [8], while Figure 7.9 illustrates the regions of impedance which can be matched with different L-networks [9].

#### 7.4.3 Matching Topologies

Due to the inherent characteristics of the antenna, some of the L-networks are preferred over the others as illustrated in the following examples. For a loop antenna, its impedance is typically inductive [10, 11]. Circuit B or F can used to achieve the impedance matching as the added capacitance can cancel out the reactance of the loop antenna while performing resistance transformation at the same time. Similarly, for a short dipole or monopole, its impedance is typically capacitive while its equivalent parallel resistance is very high. Circuit D would be the natural choice as the added inductance can cancel out the capacitance of the short dipole while transforming the impedance to a lower one of, say,  $50\Omega$  as the system impedance.

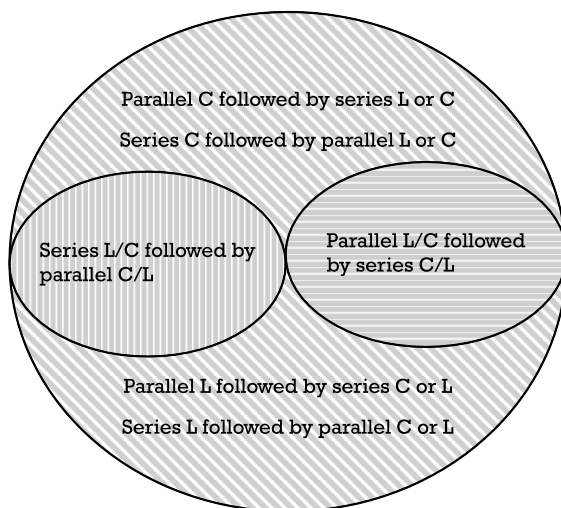


**Figure 7.9** Allowable impedance matching networks in the Smith chart.

In a typical transmitter circuit of many radio frequency integrated circuits (RFIC) on the market, a radio frequency choke (RFC) is typically used to provide DC bias to the collector or drain of a bipolar or FET transistor, respectively, acting as an output stage of the transmitter. The RFC is used instead of a resistive load as the output voltage can swing up to twice of the DC supply voltage to deliver higher output power. However, high-quality and high-value inductors are very difficult to be implemented on silicon. The output stage inductor is typically placed off-chip. The L-network G shown in Figure 7.10 is typically used for such application. Inductor L serves as an RFC to provide DC power to the collector of the output transistor and a matching element. Capacitor C is used for DC blocking and as a matching element. DC blocking is needed since there is a biasing DC level at the output of the transmitter. It will be shorted to ground if the antenna is a loop type in which one of the terminals may be grounded. Having a DC blocking capacitor can also avoid the transmitter output from shorting to ground through the internal  $50\Omega$  impedance in most RF equipment for testing and characterization.

## 7.5 Matching Elements

### 7.5.1 Inductor

The previous section suggested several matching topologies using the L-network with lumped elements. The choice of the component type is very

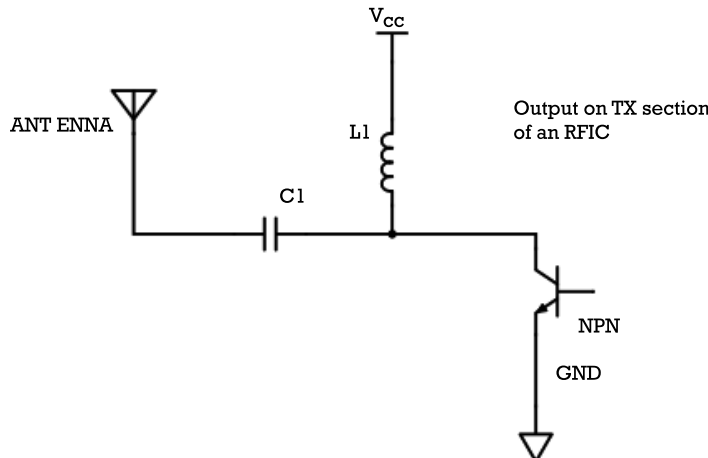


**Figure 7.10** TX amplifier with a  $V_{CC}$  feeding inductor.

important on determining the overall antenna performance at a high frequency due to the effect of the component's parasitic elements. As an illustration, the equivalent high-frequency model of an air-core inductor can be represented as an R-L-C network as shown in Figure 7.11(a). Due to the internal structure of the inductor, there is a parasitic resistor and a capacitor associated with the inductor. The resistance is caused by the loss resistance of the wire, while the capacitance is due to the coupling between turns. The quality factor  $Q$  [12, 13] of an inductor can be expressed as:

$$Q = \frac{2\pi f L}{R_l} \quad (7.11)$$

where  $L$  is the inductance of the inductor and  $R_l$  is the loss resistance.

The  $Q$  factor determines how much energy is lost on the equivalent loss resistor versus the energy stored in the inductor. It provides a figure of merit on how much loss is incurred by the inductor to the circuit when it is used at high frequency. If the frequency is high enough, the inductance and the parasitic capacitance will resonate at the self-resonant frequency (SRF) in which their reactances are the same. The  $Q$  factor of the inductor becomes minimal at SRF as shown in Figure 7.11(b). Beyond the SRF, the inductor behaves as a capacitor exhibiting negative reactance. When choosing an inductor for matching, it is recommended to choose one with SRF well above the operating frequency of the circuit to avoid the situation that it behaves as a capacitor.

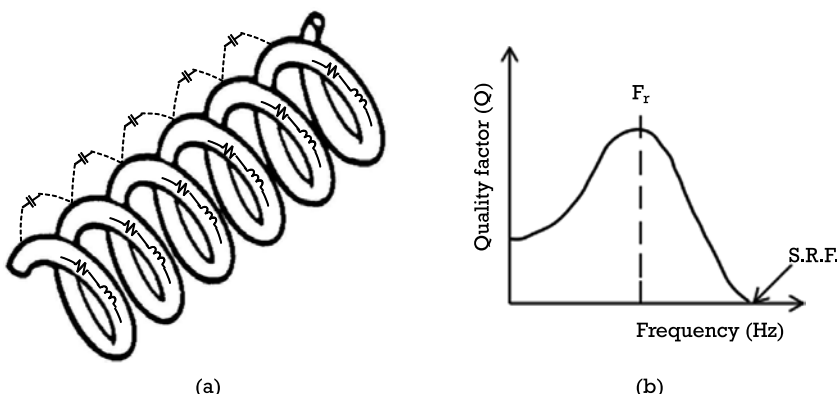


**Figure 7.11** (a) Equivalent high-frequency model of an inductor, and (b) frequency characteristic of its  $Q$  factor.

High-frequency inductors come in different forms, such as air-wound, ferrite, or ceramic chip types. Ferrite chip inductors typically have higher inductance value, but their applications are limited to megahertz operating frequency range. Air-wound type has the lowest loss but in a bigger size. Ceramic chip inductors have good compromise between performance and size, making it extensively used in many handheld wireless products. It differs in performance with different package sizes. Typically, inductors with a smaller size have a lower Q factor as the wire tends to be thinner, which results in higher resistance loss. The parasitic capacitance is also higher as the coupling between turns is higher due to the smaller separation between the turns. As an illustration of the performance difference, the high-frequency characteristics of two different inductor package types, CS0603 and CS1206, from the same manufacturer are plotted in Figures 7.12 and 7.13. The CS1206 type offers a higher Q and SRF, although it is almost twice bigger than the CS0603 type.

With either type, the inductance is relatively constant at low frequencies. It increases with frequency until it reaches a maximum at the SRF frequency due to the effect of the parasitic capacitance. In many applications, it is desirable to use the inductor at frequencies on the rising curve to obtain higher Q. Due to the inductance's dependency of frequency, the graphical design approach with the Smith chart presented previously may not work. Computer simulation and optimization with the equivalent model of the inductor will be needed to design the matching network more accurately and effectively.

### 7.5.2 Capacitor

Similarly, capacitors at a high frequency also exhibit undesirable parasitic elements but the extent will be less than that of the inductor. This is due to its simpler structure compared to the inductor, resulting in smaller parasitic elements. The high-frequency equivalent model of a capacitor is shown in Figure 7.14(a) [16]. The equivalent series resistance (ESR) is caused by the loss of the dielectric substances, electrodes, and other elements of the capacitor structure. The parasitic inductance is due to the leads and electrodes. Because of the parasitic elements, the frequency characteristic of its impedance has a V-shaped curve as shown in Figure 7.14(b). The magnitude of the impedance decreases inversely with the operating frequency, resembling the characteristic of an ideal capacitor. The impedance continues to drop and reach a minimum at the self-resonant frequency. The impedance will increase after the SRF frequency and becomes inductive as

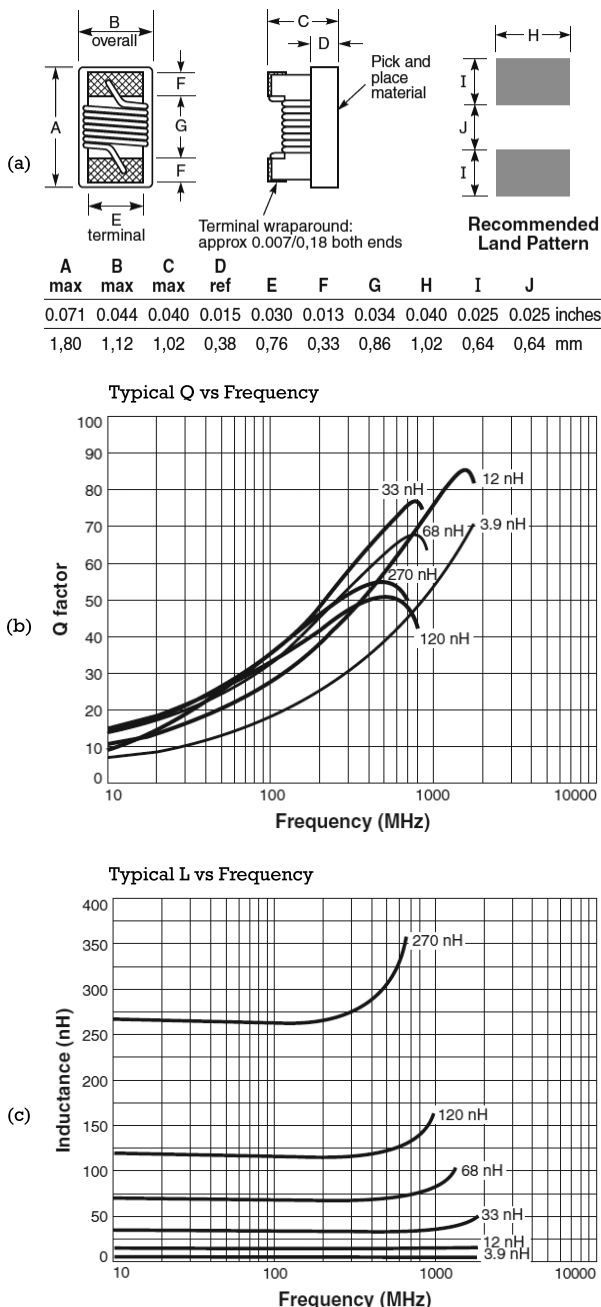


**Figure 7.12** (a) Structure of the 0603CS chip inductor, (b) Q versus frequency, and (c) L versus frequency. (From: [14]. Reprinted with permission of Coilcraft, Inc.)

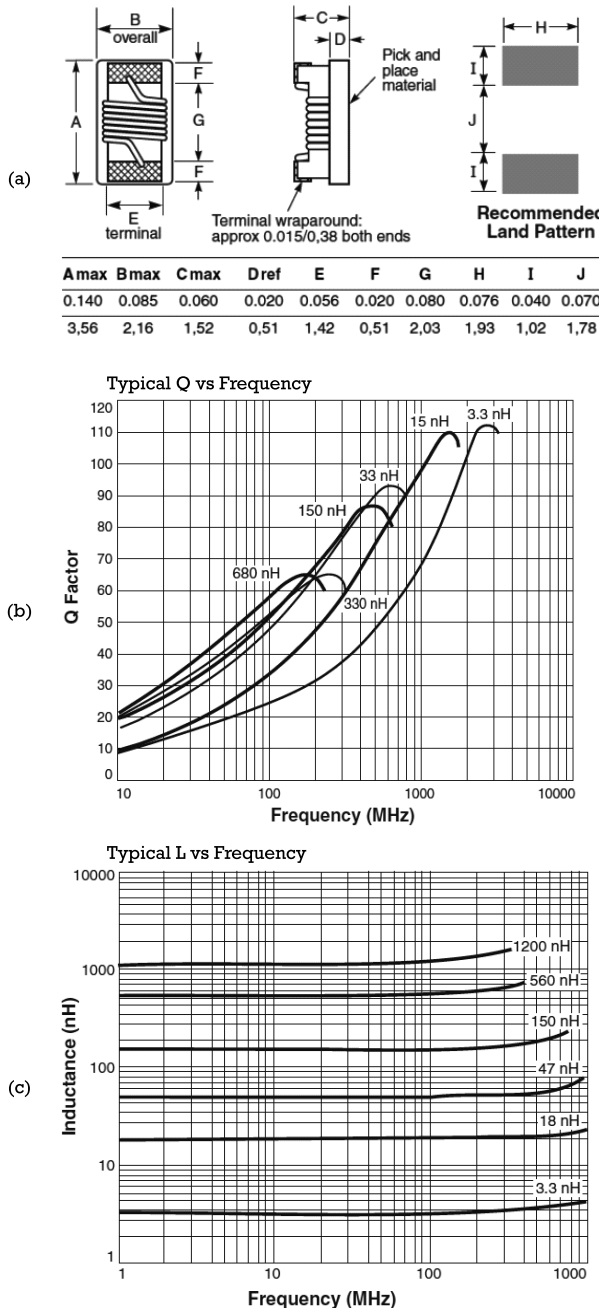


**Figure 7.13** (a) Structure of the 1206CS chip inductor, (b) Q versus frequency, and (c) L versus frequency. (From: [15]. Reprinted with permission of Coilcraft, Inc.)

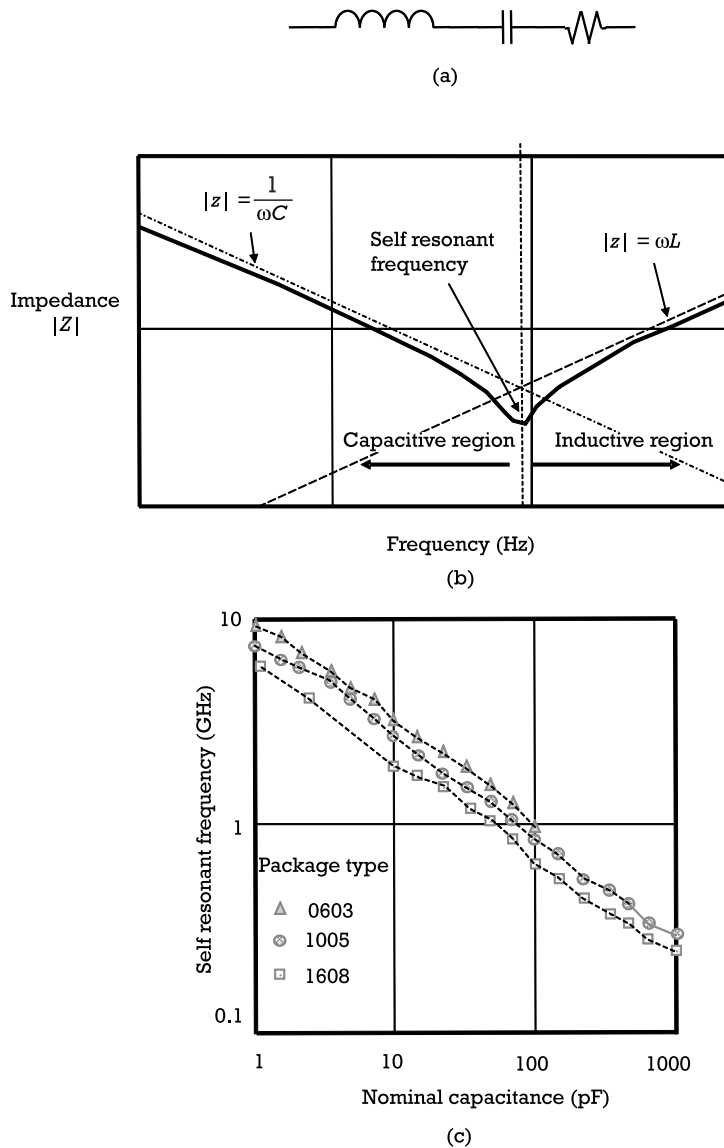


**Figure 7.14** (a) Equivalent model, (b) impedance versus frequency, and (c) SRF versus frequency for different package sizes.

dominated by the parasitic inductance. For typical matching designs, the SRF of the chosen capacitor should be well above the operating frequency. Like the ceramic chip inductors, ceramic chip capacitors are also being used

extensively in many handheld wireless products. Its high-frequency characteristic is also size-dependent as illustrated in Figure 7.14(c). The SRF typically decreases as size increases.

Although the existence of SRF in components is undesirable for circuit matching, it is often used for Vcc decoupling at RF in RFICs, modules, or subcircuits. The Vcc decoupling capacitor is placed very close to the Vcc pin of the RFIC or module. At the SRF, the impedance is at a minimum, which provides a good RF short to ground. This can prevent any signal coming out or getting into the RFIC or module through the Vcc pin, which may create undesirable oscillation or interference.

### 7.5.3 Transmission Line

Although ceramic chip inductors and capacitors are widely available for use in circuit or antenna matching, they tend to be lossy due to their parasitic elements as mentioned in the previous section and Chapter 4, particularly for frequencies higher than 2 GHz. If space is not an issue, transmission lines are often used as matching element in microwave circuits. Microstrip and striplines are commonly used in two-layer and four-layer PCB designs [17, 18]. They have much lower loss than the lumped-element inductor and capacitor at RF and microwave frequencies. A similar design technique using the Smith chart can be employed for matching [8, 19]. The only concern with transmission line is the required size as the required length of the transmission line is in the order of quarter-wavelength in order to have a significant effect on the circuit. There is therefore compromise between performance and size in both lumped and distributed matching elements. As mentioned in Chapter 4, it is best to design an antenna such that its elements are both radiating and matching element to bring the terminating impedance to be the required system impedance of, say,  $50\Omega$ .

## 7.6 Practical Considerations

### 7.6.1 Impedance Measurement with VNA

Impedance measurement is covered in this matching design section as both measurement and design tasks are always done at the same time. Impedance measurement can be done very easily with the right equipment. The VNA is commonly used to measure the impedance of an antenna and the circuit connecting to the antenna. Full two-port VNAs used to be very expensive and bulky as they can perform all four S-parameters simultaneously and automatically (see Figure 7.15). Recently, there are quite a few

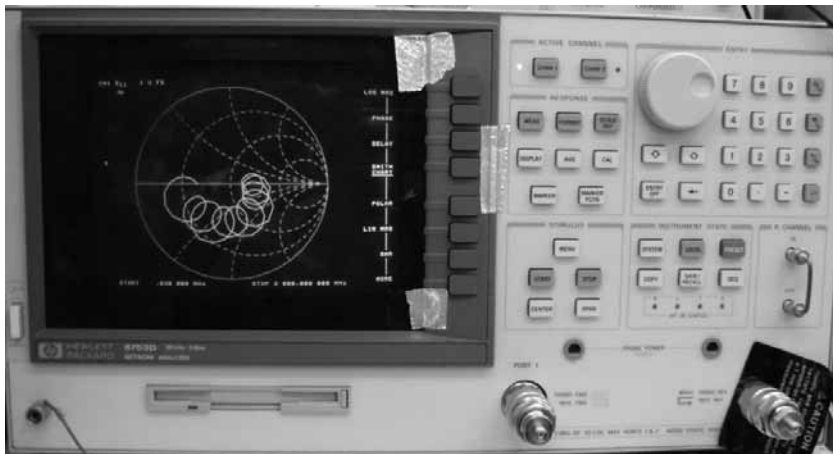


**Figure 7.15** Full two-port VNA.

vendors offering low-cost VNAs, which drive down the price significantly [20, 21]. Those low-cost VNAs as shown in Figure 7.16 can make reflection ( $S_{11}$ ) and transmission ( $S_{21}$ ) measurements but not simultaneously. If the isolation ( $S_{12}$ ) or reflection at port 2 ( $S_{22}$ ) need to be measured, the device unit test needs to be swapped physically between port 1 and port 2 of the VNA. Despite the inconvenience, the low-cost VNAs make the antenna impedance measurement more affordable to many small- to medium-sized companies nowadays.

Once the equipment is available and the matching topology is chosen, the measurement is straightforward. The VNA is then calibrated with some standards to correct any imperfections due to the measuring cable and the VNA's inaccuracies due to temperature drift, aging, and so forth [8, 22]. Even with calibration, the measured impedance always deviates from the calculated or simulated one. There are a few common mistakes which cause the inconsistency. They are to be discussed in the following sections.

### 7.6.2 Balanced or Unbalanced

Different types of antenna were introduced in the previous chapters. Some of them were differential in design such as dipole and loop antennas. Other antennas such as monopole, inverted-L, or patch were single-ended. For measuring a differential antenna such as a dipole, a typical setup is shown in Figure 7.17. Although the antenna itself is differential, the equipment and the cable (typically of a coaxial type) are not. A coaxial cable is usually

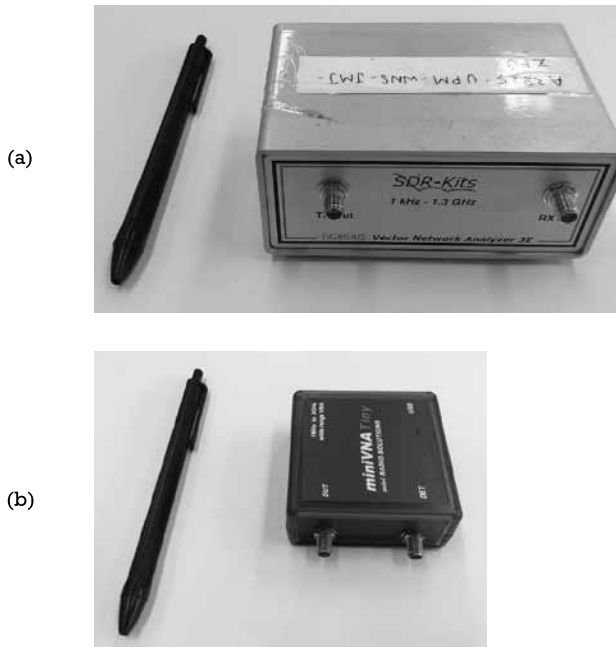


**Figure 7.16** Low-cost network analyzer: (a) DG8SAQ VNWA from SDR-Kits and (b) miniVNA Tiny from Mini Radio Solutions. (Courtesy of Lexiwave Technology (Hong Kong) Limited.)

used to connect the measuring port of the network analyzer to the antenna under test. The coaxial cable is inherently unbalanced as the inner and outer conductors of the cable are connected to the antenna differently. This results in a net current  $I_3$  flowing to the ground on the outside part of the outer conductor as shown in Figure 7.17 [23]. The unbalanced current  $I_3$  is determined by the impedance  $Z_g$  from the outer shield to the ground.  $Z_g$  is determined by the length of the cable, the size of the network analyzer, and the proximity to the surrounding objects. This makes  $I_3$  vary with the surrounding conditions. The measured impedance of the antenna is thus uncertainly subject to the surrounding conditions.

Even though the cable loss and any imperfections on the equipment can be calibrated by the calibration procedures of the network analyzer, the impedance of the antenna being measured will still depend on the antenna itself and the length of the cable due to the unbalanced current  $I_3$ . To alleviate this problem,  $Z_g$  can be made very large to minimize  $I_3$ . Devices known as baluns (balance to unbalance) can cancel or choke off  $I_3$  to make the system balanced. Typical balun devices are Bazooka, quarter-wavelength

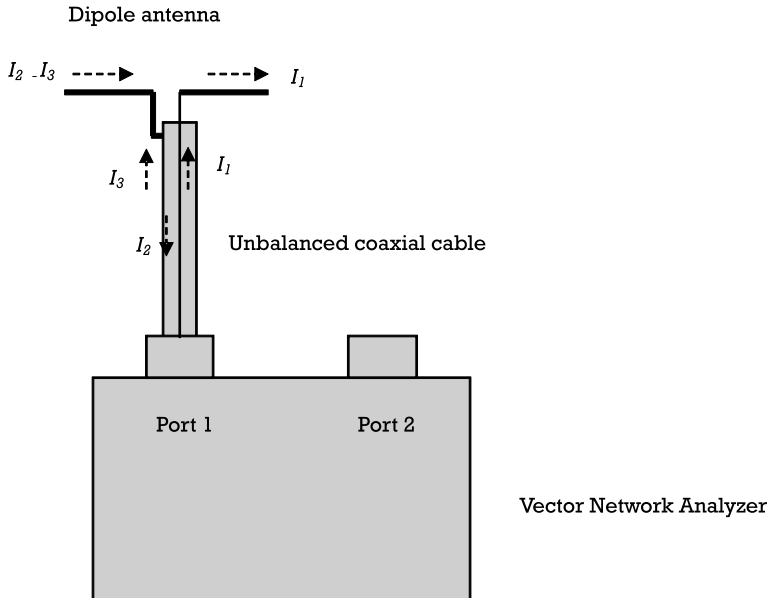


**Figure 7.17** Setup for measuring the impedance of a dipole antenna.

coaxial, or transmission-line transformer [23]. However, their operating frequency band is very narrow. Transmission-line transformers with a ferrite core can increase the bandwidth and can also provide impedance stepping up or down transformation. Ideally, differential impedance should be taken by differential equipment for differential antennas.

However, the nonideal factors of the balun such as finite insertion loss and bandwidth will make the measured impedance of the antenna inaccurate or incorrect. Instead of using baluns, with some special setups and procedures, an ordinary or a multiport network analyzer can be used to obtain the differential measurement as shown in Figure 7.18. Although the outer conductor current  $I_3$  still exists but on both feeding cables, their influence can be removed mathematically with special measurement procedures with the network analyzer [24–26].

### 7.6.3 Ground Effect

Special attention still has to be given for measuring the single-ended antenna such as monopole, inverted-F, or helix with the VNA, even though the balanced-to-unbalanced issue does not exist. Figure 7.19(a) shows the setup using a VNA to measure a helical antenna at 500 MHz [27]. The

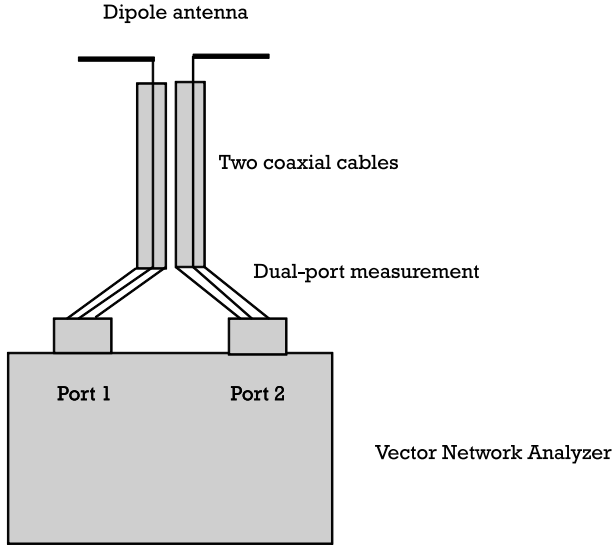


**Figure 7.18** Setup for the dual-port measurement on the impedance of a differential antenna.

antenna is connected to an SMA connector at the end of the feeding cable. Although both the antenna and the VNA are single-ended, the ground current  $I_3$  still flows on the outside part of the outer conductor as shown in Figure 7.19(b). Due to the ground current, there are couplings from the antenna to the cable. The measured impedance is a resultant impedance due to the antenna and the ground couplings. The measured impedance thus changes with the cable length and the distance from the antenna to the cable section as shown in Figure 7.19(c).

A simple way to avoid the coupling is to add a metal ground plane between the antenna and the cable as shown in Figure 7.20(a). The added ground plane confines the couplings between the antenna and itself (see Figure 7.20(b)). It makes the coupling more controllable and the measured impedance more consistent, regardless of the cable length. The measured impedance is still the resultant impedance of the antenna and the couplings. A better approach is to measure the antenna with the product in which the antenna is used. The feeding cable is soldered on the main board of the product, which presumably is flooded with large ground plane as shown in Figure 7.21(a). If there are couplings, they will only be confined to the ground of the main board. In case there are many obstacles such as existing components on the main board for the feeding cable to put on, a

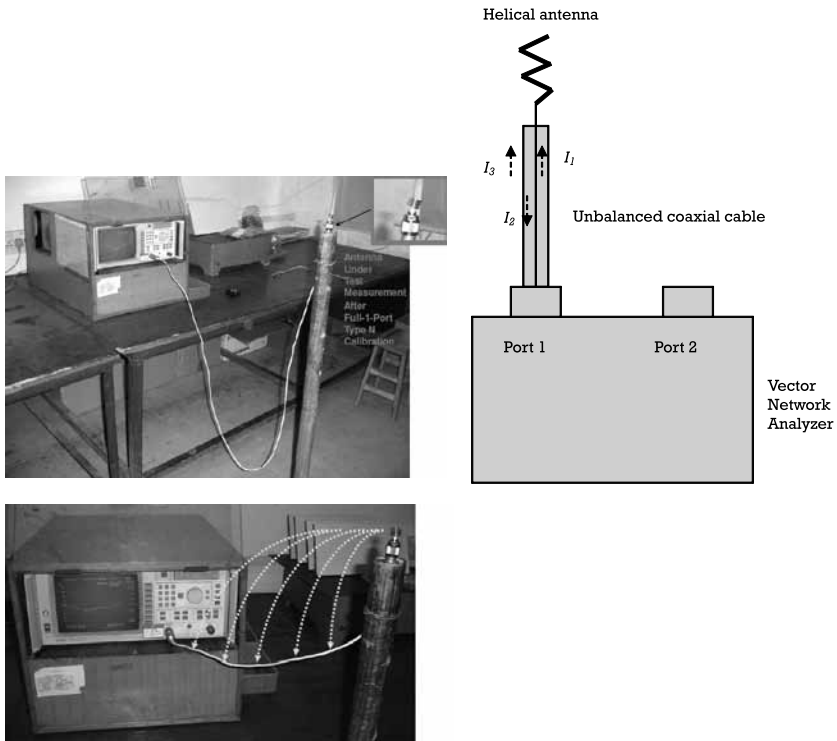


**Figure 7.19** (a) Setup measuring impedance of a helical antenna. (From: [27]. Reprinted with permission of Andrew Ko.) (b) Ground current  $I_3$  flowing on the outer conductor. (c) Coupling from the antenna to the feeding cable. (From: [27]. Reprinted with permission of Andrew Ko.)

plain PCB flooded with ground with similar size as the main PCB can be used (see Figure 7.21(b)).

If the antenna to be measured is the monopole or inverted-F antenna, a ground plane is needed to provide the lower-half image for full operation as discussed in Chapter 3. The antenna can be measured with either the product or the emulated ground PCB as suggested above. However, it is assumed that the ground plane is infinitely large to provide full radiation of the image. In practical situation, the ground size is finite as it is typically limited by the product size particularly for handheld devices. As suggested by [28], the main characteristics of the antenna such as gain, efficiency, bandwidth, and impedance are a function of the ground size. Typically, the larger the ground plane, the closer they are to the theoretical values if the ground plane is part of the antenna. Therefore, it is important to measure



(a)



(b)

**Figure 7.20** (a) Added ground plane between the antenna and cable, and (b) couplings confined from the antenna to the ground plane. (From: [27]. Reprinted with permission of Andrew Ko.)

the antenna's performance with the actual ground size to reflect the true performance. The antenna characteristics of a commercial multiband SMD antenna (see Figure 7.22(a)) are used as an illustration to show how the antenna's characteristics are affected by the length of the ground plane [29]. The antenna is mounted on a ground plane as shown in Figure 7.22(b) for measurement. The return loss and the maximum gain change with the length of the ground plane are shown Figure 7.22(c, d), respectively. The antenna gain is typically higher for larger ground plane as illustrated in Figure 7.22(d). The ground is also part of the radiating structure of the antenna. The larger the ground plane, the more radiation the antenna can generate as it has more currents flowing through the ground plane. Up to



(a)



(b)

**Figure 7.21** (a) Antenna measurement with the main PCB, and (b) measurement with a ground plane to simulate the actual main PCB.

a certain size, the gain will not increase any further. Similarly, many other antennas such as the patch antenna also works with the ground plane for effective radiation. Their antenna gain increases with the ground plane size as well [30, 31].

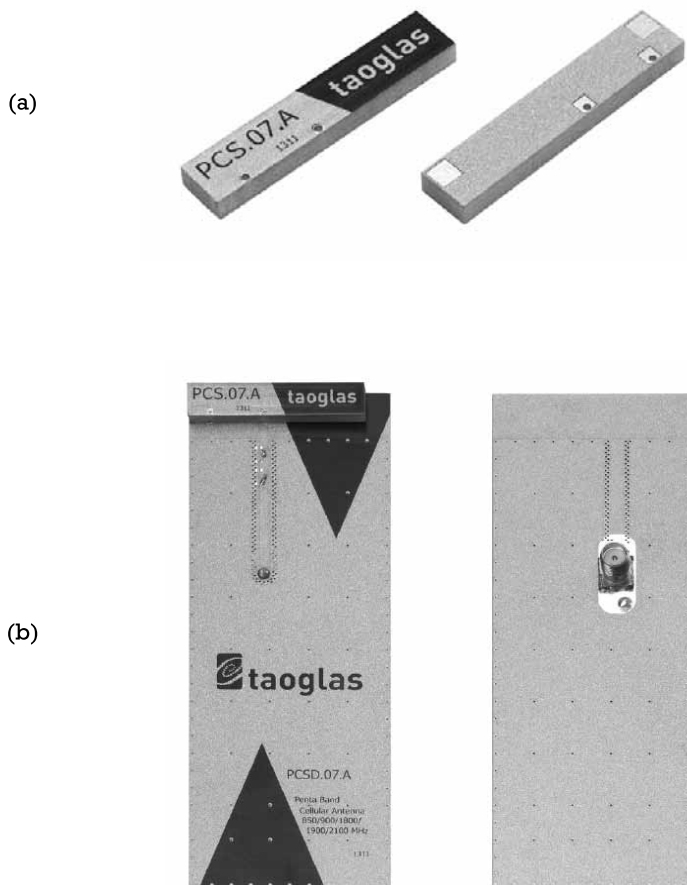


**Figure 7.22** (a) Multiband SMD dielectric antenna, (b) antenna measurement with a ground plane, (c) return loss with different ground plane lengths, and (d) maximum antenna gain with different ground plane lengths. (From: [29]. Reprinted with permission of Taoglas Ltd.)

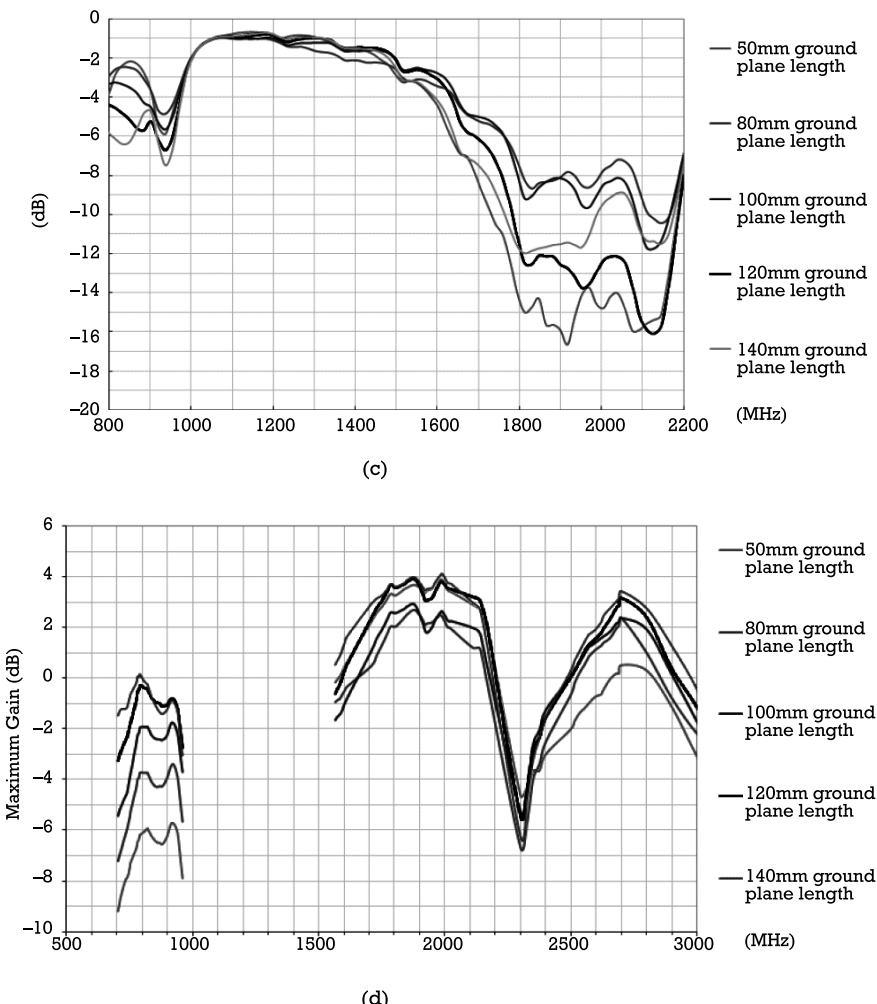


Figure 7.22 (continued)

## References

- [1] Jackson, H. W., *Introduction to Electronic Circuits*, Upper Saddle River, NJ: Prentice-Hall, 1959.

- [2] "Maximum Power Transfer Matching," last modified September 13, 2018, [https://en.wikipedia.org/wiki/Impedance\\_matching#Maximum\\_power\\_transfer\\_matching](https://en.wikipedia.org/wiki/Impedance_matching#Maximum_power_transfer_matching).
- [3] "Maximum Power Transfer Theorem," last modified September 13, 2018, [https://en.wikipedia.org/wiki/Maximum\\_power\\_transfer\\_theorem](https://en.wikipedia.org/wiki/Maximum_power_transfer_theorem).
- [4] Smith, P. H., "Transmission Line Calculator," *Electronics*, Vol. 12, No. 1, January 1939, pp. 29–31.
- [5] Smith, P. H., "An Improved Transmission Line Calculator," *Electronics*, Vol. 17, No. 1, January 1944, p. 130.
- [6] Keysight Technologies, "Understanding the Fundamental Principles of Vector Network Analysis," Application Note, December 14, 2017.
- [7] Davis, W. A., and K. K. Agarwal, *Radio Frequency Circuit Design*, New York: Wiley-Interscience, 2001.
- [8] Gonzalez, G., *Microwave Transistor Amplifiers: Analysis and Design*, 2nd ed., Boston, MA: Pearson, 1996.
- [9] "Immittance Charts: More Impedance Matching," last modified September 13, 2018, <http://www.antenna-theory.com/tutorial.smithsmithchartB.php>.
- [10] Fu, T. L., "Optimize the Performance of Pager Antennas," *Microwaves & RF*, August 1994, pp. 141–147.
- [11] Lau, H., "Performance Concerns Guide the Design of Pager Antennas," *Microwaves & RF*, December 1995, pp. 95–106.
- [12] Scott, A. W., *Understanding Microwaves*, New York: Wiley-Interscience, 1993.
- [13] Vizmuller, P., *RF Design Guide: Systems, Circuit and Equation*, Norwood, MA: Artech House, 1995.
- [14] Coilcraft, Inc., Chip Inductors – 0603CS (1608) product catalog.
- [15] Coilcraft, Inc., Chip Inductors – 1206CS (1206) product catalog.
- [16] "What Are Impedance/ESR Frequency Characteristics in Capacitors?" last modified August 28, 2018, <https://www.murata.com/en-us/products/emiconfun/capacitor/2013/02/14/en-20130214-p1>.
- [17] Edwards, T. C., *Foundations for Microstrip Circuit Design*, New York: John Wiley & Sons, 1981.
- [18] Lau, H., "Practical RF PCB Design: Wireless Networks, Products and Telecommunications," *IEEE Course Material*, Boston, MA, December 15, 2017.
- [19] "Smith Chart Tutorial - Impedance Matching with Tx Lines, Series L and C," last modified September 13, 2018, <http://www.antenna-theory.com/tutorial.smithsmithchart6.php>.

- [20] SDR-Kits, "DG8SAQ VNWA 3 Low Cost 1.3 GHz Vector Network Analyzer," product homepage, <https://www.sdr-kits.net/index.php?route=information/contact>.
- [21] Mini Radio Solutions, "miniVNA Tiny - PC Based Vector Network Analyzers," product homepage, <http://miniradiosolutions.com/54-2/>.
- [22] Anritsu Company, "Understanding VNA Calibration," 2012 ,[www.anritsu.com](http://www.anritsu.com).
- [23] Balanis, C. A., *Antenna Theory: Analysis and Design*, New York: John Wiley & Sons, 1997.
- [24] Rohde & Schwarz, "Measuring Balanced Components with Vector Network Analyzer ZVB," Application Note, September 2004.
- [25] Bockelman, D. E., and W. R. Eisenstadt, "Combined Differential and Common-Mode Scattering Parameters: Theory and Simulation," *IEEE Trans. on Microwave Theory and Techniques*, Vol. 43, No. 7, July 1995, pp. 1530–1539.
- [26] Henkes, D. D., "Ordinary Vector Network Analyzers Get Differential Port Measurement Capability," *High Frequency Electronics*, Applied Computational Sciences, November 2003.
- [27] Ko, A., "Resolving Vector Network Analyzer Measurement Issues of Antenna Resonance Frequency Variations with Different Test Port Cable Lengths," Presentation on Antenna Measurement, April 9, 2011.
- [28] Bancroft, R., "Fundamental Dimension Limits of Antennas - Ensuring Proper Antenna Dimensions in Mobile Device Designs," Centurion Wireless Technologies, Westminster, CO, 2014
- [29] Taoglas Ltd., "PCS.07.A Low Profile Cellular SMD Dielectric Antenna Specification," antenna datasheet.
- [30] Bhattacharyya, A. K., "Effects of Finite Ground Plane on the Radiation Characteristics of a Circular Patch Antenna," *IEEE Trans. on Antennas and Propagation*, Vol. 38, No. 2, February 1990.
- [31] Lolit, L., et al., "A Review on Effects of Finite Ground Plane on Microstrip Antenna Performance," *International Journal of Electronics and Communication Engineering & Technology*, Vol. 3, No. 3, October-December 2012, pp. 287–292.

## **CHAPTER**

# **8**

### **Contents**

- 8.1 Introduction
- 8.2 Understanding the Requirements
- 8.3 Implementation Considerations and Strategies

## **Practical Implementation Strategies and Design Examples**

### **8.1 Introduction**

Chapters 3 and 4 presented useful insights on designing both basic and advanced antennas. However, the focus was confined within the design of the antenna itself. When the antennas are used in a system or product, there are limitations and constraints by the system that allow only certain types of antennas to be used. The system or product will also have its own characteristics that determine the right type of antennas to be used. This chapter will address the design issues and considerations of the antenna from product and system perspectives. It will first identify the importance of understanding the specifications and requirements of the antenna, followed by system analyses and considerations. General design rules on PCB layout design, component placement, and mechanical design will be introduced since they are also the

key design elements, determining the ultimate performance of the antenna. Their relevancy and special design rules on antenna design will also be presented. The importance of teamwork will be highlighted. Several design examples on commercial products will be referenced to offer more design details and insights.

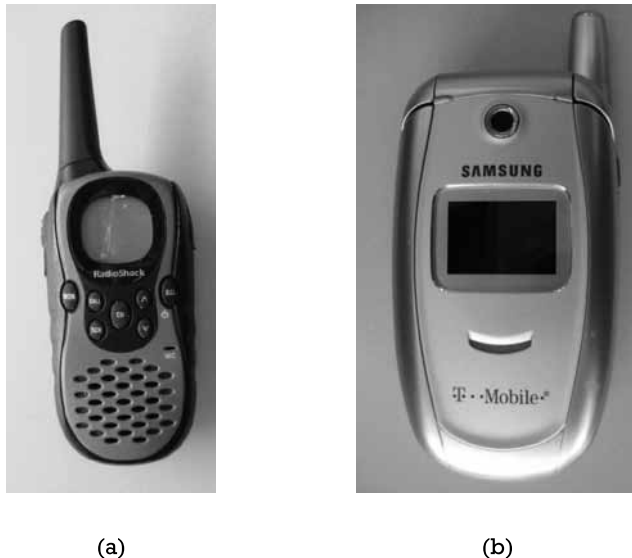
## 8.2 Understanding the Requirements

The first step to design a good antenna is to understand the requirements. Typical key requirements of an antenna can be summarized as the internal or external type, operating frequency, bandwidth, gain, polarization, directivity, and size. Depending on the products and overall product requirements, some parameters are more important than the others.

### 8.2.1 Internal or External

An external antenna typically has a higher gain than an internal one. That is because an external antenna experiences larger free space than an internal antenna within an enclosure. The typical reasons for using an external antenna are as a requirement for higher antenna gain, the antenna has to be separated from the device, and the size of the antenna is bigger than the device itself. In theory, a larger antenna has higher gain than a smaller one [1–3] as it would be much easier for an external antenna than an internal one to find more free space. Figure 8.1 shows two devices using an external antenna. The first one is a walkie-talkie operating at 433 MHz, and the second one is a clamshell cellphone operating at 900 MHz. The antennas that they are using are both monopoles. Quarter-wavelength monopoles have been used in many portable devices as they offer a near omnidirectional radiation pattern, high radiation efficiency, and simple structure. A quarter-wavelength of the walkie-talkie and the cellphone is 173 mm and 83 mm, respectively. The length of the required monopole for each product is longer than the device itself. It would be impossible to put it inside the product. It has to stay outside the casing. Even if they are put outside the casing, the required length of the antenna is still disproportionately longer than the product. For cosmetic reasons, the performance is sacrificed by using a shorter monopole as shown in Figure 8.1.

The required length of the antenna on the cellphone shown in Figure 8.1(b) is shorter since it is operating at a higher frequency. It could have been placed inside the cellphone. The product was on the market more than 15 years ago before this book was published. Having an external antenna



(a)

(b)

**Figure 8.1** Product using an external antenna: (a) a 433-MHz walkie-talkie and (b) a cellphone at 900 MHz.

was acceptable at that time. The first handheld cellular phone was demonstrated by John F. Mitchell and Martin Cooper [4, 5] of Motorola in 1973, weighing 2 kg [6] with the size as big as a brick. As the product evolved, it became a smartphone with all the advanced features inside a palm-size phone (see Figure 8.2). Many parts and components including the antenna are put inside the phone in order to implement all the advanced features offered by a smartphone. Those components and parts compete on the scarce board space and pose great challenges to the PCB, mechanical, and antenna designers. Collaboration among different design members is imperative on products with an internal antenna. Those issues will be addressed in detail throughout the rest of the chapter.

### 8.2.2 Polarization and Directivity

As introduced in Chapter 2, polarization is one of the key antenna parameters for wireless communications. The transmitting and receiving antennas should be designed to have the same polarization to receive the maximum signal strength. For example, if the transmitting antenna is a vertical monopole, the corresponding receiving antenna should be designed to be verti-



**Figure 8.2** Evolution of the cellular phone to the smartphone.

cally polarized. The obvious choice would be another vertical monopole for the receiving antenna.

To illustrate the antenna design for optimum polarization, a wireless product shown in Figure 8.3 is used. The product is a wireless doorbell operating at 433 MHz for the European market. It has a doorbell unit as a transmitter and a base unit as a receiver. The transmitter is in a rectangular shape and attached to the front or back door in a vertical position by convention. In addition to its functional features and outlook, the communication range is also important for consumers to consider in buying the product. The antenna thus plays a crucial role in determining the communication range and an optimization of the antenna design is needed. The transmitter is very small and thus having an external antenna would not be appropriate for cosmetic reasons. Also, since most similar products on the market use internal antennas, an internal antenna was implemented in the product.

A monopole could be a candidate for the internal antenna. As indicated in the previous section, the quarter-wavelength is 173 mm at 433 MHz for optimum performance. It is too long as compared to a length of 80 mm of



**Figure 8.3** Wireless doorbell.

the product. A short vertical monopole with lower gain could be used instead. The base unit is also in a rectangular shape but is bigger and thicker. It could be placed horizontally on a table or mounted onto a wall. Assuming that the base unit is placed on a table and the antenna is a monopole placed horizontally inside the casing, the antenna could not receive any signal at all from the transmitting signal. This is due to the polarization mismatch between the antennas since the transmitting antenna is a vertical monopole. However, full power would be received if the base unit is mounted against the wall since both antennas are vertically polarized. Since the orientation of the base unit is not fixed, one of the antennas would have fields in both  $x$ - and  $y$ -directions in order not to lose any receiving signals. The transmitter unit actually uses a printed spiral antenna [7] on a PCB as shown in Figure 8.4. The spiral antenna transmits or receives electromagnetic fields with circular polarization, meaning that it can receive linearly polarized fields in any orientations. However, it will reject signals with an opposite circular polarization. A spiral antenna could not be used in the base unit as it could reject receiving signals when the base unit is placed in a position where the TX and RX antennas have the opposite polarization. A wire monopole is actually used as shown in Figure 8.5. It has two sections, one internal and one external. The internal section is placed along the inner edge of the plastic casing while the external section is inserted into the body of an external and turnable antenna. When the base unit is placed on a table, it would receive

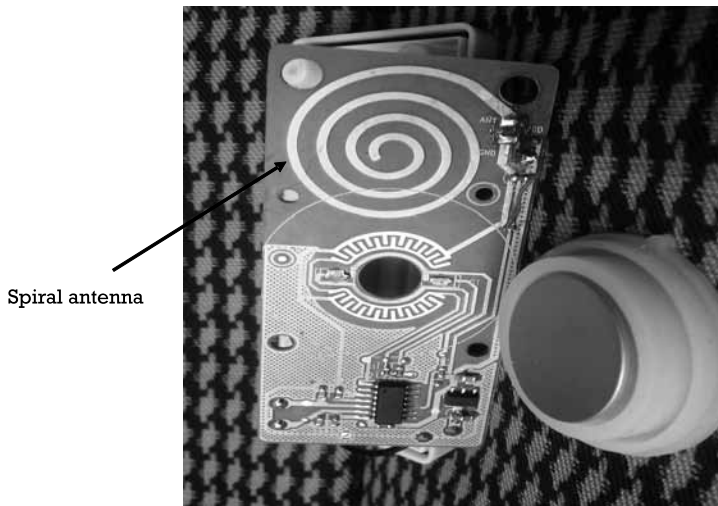


**Figure 8.4** Transmitter of the doorbell.

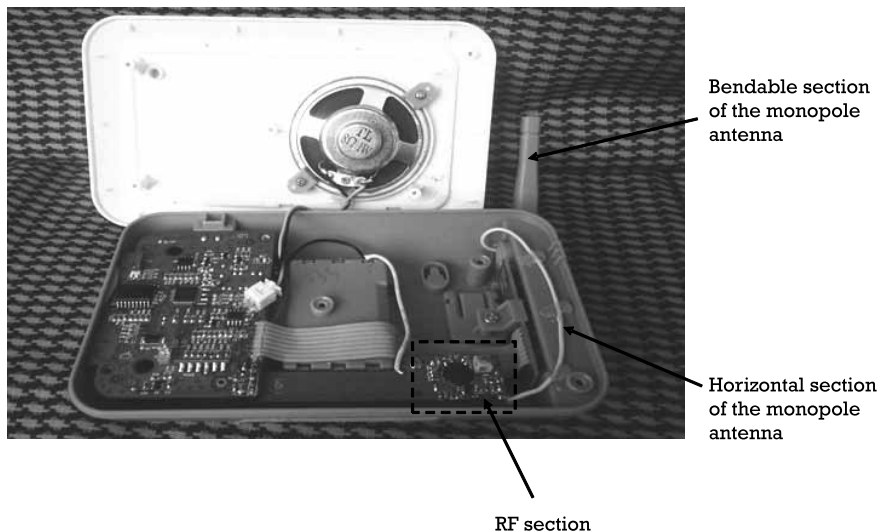


**Figure 8.5** PCB on the base unit of the wireless doorbell.

signals regardless of the position of the external antenna. For a maximum range, a user could turn the external antenna to align with the orientation

of the internal section to receive a full signal level. For example, the external section would be bent horizontally or vertically when the base unit is placed on a table or mounted against a wall, respectively.

Another key antenna parameter to be discussed is directivity. It is a measure of how directionally an antenna radiates. It is defined as the ratio of the maximum radiation intensity to the average radiation intensity over the entire sphere. Table 8.1 provides a comparison summary on directivity of different types of antenna [8]. The directivity of those antennas varies over several orders of magnitude. It is therefore important to know their directivity in choosing the right antenna for the specific applications. An antenna with low directivity is preferred if the signal being transmitted or received comes from different directions such as cellphones, WiFi routers, or car radios. However, if the direction of the target is fixed and known such as satellite communication, a high directivity antenna should be used to maximize the signal transmission and minimize signal from unwanted directions.

As a practical illustration, a 2.4-GHz tracking system Iseeka demonstrates the importance of antenna directivity in system considerations. Iseeka is a child-tracking system developed a few years ago when cellphones and data usage were still expensive to consumers. The product has two units, the finder unit and tracking tag, as shown in Figure 8.6. The tracking tag is to be worn on the wrist of a child while the finder unit is to be kept by a parent. When children go to a public place such as a playground with their parents, their parents can use the system to locate where they are.

The tracking tag transmits a radio signal periodically. The radio signal will then be picked up by the finder unit. The LCD screen on the finder unit will show the corresponding receiving signal strength (RSSI). If the child is out of range, the finder unit will not receive any broadcasting signal and it will provide an alert sound. Also, the child can press a panic button on the tag to broadcast an emergency signal when he or she is in danger. If the

**Table 8.1**  
Comparison on Directivity of Different  
Types of Antenna

Antenna Type	Typical Directivity (dB)
Short dipole	1.76
Half-wavelength dipole	2.15
Dish	10 to 30
Patch	3 to 8

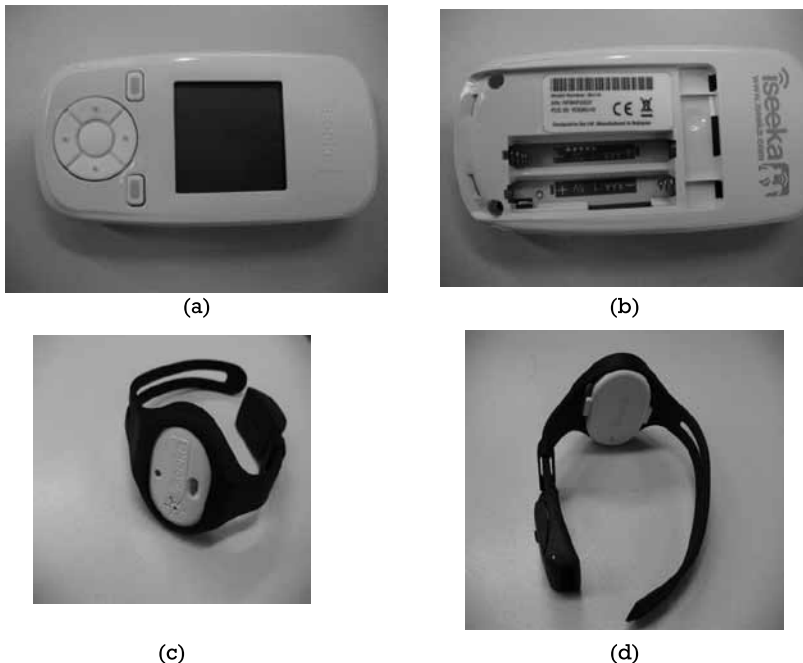


**Figure 8.6** Iseeka: (a) finder unit, front side; (b) finder unit, back side; (c) tracking tag, front; and (d) tracking tag, back.

tag is within the communication range, the parent can hold the finder and move around to check the corresponding RSSI reading. The direction to which the RSSI reading is the highest is the child's location. To achieve the seek function, the tag prefers to have an omnidirectional property on the antenna since it wants to be found by the finder unit from all directions. Figure 8.7 reveals the design of the PCB on the tag. Since the tag is worn on the wrist of the child, the size is desired to be small. With such a small size, the whole PCB is occupied by all components and leaves no space for the antenna. Even if it has space for the antenna, the radiation pattern will be dominated by the child's hand as it is so close to the antenna. There is no antenna on the board. The RF signal is capacitively coupled from the RF circuit to the wristband and it radiates out through the human body. The radiation is actually more desirable as the signal radiates from all direction from the body. The resultant radiation pattern is near omnidirectional.

However, the finder unit prefers to have directivity on the antenna so that the parent can search for the child more easily and precisely. To achieve the required directivity, the device uses a three-element Yagi-Uda antenna

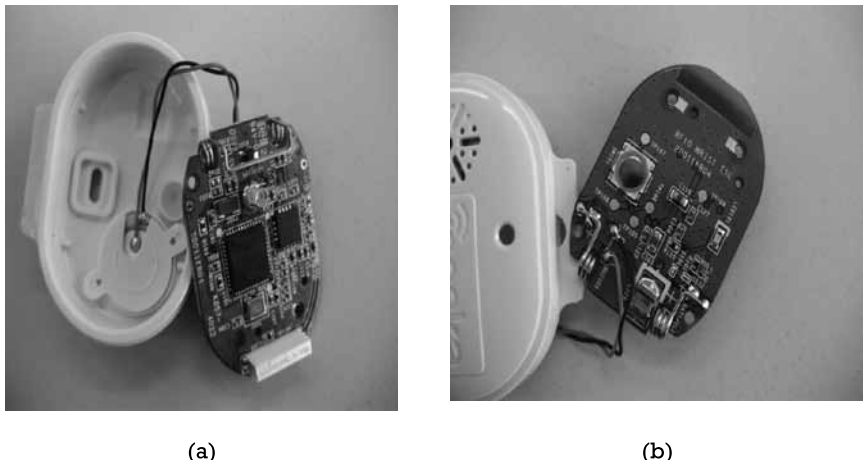
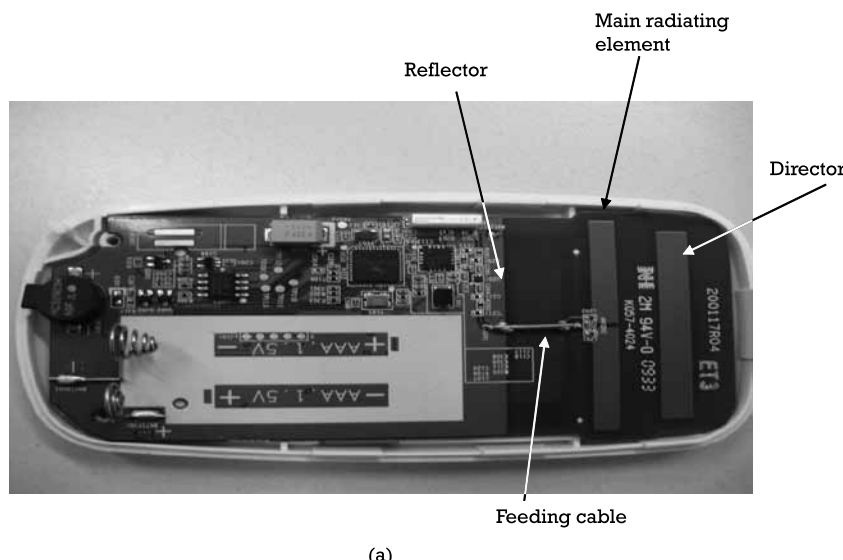


**Figure 8.7** (a) Top side of the PCB of the tracking tag, and (b) bottom side of the PCB of the tracking tag.

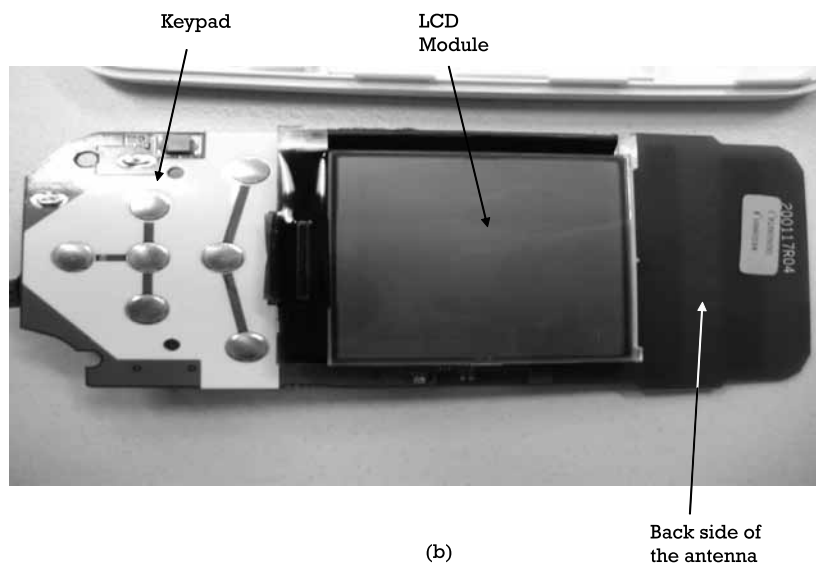
as shown in Figure 8.8. It is printed on the PCB and consists of a main radiating element, director, and reflector. The reflector is actually emulated by the ground plane of the main PCB to save space. Empty space on the bottom side of the antenna as shown in Figure 8.8(b) is reserved in order not to affect the antenna's characteristics. The design of the PCB was very well planned and done so that it can accommodate all the elements as well as the Yagi-Uda antenna. The size of the device is only about the same size of a regular smartphone.

### 8.2.3 Operating Frequency, Size, and Geometry

Besides being internal or external, antennas come in different shapes and sizes and are used for many different applications. The most important parameter is the operating frequency. The operating frequency determines four key parameters: (1) size, (2) product compliance requirement, (3) system link budget, and (4) implementation cost. Already discussed in Section 8.2.1, the size of a small antenna for optimum performance [1–3] is a function of its wavelength. The size of the antenna can be reduced significantly for higher operating frequencies. As illustrated in Chapter 3, the length of a quarter-wavelength monopole is 24 cm and 8.2 cm for 315 MHz and 915 MHz, respectively, for a short range device (SRD). For 315 MHz, the antenna would most likely be external due to its long length. SRDs are also allowed to operate at 2.4 GHz, having the quarter-wavelength of only 3 cm.



(a)

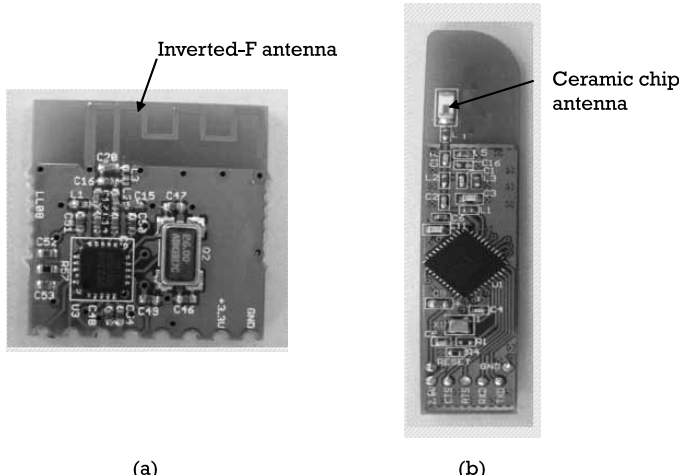


(b)

**Figure 8.8** (a) Main PCB (top side) showing the Yagi-Yuda antenna, and (b) main PCB (bottom side) showing back side of the antenna.

For 3 cm, the antenna can either be external or internal. For most handheld devices, an internal antenna will be preferred since it will not occupy too much space. Figure 8.9(a) shows a 2.4 GHz transceiver module using an inverted-F PCB antenna. The complete antenna module occupies only 3 cm × 3 cm and can fit into any small handheld device. With a higher cost, a ceramic chip antenna can be used which occupies even less board space as shown in Figure 8.9(b).

However, the operating frequency at which a wireless product can operate is determined by the local telecommunication authority in each country. For a short-range device (SRD) in the United States, the allowed operating frequencies are 315/433 MHz, 915 MHz, and 2.4/5.8 GHz [9, 10]. The required fundamental and harmonic power levels, modulation type, and transmit duration differ in their respective operating frequencies. Some are more restrictive than the others and thus the system designer should be very careful on choosing the right operating frequency. Besides the mentioned parameters governed by the telecommunication authority, other system performances such as signal immunity and range need to be considered as well. For example, many Internet of Things (IoT) devices these days try to include radar motion detector in the product to detect occupancy, motion or speed. Radar detectors can operate at 2.4 GHz, 5.8 GHz, 10.5 GHz, 24 GHz, and 77 GHz in the United States. Similar to any SRDs, each operating



frequency has its own requirements on fundamental and harmonic power levels and modulation bandwidth. Although allowed in 2.4 GHz and 5.8 GHz, radar detectors can be interfered with very easily by the Bluetooth and WiFi signals. For better signal immunity and smaller antenna size, operating at a higher frequency such as 10.5 GHz and 24 GHz is a better choice.

Although a quarter-wavelength monopole is shorter, the free-space path loss is higher for higher operating frequencies as introduced in Chapter 2. This means that the receiving signal would be lower and the communication range would be shorter. The system link budget has to be calculated for each operating frequency since the free-space path loss is different. Unfortunately, unless using the spread spectrum technology, the maximum allowable output power remains almost the same for 900 MHz, 2.4 GHz, and 5.8 GHz [9, 10], which means that the receiving power is lower at higher frequencies due to its higher free-space path loss. This results in a short communication distance for operating at higher frequencies.

Assuming that there is a size limitation, the SRD has to operate at 2.4 GHz and use an internal antenna. The designer can still choose antennas with different geometries and shapes for optimum performance. For example, in the 2.4-GHz remote controller, an inverted-L or inverted-F antenna can be used (see Figure 8.9(a)). If space is a concern, a ceramic chip antenna as a shrunk down monopole can also be used (Figure 8.9(b)) but with a higher cost. Those suggested designs are strictly 2-D or planar structure and they may not fully utilize the available volume of the product. The studies on the limitations of small antenna [11–14] have suggested that creative designs can be developed with 3-D structures to fully utilize the available volume of the product to optimize the antenna performance. Reference [15] suggested a 3-D technique to make volumetric dipoles, helix, spiral, and sphere, to optimize antenna efficiency.

### 8.3 Implementation Considerations and Strategies

Following the design techniques and using the simulation tools mentioned in the previous chapters, antennas with optimal performance can be designed without too many difficulties. However, once the antennas are placed inside the casing or on the main PCB of products, the characteristics of the antenna will change drastically and the radiation performance decreases significantly. Typical design areas on the product that affect the antenna's performance are antenna location and placement, ground plane, enclosure, PCB design practices, and mechanical design (board size and area).

### 8.3.1 RF PCB Layout Techniques and Practices

A well-designed RF PCB is crucial to the success of any wireless product as the layout of the PCB greatly affects the performance, stability, and reliability of the product. For example, an RF amplifier will become an oscillator if the layout is not done properly. Similarly, an oscillator may become an amplifier if the layout is poor. The products will also have many electromagnetic interference/ electromagnetic compatibility (EMI/EMC) issues and may fail in product compliance tests if the layout and shielding of the product are not done properly. General design rules and guidelines can be found from [16–20] while RF-specific PCB design guidelines can be found from [21, 22]. The design guidelines related to RF and antenna designs can be summarized in Table 8.2 for quick reference.

Those guidelines are typically applicable on making the PCB itself. When the products have an antenna, the layout will directly or indirectly affect the radiation performance. The requirements on making good RF or high-speed PCB could be contradictory to those for good antenna performance. It is therefore important to identify those special PCB design items when an antenna is in place. They will be discussed in the following sections.

### 8.3.2 Antenna Location and Placement

In free space, the actual radiation characteristics of an antenna match very well with the simulated or designed ones. However, when the antenna is placed inside the product as an internal antenna, its characteristics will change significantly particularly if it is too close to metal parts or the ground plane. The changes are due to the cancellation on the radiating current on the antenna and by the ground plane [7]. As a general practice, the antenna should be placed at the corner or the edge of the PCB with sufficient clearance from the rest of the circuit [21–23] to avoid the field-cancellation current induced on nearby metal objects or the ground plane. The electromagnetic fields generated by the antenna will radiate out into free space rather than going back to the source on the main PCB.

The cellular phones shown in Figures 8.1 and 8.2 are good examples of placing the antenna at a corner. The PCB layout of the cellular phone was very well designed so that the circuits were grouped and partitioned in individual functional blocks as shown in Figure 8.10. The layout was done in a strategic way so that the digital parts were on the right side while the RF and analog parts were on the upper left corner. The RF and analog parts were placed right next to the antenna. Such close proximity can eliminate

**Table 8.2**  
Design Guidelines Related to RF and Antenna Designs

Layout item	Design Guideline
Layer stack-up assignment	Assign proper layers for main signal, auxiliary signal, power, main ground and auxiliary ground planes
Component placement	Identify and group circuits of antenna, analog, digital, switching, audio; identify critical components; place components as close to integrated circuits as possible with the priority of RF, IF and audio components; maximize the area of ground plane; separate input and output ports of circuits as far as possible
Grounding method	Prerequisite of good RF and EMC performance; make ground traces as short and wide as possible; make ground plane as large as possible; make complete ground plane by avoiding interruptions due to via holes and signal traces
Bypassing and decoupling	Prevent energy transferring from one circuit to another; decouple each circuit block individually; location of decoupling components is critical; avoid unnecessary long connection traces; decouple each supply pin individually; provide different VCC decoupling capacitors: 10–100 $\mu\text{F}$ for audio frequency, 0.01 to 0.1 $\mu\text{F}$ for IF, 30~100 p for RF; use the right decoupling component for the right frequency
Via holes	Avoid interruptions on ground plane; use the right size for signal, power, and ground via holes; use a sufficient number of ground via holes, depending on current and frequency; use multiple via holes for ground connection
Trace routing	Keep traces as short as possible and minimize stitches between layers; good routing can minimize parasitic inductance, capacitance, and resistance; maximize board space to leave space for trace routings; can use trace as PCB antenna; avoid unintended radiation due to long traces
Shielding	Provides an effective solution for EMI and EMC; provide circuit partitioning and isolation
Design for evaluation boards	Performance is most important and cost is a less concern; make the board larger for easy routing and larger ground plane

the feeding cable and or shorten the feeding path from the RF output to the antenna so that the insertion loss can be minimized.

As other examples, Figure 8.9(a, b) show RF modules using internal antenna being placed at the edge and corner, respectively. Their circuits and layouts are not as complicated as the cellular phone example, but they share the same layout principle that the RF-related sections are placed very close to the antenna. As a general RF layout guideline [21], the high-speed digital circuit should be separated as far as possible from the RF circuit. The digital part typically has a high-speed clock with high harmonic signal levels. Those harmonic signals can get into the RF part very easily by either conduction or radiation and create self-quenching effect [24] (jamming) on the receiver degrading the sensitivity.

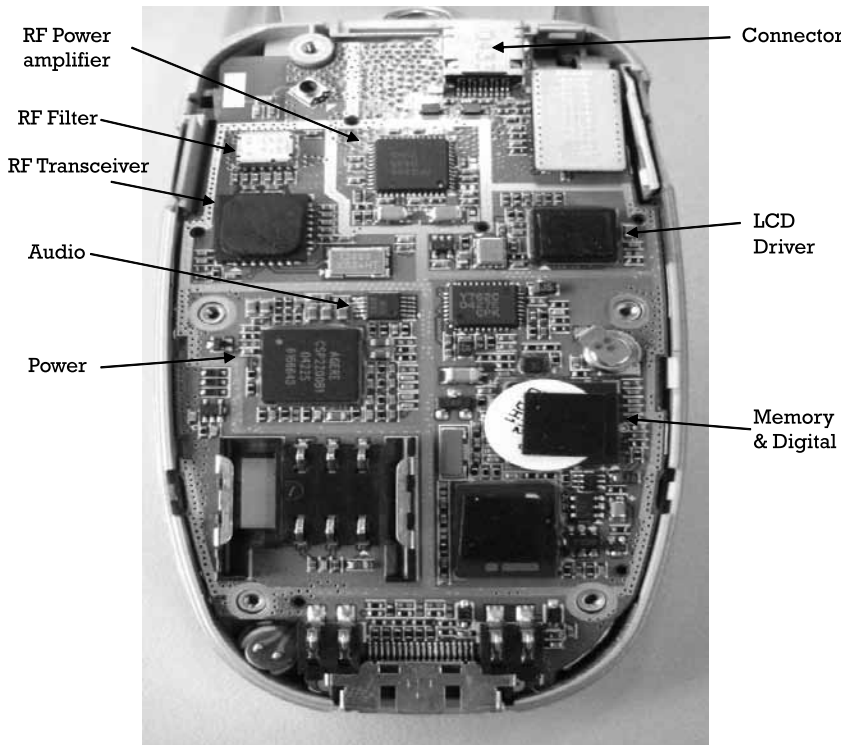


**Figure 8.10** PCB design of a cellular phone.

### 8.3.3 Ground Plane

The effect of the size of the ground plane on the antenna performance was discussed in detail in Chapter 7. The ground plane is actually part of the antenna for some types of antenna such as monopole or patch. Besides those considerations for antenna performance, the PCB design on the ground is also important on system performance. According to the RF layout design guidelines suggested in [21, 22], the ground is supposed to be as big and complete as possible and avoid any signal lines running across it to minimize signal disruption. Furthermore, the top and bottom grounds should be connected with as many ground via holes as possible. As an example, Figure 8.11(a) shows an ISM band RF transceiver module [25]. The module is using a ceramic antenna for overall size reduction. It has reserved a good amount of free space for the antenna such that the antenna can radiate close to the free-space condition. On the PCB, a complete ground plane was put on the inner ground layer.

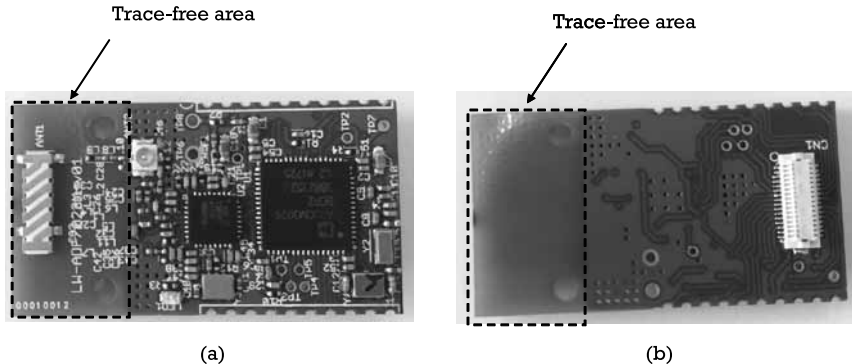


**Figure 8.11** (a) Top side of the ISM band RF transceiver module. (b) Bottom side. (From: [25]. © 2018 Reprinted with permission of Lexiwave.)

RF module is typically put on a motherboard for further signal processing or evaluation as shown in Figure 8.12. Although the layout of the module is done according to the RF layout design rules, special attention should be made to treat the ground on the motherboard or the evaluation board since the module has an on-board antenna. The main board should

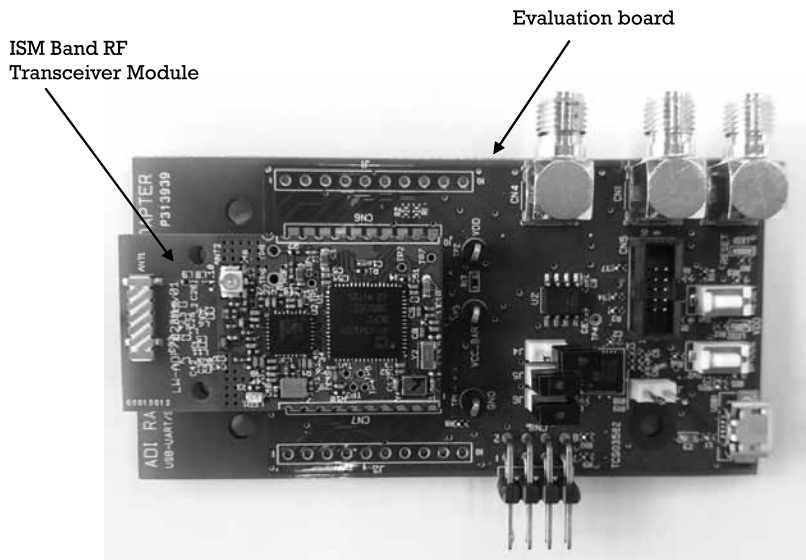


**Figure 8.12** ISM band RF transceiver module on an evaluation board. (From: [26]. Reprinted with permission of Analog Devices.)

be filled with as much ground as possible by default for RF considerations. That can be done very easily using the automatic copper-flooding feature found in most PCB layout design tools. The area underneath the RF module would have been filled with ground very easily without knowing the presence of the antenna on the module. The filled ground underneath the antenna could block the electromagnetic signals and lower the antenna gain significantly. However, the layout of the evaluation board shown in Figure 8.13 was done nicely with a dedicated copper keep-out area underneath the antenna of the RF module.

### 8.3.4 Enclosure

The enclosure, typically made of plastic, will affect the antenna's characteristic when it is too close to the antenna. An antenna can be treated as a resonator when designed properly with or without a matching network. It can be modeled as an indicator-capacitor (LC) resonating network whose frequency changes with its equivalent capacitance or inductance. Plastic has a higher dielectric constant than air or the FR-4 material in PCB. If the antenna is close to the casing, the capacitance of the casing will couple to it. The resultant capacitance of the antenna will then increase, leading to a lower resonant frequency. Reference [23] demonstrated such an effect on the resonant frequency of an antenna placed in a wireless mouse with a plastic casing. The wireless mouse has both top and bottom plastic covers. Due to slim nature of the product, the antenna is placed between the two covers with a very narrow gap. The coupling capacitance from the antenna

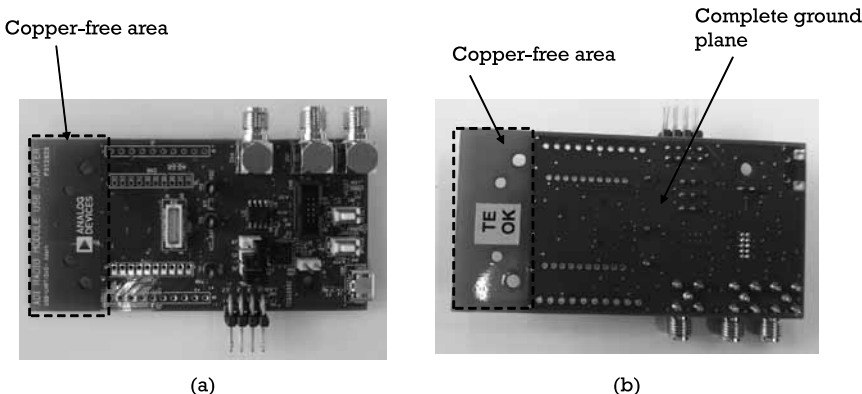


**Figure 8.13** (a) Top side of the evaluation board and (b) bottom side showing copper keep-out area for the antenna on the RF module.

will shift the resonant frequency down as observed on the change in the return loss over frequency as reported in [23]. Due to the potential shift in the antenna characteristic, it is recommended to characterize and tune the antenna with enclosure in place.

For RF considerations, the main PCB in wireless products is typically flooded with a complete ground in at least one PCB layer. The RF layout practice is contradictory to the requirement of leaving more free space for the antenna. One way to satisfy both requirements is to increase the size of the product, which is not desirable from cost and cosmetic perspectives. Figure 8.14 shows a tablet PC on the market to illustrate the dilemma of having good PCB ground and good antenna performance. The tablet PC has top and bottom covers that are both made of plastic. On the top side of the PCB, there is a big liquid crystal display (LCD) panel occupying most of the available space of the product. The liquid crystal material of the LCD and its associated coating for connections have very high conductivity at RF and microwave frequencies. They can be treated as an equivalent solid metal. The antenna is not recommended to be put on or near it although the top cover is plastic. The bottom side is the main PCB and flooded with complete ground plane. This is also not a good place to put the antenna. To leave room for the required antennas for the WiFi (2.4 GHz), GPS (1.5 GHz), and cellular (800/900/1,800/1,900 MHz) connectivity, the casing is extended out (see Figure 8.15(a)). It has two antennas, one for WiFi and one for the GPS and cellular bands. Both antennas are inverted-F type with flexible PCB material so that they can be attached to the curved surface of the casing as shown in Figure 8.15(b). Due to its proximity to the either the ground of the PCB or the LCD, the radiation resistance will be very low.



**Figure 8.14** Tablet PC: (a) front side and (b) back cover.

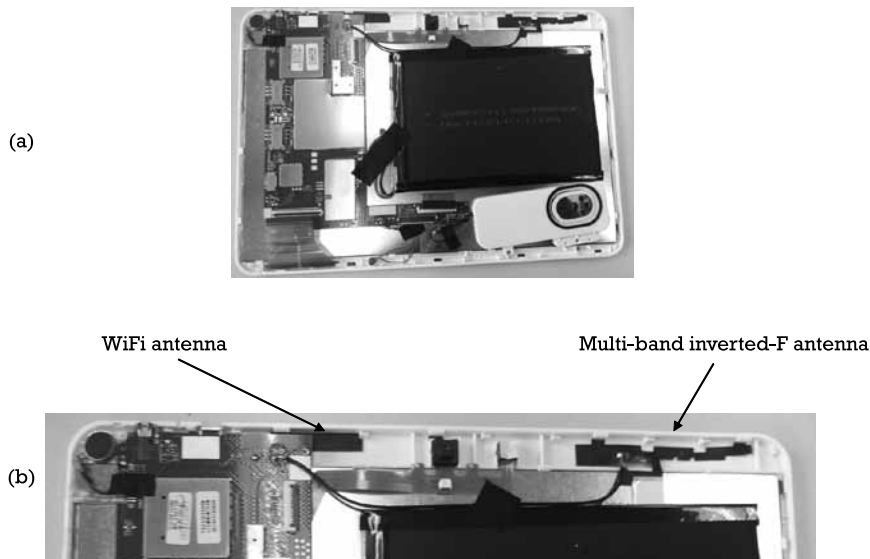


**Figure 8.15** Tablet PC: (a) PCB inside and (b) WiFi and cellular band antennas.

Although plastic is a popular material for making product enclosures, metal is commonly used for ruggedness, stylish, and mechanical strength reasons. Many recent smartphones and tablet PCs use metal material, at least on the back cover. They need to support multiple frequency bands for WiFi, GPS, and GSM/3G/4G signals. These handheld devices are preferred to be thin and small. It is thus very difficult to find space to put separate antennas for each frequency band and it is the metal enclosure posing the greatest challenge to the antenna designer as it is shielding all the RF signals. Fortunately, slot antennas are very suitable for tight-space devices and devices having a metal environment. The antennas used in the tablet PC mentioned could be replaced by a slot antenna for higher radiation resistance as shown in Figure 8.16. Since the body of a slot antenna is made of metal, its antenna characteristics will only change slightly even if the antenna is placed next to other metal objects such as the ground of the PCB or the LCD. With creative designs, wideband slot antennas can be realized without increasing too much in size [27–29].

### 8.3.5 Mechanical Design, PCB Design, and Teamwork

There are typically several teams in a company involved in developing a wireless product such as the marketing, system, electronic, software, and

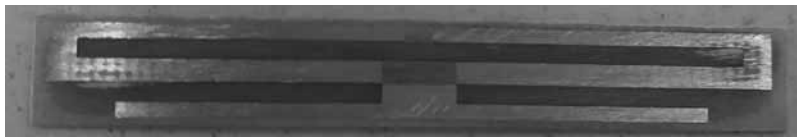


**Figure 8.16** A slot antenna.

mechanical design teams. As already discussed throughout this chapter, an antenna has better performance if it has larger volume and more free space. Unfortunately, the design teams always compete with each other on the scarce space available by the product, particularly in handheld devices since each design team has its respective design requirements and objectives. As an illustration of the group design challenge, Figures 8.17 through 8.19 along with Figure 8.10 all show the design details of a clamshell cellphone on the market a few years ago. The marketing team would try to add as many features as possible in the product with the smallest size. At a minimum, the speaker, earphone, microphone, keypad, camera, battery, and LCD would be needed to form a basic cellphone. However, the mechanical engineer prefers to make the product as big as possible to house all the parts and the PCB. For the electronic design team, they would need a PCB as

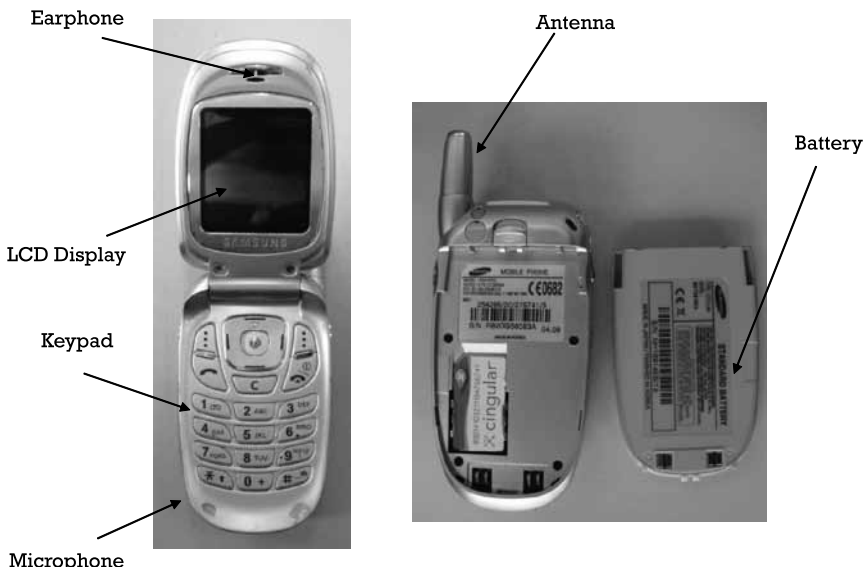


**Figure 8.17** A clamshell cellular phone showing the basic features.

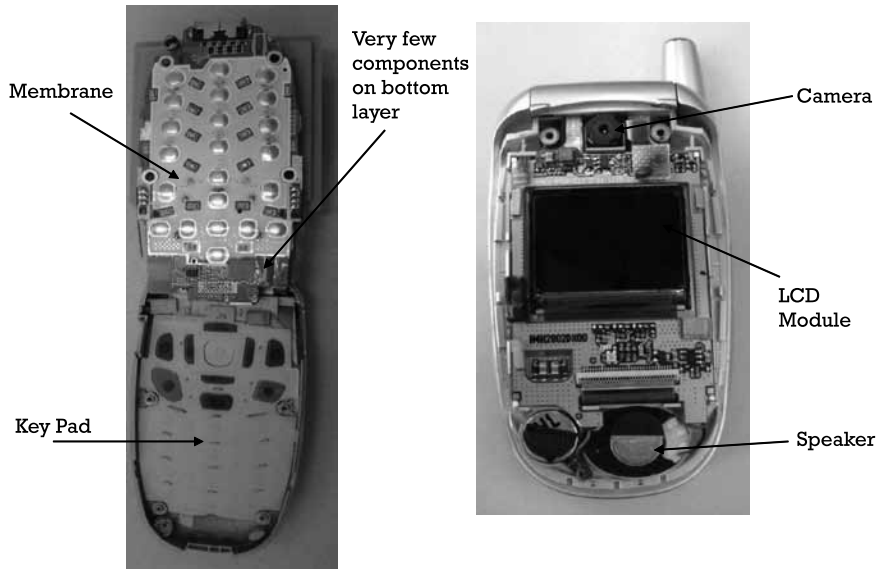


**Figure 8.18** Internal structure of a clamshell cellular phone.



**Figure 8.19** Internal circuit partitioning and metallization.

big as possible to place all the components and routing to make a good RF layout for best RF performance. Some space is also reserved on the PCB for isolation walls for EMI/EMC considerations. Given all the requirements and

constraints, the antenna has to be placed outside the casing to leave internal space for all the components and parts.

With the advance of semiconductor technology and design, many circuits and parts can be integrated into an integrated circuit (IC) or system on chip (SoC). The RF, analog, and digital circuits can now be integrated into one single SoC. This leaves space for smartphones found nowadays to use internal antennas as introduced in Section 8.2.1. Despite the integration, more parts, components, and RF connectivities are incorporated into smartphones to offer more advanced features to users. Smartphones with sensors of accelerometer and gyroscope and RF connectivities of GPS, BLE, WiFi, and GSM/GPRS/3G or 4G are standard. They also have to house a large LCD, batteries, and multiple cameras. The challenge to put all the components and parts into smartphones with scarce board space remains. To be compatible to the existing cellular networks, most cellphones have to operate in multiple frequencies to cover all the available frequency bands of different cellular generations of network (i.e., GSM/GPRS, 3G or 4G). To design a compact, multiband antenna to cover those cellular standards, it is important to leave space for other parts and components. It is also helpful for engineers to apply the same technique to develop future wireless handheld devices with space limitations.

Reference [30] conducted a survey of internal antennas in more than 60 mobile phones on the market and provides a good source of information on antenna design techniques, antenna manufacturing technologies, and the effect of handset materials. Table 8.3 summaries the key parameters of the studied smartphones including antenna types and covered frequency bands. It can be noticed that the planar inverted-F antenna (PIFA) is the most common configuration on multiband designs. The design technique for multiband on PIFA is similar to that for the inverted-F antenna as illustrated in Section 4.2.3 by introducing radiating branches, slots, and parasitic elements. Several GSM smartphones using PIFA for tri-band operation are shown in Figure 8.20. They are all operating at GSM bands of 800 MHz, 900 MHz, and 1,800 MHz. As illustrated in Figure 8.20(b), the antenna has two radiating branches and one parasitic element to resonate at 800 MHz, 900 MHz, and 1,800 MHz. They are all placed near the edge of the board and at the top part of the product for best radiation performance as discussed in Section 8.3.2.

MIMO systems become very popular due to the increased demand in handheld devices using WiMax and Long Term Evolution of 4G standards as mentioned in Section 1.2.2 for high transmission rate and channel capacity. In these MIMO systems, multiple antennas are used at both transmitters

**Table 8.3**  
Various Mobile Phones on the Market

<b>Model</b>	<b>Antenna</b>	<b>Effective Volume (cc)</b>				<b>Form Factor</b>	<b>Frequency Bands</b>
		<b>Length</b>	<b>Width</b>	<b>Height</b>			
Apple iPhone 2G	Planar Monopole	55.6	22.8	10.4	6.9	Candybar	GSM850/900/1800/1900
Apple iPhone 3G	Planar Monopole	55	20	8.5	9.0	Candybar	GSM850/900/1800/1900+3G
Apple iPhone 4	Planar Monopole	58	14	6.1	4.8	Candybar	GSM850/900/1800/1900+3G
ASUS M307	Planar Monopole	35	24	0.2	1.6	Clamshell	GSM900/1800/1900
ASUS P525	PIFA	34	20	7.6	5.1	Candybar	GSM850/900/1800/1900
BenQ Siemens EF-71	Planar Monopole	38	10.1	5.3	2.0	Clamshell	GSM900/1800/1900
Blackberry 8100	Planar Monopole	42	9	6.7	7.7	Candybar	GSM850/900/1800/1900
Blu 233/ Sendo M570	Planar Monopole	35	16.4	1.5	0.9	Clamshell	GSM900/1800
Geo GC688	PIFA	36.5	10.7	5.8	2.3	Slider	GSM850/900/1800/1900
Hagenuk	Slot	72.4	49.6	6.0	12.6	Candybar	GSM900
Motorola E398	PIFA	37.2	20.1	8.7	5.5	Candybar	GSM900/1800/1900
Motorola KRZR K1	Planar Monopole	37.5	7.6	7.0	2.4	Clamshell	GSM850/900/1800/1900
Motorola L2000/ P7389	Helix	44.2	5	5.0	2.1	Candybar	GSM900/1800/1900
Motorola L6	Planar Monopole	36.1	7.5	7.0	1.9	Candybar	GSM900/1800/1900
Motorola T193	PIFA	27	17.8	8.1	2.9	Candybar	GSM1900
Motorola T720i	Helix	29	10	10	1.6	Clamshell	GSM900/1800
Motorola V690	PIFA	38	16.9	9.5	6.1	Clamshell	GSM900/1800/1900
Motorola W208	PIFA	35.6	24	6.5	2.1	Candybar	GSM900/1800
Nokia 2626	PIFA	38	22.3	7.7	3.0	Candybar	GSM900/1800
Nokia 2652	PIFA	41.4	18.6	6.6	5.1	Clamshell	GSM900/1800
Nokia 5210	PIFA	34	18	6.6	4.4	Candybar	GSM900/1800

**Table 8.3** (continued)

<b>Model</b>	<b>Antenna</b>	<b>Length</b>	<b>Width</b>	<b>Height</b>	<b>Effective Volume (cc)</b>	<b>Form Factor</b>	<b>Frequency Bands</b>
Nokia 5300	Planar Monopole	36.5	8.4	9.3	2.8	Slider	GSM900/1800/1900
Nokia 5320	PIFA	42.6	28.5	8	6.4	Candybar	GSM850/900/1800/1900+3G
Nokia 5500	PIFA	34.4	38.8	8.5	10.5	Candybar	GSM900/1800/1900
Nokia 6030	PIFA	38	22.3	9.1	6.6	Candybar	GSM900/1800
Nokia 6100	PIFA	37.9	28.6	6.3	6.1	Candybar	GSM900/1800/1900
Nokia 6108	PIFA	37.9	28.6	5.6	5.5	Candybar/Flip	GSM900/1800/1900
Nokia 6111	Planar Monopole	41.4	9.1	6.8	2.5	Slider	GSM900/1800/1900
Nokia 6210	PIFA	42.6	19.8	9.9	8.4	Candybar	GSM900/1800
Nokia 6260	Planar Monopole	45	8.5	1.1	1.5	Clamshell	GSM900/1800/1900
Nokia 6270	PIFA	47.7	28.9	6	6.3	Slider	GSM850/900/1800/1900
Nokia 6300	PIFA	33	24.2	3.3	3.4	Candybar	GSM900/1800/1900
Nokia 6630	PIFA	33	34.4	6.5	7.0	Candybar	GSM850/900/1800/1900+3G
Nokia 6680	PIFA	28	34.8	10.6	10.0	Candybar	GSM850/900/1800/1900+3G
Nokia 6708	PIFA	33	28	11.1	9.0	Candybar	GSM900/1800/1900
Nokia 6800	PIFA	35.4	20.5	10.7	6.1	Candybar/Flip	GSM900/1800
Nokia 7210	PIFA	38.3	32.9	8.1	8.8	Candybar	GSM900/1800/1900
Nokia 7270	PIFA	84	40	3.8	12.8	Clamshell	GSM900/1800/1900
Nokia 7280	PIFA	29.4	26	10.5	3.3	Candybar	GSM900/1800/1900
Nokia 7370	PIFA	40	28	7	8.2	Clamshell	GSM900/1800/1900
Nokia 8110	Helix	33	4.5	4.5	1.7	Candybar/Slider	GSM900
Nokia 8210	PIFA	36	15.8	12.5	6.7	Candybar	GSM900/1800
Nokia 8850	PIFA	34.9	14.1	7.4	5.9	Candybar/Slider	GSM900/1800

**Table 8.3** (continued)

<b>Model</b>	<b>Antenna</b>	<b>Length</b>	<b>Width</b>	<b>Height</b>	<b>Effective Volume (cc)</b>	<b>Form Factor</b>	<b>Frequency Bands</b>
Nokia 9300	PIFA	43	23	7.2	7.1	Candybar/Flip	GSM900/1800/1900
Nokia E60	PIFA	40	19.4	10.4	8.1	Candybar	GSM900/1800/1900 + 3G
Nokia N-Gage	PIFA	44.9	24.8	7.5	8.4	Candybar	GSM900/1800
Samsung P300/308	Planar Monopole	48.4	6.2	5	1.2	Candybar	GSM900/1800/1900
Samsung SGH-2200	Helix	38.5	5.1	5.1	1.4	Candybar/Flip	GSM900/1800
Samsung SGH-C408	Planar Monopole	33.6	16	4	1.9	Clamshell	GSM900/1800/1900
Sony Ericsson J200i	PIFA	33	25.6	6.2	4.5	Candybar	GSM900/1800/1900
Sony Ericsson K660i	PIFA	40	22	8	6.2	Candybar	GSM850/900/1800/1900+3G
Sony Ericsson P910i	Planar Monopole	35	9.7	8.4	2.9	Candybar/Flip	GSM900/1800/1900
Sony Ericsson W800i	PIFA	37.1	20	6.2	4.6	Candybar	GSM900/1800/1900
Sony Ericsson W850i	PIFA	33	31	7.5	5.4	Slider	GSM900/1800/1900 + 3G
Sony Ericsson Z200	Planar Monopole	32	28.8	0.3	0.8	Clamshell	GSM900/1800/1900
Sony Ericsson Z300i	PIFA	38.4	10	10.9	3.3	Clamshell	GSM900/1800
Sony Ericsson Z600	PIFA	43.6	39	4.4	7.5	Clamshell	GSM900/1800/1900
Toshiba TS30/TS32	Planar Monopole	42.6	6.7	4.7	1.3	Candybar	GSM900/1800/1900

Source: [30].

and receivers. The signal paths from different antennas between the transmitters and receivers should be uncorrelated to obtain high capacity. Diversity antennas are thus required and antenna diversity can be accomplished by polarization, space, pattern diversities, or a combination of these

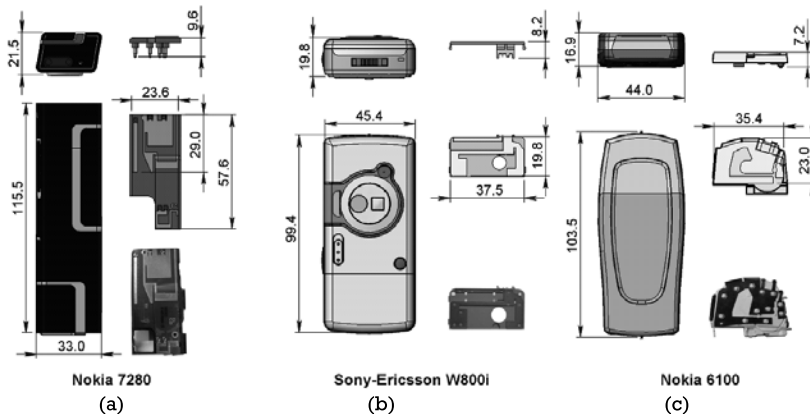


**Figure 8.20** Tri-band GSM smartphones. (From: [30]. Reprinted with permission of IEEE.)

techniques. Space diversity can be achieved by using more antennas but finding space in smartphones is extremely difficult. Other diversity methods occupying less space are preferred for handheld devices. Research in [31] proposed a creative dual-port PIFA MIMO antenna, which has polarization and pattern diversities. The design is shown in Figure 8.21, which has only one PIFA element with two feed points to make the antenna compact. Polarization and pattern diversities are achieved by having the two feed plates at different sides of the top plate and perpendicular to each other. However, there is a signal coupling between the two ports through the ground plane. A rectangular slot is added on the ground plane between the two ports to increase the isolation. Although only one single element is needed to achieve the required diversities, no components are allowed to be put inside the slot area at the bottom side of the PCB which effectively leaves less usable space for the phone. Nevertheless, the designed PIFA antenna can cover a frequency band of 2.35 to 2.8 GHz for BLE/WLAN and LTE (2.5–2.7 GHz) applications.

The cellular technology is soon going into the 5G era and new antenna designs for 5G base stations and mobile stations will be in great demand. Current antennas for 4G application require a  $2 \times 2$  MIMO operating scheme. They are not suitable for 5G application as the data rate of 5G is almost 1,000 times faster than that of 4G. Multiple antenna elements of more than 4 are required to have a more reliable radio link for 5G massive MIMO applications [32, 33]. This will pose great challenges for the handset manufacturers to put extra antennas into already crowded handsets.

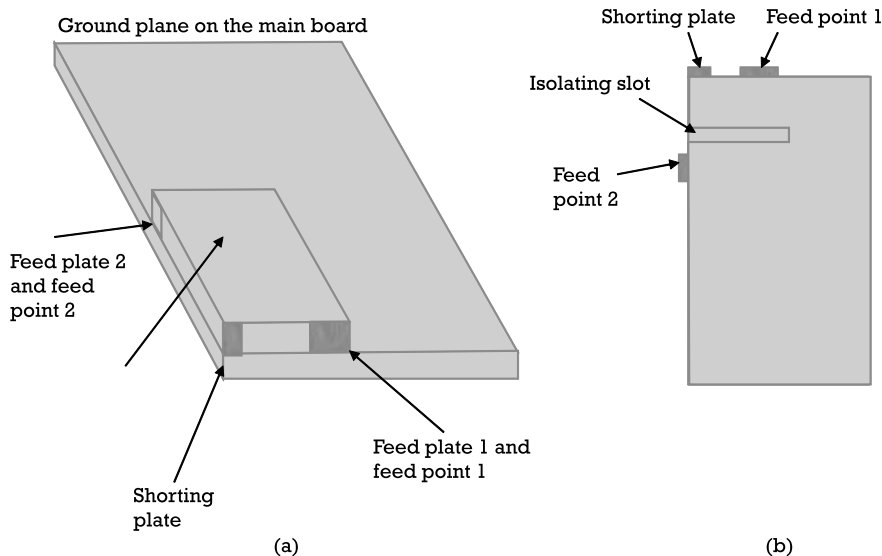


**Figure 8.21** Two-port PIFA: (a) configuration and (b) ground plane with slot for isolation.

As illustrated throughout this chapter, the design objectives of each team are different and most of the time they conflict with each other. Teamwork and joint effort would be the most effective way to come up with an optimal design from marketing, electronic, and mechanical design perspectives.

## References

- [1] Wheeler, H. A., "Fundamental Limitations of Small Antennas," *Proceedings of the IRE*, Vol. 35, December 1947, pp. 1479–1484.
- [2] Hansen, R. C., "Fundamental Limitations in Antennas," *Proceedings of the IEEE*, Vol. 69, No. 2, February 1981, pp. 170–182.
- [3] Harrington, R. F., "Effect of Antenna Size on Gain, Bandwidth, and Efficiency," *Journal of Research of the National Bureau of Standards*, Vol. 64D, January–February 1960, pp. 1–12.
- [4] "John Francis Mitchell Biography," <http://www.brophy.net/PivotX/?p=john-francis-mitchell-biography>.
- [5] "[http://www.infobarrel.com/Who\\_Invented\\_the\\_Cell\\_Phone](http://www.infobarrel.com/Who_Invented_the_Cell_Phone), [http://www.infobarrel.com/Who\\_Invented\\_the\\_Cell\\_Phone](http://www.infobarrel.com/Who_Invented_the_Cell_Phone).

- [6] "Meet Marty Cooper: The Inventor of the Mobile Phone," [http://news.bbc.co.uk/2/hi/programmes/click\\_online/8639590.stm](http://news.bbc.co.uk/2/hi/programmes/click_online/8639590.stm).
- [7] Balanis, C. A., *Antenna Theory: Analysis and Design*, New York: John Wiley & Sons, 1997.
- [8] "Directivity—Antenna Theory," <http://www.antenna-theory.com/basics/directivity.php>.
- [9] Loy, M., R. Karingattil, and L. Williams, "ISM-Band and Short Range Device Regulatory Compliance Overview," *Texas Instruments Application Report SWRA048* May 2005.
- [10] Micrel Incorporated, "How to Go Through FCC Compliance Testing Using the MICRF112," *Application Note 55*, 2007.
- [11] Gustafsson, M., C. Sohl, and G. Kristensson, "Physical Limitations on Antennas of Arbitrary Shape," *Proceedings of the Royal Society of London A*, Vol. 463, No. 2086, 2007, pp. 2589–2607.
- [12] Behdad, N., and K. Sarabandi, "Bandwidth Enhancement and Further Size Reduction of a Class of Miniaturized Slot Antennas," *IEEE Trans. on Antennas and Propagation*, Vol. 52, No. 8, August 2004, pp. 1928–1935.
- [13] Nakano, H., et al., "Shortening Ratios of Modified Dipole Antennas," *IEEE Trans. on Antennas and Propagation*, Vol. 32, No. 4, April 1984, pp. 385–386.
- [14] Best, S. R., "The Radiation Properties of Electrically Small Folded Spherical Helix Antennas," *IEEE Trans. on Antennas and Propagation*, Vol. 52, No. 4, April 2004, pp. 953–960.
- [15] Sarrazin, F., S. Pflaum, and C. Delaveaud, "Radiation Efficiency Optimization of Electrically Small Antennas: Application to 3D Folded Dipole," *International Workshop on Antenna Technology*, 2016, pp. 29–32.
- [16] Montrose, M. I., *Printed Circuit Board Design Techniques for EMC Compliance*, New York: Wiley-IEEE Press, 1996.
- [17] Khandpur, R. S., *Printed Circuit Boards: Design, Fabrication, Assembly and Testing*, New York: McGraw-Hill, 2006.
- [18] Blankenhorn, J. J. C., "PCB Design of High Speed Circuits," *SMT Plus*, 2004.
- [19] Montrose, M. I., "EMC and the Printed Circuit Board: Design, Theory, and Layout Made Simple," New York: Wiley-Interscience/IEEE, 1999.
- [20] Thierauf, S. C., *High-Speed Circuit Board Signal Integrity*, Norwood, MA: Artech House, 2004.
- [21] Lau, H., "Practical RF PCB Design: Wireless Networks, Products and Telecommunications," *IEEE Course Material*, Boston, MA, December, 2017.
- [22] Lau, H., "Practical Antenna Design for Wireless Products," *IEEE Course Material*, Boston, MA, June 2017.

- [23] Pattnayak, T., and G. Thanikachalam, "Antenna Design and RF Layout Guidelines," *Cypress Semiconductor Corporation Application Note AN91445 Revision H.*, September, 2018.
- [24] Vizmuller, P., *RF Design Guide: Systems, Circuits, and Equations*, Norwood, MA: Artech House, 1995.
- [25] Lexiwave Technology (Hong Kong) Limited, "LWADF7023M RF Transceiver Module," *Product Datasheet*, September 2018.
- [26] Analog Devices, Inc., "WiSUN RF Module USB Adapter Board," *Connected Sensor User Guide*, May 17, 2017.
- [27] Chang, T. -H., and J. -F. Kiang, "Compact Multi-Band H-Shaped Slot Antenna," *IEEE Trans. on Antennas and Propagation*, Vol. 61, No. 8, August 2013, pp. 4345–4349.
- [28] Zhong, J., et al., "Multiband Slot Antennas for Metal Back Cover Mobile Handsets," *Progress in Electromagnetics Research Letters*, Vol. 39, 2013, pp. 115–126.
- [29] Lee, Y. C., and J. S. Sun, "Compact Printed Slot Antennas for Wireless Dual- and Multi-Band Operations," *Progress in Electromagnetics Research*, PIER 88, 2008, pp. 289–305.
- [30] Rowell, C., and E. Y. Lam, "Mobile-Phone Antenna Design," *IEEE Antennas and Propagation Magazine*, Vol. 54, No. 4, August 2012, pp. 14–34.
- [31] Chattha, H. T., et al., "Single Element Two Port Planar Inverted-F Diversity Antenna for Wireless Applications," *Antennas & Propagation Conference*, Loughborough, UK, November 2013, pp. 321–324.
- [32] Masterson, C., "Defining Massive MIMO in a 5G World," *Microwave & RF*, October 30, 2017.
- [33] Li, Y., et al., "12-Port 5G Massive MIMO Antenna Array in Sub-6GHz Mobile Handset for LTE Bands 42/43/46 Applications." *IEEE Access*, Vol. 6, 2018, pp. 344–354.



## **CHAPTER**

# **9**

### **Contents**

- 9.1 Introduction
- 9.2 IoT Technology
- 9.3 Antenna Designs for IoT Applications
- 9.4 Antenna Technologies for the Future

## **Future Trends**

### **9.1 Introduction**

Antennas continue to play an important role in the success of many consumer, commercial, and industrial applications. The Internet of Things (IoT) has become particularly popular in the business and technology worlds in recent years. IoT refers to physical devices around the world that are connected to the internet, sharing and collecting data through wired and wireless connections [1–4]. It is predicted that IoT will disrupt the technology in the near future. Due to its huge market potential, it is worth the effort to identify the trend and provide more details on the antennas for the IoT devices. Since there are a vast number of different IoT applications across different sectors, only a few examples in some selected categories with volume potential will be discussed in this chapter. In addition, many technology-specific designs are emerging

as there are many researchers and companies working on new materials or design approaches that can improve antenna performance dramatically [5]. Newer applications can be realized as a result of the new technologies. They will also be discussed towards the end of the chapter so readers can be aware of those new technology trends.

It is anticipated that more different materials, structures, fabrication processes, and combinations of them are expected to come out in the future.

## 9.2 IoT Technology

### 9.2.1 IoT Devtices

Traditionally, only standard devices, such as smartphones, iPads, desktops, and laptop computers, are IoT devices due to their internet connectivity. The IoT era started early from the proliferation of machine-to-machine (M2M) communication, which is also called the industrial IoT. M2M focuses on industrial telematics in which data transfers between devices in an industrial environment for productivity improvement and commercial benefits. With the drops in prices of microprocessor and wireless networks, it is now possible to turn anything from a “dumb” or non-internet-enabled physical device and everyday object to become connected to the internet.

According to Gartner’s report [6], there were 8.4 million more IoT devices being used in 2017, which is more than the number of people in the world. The number is up 31% from 2016 and will likely hit 20.4 billion by 2020. The total spending was \$2 trillion in 2017 on IoT end devices and services. IDC [7] has also estimated that the worldwide spending on IoT will be \$745 billion in 2019 and will increase to \$1 trillion in 2022. In terms of spending, hardware will be the largest technology item in 2018 with \$239 billion spent on modules and sensors and some spending on infrastructure and security. Services will be the second largest spending item followed by software and connectivity.

### 9.2.2 Enabling Technologies

The applications for IoT devices [8] can be broadly classified into consumer, commercial, industrial, and infrastructure spaces [9, 10]. The enabling wireless technologies can also be classified as short-range, medium-range, and long-range applications [11–13]. The most commonly used and potential technologies are summarized in Table 9.1 and are explained briefly in the following sections.

**Table 9.1**  
Enable Technologies for IoT

Type	Standard	Connection	Frequency	Range	Security
WiFi	IEEE 802.11x	WLAN	2.4, 5.6 GHz	100m	WEP, WPA, WPA2
Z-wave	Z-wave	Mesh	314, 433, 868, 915 MHz	30m	Triple DES
Bluetooth Smart	IoT Interconnect	WPAN	2.4 GHz	50m	128-bit AES
Zigbee	IEEE 802.15.4	Mesh	868, 915 MHz, 2.4 GHz	30m	128 bit
6LowPan	IEEE 802.15.4, 6LoWPAN	Mesh	314, 433, 868, 915 MHz, 2.4 GHz	11m	128-bit AES
Sigfox	Sigfox	Star	868, 915 MHz	1 km	AES
Lora	Lora	Star	433, 868, 915 MHz	3 km	AES
RFID	Many standards	Point to point	13.56 MHz	1m	Possible
NFC	ISO/IEC 13157	Point to point	13.56 MHz	5 cm	Possible
GPRS	2.5G	GERAN	850, 1,900 MHz	20 km	GEA2/GEA3/GEA4
HSDPA/ HSUPA	3G	UTRAN	850, 1,700, 1,900 MHz	20 km	USIM
LTE	4G	GERAN/ UTRAN	700–2,600 MHz	20 km	SNOW 3G
NB-IoT	NB-IoT	LPWAN	700–2,600 MHz	20 km	LTE

### 9.2.2.1 Short-Range Wireless

Bluetooth Smart is a variant of Bluetooth Low Energy (BLE) providing a mesh network with an increased number of nodes and standardized application layers. Near-field communication (NFC) is a very short distance communication technology for two electronic devices to communicate within a 5-cm range. RFID is a technology using electromagnetic fields to read and write data stored in tags or in other embedded forms. ZigBee is a communication protocol based on an IEEE 802.15.4 standard providing a low data rate, low cost, and low power consumption. WiFi is a local networking technology based on the IEEE 802.11 standard providing communication through an access point or directly between devices.

### 9.2.2.2 Medium-Range Wireless

LTE is a 4G mobile communication technology providing higher throughput and lower latency.

### 9.2.2.3 Long-Range Wireless

A low power wide area network (LPWAN) is a low data rate, low power consumption, and low-cost wireless networks for large area coverage with available technologies of LorRaWan, Sigfox, and narrowband IoT (NB-IoT).

## 9.3 Antenna Designs for IoT Applications

Since there are a vast number of different IoT applications across different sectors, only a few examples in some selected categories with volume potential will be discussed to provide some design insights. The majority of IoT devices are created for consumer use such as home automation devices and appliances with remote monitoring, connected vehicles, wearable devices, and e-health devices. The following sections will address the antenna designs for those applications.

### 9.3.1 Smarthome Applications

Home automation, also more recently referred to as smarthome devices, include traditional home automation systems for lighting, heating, and air conditioning control as well as new smarthome devices. The basic system could be a remote controller sending or receiving signals to control an in-wall thermostat or an LED lightbulb. The typical operating frequency is 315 or 433 MHz. Very low cost with an acceptable range can be achieved without difficulty. Typical antennas such as PCB printed antennas, wire, and chip antennas can be used. As the product evolves, BLE connectivity is now added on the system so that users can use their smartphones to control the devices or appliances.

The new smarthome system could be a single device controlled by a smartphone or a platform or hub that controls smart devices and home appliances [14–16]. They use BLE and WiFi for user-hub and hub-cloud communications. Regular PCB or chip antennas are the typical antennas used in the device and hub since the operating frequency is 2.4 GHz for both BLE and WiFi. As the smarthome product continues to evolve, more sensors and features such as video surveillance are being incorporated into the products. Due to the propagation property of the RF signal at 2.4 GHz, the BLE and WiFi signals cannot penetrate through walls. Their applications are usually confined to a single-room use. Other communication technologies such as Z-wave and Lora are also being incorporated into smarthome systems. Z-wave has been used in industrial and commercial applications for years and is becoming popular in smart home applications. Lora is a

long-range and star-network technology targeted for city-wide infrastructure applications. They can both operate at 868 and 915 MHz. More importantly, they can penetrate through walls covering the whole house from the front yard to the basement. Some hub devices of the smarthome systems also have 3G/4G connectivity for security monitoring. The addition of more connectivities pose a great challenge to antenna designers as they have to find space to put multiple antennas into the products. To alleviate the space limitations, many researchers are developing miniature wideband antennas for IoT applications covering several gigahertz [17–19]. It is anticipated that more wideband antennas covering from subgigahertz up to 6 GHz will come to the market [20–22].

### 9.3.2 Wearable Devices

Another key application of IoT is the wearable device. Wearable devices have entered the market with great acceptance. Product types vary from smartwatch, glasses, apparel, and clothing to monitor everything from fitness, health, and physical conditions. Many different sensors such as temperature, accelerometer, gyroscope, and sound and light sensors are put inside the devices to track movement, sleep pattern, emotion, and breath rate. The section will focus on the recent developments of smartwatches and textile antennas due to their popularities and future growths.

#### 9.3.2.1 Smartwatches

One of the most popular wearable devices is the smartwatch as shown in Figure 9.1. The basic one is a smartwatch having just BLE connectivity to send/receive messages with a smartphone. The device can provide alerts by display, audible sounds, or colors. Equipped with an accelerometer and gyroscope, the BLE smartwatch can be used as a pedometer to check the distance walked and calories burnt by the users and their sleep pattern and quality as a fitness and wellness device. If equipped with an infrared sensor with suitable software algorithm, the watch can also check the heart rate and blood pressure of the user.

Another important watch type is the tracking smartwatch. It uses GPS technology to find the user's location precisely. Equipped with various sensors, the watch can monitor body temperature and heart rate to check the vital signs of the wearer. It can also detect other critical conditions such as a sudden fall. With cellular connectivity, it is typically used as part of a remote health monitoring system to monitor remotely the elderly or individuals who require special needs and attention. The system can identify

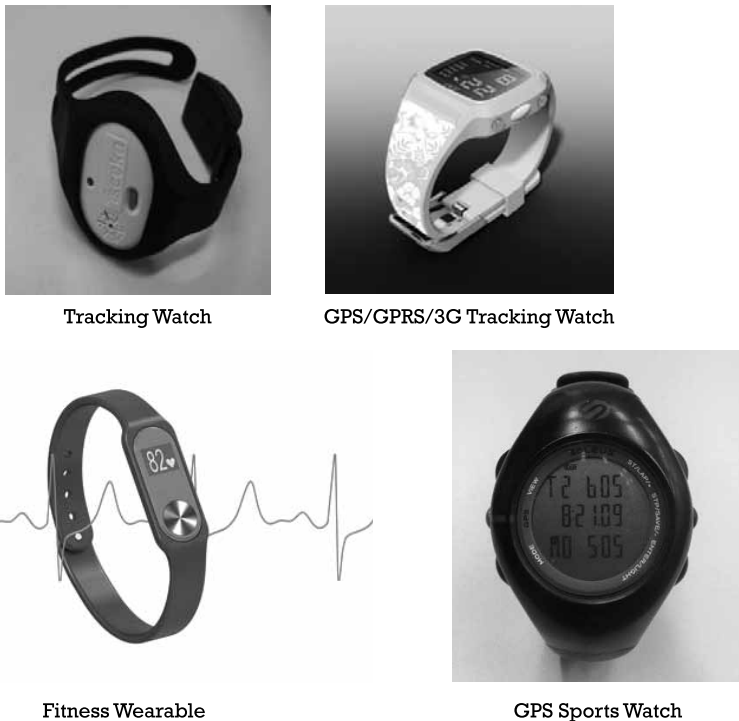


**Figure 9.1** Different types of wearable electronic products.

the person's location as well as their body vital signals. The system typically consists of a smartwatch and a cloud server. The smartwatch collects health parameters of the user periodically and sends the information to the cloud server for remote health and well-being monitoring.

Since more wearable devices are entering the market with more sensors, features, and connectivities, there is a huge demand for wearable antennas. Nevertheless, there are unique challenges to wearable devices that make antenna design particularly difficult such as having too many features and wireless connectivities, limited space, and proximity to the body. The smartwatches now have BLE connection as the basic feature and the tracking one may have GPS, 3G/4G, and even WiFi and ZigBee technologies. It becomes very difficult to find space to put all the antennas inside the watch to accommodate all the wireless connectivities. Wearable devices have to be small to be appealing to the consumers and therefore it is impossible to put a big dipole antenna hanging outside the device. In addition, space is extremely limited for the designers to put all the sensors, associated

circuitries, and antennas inside a tiny watch. Human tissue is lossy at RF/microwave frequencies. When an antenna is put near the human body, its electromagnetic waves will be absorbed and turned into heat. This results in lower antenna efficiency of the wearable antenna and thus has a significant impact on the performance of the wearable product. To mitigate those problems, researchers have been developing new and creative antennas for wearables. Their main design technique is to either come up with creative internal antennas to work better in proximity to the surroundings or to put the antenna outside the watch but hidden from the users.

### *Creative Internal Antennas*

With regard to a new component design, for a basic smartwatch, it may only have the Bluetooth antenna to pair up with a smartphone for message exchange. At 2.4 GHz, commonly used antennas are PCB, wire, or ceramic chip antennas as discussed in Section 8.2.3. Despite their higher cost, ceramic chip antennas are preferred due to their small size. Similar to other antennas, ceramic chip antennas are typically ground-plane dependent. There are certain requirements on the size and position of the ground plane to form a complete resonant circuit [23]. Assuming that the ground plane is large enough, the antenna should be placed near the edge of PCB as suggested in Chapter 8 for optimum performance. A certain keep-out area must also be reserved to free the antenna from metal objects and ground to prevent its radiated fields from being distorted. Having the keep-out area ensures that the antenna radiates effectively. Although the antenna itself is small, the required keep-out area is relatively big for a small device such as the smartwatch. It would be ideal if the keep-out area were not required for the chip antennas. The company in [24] has come up with a new chip antenna that eliminates the needs of a designated keep-out area. The antenna can be mounted directly onto the ground plane through the optimization of circuit design and materials of ceramic and conductive ink. This opens up opportunities for many small products from jewelry to other wearables in different sizes and shapes to incorporate wireless technology.

With regard to an integrated antenna, although using the new ceramic antenna introduced in the previous section can eliminate the need of the keep-out area, it is still necessary to find space to put the antenna on the PCB. Many researchers are trying to integrate the antenna into the body of the watch so that the antenna does not occupy any board space. Figure 9.2 shows such a design of using the metal frame of a smartwatch as a loop antenna with a dimension of 5 mm × 40 mm × 50 mm [25]. It encircles the main PCB of the watch with a separation distance of 2 mm between the

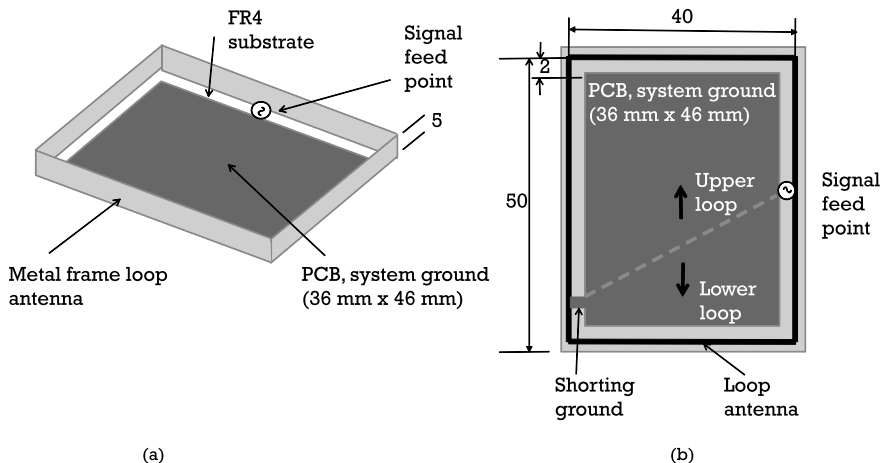


**Figure 9.2** (a) Integrated metal frame antenna of a smartwatch, and (b) detailed dimensions.

antenna and the ground to minimize their couplings. With the appropriate signal feeding and ground-shorting points, the antenna performs reasonably well with an antenna efficiency of around 68% at the Bluetooth operating frequency of 2.4 GHz. Even placed on a hand model, an antenna efficiency of 26% can still be achieved.

With regard to creative design, the casing of a smartwatch is typically either plastic or metal. Metal casing is more appealing over plastic as it looks like a jewelry and makes the watch look more valuable [26]. In addition to the visual appeal, the metal casing provides mechanical strength and rigidity for durability and reliability. However, having metal casing is a major challenge to the antenna design on smartwatches as the metal casing forms a complete Faraday cavity shielding all RF signals. The second example of using an internal antenna is a smartwatch operating at 2.4 GHz for BLE or WiFi connectivity with a round shape and metal casing. Its rim, top plate, and casing are all metal. If it were a traditional watch with all metal in the whole body, no radiation occurs due to the shielding cavity formed by the casing. The new design uses a new integrated approach to alleviate the shielding effect by cutting a slot along the perimeter of the top plate. The top plate, slot, and the casing form an annular slot antenna [27] with the annular slot as a radiating aperture as shown in Figure 9.3. With the slot's circumference of about one wavelength, the antenna will resonate at the required frequency. The measured efficiency is quite impressive with 70%

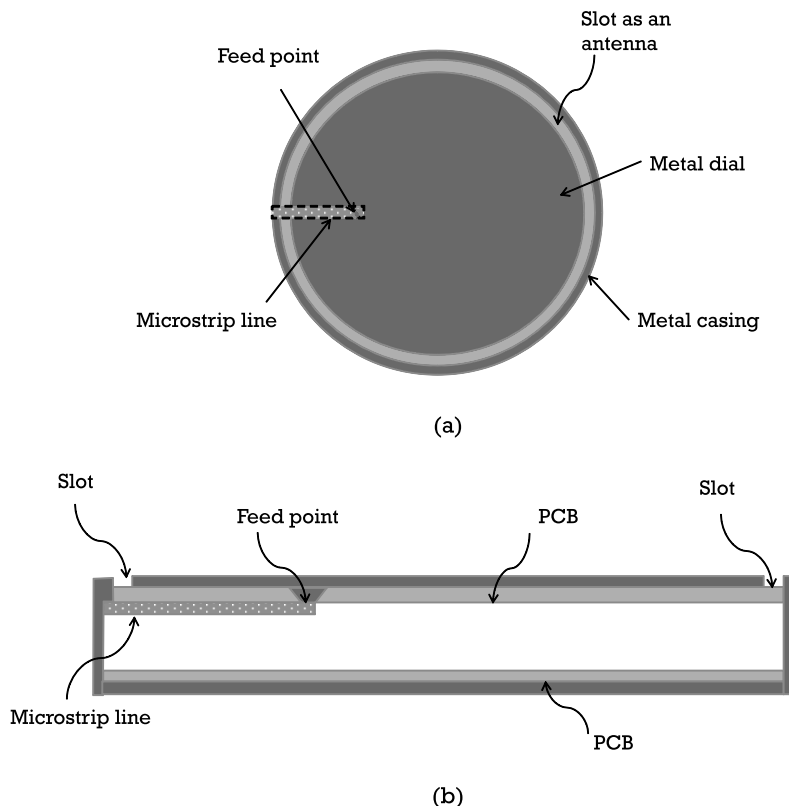


**Figure 9.3** Annular slot antenna for a smartwatch: (a) top view, and (b) side view.

to 78% and 57% to 66% in free space and on a phantom hand, respectively, across the Bluetooth/WiFi frequency band. Such good antenna performance allows many other metal wearables such as bracelets or earrings to incorporate wireless technology.

With regard to the external antenna that is invisible to the user, the previous smartwatch design examples use creative industrial design to integrate the antenna into the main body of the watch. In order to get the best range, a large antenna will unavoidably be required. It is best to increase the volume of the watch without making it look bigger in appearance. The GPS watch shown in Figure 9.4 illustrates such a design. It is a GPS fitness watch using a GPS signal to record speed, distance, and average pace walked by the user. Data can be uploaded to a computer by Universal Serial Bus (USB) connection. The GPS patch antenna is typically big, ranging from  $12\text{ mm} \times 12\text{ mm}$  to

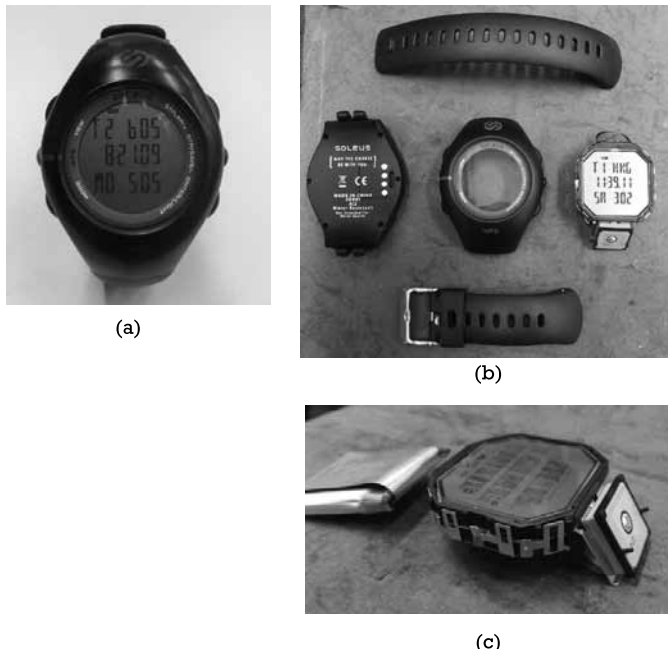


**Figure 9.4** (a) A sports GPS watch, (b) all of its parts, and (c) placing the patch antenna between the body and the band with a tilt angle.

35 mm × 35 mm depending on the required gain. For an optimal reception, it is best placed horizontally with the main board pointing to the sky for maximum signal level. However, this leaves no room for other components and the LCD display blocks the GPS signal. Instead of using the regular shape of circle or square, the housing is designed in ellipse shape. It has a curved section connecting the main body to the wrist band. The curved section is large enough to put the patch antenna inside without being obvious to users. The GPS reception would still be good even if the patch were tilted by around 45°.

Smartwatches now add more features than just the plain GPS or Bluetooth (BT) watch mentioned in the previous sections. Some watches have cellular connectivity and BT/WiFi connectivities in addition to GPS to work as real-time tracking devices for elderly or children. Multiband or wideband antennas will be needed for more advanced smartwatches. It would be very difficult to design a multiband or wideband antenna in the main casing of the watch due to its small size. The strap would be a better place to house the required antenna(s) as it has a bigger area and larger volume than the watch body does. However, there is a significant reduction in antenna efficiency

when the strap is worn on the human arm as reported in [28]. The study examined the impedance and radiation performance of three different types of antennas: wideband dipole, slot, and loop. The antennas were constructed by a slab of copper tape of  $1 \times 3.5$  inches as shown in Figure 9.5. To show the effect that a human body placed near the antenna can have, the antennas were placed 2.7 mm above a lossy block, which was specifically designed to model the human body. It was found that the wideband dipole has a better voltage standing wave ratio (VSWR) than the slot and the loop for a measured frequency of 1 to 6 GHz with and without the lossy block. At 2.4 GHz, the antenna efficiency of the dipole is 50% in free space. The efficiency drops to only 5% when placed on the body. The efficiencies of the loop and slot antennas are several decibels lower than the dipole one as expected. As illustrated, designing wearable antennas is a significant challenge to antenna designers as the human body can degrade the performance of the antenna to a great extent. More future efforts are still needed to come up with wideband or multiband antennas with high performance for wearable devices.

The following shows another good example of embedding the antenna on the wristband. Researchers in [29] explored the possibility of using the metal strap of a smartwatch as a slot antenna. An existing analog watch on the market with a metal strap was used for analysis and experiment. The structure of the watch is shown in Figure 9.6 along with the model of a human arm. The metal strap has a large number of air slots in square and rectangular shapes. The watch has a round metal frame with a metal dial

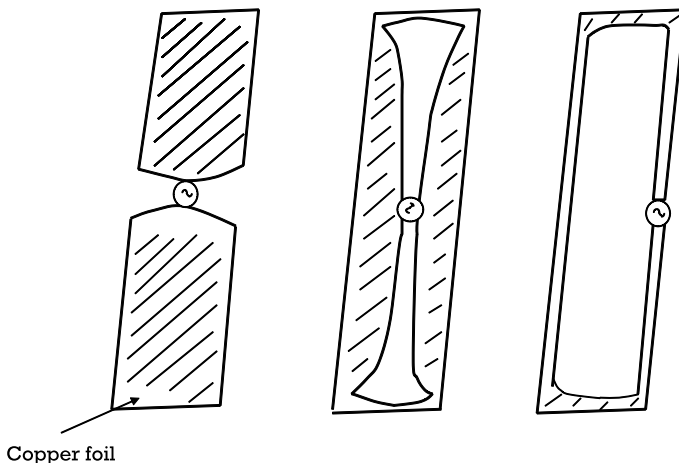
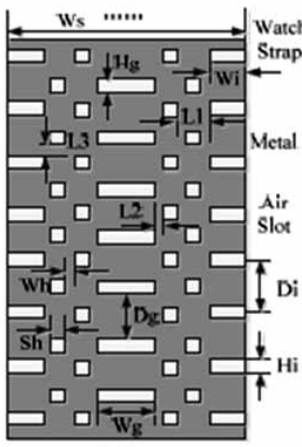
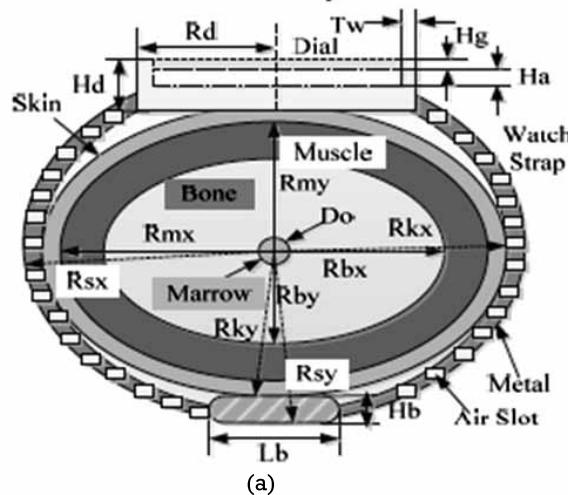
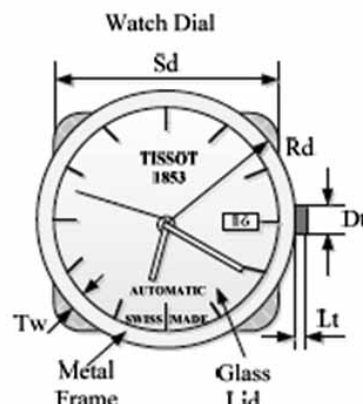


**Figure 9.5** Strap planar antennas, dipole, slot, and loop (from left to right).



(b)



(c)

**Figure 9.6** Watch strap antenna: (a) cross-section, (b) structure of the strap showing the slot antennas, and (c) top view showing the dial of the watch. (From: [29]. Reprinted with permission of the IEEE.)

plate and a glass lid at the top. Experiments on impedance and radiation performance changes with different signal-feeding locations and number of slot holes were conducted. It was found that, with the right feeding location and number of slot holes, good impedance match with a maximum antenna gain of 5 dBi can be achieved at the operating frequency of 2.4 to 2.5 GHz.

### 9.3.2.2 Textiles Antennas

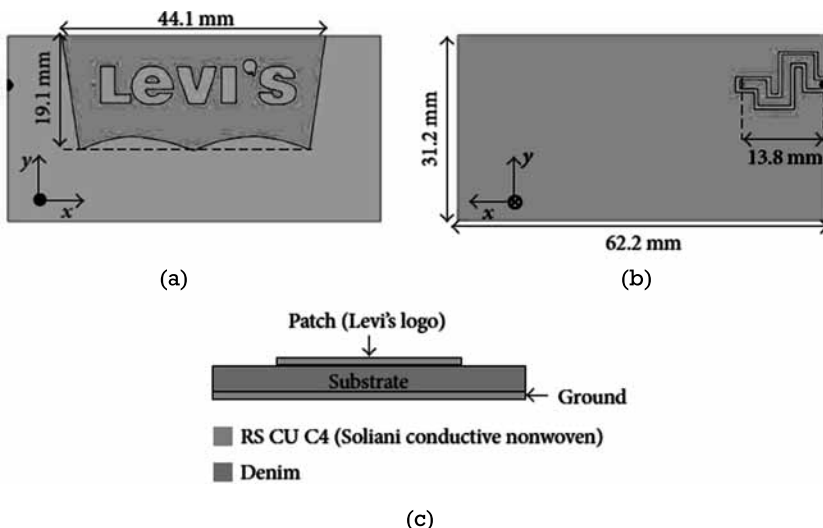
As a type of wearable antenna, the textile antenna is gaining more attention recently due to its wide range of applications. Textile antennas are typically embedded into clothes for wireless applications such as wireless body area networks (WBAN) for healthcare and medical monitoring, RFID, and smart coats with an energy harvesting feature [30–34]. The designs of these on-body antennas are particularly challenging as they are traditionally built on rigid substrates. The rigid substrates make them invasive and less comfortable to the wearers. Researchers have recently developed new ways to embed antennas into clothing as textile antennas to enhance the interactivity between users and electronic devices while making them less invasive. A typical example of using textile antennas is a remote healthcare monitoring system. In telehealth systems, the remote monitoring should not affect the user's regular activities. To achieve this, researchers in [30] blended all the components and antenna into the user's daily routine by integrating the sensors and antenna into the clothes to ensure constant sensor data collection since the user will wear the clothes at all times.

Textile antennas use traditional textile materials and are typically in microstrip patch type so they can adapt to any surface with light weight and low cost for manufacturing. As discussed in Section 3.2.3, typical shapes of patch antennas are rectangular, square, elliptical, or circular, with the rectangular patch being the most common type. The patch typically consists of two metal layers with the top layer as the radiating element and the bottom layer as the ground. Between the two metal layers is the substrate consisting of a dielectric material, which is textile in this case for bendability and easy manufacturing. Due to the ground plane, the antenna characteristic of a microstrip patch antenna will not change even when it is attached to the body. This makes patch antennas particularly suitable for clothing application. The properties of textile materials and the manufacturing techniques are critical to determine the antenna properties as the textile materials are deformable. The dimensions of the antenna should not change when the materials are connected together in production. The stability of the materials, geometrical precision of the patch, and production techniques are all crucial to maintain the desired characteristics of the antenna.

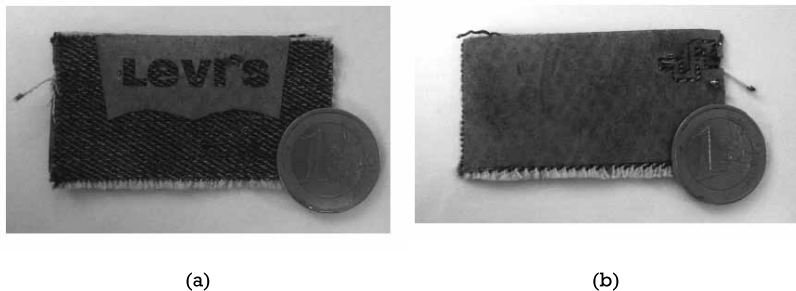
The major difference among different manufacturing methods is the material used for the conductive parts. The four major materials that can be used are categorized as: (1) nonwoven conductive fabrics (NWCFs), (2) conductive threads, (3) electro-textiles, and (4) conductive inks. The NWCF and conductive thread materials provide higher spatial resolution and higher integratability with clothes and surface mounted components. There are

three major techniques on fabricating wearable antennas: (1) NWCF in combination with a cutting plotter, (2) thermal adhesive, and (3) embroidery of conductive threads. Since the NWCF with cutting plotter method is gaining popularity due to its low cost and integratability with sensors and electronic chips, only this method is discussed.

In the fabrication method using NWCFs, the antenna is cut out from an adhesive conductive fabric by a cutting plotter. An adhesive vinyl foil is attached onto the conductive fabric with the backing material removed. The conductive fabric is then pasted on the textile substrate. Any extra conductive fabric and adhesive vinyl foils are removed in the final stage. Researchers in [30] have designed and fabricated a logo antenna as shown in Figure 9.7 using this manufacturing technique to validate the antenna's performance. The antenna is a patch type with a conductive fabric made by an NWCF material with a surface resistivity of  $0.03 \Omega/\text{sq}$ . The substrate was made of a layer of denim with a thickness of 0.5 mm and a relative dielectric constant  $\epsilon_r$  of 1.67. The logo letters were created by cutting the edges of the patch and creating slots inside by a cutting plotter. As a signal feed line, a coplanar transmission line was slotted on the ground plane and connected to the radiating patch by via holes. The prototype was fabricated with the NWCF material by a cutting plotter as shown in Figure 9.8. The simulated



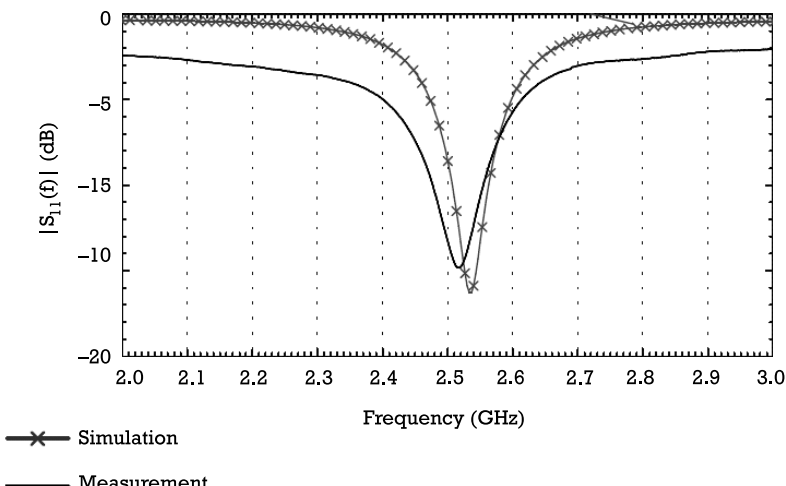
**Figure 9.7** Logo antenna design: (a) front view, (b) back view, and (c) side view showing a patch antenna structure. (From: [30].)



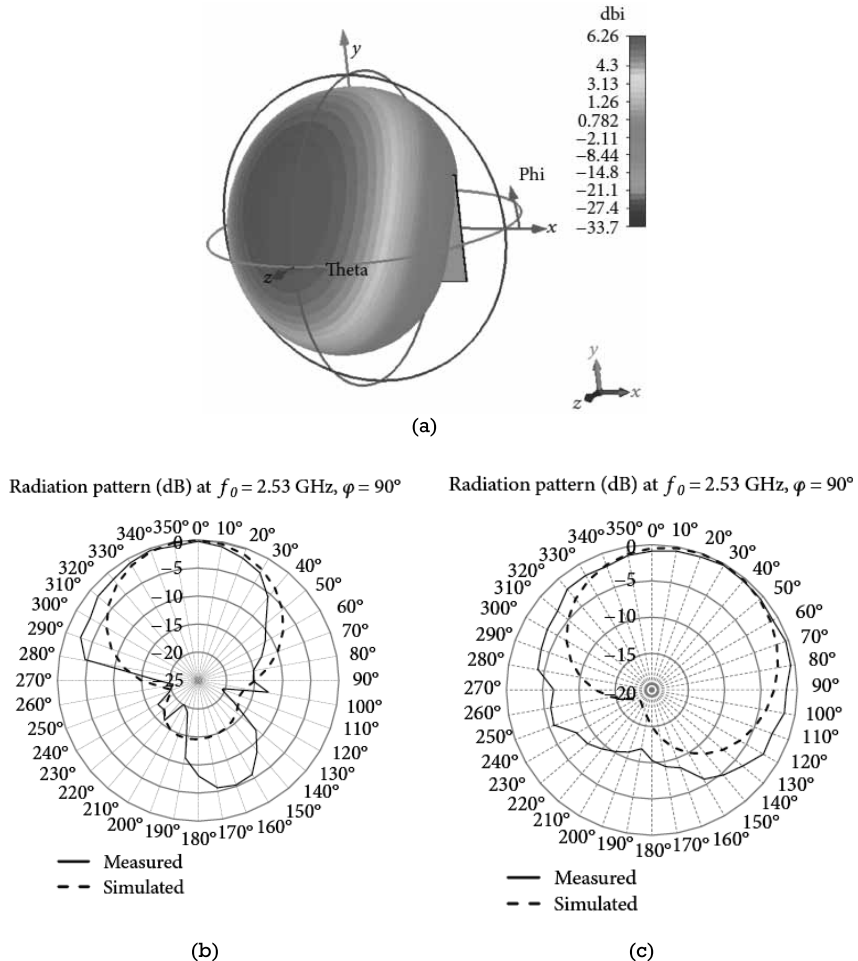
**Figure 9.8** Prototype of an NCWF-based logo antenna: (a) front view and (b) back view. (From: [30].)

and measured input reflection coefficient  $S_{11}$  and radiation properties are plotted in Figures 9.9 and 9.10, respectively, with overall good agreement.

With the same fabrication technique and material, miniaturized antennas with complicated geometries and creative designs can also be made. As shown in Figure 9.11(a), a very small logo antenna with an overall dimension of 25 mm  $\times$  25 mm operating at 1.8 GHz was designed. Two slits of 1 mm were used to disturb the current path on the letter A of the logo to achieve a dipole-like radiation pattern. Surface mount device (SMD) inductors were

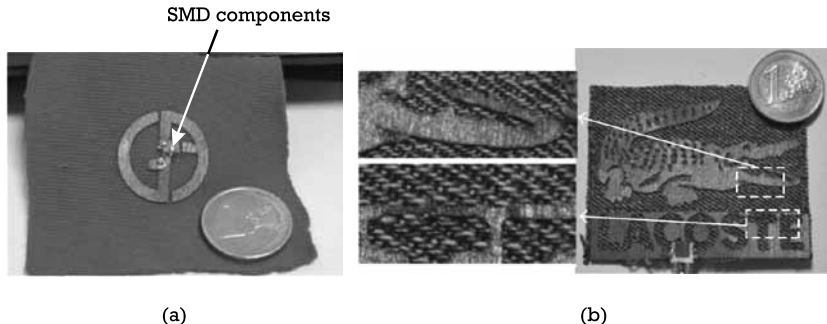


**Figure 9.9** Comparison between the simulated and measured input reflection coefficient  $S_{11}$ . (From: [30].)



**Figure 9.10** Radiation pattern of logo antenna prototype: (a) simulated 3-D radiation pattern, (b) simulated and measured radiation pattern in the x-z plane, and (c) simulated and measured radiation pattern in the y-z plane. (From: [30].)

attached on the antenna for impedance matching. Figure 9.11(b) shows an antenna design with a complicated shape and design. It consists of a planar monopole on a ground plane operating at 1.8 GHz with a substrate of a 0.5-mm-thick layer of denim. The monopole was implemented in a crocodile shape with details of jaws and legs to provide a Vivaldi-like radiation pattern with a maximum directivity of 4.55 dBi. Both design examples confirm that the fabrication technique offers high spatial resolution and complex geometries. However, the signal feed line on the logo patch antenna shown in



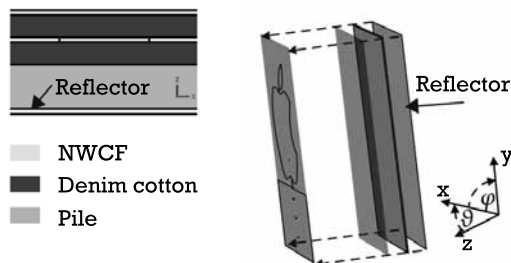
**Figure 9.11** Miniaturized logo antenna with complicated geometries: (a) designer logo with SMD components, and (b) complicated design with a crocodile figure. (From: [30].)

Figure 9.7 is on the ground side. The impedance of the antenna will shift when the back side of the antenna or the matching SMD inductors are placed close to a human body (see Figure 9.11(a)). The SMD inductors will also be damaged very easily due to possible scratches since they are exposed. To alleviate those problems, future developments can use multilayer structures similar to the logo antenna design used in [33]. As shown in Figure 9.12, the multilayer structure consists of denim, cotton, pile, and NWCF layers. It is envisioned that future designs may use more layers, particularly ground planes, to embed all the signal lines and components.

### 9.3.3 Commercial Application

#### 9.3.3.1 Building and Home Automation

The home automation IoT technology can be extended to provide building automation. The devices can monitor and control all the mechanical,



**Figure 9.12** Multilayer logo antenna: (a) side view showing all layers and (b) 3-D view. (From: [33].)

electrical, and electronic systems in different buildings. Since many different sensors such as temperature, vibration, motion, and light sensors will be provided by the device, space is a major concern. External antennas not preferred as they should be hidden from the users or residents of the buildings. A compact and high-efficiency antenna is thus required by the device as the operating environment may not be RF-friendly, having too much metal or walls around the antenna.

### 9.3.3.2 Transportation

There is an increasing number of wireless technologies that are being implemented for entertainment, communication, and safety in cars as people are spending more time in their cars now [34]. An entry-level car typically has short-wave (SW), medium-wave (MW), and frequency modulation (FM) radio receptions and the keyless remote entry feature. In addition, a luxury car is also equipped with tire-pressure sensing, GPS, RFID, Advanced Driver Assistance Systems (ADAS) radars, and cellular and BLE wireless technologies. Vehicle-to-vehicle and vehicle-to-infrastructure communications are some of the most popular fields of research today. These technologies not only help drivers find the most efficient route, but also provide the current traffic condition. With all these systems in place, the estimated number of antennas required ranges from 10 to 30 [35]. The antenna business opportunities are huge and so is the challenge to place all the antennas on the vehicles.

To get the best signal reception, an antenna should be as high as possible over the ground on the vehicle. The antenna is also supposed to receive signal from all azimuth directions. It should keep a maximum distance from other metallic structures or antennas. The distance from the antenna to the receiver/transceiver should be short to minimize the cable loss. The antenna should be placed as far as possible from the engine as the engine could generate spurious noise interfering the receiving signal. There are quite a few places on the vehicle suitable for installing the antennas such as mirrors, roof, spoiler, windows and screens, fender, bumper, and trunk cover as shown in Figure 9.13 [35].

There are many possible antenna options that can be used for vehicle antennas. Monopoles or rod antennas are the most popular type due to their low cost and easy installation. They are also versatile in operating frequency, covering the VHF FM radio band to vehicle-to-vehicle communication at 5.9 GHz. For SW and MW bands, the required length  $\lambda/4$  for optimum performance is too long to place on the vehicle. Instead, a short monopole is implemented, and the FM rod antenna is shared for SW and

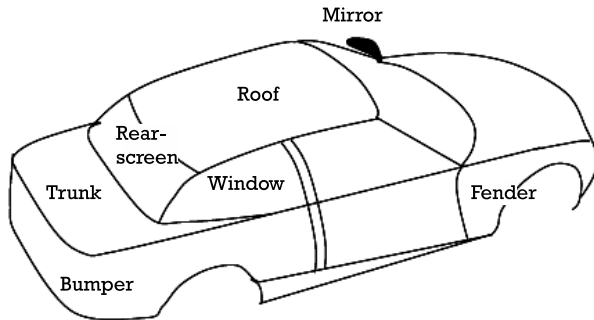


**Figure 9.13** Possible places for an antenna in a regular passenger car. (From: [35].)

MW receptions as well. Depending on the type and model of the vehicle, the antenna can be put at the center or edge of the roof. With a higher cost, a retractable rod antenna with an electric motor can be used to hide and protect the antenna when it is not in use.

Despite its low cost and versatility, the rod antenna is not preferred in middle-end to high-end car manufacturers for cosmetic reasons. Instead, the rod antenna can be hidden in the spoiler and fender or bumper if they are plastic. For a higher price, the on-glass antenna would be a good alternative as well. There are two on-glass antenna types and both are typically placed in the rear windshield. The first one is the wire-grid type. It uses conductive lines printed on glass to form grid or meandering geometries. The early designs are integrated with the defogger elements while newer designs are an invisible, standalone element sitting aside the defogger, which occupies most of the glass area as shown in Figure 9.14. The second type is the slot antenna. Since the car structure is metal, it is part of the antenna with the windscreens as the slot opening of the antenna. Different modes can be excited for certain polarities and radiation behavior with careful selection for the feeding position as shown in Figure 9.15. With a suitable DC-decoupling network, the defrosting elements can be used as part of the antenna since they are already placed on the window [36].

The deployment of the patch antenna in vehicles has been increasing due to the increase in GPS service at 1.5 GHz and the satellite broadcasting radio reception service (SDARS) at 2.3 GHz. Due to its small size and unobtrusively flat shape, it can be placed in several locations in the vehicle such as the fender, bumper, or top of the roof.

Traditionally, shark-fin antennas [36] have been used in premium automobiles. It has several advantages over other types of antennas. They are

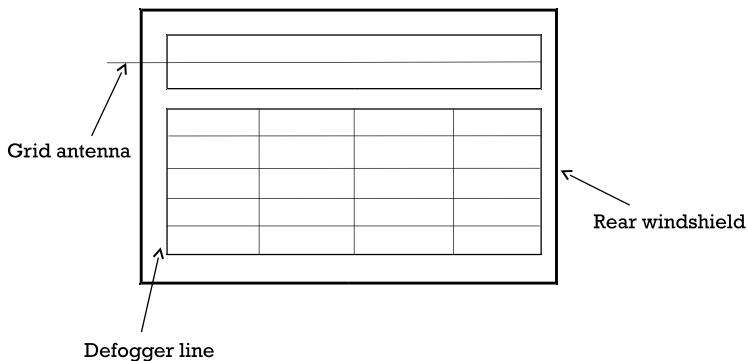


**Figure 9.14** On-glass antenna.

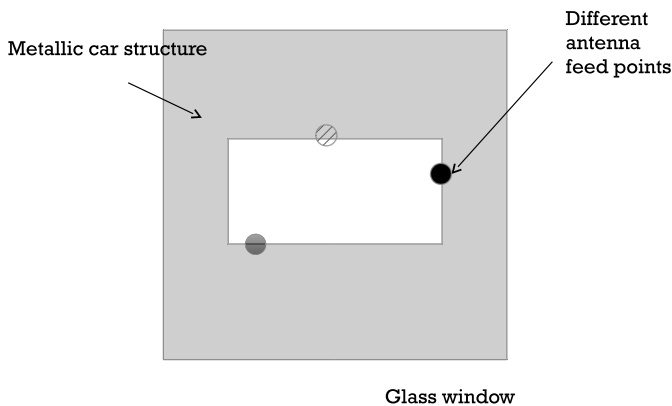


**Figure 9.15** On-glass slot antenna.

small, aerodynamic, and aesthetically pleasing in the shape of a blade or dorsal fin. They are usually located on the roof near the rear of the vehicle as shown in Figure 9.16. Due to its distinct advantages, it is gaining popularity even in the low-end to mid-end markets. Although the antenna size is small as compared to the size of the vehicle, it is still relatively large for antennas operating from UHF to gigahertz. It can combine several antennas in a single housing to accommodate multiple wireless technologies. Figure 9.17 shows an example of using multiple antennas. It has a ceramic GPS antenna with a high dielectric constant placed at the leftmost position to provide a hemispherical radiation pattern receiving satellite signals from



**Figure 9.16** Sharkfin antenna.

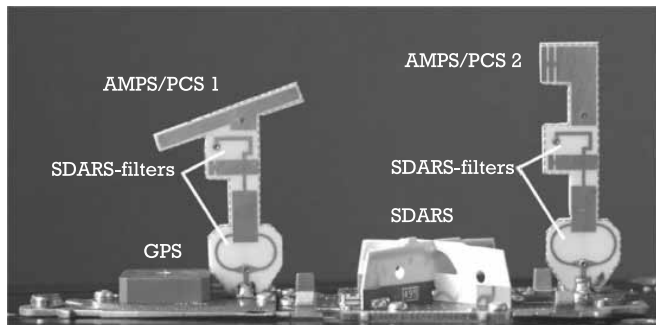


**Figure 9.17** Detailed design of a sharkfin antenna. (From: [37]. Reprinted with permission of the IEEE.)

the sky. The SDARS antenna is a crossed frame type and placed between two cellphone antennas. Both cellphone antennas are quarter-wavelength monopoles with a top loading element for electrical length extension. Since there are many small parts in a shark-fin antenna, it is expensive to produce. The radiation performance may be affected by the mutual coupling between the various antennas in the same housing due to their proximity.

Besides the antennas discussed so far in this section, there are many other advanced antenna technologies such as patch antenna arrays for ADAS at 24 and 77 GHz. TV antennas on glass and body-integrated spiral antenna have been developed with their unique structures and advantages. For future developments, further integration of antennas with the vehicle structure will be expected [36]. The use of radar for ADAS and security purpose may be mandatory in vehicles, which drives the demand for more advanced radar antennas. The vehicle-to-vehicle communication technol-

ogy will become more mature and the service will be widely used, which requires more advanced antennas.

## 9.4 Antenna Technologies for the Future

In addition to the predicted growth to meet the demands of today's IoT, 5G, radar, and automobile applications, there are other main trends to discuss. Future antennas will be in smaller forms, a trend that is mainly driven by the requirement of smaller IoT sensors and devices. More 3-D antenna structures will emerge in addition to the traditional planar type due to the availability of new manufacturing materials and equipment. More creative antennas with greater performance such as wideband and multiband in smaller size will come into play. The cost of antennas will continue to drop due to the higher economy of scale as their demands increase. Beyond those general trends, some technology-specific designs will emerge as there are many researchers and companies working on new materials or design approaches. Newer designs can be realized as a result of the new developments which can improve the antenna performance dramatically.

### 9.4.1 Fractal Antennas

Fractal shapes were proposed by Mandelbrot originally and were considered for electromagnetic analyses and applications in the 1990s [38, 39]. They have been used in antennas since 2010s. A fractal is built from the repetition of a simple shape to form a self-similar and complex pattern. A fractal antenna is an antenna that uses the fractal geometry to maximize the effective length or increase the perimeter of the material receiving or transmitting electromagnetic waves given a total surface area or volume. Due to the inherent properties of fractal elements, fractal antennas can be 50% to 75% smaller than traditional antennas [5]. In addition, they have good to excellent performance at many different frequencies simultaneously over the traditional antennas. Unless specially treated, the traditional antennas are designed for a particular frequency. They will not work well beyond the designed frequency. The typical advantages of fractal antennas are better multiband performance, wider bandwidth, smaller cross-sectional areas, and higher gain in some cases [39]. Also due to the fractal nature of the antenna, no impedance matching network is required. In spite of their advantages, the fractal antennas suffer from a few disadvantages such as complicated design and fabrication, mathematical limitations, and lower gain in some cases [39]. New developments and further research will overcome

those disadvantages in the near future. Putting fractal antennas in volumetric shape may open up opportunities for newer and more creative designs.

### 9.4.2 Polymer

New opportunities for antenna miniaturization and RF packing are being realized recently by novel-engineered materials. Polymer-ceramic composite is an excellent material for antennas as polymer-based antennas are flexible, lightweight, low cost, and highly integratable [5, 40, 41].

Having the capability to change the dielectric constant  $\epsilon_r$  by controlling the ceramic mixture is a key advantage of using polymer-ceramic composite. The composite is made by introducing ceramic into the polymer using a particle-dispersion process. This can be done at room temperature and is low cost. The complete procedure can take only a day without using expensive machinery for composite fabrication. The method also avoids typical issues encountered with ceramic substrates such as cracks and thermal mismatches.

Another advantage of using polymer-ceramic composite is that its dielectric constant  $\epsilon_r$  can be changed from 2 to 20 or even 100 very easily with a typical dielectric loss  $\tan \delta < 0.02$  for frequency up to several gigahertz. Ceramic powder with a different dielectric constant is dispersed into the polymer while the polymer is wet. Polydimethylsiloxane (PDMS), a silicone-based organic polymer with a low cost, can be used as the base material [42]. It is hydrophobic and stable at a temperature up to 200°C and is suitable for microwave applications due to its low dielectric loss for frequencies up to several gigahertz. To achieve higher dielectric constant for the compound, various ceramic powders such barium titanate (BT), Mg-Ca-Ti (MCT), strontium titanate (D270), or Bi-Ba-Nd-Titanate (BBNT) can be used with the polymer.

BT has a wide range of dielectric constants from 10 to 1,000 depending on its chemical combinations, while BBNT, MCI, and D270 have dielectric constants of 95, 140, and 270, respectively [42]. To evaluate their material properties at high frequencies, researchers [41, 42] have fabricated the composites and measured their permittivity and loss tangent versus frequency in different volume percentages of BT-PDMS, MCT-PDMS, and BBNT-PDMS. The results show that the BT-PDMS composite has a high dielectric constant  $\epsilon_r$  of up to 20 with a loss tangent  $\tan \delta$  of less than 0.04 while MCT/PDMS and BBNT/PDMS exhibit a lower loss tangent  $\tan \delta$  of less than 0.009 and a dielectric constant of 8.5. Patch antennas and a microwave filter using

the ceramic-PDMS substrate were built and they showed satisfactory results in predicting the substrate permittivity and loss behavior.

Their flexibility and possibly high dielectric constant make polymer antennas very useful in applications from VHF to microwave frequencies. Wearable and IoT devices may employ them due to their small size and conformability. Further developments on polymer antennas may include researches of new ceramic composites with higher dielectric constant and lower loss, and efficient volume-manufacturing process.

#### 9.4.3 Metamaterials

Traditional antenna miniaturization techniques such as meandering, dielectric loading, or terminal loading will lower the radiation efficiency, narrow the bandwidth, and produce undesired radiation patterns. Because of those undesired results, a great interest in the research of metamaterials or engineered materials has been observed. The word “meta” is a prefix word in Greek meaning “beyond.” Metamaterials are constructed by arranging naturally available materials in a periodic pattern such that the metamaterials exhibit electromagnetic characteristics not found in nature. In other words, they extract their electromagnetic responses from their structure rather than their bulk individual constituents. Two major metamaterials gaining much attention for antenna application are the negative reflective indexes (NRI) ( $\epsilon < 0$  and  $\mu < 0$ ) and electromagnetic bandgap (EBG) media. Since its periodic structure is created at a scale smaller than the wavelength, the NRI metamaterial can control electromagnetic energy in ways natural materials cannot. The EBG metamaterial created by photonic crystal or left-handed materials (LHM) [38] has an artificial structure that can control and manipulate the propagation of electromagnetic waves.

Due to the novel periodic structure and the bandgap feature found in NRI and EBG, respectively, metamaterials are being used in various antennas with greater miniaturization [43, 44] and enhanced performance compared to conventional antennas. Signal will be reflected back to the source in conventional small antennas, whereas energy can be stored and re-radiated in metamaterial antennas. This characteristic makes metamaterial antennas smaller and become effective radiators.

If the transmission lines of the unit cell of NRI metamaterials employ reactive loads, the operational frequency can be reduced. In addition, NRI metamaterials can exhibit multiple resonating modes when used as a microwave resonator. Due to those unique features, printed NRI metamaterials have been used extensively to make miniature and multiband antennas.

Also, the capability of having backward and forward waves by printed NRI metamaterials allows them to realize back-fire to end-fire scanning leaky wave antennas.

Since EBG metamaterial can prevent electromagnetic wave propagation in specified frequency bands and directions, it can be designed to block propagation in single or multiple directions with either narrow or wide bandwidth. Due to this unique propagation property and design flexibility, EBGs have been employed to enhance performance of various microwave devices such as filters, waveguides and antennas. Their bandgap characteristic is particularly useful if used as high-impedance ground plane for antennas to suppress undesired surface waves and mutual couplings. This unique property can enhance the radiation performance of gain, pattern, and side or back lobes of antennas. When defects are introduced in the EBG periodic structure, localized electromagnetic modes can be realized within the bandgap frequencies. Antennas embedded with such defects can radiate in a particular direction since the transmission propagation direction is affected by localized electromagnetic modes. High gain can thus be achieved by this EBG with much simpler structures than conventional high-gain 2-D antenna arrays of complex structures.

#### 9.4.4 3-D Printed Antennas

Additive manufacturing, also known as 3-D printing, is gaining popularity in recent years in fabricating 3-D electromagnetic structures such as passive microwave components, especially antennas. The 3-D printing technology can make antennas smaller, lighter, and cheaper than those made by traditional fabrication methods. Many different types of antennas have been fabricated [45, 46] by 3-D printing over the past few years including multiband GSM/UMTS/LTE, fractal bowtie, spiral, Yagi-Uda, and horn. Various 3-D printing approaches were used to realize the designs. In some of the designs, the antenna structure was first 3-D-printed with the base substrate material. The radiator part was then created by coating the 3-D-printed layer with a conductive material, whereas, in some designs, both the conductive and dielectric sections were created by the same 3-D printing process. Direct printing of conductive traces on the antenna substrate was also possible. In a more novel printing approach, silver nanoparticle ink was written directly on the internal surfaces of a glass hemisphere to explore the possibility of the integration of an antenna onto a small wireless sensor node. Lens antennas at millimeter-wave frequencies have been

realized by 3-D printing with comparable performance to those built with conventional approaches.

More creative and innovative designs are being developed and have been experimented with many companies and research institutes [5]. Using metamaterials or polymers as the antenna substrate has a great potential for higher performance and compact designs. Putting them in volumetric designs may offer performances that traditional antennas can never achieve [47]. Despite all the advantages of 3-D printing, there are still a few design and manufacturing challenges to tackle. Direct metal printing is still very expensive as compared to traditional approaches. However, researchers in [48] have demonstrated the possibility of fabricating 3-D-printed microwave horn antennas in plastic by using a basic 3-D printer with several coats of commercial, conductive paint. The developed horn antennas have a performance comparable to that of a solid metal antenna up to 40 GHz. The fabrication time for making prototypes is relatively short but still long for volume production.

## References

- [1] Brown, E., "Who Needs the Internet of Things?" *Linux.com*, September 13, 2016, last modified January 19, 2019, <https://www.linux.com/news/who-needs-internet-things>.
- [2] Brown, E., "21 Open Source Projects for IoT," *Linux.com*, September 20, 2016.
- [3] "Internet of Things Global Standards Initiative," ITU, <https://www.itu.int/en/ITU-T/gsi/iot/Pages/default.aspx>.
- [4] Hendricks, D., "The Trouble with the Internet of Things," *London Datastore*, Greater London Authority, last modified August 10, 2015, <https://data.london.gov.uk/blog/the-trouble-with-the-internet-of-things/>.
- [5] Hindle, P., "Antenna Technologies for the Future," *Microwave Journal*, January 12, 2018.
- [6] van der Meulen, R., "Gartner Says 8.4 Billion Connected 'Things' Will Be in Use in 2017, Up 31 Percent from 2016," Gartner, <https://www.gartner.com/en/newsroom/press-releases/2017-02-07-gartner-says-8-billion-connected-things-will-be-in-use-in-2017-up-31-percent-from-2016>.
- [7] "IDC Forecasts Worldwide Spending on the Internet of Things to Reach \$745 Billion in 2019, Led by the Manufacturing, Consumer, Transportation, and Utilities Sectors," IDC, last modified January 3, 2019, <https://www.idc.com/getdoc.jsp?containerId=prUS44596319>.

- [8] Vongsingthong, S., and S. Smachat, "Internet of Things: A Review of Applications & Technologies," *Suranaree Journal of Science and Technology*, 2014.
- [9] "The Enterprise Internet of Things Market," *Business Insider*, last modified February 25, 2015, <https://www.businessinsider.com/the-enterprise-internet-of-things-market-2014-12>.
- [10] Perera, C., C. H. Liu, and S. Jayawardena, "The Emerging Internet of Things Marketplace from an Industrial Perspective: A Survey," *IEEE Trans. on Emerging Topics in Computing*, Vol. 3, No. 4, December 2015, pp. 585–598.
- [11] Want, R., B. N. Schilit, and S. Jenson, "Enabling the Internet of Things," *IEEE Computer Society*, 2015, pp. 28–35.
- [12] "The Internet of Things: A Jumbled Mess or a Jumbled Mess?" *The Register*, [https://www.theregister.co.uk/2015/05/14/the\\_internet\\_of\\_things\\_a\\_jumbled\\_mess\\_or\\_a\\_jumbled\\_mess/](https://www.theregister.co.uk/2015/05/14/the_internet_of_things_a_jumbled_mess_or_a_jumbled_mess/).
- [13] "Can We Talk? Internet of Things Vendors Face a Communications 'Mess,'" *Computerworld*, <https://www.computerworld.com/article/2488373/emerging-technology/can-we-talk--internet-of-things-vendors-face-a-communications-mess-.html>.
- [14] Greengard, S., *The Internet of Things*, Cambridge, MA: MIT Press, 2015.
- [15] Apple Inc., "HomeKit - Apple Developer," *developer.apple.com*, last modified September 19, 2014, <https://developer.apple.com/homekit/>.
- [16] Wollerton, M., "Here's Everything You Need to Know about Apple HomeKit," *CNET*, <https://www.cnet.com/news/apple-homekit-everything-you-need-to-know/>.
- [17] Arif Khan, M., M. Aziz ul Haq and S. ur Rehman, "A Practical Miniature Antenna Design for Future," *10th International Conference on Signal Processing and Communication Systems*, 2016.
- [18] Aziz ul Haq, M., and S. Kozieł, "Design Optimization and Trade-Offs of Miniaturized Wideband Antenna for Internet of Things Applications," *Metrol. Meas. Syst.*, Vol. 24, No. 3, 2017, pp. 463–471.
- [19] Vyshnavi Das S K, T. Shanmuganantham, "CPW FED Dual Band Antenna for IOT Application," *International Journal of Engineering & Technology*, 2018, pp. 822–825.
- [20] Manohar, M., R. S. Kshetrimayum, and A. K. Gogoi, "Super Wideband Antenna with Single Band Suppression," *International Journal of Microwave and Wireless Technologies*, 2015, pp. 1–8.
- [21] Seyfollahi, A., and J. Bornemann, "Printed-Circuit Monopole Antenna for Super-Wideband Applications," *12th European Conference on Antennas and Propagation*, January 2018.

- [22] Chen, K. -R., C. -Y. -D. Sim, and J. -S. Row, "A Compact Monopole Antenna for Super Wideband Applications," *IEEE Antennas and Wireless Propagation Letters*, Vol. 10, 2011, pp. 488–491.
- [23] "Miniaturizing Smart Wearables," [https://www.ecnmag.com/node/388197?cmpid=horizontalcontent&\\_\\_hstc=753710.b6204cdbf97306a4f1c5180856691039.1546314691459.1546314691459.1546314691459.1&\\_\\_hssc=753710.1.1546314691460&\\_\\_hsfp=1212338885](https://www.ecnmag.com/node/388197?cmpid=horizontalcontent&__hstc=753710.b6204cdbf97306a4f1c5180856691039.1546314691459.1546314691459.1546314691459.1&__hssc=753710.1.1546314691460&__hsfp=1212338885).
- [24] 2450AT42E0100, "2.4 GHz Surface Mount, Above Metal, Low Profile Mini Chip Antenna," Johanson Technology, Inc.
- [25] Su, S. -W., and Y. -T. Hsieh, "Integrated Metal-Frame Antenna for Smartwatch Wearable Device," *IEEE Trans. on Antennas and Propagation*, Vol. 63, 2015, pp. 3301–3305.
- [26] TE Connectivity Ltd., Schaffhausen, Switzerland, *Antenna Technologies for Wearables*, last modified October 12, 2016, <http://www.te.com/usa-en/industries/consumersolutions/insights/antenna-technologies-for-wearables.html>.
- [27] Wu, D., and S. W. Cheung, "A Cavity-Backed Annular Slot Antenna with High Efficiency for Smartwatches with Metallic Housing," *IEEE Trans. on Antennas and Propagation*, Vol. 65, 2017, pp. 3756–3761.
- [28] "Wearable Antennas," last modified January 6, 2019, <http://www.antenna-theory.com/antennas/wearable-antennas.php>.
- [29] Li, G., et al., "A Watch Strap Antenna for the Applications of Wearable Systems," *IEEE Access*, Vol. 5, 2017, pp. 10332–10338.
- [30] Corchia, L., et al., "Wearable Antennas for Remote Health Care Monitoring Systems," *International Journal of Antennas and Propagation*, Vol. 2017, 2017, Article ID 3012341.
- [31] Loss, C., et al., "Smart Coat with a Fully-Embedded Textile Antenna for IoT Applications," *Sensors*, Vol. 16, 2016, p. 938.
- [32] Monti, G., L. Corchia, and L. Tarricone, "Logo Antenna on Textile Materials," *Proceedings of the 44th European Microwave Conference*, October 2014, pp. 516–519.
- [33] Corchia, L., G. Monti, and L. Tarricone, "Durability of Wearable Antennas Based on Nonwoven Conductive Fabrics: Experimental Study on Resistance to Washing and Ironing," *International Journal of Antennas and Propagation*, Volume 2018, 2018, Article ID 2340293.
- [34] "Antenna Design and Placement for the Automotive Market," *CST Webinar*, 2014, last modified December 19, 2018, <http://cst2cd.acceptance.brimit.com/solutions/article/antenna-design-and-placement-for-the-automotive-market>.
- [35] Koch, N., "Antennas for Automobiles," *New Advances in Vehicular Technology and Automotive Engineering, InTech*, 2012.

- [36] Pell, B. D., et al., "Advancements in Automotive Antennas, New Trends and Developments in Automotive System Engineering," *InTech*, <http://www.intechopen.com/books/newtrends-and-developments-in-automotive-system-engineering/advancements-in-automotive-antennas>.
- [37] Hopf, J., L. Reiter, and S. Lindenmeier, "Compact Multi-Antenna System for Cars with Electrically Invisible Phone Antennas for SDARS Frequencies," *2nd International ITG Conference on Antennas*, 2007, pp. 171–175.
- [38] Mohd, S., et al., "Introduction to Fractal Antenna," *International Journal of Innovative Research in Electrical, Electronics, Instrumentation and Control Engineering*, Vol. 4, No. 2, February 2016, pp. 152–155.
- [39] Volakis, J., C. -C. Chen, and K. Fujimoto, *Small Antennas: Miniaturization Techniques & Applications*, New York: McGraw-Hill, 2009.
- [40] Chen, S. J., "Flexible, Wearable and Reconfigurable Antennas Based on Novel Conductive Materials: Graphene, Polymers and Textiles," Ph.D. thesis, School of Electrical & Electronic Engineering, University of Adelaide, 2017.
- [41] Koulouridis, S., et al., "Polymer–Ceramic Composites for Microwave Applications: Fabrication and Performance Assessment," *IEEE Trans. on Microwave Theory and Techniques*, Vol. 54, No. 12, December 2006, pp. 4202–4208.
- [42] Rashidian, A., et al., "Development of Polymer-Based Dielectric Resonator Antennas for Millimeter-Wave Applications," *Progress in Electromagnetics Research*, Vol. 13, 2010, pp. 203–216.
- [43] Acharya, R., et al., "A Review on Antenna Application of Metamaterials," *Journal of Electronics and Communication Engineering*, Vol. 12, No. 5, 2017, pp. 6–8.
- [44] Singh, G., Rajni, and A. Marwaha, "A Review of Metamaterials and Its Applications," *International Journal of Engineering Trends and Technology*, Vol. 19, No. 6, January 2015, pp. 306–310.
- [45] Mandke, Y., and R. Henry, "Review of Additive Manufacturing 3D Printed Microwave Components for Rapid Prototyping," *International Journal of Control Theory and Applications*, Vol. 10, No. 29, 2017, pp. 11–14.
- [46] Bjorgaard, J., et al., "Design and Fabrication of Antennas Using 3D Printing," *Progress in Electromagnetics Research*, Vol. 84, 2018, pp. 119–134.
- [47] Elsallal, M. W., J. Hood, and I. McMichael, "3D Printed Material Characterization for Complex Phased Arrays and Metamaterials," *Microwave Journal*, October 14, 2016.
- [48] Robb, G., "Assemble Antennas with 3D Printing," *Microwave & RF*, October 2018.



## **About the Author**

Henry Lau received an M.Sc. and an M.B.A. in the United Kingdom and the United States, respectively. He has more than 27 years of experience in designing radio frequency (RF) systems, products, and radio frequency integrated circuits (RFICs) in both Hong Kong and the United States. He worked for Motorola and Conexant in the United States as the principal engineer on developing RFICs for cellular phone and silicon tuner applications. Mr. Lau holds five issued patents and has two pending patents, all in RF designs. He is currently running Lexiwave Technology, a wireless and Internet of Things (IoT) solutions company in Hong Kong and the United States that designs and sells RFICs, RF modules, RF solutions, radar solutions, and antennas. He has also taught numerous RF-related courses internationally. In addition, Mr. Lau chaired two symposiums and three seminars in wireless and IoT technologies in Hong Kong during 2016 and 2017.



# Index

3-D printed antennas, 211–12

## A

Admittance, 132

Advanced Driver Assistance Systems (ADAS) radars, 204, 207

Alternating current element, 28, 29

Anechoic chamber, 115

Antenna diversity, 181

Antenna elements

advanced, 75–88

basic, 55–72

half-wavelength dipole

antenna, 55–62

loop antenna, 62–66

monopole antenna, 55–62

patch antenna, 66–72

quarter-wavelength

antenna, 55–62

Antenna future technologies

fractal antennas, 208–9

metamaterials, 210–11

polymer-ceramic

composite, 209–10

3-D printed antennas, 211–12

Antenna Magus, 104–6

Antenna ranges

anechoic chamber, 115

compact, 115–16

defined, 113

elevated, 114

free-space, 113–14

outdoor, 113–14

slant, 114, 115

Antennas

amount of current flowing through, 33

aperture concept, effective aperture, and directivity, 41–43

basic types of, 16–20

beam solid angle, 38–39

designs for IoT

applications, 190–208

directivity and effective

aperture, 40–41

efficiency, 48–49

Friis transmission and receiving formulas, 51–53

fundamentals of, 16–23

gain, 43–45

impedance matching, 49–51

location and placement, 169–71

main functions of, 59

miniature, for portable

electronics, 76–88

polarization, 45–48

radiation mechanism, 23–33

radiation pattern, 35–38

- A**
- Antennas (continued)
    - radiation power intensity, 39–40
    - specifications and performances, 35–53
    - as transformation devices, 24
    - See also specific types of antennas*
  - AntSyn, 106
  - Aperture
    - concept, 41–43
    - effective, 40–43
    - field experienced at observation point due to, 42
    - radiating, 42
  - APLAC, 103
  - Attenuation, 23
  - AWR Microwave Office, 103–4
  - AXIEM
    - automatic meshing on patch antenna with, 106
    - complex antenna array simulation with, 103
    - defined, 103
    - single patch antenna modeling with, 104
- B**
- Beam solid angle
    - approximation, 39, 40
    - defined, 38–39
    - directivity and, 41
    - See also* Specifications and performances
  - BLE smartwatch, 191
  - Bluetooth Low Energy (BLE), 189, 190, 204
  - Building and home automation IoT technology, 203–4
- C**
- Capacitance, 173–74
  - Capacitors, 141–45
  - Cellphones
    - basic, minimum elements of, 176
    - clamshell, 176
    - evolution to smartphone, 160
    - internal circuit partitioning and metallization, 177
    - PCB design of, 171
    - required antenna length, 158–59
    - table of, 179–81
- D**
- Ceramic chip capacitors, 144–45
  - Ceramic types, 86–87
  - Channel state information (CSI), 22
  - Characteristic impedance, 129
  - Circular loop antenna, 63
  - Circular polarization, 46
  - Clamshell cellular phone, 176
  - Compact ranges, 115–16
  - Composite vector field, 47
  - Conduction efficiency, 48–49
  - Coupling capacitance, 173–74
  - CST Microwave Studio, 101
  - Current density, 26
  - Current distribution, 28, 56
- Dipole antennas**
- current distribution, 56
  - defined, 16
  - directional property of, 59–61

- half-wavelength, 55–62  
illustrated, 16  
radiation characteristics, 55  
radiation field strength, 59–60  
setup for measuring impedance  
of, 148  
short dipole, 16, 56  
sinusoidal current distribution, 57  
vertical placement of, 59  
*See also* Antennas
- Directivity  
beam solid angle and, 41  
comparison of antenna types, 163  
defined, 40–41, 119  
expression of, 41  
implementation and, 163–65  
measurement, 119–20  
of test antenna, 120
- Diversity coding, 22
- Doorbell, wireless, 161, 162
- Dual-port measurements, 149
- E**
- Effective aperture  
aperture concept and, 41–43  
directivity and, 40–41  
maximum, 43  
physical area and, 42
- Effective isotropic sensitivity (EIS), 124
- Efficiency  
conduction, 48–49  
impedance mismatch, 48  
loop, 65  
measurements, 120  
patch antenna, 69  
radiation, 62, 82–83  
receiver sensitivity and, 53  
total antenna, 44–45, 48
- Electric fields  
as function of time and  
position, 46  
half-wave dipole, 57–58  
quarter-wave monopole, 57–58
- retarded potential, 28  
scalar potential, 27  
strength, 30, 43  
of wave traveling in  $z$ -direction, 46
- Electromagnetic bandgap media,  
210–11
- Electromagnetic horn, 41, 42
- Electromagnetic simulation  
Antenna Magus, 104–6  
AntSyn, 106  
AWR Microwave Office, 103–4  
CST Microwave Studio, 101  
differential equation techniques,  
94, 95–97  
EM.Cube, 102  
FEKO, 100–101  
high-frequency structure simulator  
(HFSS), 101  
introduction to, 93–94  
methods, 94  
MoM, 94–95  
Momentum, 100  
Numerical Electromagnetics Code  
(NEC), 98–100  
software, 93–94, 97–106  
Sonnet, 102  
tools, 97–106  
WIPL-D Pro, 102–3
- Elevated ranges, 114
- Elliptical polarization, 46
- EM.Cube, 102
- Enclosure  
antenna characteristics and, 173  
illustrated, 174  
LCD and, 174  
as plastic, 173  
RF considerations and, 174
- Equivalent series resistance (ESR), 141
- F**
- Family Radio Service (FRS), 17
- Far-field pattern measurement, 116
- FEKO, 100–101

- Field pattern, 36, 38, 39, 60
  - Finite-difference time-domain method (FDTD), 94, 96
  - Finite element method (FEM), 94, 95–96
  - Finite integration technique (FIT), 94, 96–97
  - Fractal antennas, 208–9
  - Free-space ranges, 113–14
  - Friis receiving equation, 52
  - Friis transmission equation, 51, 52, 117
  - Future trends
  - Antenna technologies, 208–12
    - introduction to, 187–88
    - IoT applications, 190–208
    - IoT technology, 188–90
- G**
- Gain
    - characteristics of, 43
    - defined, 44
    - measurement, 116–19
    - total antenna efficiency and, 44–45
  - See also* Specifications and performances
- Gain-comparison method, 117, 118
  - Global Positioning System (GPS)
    - antennas, 70, 71
  - Green’s function tensor, 94
  - Ground effect, 148–54
  - Ground plane
    - between antenna and cable, 151
    - effect of size on performance, 171
    - implementation and, 171–73
    - lengths, 153–54
    - measurement to simulate
    - PCB, 152
    - with slot for isolation, 183
- H**
- Half-wavelength dipole antennas
    - elements of, 55–62
- magnitude of electric and magnetic field, 57–58
  - radiation pattern, 61
  - for wireless communication devices, 61–62
  - Heat dissipation, 23
  - Helical antennas
    - advantage of, 17
    - characteristics of, 16–18
    - with ground plane, 18
    - impedance measurement setup, 150
    - with major lobe along its axis, 18
    - traveling wave, 16
  - See also* Antennas
  - Hex-band antenna, 83
  - High-frequency structure simulator (HFSS), 101
  - High-temperature cofired ceramic (HTCC), 87
  - Home automation IoT technology, 203–4
  - Horizontal field pattern, 60
- I**
- Impedance
    - characteristic, 129
    - as function, 33
    - helical antenna, measurement setup, 150
    - load, 135
    - loop antennas, 138
    - measurement with VNA, 145–46
    - multiband antennas, 85
    - normalized, 129–30
    - reference, 49
    - system, 138
    - terminal, 48
  - Impedance matching
    - adding a series inductor and then a parallel shunt capacitor for, 136

- adding a shunt inductor and then a series capacitor for, 137  
adding a shunt inductor and then a series inductor for, 137  
adding parallel inductor for, 136  
adding series capacitor for, 134  
adding series inductor for, 134, 136  
defined, 49, 129  
introduction to, 127–28  
L-type networks, 50  
matching elements and, 139–45  
matching topology and, 138–39  
maximum power transfer and, 128–29  
Smith chart and, 129–32
- Impedance mismatch efficiency, 48
- Implementation
- considerations and strategies, 168–83
  - enclosure and, 173–75
  - ground plane and, 171–73
  - internal versus external, 158–59
  - introduction to, 157–58
  - mechanical design and, 175–83
  - operating frequency, size, and geometry and, 165–68
  - PCB design and, 175–83
  - polarization and directivity and, 159–65
  - requirements, understanding, 158
  - RF PCB layout techniques and practices, 169
  - teamwork and, 175–76
- Inductors
- 0603CS chip, 142
  - 1206CS chip, 143
  - air-core, 140
  - ceramic chip, 145
  - high-frequency, 140, 141
  - Q factor of, 140, 141
  - Vcc feeding, 139
- Instantaneous power flow density, 31
- Internet of Things (IoT). *See* IoT applications; IoT devices
- Inverted-F antenna
- analysis of characteristics, 77
  - illustrated, 20
  - impedance variation, 78
  - layout, 79
  - lumped-element model, 78, 79
  - mounted on ground plane, 78
  - multiband, 84
  - as open-ended transmission line, 77
  - planar, 83
  - printed PCB, 80
  - segments, 77
  - shunting shorted-conductor, 80
  - simulated input impedance of, 81
  - in 3-D layout view, 80
  - transceiver module using, 167
- Inverted-L antenna, 76–77
- IoT applications
- antenna designs for, 190–208
  - building and home automation, 203–4
  - commercial, 203–8
  - enabling technologies, 188–90
  - smarthome, 190–91
  - smartwatches, 191–98
  - textile antennas, 199–203
  - transportation, 204–8
  - wearable devices, 191–203
- IoT devices, 167, 188
- Iseeka, 163, 164
- ISM band RF transceiver module, 171, 172
- L**
- Left-hand circularly polarized (LHCP), 71
- Left-handed materials (LHM), 210
- Linear polarization, 46, 119
- Liquid crystal display (LCD), 174, 178
- L-network, 137, 139

- Load impedance, 135
- Logo antennas
  - design, 200
  - miniaturized, 203
  - radiation pattern, 202
- Long-range wireless, 190
- Long Term Evolution 4G standards, 178
- Loop antennas
  - characteristics of, 18–20
  - circular, 63
  - coplanar loops, 66
  - defined, 18
  - efficiency, 65
  - electromagnetic interference/electromagnetic compatibility, 65
  - forms of, 62
  - frequency range of operation, 18–19
  - illustration of types of, 19
  - impedance, 138
  - as inductive, 65
  - radiation efficiency, 62
  - radiation pattern, 19–20
  - radiation resistance, 64
  - radiation sufficiency, 66
  - rectangular, 19
  - square, 64
  - use of, 62
- See also* Antennas
- Low-cost VNAs, 146
- Low noise amplifier (LNA), 53
- Low-temperature cofired ceramic (LTCC), 87
- Lumped-element model, 78, 79
- M**
- Machine-to-machine (M2M) communication, 188
- Magnetic fields
- half-wave dipole, 57–58
  - quarter-wave monopole, 57–58
  - retarded potential, 28
  - scalar potential, 27
- Magnetic potential, 30
- Matching elements
  - capacitor, 141–45
  - high-frequency behavior of, 77
  - inductor, 139–41
  - losses associated with, 76
  - series element, 132–35
  - shunt element, 135–38
  - transmission line, 145
- Matching networks, 76–77
- Matching topology, 138–39
- Material loading, 85
- Maximum effective aperture, 43
- Maximum power transfer, 128–29
- Maxwell equations, 28, 94
- Meander line antennas
  - physical length, 81
  - radiation efficiency, 82–83
  - radiation resistance, 83
  - resonant frequencies, 82
  - in 3-D layout view, 86
  - use of, 81
- Measurements
  - antenna ranges in, 113–16
  - antenna system for, 112
  - challenges in, 113
  - directivity, 119–20
  - dual-port, 149
  - efficiency, 120
  - far-field pattern, 116
  - gain, 116–19
  - with ground plane, 151, 152, 153–54
  - impedance, with VNA, 145
  - introduction to, 111–12
  - phase, 120–21
  - place and environment for taking, 113
  - polarization, 121–22
  - SAR, 124–25
  - TIS, 122–24
  - TRP, 122–24
  - in validating antenna design, 111

- Measuring equipment, 112–13  
Mechanical design, 175–83  
Medium-range wireless, 189  
Metamaterials, 210–11  
Method of Moments (MoM), 94–95  
Microstrip antennas  
    advantages of, 66  
    performance limitations, 66–67  
    width of, 68  
Microwave monolithic integrated circuit (MMIC), 87  
MIMO antennas  
    cellular, 22  
    channel capacity and, 178–81  
    defined, 21  
    diversity performance, 23  
    popularity of, 178  
    techniques, 22  
    transmission rate and, 178–81  
    use of, 21  
    in wireless router, 22  
    *See also* Antennas  
Miniature antennas, for portable electronics  
    dielectric loaded, 85–88  
    inverted-F antenna, 77–81  
    inverted-L antenna, 76–77  
    meander line, 81–83  
    multiband, 83–85  
Mismatch loss, 23  
MMANA-GAL antenna design software, 98–99  
Mobile phones on market, 179–81  
Momentum, 100  
Monopole antennas  
    defined, 16  
    dielectric-loaded, 88  
    elements of, 55–62  
    as external to wireless devices, 62  
    on handheld device, 17  
    illustrated, 17  
    for internal use, 160  
modeling with WIPL-D, 103  
radiation pattern, 16  
total radiated power, 58  
Moving charge, 25–26  
Multiband antennas  
    design techniques, 83  
    hex-band, 83  
    impedance, 85  
    inverted-F, 84  
    penta-band, 83  
    sizing, 84  
    SMD, 151, 153  
    use of, 20–21  
    WiMAX band, 85  
    WLAN band, 85  
    Multilevel Fast Multipole Method (MLFMM), 101
- N**
- Narrowband IoT (NB-IoT), 190  
Nonwoven conductive fabrics (NWCFs), 199–200, 201  
Normalized impedance, 129–30  
Numerical Electromagnetics Code (NEC), 98–100
- O**
- On-glass antennas, 206  
Operating frequency, 165–68  
Outdoor ranges, 113–14
- P**
- Patch antennas  
    bandwidth and efficiency, 69  
    center frequency of operation, 68  
    with fringing E-fields, 68  
    input impedance, 68–69  
    with insert feed, 70  
    performance limitations, 67  
    permittivity of free space, 68  
    with quarter-wavelength impedance transformer, 70

- Patch antennas (continued)
- quarter-wavelength transmission line, 69
  - radio frequency identification device (RFID), 70–72
  - total radiated field, 69
  - typical shapes of, 67
  - in vehicles, 205
- PCB
- antenna placement at edge of, 169
  - design, 175–83
  - design of cellular phone and, 171
  - flooded with complete ground, 174
  - RF, layout and practices, 169
  - in tablet PC, 174
- PCB antennas
- layout design rules, 157
  - printed inverted-F, 80
  - use of, 20
- Penta-band antenna, 83
- Permittivity, 27
- Phase angle, 46
- Phase measurement, 120–21
- Physical optics (PO), 101
- Planar inverted-F antenna (PIFA), 83, 178, 182–83
- Polarization
- of antenna, 47–48
  - antenna diversity by, 181
  - in antenna-to-antenna communication, 47
  - circular, 46
  - determination, 121
  - elliptical, 46
  - implementation and, 159–63
  - linear, 46, 119
  - measurement, 121–22
  - optimum, antenna design for, 160
  - of plane electromagnetic wave, 45–47
- See also* Specifications and performances
- Polarization loss factor (PLF), 47
- Polymer-ceramic composite, 209–10
- Power density
- non-isotropic antenna and, 51
  - radiation pattern expressed as, 38
  - in total power received by horn, 41
- Poynting vector, 31, 38, 41, 58
- Precoding, 22
- Q**
- Q factor, 140, 141
- Quarter-wavelength monopole antennas
- elements of, 55–62
  - free-space path loss, 168
  - magnitude of electric and magnetic field, 57–58
  - radiation resistance, 58–59
  - for wireless communication devices, 61–62
- R**
- Radiated field, 36–37
- Radiation
- characteristics of, 26–33
  - due to motions of electric charge, 25
  - efficiency, 62, 82–83
  - intensity, 119
  - loss, 23
  - mechanism, 23–33
  - moving charge, 25–26
  - potential functions due to current source, 26
  - power intensity, 39–40
  - source of, 23–26
  - stationary charge, 25, 27

- Radiation pattern  
defined, 35–36  
defined by radiated field and, 36–37  
as function of distance, 36  
half-wavelength dipole antennas, 61  
logo antenna prototype, 202  
monopole antennas, 16  
normalized field pattern, 37–38  
one-and-a-half-wavelength dipole, 61  
power density expression, 38  
presentation of, 36  
principal planes, 37, 38  
representation of radiation characteristics, 38  
wavelength dipole, 61  
*See also* Specifications and performances
- Radiation resistance  
analytical expression of, 32  
defined, 32  
impedance as function of, 33  
loop antennas, 64  
meander line antennas, 83  
quarter-wavelength antenna, 58–59
- Radio frequency integrated circuit (RFIC), 139
- Receiving signal strength (RSSI), 163, 164
- Reference impedance, 49
- Reflection coefficient, 130
- Retarded potentials, 28
- RFID patch antennas  
with ceramic and FR-4 dielectric materials, 72  
installed in vending machine, 71  
operating frequency, 70–71  
reader, 71  
RFID tags, 70
- RF PCB  
design guidelines related to, 170  
techniques and practices, 169
- RF transceiver module, 171, 172
- Right-hand circularly polarized (RHCP), 47, 71
- S**
- SAR  
defined, 124  
importance of, 124  
measurement, 124–25  
test set, 125
- Satellite broadcasting radio reception service (SDARS) antenna, 205, 207
- Scalar potential, 26–27
- Self-quieting effect, 170
- Semiconductor technology, 178
- Series element, 132–35
- Shark-fin antennas, 205–6, 207
- Shooting and bouncing rays (SBR), 101
- Short dipole, 16, 56
- Short-range device (SRD), 61–62, 165–68
- Short-range wireless, 189
- Shunt element, 135–38
- Shunting shorted-conductor, 80
- Slant ranges, 114, 115
- Slot antennas, 176
- Smartwatches  
annular slot antenna, 194–95  
BLE, 191  
casing for, 194  
ceramic antenna, 193–94  
component design, 193  
creative internal antennas, 193–98  
external antenna, 196–97  
features of, 196–97  
GPS patch antenna, 195–96  
illustrated, 192

- Smartwatches (continued)  
integrated metal frame antenna, 194  
strap antenna, 198  
strap planar antennas, 197  
tracking, 191–92  
*See also* IoT applications
- Smith chart  
as admittance chart, 132  
conformal mapping from impedance to, 131  
constant resistance circle on, 132–35  
defined, 129  
illustrated, 130  
use of, 129  
 $Y$ , 133  
 $ZY$ , 133
- Sonnet, 102
- S-parameters, 127
- Spatial multiplexing, 22
- Specifications and performances  
aperture concept, effective aperture, and directivity, 41–43  
beam solid angle, 38–39  
directivity and effective aperture, 40–41  
efficiency, 48–49  
Friis transmission and receiving formulas, 51–53  
gain, 43–45  
impedance matching, 49–51  
polarization, 45–48  
radiation pattern, 35–38  
radiation power intensity, 39–40
- Spherical coordinate system, 117
- Square loop antenna, 64
- Stationary charge, 25, 27
- Stimulation tools  
Antenna Magus, 104–6  
AntSyn, 106  
AWR Microwave Office, 103–4  
CST Microwave Studio, 101
- EM.Cube, 102  
FEKO, 100–101  
high-frequency structure simulator (HFSS), 101  
Momentum, 100  
Numerical Electromagnetics Code (NEC), 98–100  
Sonnet, 102  
WIPL-D Pro, 102–3
- T**
- Textile antennas  
embedding of, 199  
fabrication method, 200  
logo antenna design, 200  
miniaturized logo antenna, 203  
NWCF-based, 200–201  
radiation pattern, 202  
surface mount device (SMD) inductors, 201–2  
textile materials, 199  
*See also* IoT applications
- 3-D printed antennas, 211–12
- TIS measurement, 122–24
- Total antenna efficiency, 44–45, 48
- Total noise figure, 52–53
- Total radiated power, 39–40, 58
- Tracking smartwatch, 191–92
- Tracking tag, 163, 165
- Transmission line  
inverted-F antenna as, 77  
as matching element, 145  
transition region between free-space and, 23
- Transmission line matrix (TLM) method, 97
- Transportation. *See* Vehicles
- Traveling wave antennas, 16
- Tri-band GSM smartphones, 182
- TRP measurement, 122–24
- Two-port PIFA, 182, 183
- Two-port VNAs, 145–46, 147

**U**

Ultrahigh frequency (UHF), 49  
Unified Theory of Diffraction (UTD), 100

**V**

Vector network analyzer (VNA)  
defined, 129  
ground effect and, 148–49  
impedance measurement with, 145–46  
low-cost, 146, 147  
two-port, 145–46

Vector potential, 29

Vehicles  
Advanced Driver Assistance Systems (ADAS) radars, 204, 207  
antenna locations for, 205  
on-glass antennas, 206  
patch antenna, 205

radio receptions, 204

rod antenna, 205  
SDARS antenna, 205, 207  
shark-fin antennas, 205–6, 207  
wireless technologies in, 204–8

Vertical field pattern, 60

Very high frequency (VHF), 49

**W**

WiMAX band, 85, 178  
WIPL-D Pro, 102–3  
Wireless body area networks (WBAN), 199  
Wireless doorbell, 161, 162  
WLAN band, 85

**Y**

Yagi antenna, 99  
Yagi-Uda antenna, 164–65, 166

